UNIVERSITÉ DE LORRAINE | BIBLIOTHÈQUES UNIVERSITAIRES

AVERTISSEMENT
DROIT D'AUTEUR

Ce document est le fruit d'un long travail approuvé par le jury de soutenance et mis à disposition de l'ensemble de la communauté universitaire élargie.

Il est soumis à la propriété intellectuelle de l'auteur. Ceci implique une obligation de citation et de référencement lors de l'utilisation de ce document. Toute contrefaçon, plagiat ou reproduction illicite encourt une poursuite pénale.

Contact bibliothèque : ddoc-theses-contact@univ-lorraine.fr
(Cette adresse ne permet pas de contacter les auteurs)

Code de la Propriété Intellectuelle. articles L 122. 4
Code de la Propriété Intellectuelle. articles L 335.2- L 335.10

UNIVERSITÉ DE LORRAINE
34 COURS LÉOPOLD — CS 25233
54052 NANCY CEDEX
TÉL : 03 54 50 54 00
CONTACT@UNIV-LORRAINE.FR
WWW.UNIV-LORRAINE.FR

Thèse

Présentée et soutenue publiquement pour l'obtention du titre de

DOCTEUR DE l'UNIVERSITE DE LORRAINE

Mention : Génie des procédés, des Produits et des Molécules

par **Mathilde LAFONT**

Sous la direction de Pr. Christophe CASTEL & Pr. Romain PRIVAT

Energy analysis of a compression-separation system using membrane in transient state: the Membrane Piston

Présentée en vue d'une soutenance le 12 décembre 2025

Membres du jury :

Directeurs de thèse :	**Christophe CASTEL**	**Professeur à l'Université de Lorraine, LRGP, Nancy**
	Romain PRIVAT	**Professeur à l'Université de Lorraine, LRGP, Nancy**
Président de jury :	**Christophe COQUELET**	**Professeur des Universités, IMT Mines, Albi**
Rapporteurs :	**Xuan-Mi MEYER**	**Professeure à l'Université de Toulouse, LGC, Toulouse**
	Pierrette GUICHARDON	**Professeure des universités, Centrale, Marseille**
Examinateurs :	**Christophe COQUELET**	**Professeur des Universités, IMT Mines, Albi**
	Torsten BRINKMANN	**Head of Process Engineering Department, Institute of Membrane Research, Hereon, Geesthacht,**
Membres invités :	**Eric FAVRE**	**Professeur à l'Université de Lorraine, LRGP, Nancy**
	Yann LE MOULLEC	**Docteur Ingénieur, EDF, Saint Denis**

Contents

Introduction **1**

General context 1

Thesis objective and outline 2

1 State of the art **5**

Introduction to membrane separation history 5

1.1 Steady-state gas permeation 6

1.1.1 Principle of Gas Permeation 7

1.1.2 Transport through the membrane 9

1.1.3 Materials 12

1.1.4 Membrane Modules and Flow Configurations models 14

1.2 Transient membrane separation 17

1.2.1 Time-lag measurement 17

1.2.2 Paul's work: the Steady Cyclic Operation 19

1.2.3 Pressure(-Vacuum) Swing Permeation 20

1.2.4 Cyclic batch mode/Free diffusion 24

1.2.5 Pulsed retentate separation 28

1.2.6 Summary of transient processes 29

1.3 Efficiency and steady-state membrane gas separation 33

1.3.1 Minimum work of separation 33

1.3.2 Improving energy efficiency 34

1.4 A few interrogations 36
1.5 Nomenclature 37

2 Membrane Piston concept **39**
2.1 Concept 39
2.1.1 Steady-state membrane process 40
2.1.2 Membrane piston 42
2.1.3 How could we compare the performances of the steady-state compression and the Membrane Piston? 45
2.1.4 Synthesis 48
2.2 Membrane-piston modelling 48
2.2.1 Gas model for pressure estimation 49
2.2.2 Mass transfer 49
2.2.3 Volume variation of the two compartments within the system 52
2.2.4 Energy balances 52
2.2.5 Compression-Separation work 54
2.2.6 Summary: final expression of the model 55
2.3 Study of boundary limitations on flux 56
2.4 Study of temperature dependency of selectivity 61
2.5 Dimensionless numbers for the Membrane Piston 64
2.5.1 Model & numbers 64
2.5.2 Results 66
2.6 Conclusion 69
2.7 Nomenclature 70

3 Numerical investigation of Membrane-Piston behavior **73**
3.1 Case study on Air separation 73
3.2 Sensitivity analysis on case studies 76
3.2.1 Air separation for Nitrogen Enriched Air 78

3.2.2 Biogas separation 81
3.3 Global parametric analysis 84
3.3.1 Minimal work requirement for velocity, permeance & selectivity study 84
3.3.2 Comparison of molar work necessary for slow component enrichment to the steady-state 87
3.4 Prospective impact of the Membrane-Piston 89
3.4.1 Results 90
3.4.2 Discussion & Conclusion 96
3.5 Conclusion 96
3.6 Nomenclature 97

4 Experimental validation 99
4.1 Aim of the experimental set-up 99
4.2 Materials 100
4.2.1 Experimental set-up description 100
4.2.2 Membrane 102
4.2.3 Piston 103
4.2.4 Gas Chromatography 105
4.3 Methods 105
4.3.1 Pressure and temperature measurements 105
4.3.2 Composition measurements 106
4.3.3 Simulation framework for comparison 106
4.4 Results and discussion 108
4.4.1 Pressure evaluation 108
4.4.2 Composition evaluation 112
4.5 Conclusion 114
4.6 Nomenclature 115

5 Efficiency analysis **117**

5.1 Theoretical framework 117

5.1.1 Estimation of the thermodynamic properties of perfect-gas mixtures 118

5.1.2 Minimum work required for membrane separation 119

5.1.3 Entropy analysis of the Membrane Piston 126

5.1.4 Optimization framework 128

5.2 Results and discussion 129

5.2.1 Membrane Piston efficiency 129

5.2.2 Optimization of the system 131

5.3 Conclusion 137

5.4 Nomenclature 138

Conclusion & Perspectives **141**

Conclusions 141

Perspectives 142

Bibliography **145**

Appendix A Robeson plot for O_2/N_2, CO_2/N_2 and CO_2/CH_4 **157**

Appendix B Compressibility factor **161**

Appendix C Minimal molar work for multiple $(\alpha^*, \mathscr{P}_0)$ at different $x_{\text{in, slow component}}$ and $x_{\text{I, obj}}$ **163**

C.1 $x_{\text{in, slow component}} = 0.95$ 163

C.2 $x_{\text{in, slow component}} = 0.80$ 164

C.3 $x_{\text{in, slow component}} = 0.6$ 165

C.4 $x_{\text{in, slow component}} = 0.4$ 166

C.5 Summary 167

Appendix D N2 selective membranes literature review **169**

Appendix E Supplementary experimental data 171

List of Figures 173

List of Tables 181

Abstract 185

Résumé 187

Résumé étendu en français 189

Remerciements 199

Introduction

General context

Separation processes such as cryogenics, adsorption, or absorption have long been employed for industrial gas separations [1]. More recently, membrane operations have emerged as an attractive alternative and are now considered among the most effective technologies for several applications, including nitrogen production from air (NEA), natural gas or biogas upgrading, hydrogen purification, or volatile organic compound (VOC) recovery [2, 3]. Their appeal lies in their modularity, low footprint, absence of solvents, and potential energy savings compared to traditional methods like distillation [4, 5].

Energy efficiency is a central concern in separation processes. While membranes are often promoted as energy-efficient due to the absence of phase change, reported performances vary widely. Some studies underline the large energy requirements of gas membrane separations [6], while others highlight their potential for drastically reducing industrial energy consumption [7, 8]. Practically, two steady-state strategies are used to generate the driving force for mass transfer: feed compression or vacuum pumping [9]. Feed compression remains the most classical approach, minimizing membrane area but requiring large processed flowrates. Conversely, vacuum pumping reduces the treated quantity of gas but is limited by equipment efficiency and scalability at low pressure. In both cases, the energy consumption depends on the processed flowrate, the pressure ratio, and the efficiency of the compression or pumping devices.

Beyond steady-state operation, several studies have investigated transient membrane processes to overcome intrinsic limitations. The pioneering work of Paul (1971) introduced "Pulsed Membrane Operation" to enhance selectivity [10]. Since then, various unsteady-state concepts have been explored, such as pressure swing permeation [11–13], pulsed retentate operation [14], or cyclic strategies [15, 16]. These approaches demonstrated that transient operations could significantly improve selectivity, even with low-performance membranes. However, productivity and energy efficiency often remained limiting factors.

In today's context of increasing energy constraints and the need for decarbonization, energy efficiency must be addressed explicitly. This consideration has led to the exploration of a new concept: the Membrane Piston process. This system combines compression and separation in a single operation, taking advantage of the decreasing processed flowrate while benefiting from the high mechanical efficiency of piston compression.

Thesis objective and outline

The objective of this thesis is to develop an innovative concept that reduces energy requirements and improves overall process efficiency by integrating the operations of separation and compression into a single system, called the Membrane Piston. To achieve this goal, a comprehensive theoretical model of the process is established and subsequently analyzed through a parametric study and sensitivity analysis in order to identify the most influential operating parameters. In parallel, an experimental proof of concept is carried out to demonstrate the technical feasibility of the proposed approach, with the theoretical framework being validated against the experimental results to ensure both accuracy and predictive reliability. Furthermore, particular attention is devoted to the thermodynamic assessment of the system, with a specific focus on entropy generation, in order to evaluate its potential as an optimization tool and as a means of guiding process design towards improved efficiency.

This thesis is organized into five chapters, each addressing a specific aspect of the work described above. The research behind this concept has led to two published articles [17, 18] and two additional manuscripts currently in preparation, which together form the basis of three of these chapters. Experimental validations and a detailed state of the art have been incorporated, along with several complementary analyses that, while not yet published, enrich the overall understanding of the system. The structure of this thesis has been designed to facilitate readability and coherence, with relevant parts of the accompanying papers integrated where appropriate.

Chapter 1: *State of the Art.*
This introductory chapter presents the fundamental concepts and definitions related to membrane separation processes. It provides an overview of the historical development of transient membrane operations and their main modes of operation. The chapter concludes with a discussion on process energy efficiency, highlighting previous attempts at improvement and identifying the remaining gaps that motivate this research.

Chapter 2: *The Membrane Piston Concept* ([18]).
This chapter introduces the core concept of this thesis: the Membrane Piston. It offers a detailed description of the model, its physical foundations, and the associated dimensionless numbers that help characterize the system's behavior.

Chapter 3: *Numerical Investigation of Membrane-Piston Behavior* ([17, 18], in preparation).
This chapter presents a series of numerical studies exploring the dynamic behavior of the Membrane Piston. The system is first examined for an air separation case to illustrate its operating principles. A subsequent parametric study investigates the influence of various parameters, such as piston velocity and membrane properties, across different gas mixtures. The potential application of the Membrane Piston for carbon capture, using reverse-selectivity membranes, is then analyzed.

Chapter 4: *Experimental Validation.*
Here, the experimental validation of the Membrane Piston system is described. This includes the design and construction of a proof-of-concept setup, along with pressure and composition measurements for selected gas mixtures.

Chapter 5: *Efficiency Analysis* (In preparation).
The final chapter focuses on the thermodynamic efficiency of the process. It examines the minimum work required and explores the use of entropy as an objective function to optimize the piston's velocity profile, aiming to minimize energy losses.

Conclusion & Perspectives.
The concluding section summarizes the main findings and key insights of the thesis, emphasizing the significance of the Membrane Piston concept. It also outlines potential avenues for improvement and future research directions.

Chapter 1

State of the art

Introduction to membrane separation history

Membrane separations, once a scientific curiosity observed in early osmosis experiments, have evolved into indispensable industrial technologies, used in a wide range of applications from water desalination to gas purification, progressing through key milestones that connect fundamental physical principles to modern applications. [19]

The first observation of membrane phenomena dates back to 1748, when Jean-Antoine Nollet observed water permeating through a diaphragm [20]. Subsequent observations throughout the 19th and early 20th centuries employed available diaphragms to study osmosis and diffusion processes. In the mid-19th century, Adolf Fick formulated his law of diffusion [21], laying a theoretical foundation for understanding how substances move through semipermeable barriers. Practical work with synthetic membranes began in the early 1900s, particularly in applications of ultrafiltration and microfiltration for laboratory separations. [19]

Despite these early advances, membranes at that time were often too expensive, unselective, unreliable, and slow for practical large-scale use [19]. The industrial development of membranes began to advance significantly with the work of Loeb and Sourirajan in the early 1960s [22], who succeeded in producing defect-free asymmetric cellulose acetate membranes suitable for reverse osmosis desalination. This breakthrough laid the foundation for the modern membrane separation industry and spurred further innovations such as thin-film composite membranes, improved polymeric and inorganic materials, and module designs optimized for high flux and selectivity.

Today, membrane technologies are indispensable across multiple industrial sectors. Reverse osmosis and nanofiltration dominate water and wastewater treatment for desalination and

contaminant removal. Gas separation membranes are applied in natural gas sweetening, hydrogen recovery, and carbon dioxide capture. In the food and beverage industry, ultrafiltration and microfiltration are widely used for protein concentration, juice clarification, and dairy processing. The biotechnology and pharmaceutical industries rely on membranes for sterile filtration, dialysis, and bioreactor operations. Furthermore, membrane bioreactors and forward osmosis systems are increasingly used for sustainable resource recovery and zero-liquid-discharge strategies.

Since then, advances including thin-film composite membranes, integration into large-scale modules (e.g., spiral wound modules), improved materials (both polymeric and inorganic), and module design have steadily expanded the industrial applicability of membrane separations in water treatment, gas separation, biotechnology, and more [23].

More specifically, modern theories of gas separation were established in the 1950s, most notably by Barrer et al. [24, 25], through the development of the solution–diffusion model, which remains the standard framework for describing gas transport in polymer membranes today. At that time, however, available materials lacked the necessary performance for large-scale industrial use. A major breakthrough occurred in the 1980s, when Monsanto produced and commercialized a hydrogen separation module, initiating the development of numerous other membrane systems targeting different applications, such as nitrogen separation from air [26]. This latter application has since become a significant segment of the gas permeation market [9]. Figure 1.1, adapted from [19], provides an overview of the historical development of gas permeation.

Given that the central theme of this thesis is gas permeation, the subsequent state-of-the-art review has been deliberately restricted to research and technological progress directly related to gas permeation, excluding other membrane-based separation processes.

1.1 Steady-state gas permeation

This section provides a concise overview of membrane gas permeation. The detailed description of the processes, including the relevant equations, is presented in later chapters where appropriate for context (see section 2.1.1). Therefore, the purpose here is solely to introduce the fundamental definitions and modeling aspects, which will not be revisited in depth in the subsequent sections.

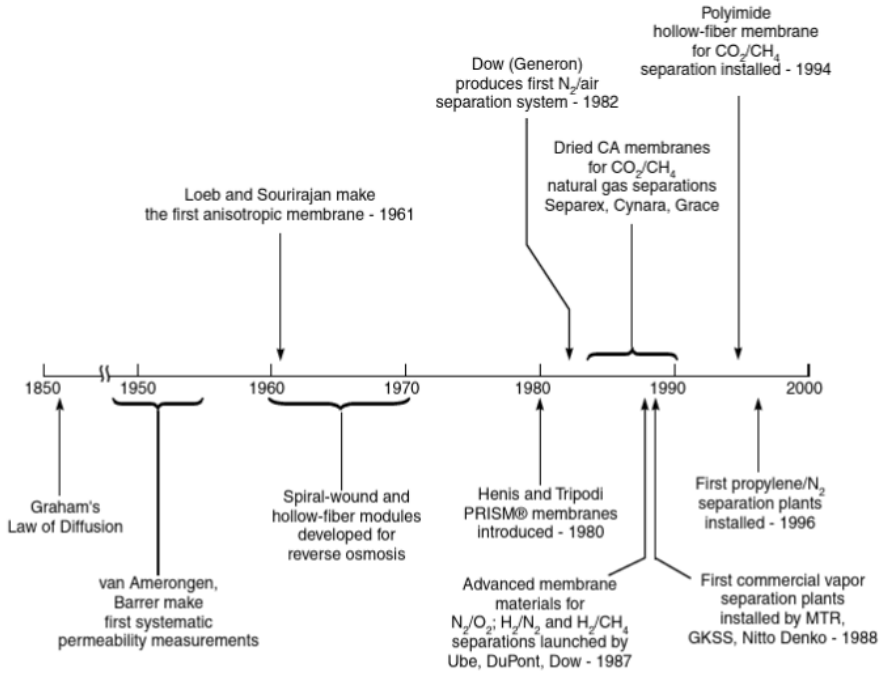


Figure 1.1 Gas permeation history [19]

1.1.1 Principle of Gas Permeation

Gas permeation is a separation process based on a membrane's ability to transport one gas component at a different transmembrane flux than another, leading to a variation in composition between two compartments. In this process, a membrane acts as a permselective barrier, allowing certain gas species to pass preferentially while retaining others [27].

As illustrated in Figure 1.2, a gas mixture, referred to as the *feed*, is introduced on one side of the membrane. The slowest permeating components through the membrane form the *retentate*, while those that successfully cross the membrane constitute the *permeate*.

A fundamental property characterizing membrane performance is the permeability of a gas component, defined as the volumetric flux per unit membrane area per unit driving force. In gas separation, permeability $\mathbb{P}$ is often reported in barrer, a non-SI unit defined such as $1\ \text{barrer} = 3.347 \times 10^{-16}\ \text{mol m m}^{-2}\,\text{s}^{-1}\,\text{Pa}^{-1}$ [9]. Permeance $\mathscr{P}$, defined as:

$$\mathscr{P}_i = \frac{\mathbb{P}_i}{\varepsilon_{mem}}, \tag{1.1}$$

provides a more practical measure for engineering applications, as it accounts for membrane thickness ε_{mem} in m and is often expressed in GPU, following :
$1\ \text{GPU} = 3.347 \times 10^{-10}\ \text{mol}\,\text{m}^{-2}\,\text{s}^{-1}\,\text{Pa}^{-1}$.

The selectivity $\alpha_{i/j}$ of a membrane quantifies its ability to preferentially separate two gases i and j:

$$\alpha_{i/j} = \frac{\mathscr{P}_i}{\mathscr{P}_j} \tag{1.2}$$

where i denotes the more permeable gas and j the less permeable gas. Typically, α is defined such as $\alpha > 1$, although some advanced materials exhibit reversed selectivity ($\alpha < 1$) [28]. Permeability is usually measured for pure gases, and the ideal selectivity α^* is calculated accordingly. In practical applications involving gas mixtures, the selectivity may differ due to interactions between the gas and membrane material. For instance, CO_2 often exhibits specific interactions that modify selectivity compared to the ideal case. Depending on the material, the selectivity value can also be influenced by operating parameters like temperature or pressure (see section 1.1.2).

The transmembrane flux of component i can be expressed analogously to other types of transport processes [19, 9]:

$$\Phi_i = \frac{\mathbb{P}_i}{\varepsilon_{mem}} \cdot A \cdot \Delta P_i = \mathscr{P}_i \cdot A \cdot \Delta P_i \tag{1.3}$$

where Φ_i is the molar flux of species i in $\text{mol}\,\text{s}^{-1}$, $\mathbb{P}_i$ is the permeability (barrer) and $\mathscr{P}_i$ the permeance (GPU), ε_{mem} is the membrane thickness (m), A is the membrane area (m^2), and ΔP_i is the partial pressure difference across the membrane (Pa).

In gas permeation, the driving force is the partial pressure difference of each component across the membrane. However, when moving from the molecular description of flux to the process-scale description of separation performance, it becomes useful to introduce additional dimensionless parameters, also detailed in Section 2.1.1. Among the most relevant are the stage cut:

$$0 < \theta = \frac{Q_{\text{perm}}}{Q_{\text{feed}}} < 1 \tag{1.4}$$

and the pressure ratio across the membrane:

$$0 < \Psi = \frac{P_{\text{down}}}{P_{\text{up}}} < 1 \tag{1.5}$$

These parameters are particularly valuable because they not only provide a compact way of characterizing the process but also facilitate scale-up and enable mathematical optimization of membrane systems.

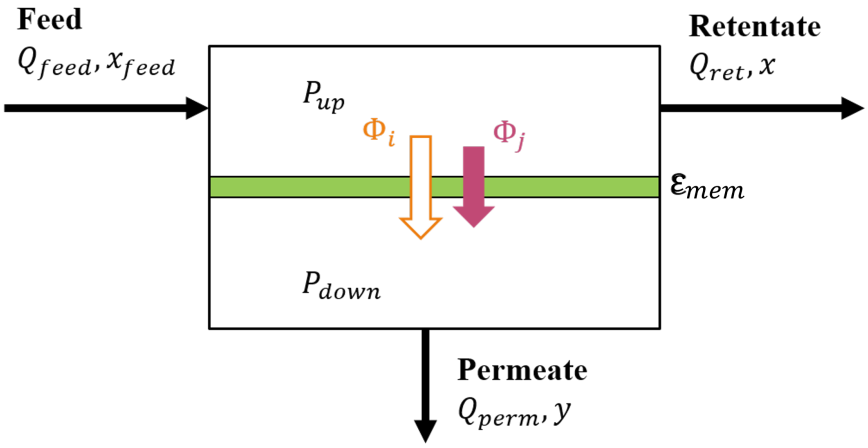


Figure 1.2 Schematic representation of a gas separation membrane module. The feed mixture is separated into permeate and retentate streams [18].

Ultimately, permeability (or permeance) and selectivity are critical parameters governing membrane performance. These properties are inherently tied to the membrane material, which partly explains the delayed industrial adoption of membrane technology. Historically, many materials did not offer sufficient performance, limiting early practical applications [19]. The effect of membrane material properties on separation performance will be discussed in detail in later sections.

Key industrial applications of gas permeation include the separation of hydrogen from nitrogen, argon from methane in ammonia plants, the production of nitrogen-enriched air (NEA) or oxygen-enriched air (OEA), and the removal of CO_2 from methane in natural gas processing [19, 9, 29, 30].

1.1.2 Transport through the membrane

The transport phenomenon through membranes is, of course, dependent on the material type, as membrane are generally either dense or porous. Currently, most of the industrial gas separation call for polymers, glassy or elastomers [30], that are considered to be dense material making the associated model of solution-diffusion prevalent [19].

In dense (i.e., non-porous) membranes, gas transport is commonly described using the **Solution-Diffusion model** [9, 19]. According to this model, gas molecules first dissolve into

the membrane material, then diffuse through the polymer matrix, and finally desorb on the opposite side of the membrane, as shown on the right hand-side of Figure 1.3. The separation comes from differences in the gas–polymer affinity, which manifest as distinct solubilities and diffusivities for each gas species.

Several key assumptions are made:

- The gas on either side of the membrane is in thermodynamic equilibrium with the membrane at the interface.
- The concentration gradient within the membrane is continuous from one side to the other, implying that absorption and desorption at the interfaces occur much faster than diffusion through the membrane bulk.
- The pressure within the membrane is assumed to be uniform and equal to the higher of the two external pressures.
- No concentration polarisation, the transfer limitations are located in the membrane.

This model provides a framework for understanding how dense membranes achieve selective gas transport and is widely used in modeling polymer-based membrane systems.

In the Solution-Diffusion framework, the transport of a gas component i through a dense membrane is described by:

$$\Phi_i = \frac{D_i \cdot \mathscr{S}_i}{\varepsilon_{mem}} \cdot A \cdot \left(P_{up,i} - P_{down,i}\right) \tag{1.6}$$

where D_i is diffusion coefficient of component i though the membrane ($\mathrm{m^2\,s^{-1}}$), $\mathscr{S}_i$ is its solubility (analogous to Henry's law constant, in $\mathrm{cm^3(STP)/(cm^3{\cdot}cmHg)}$, i.e $\mathrm{mol\,m^{-3}\,Pa^{-1}}$), and P_i^{up} and P_i^{down} are the partial pressures on the upstream and downstream sides, respectively.

The transport equation can be conveniently rewritten to correspond to the previous definition including permeability, $\mathbb{P}_i$, as the product of solubility and diffusivity in this model:

$$\Phi_i = \frac{\mathbb{P}_i}{\varepsilon_{mem}} \cdot A \cdot \left(P_{up,i} - P_{down,i}\right), \quad \text{with} \quad \mathbb{P}_i = D_i \cdot \mathscr{S}_i \tag{1.7}$$

The expression $\mathbb{P}_i = D_i \cdot \mathscr{S}_i$ holds true exclusively for dense membranes, where the solubility of permeating species obeys Henry's law and diffusion is governed by Fick's law. Freeman [31] developed a fundamental theoretical basis to extend Robeson's trade-off representation,

interpreting the permeability behavior of polymer membranes through the principles of the solution–diffusion model [31].

Finally, the ideal selectivity of the membrane for component i and component j can then be expressed as:

$$\alpha^*_{i/j} = \frac{\mathscr{P}_i}{\mathscr{P}_j} = \frac{D_i}{D_j} \cdot \frac{S_i}{S_j} \tag{1.8}$$

In polymeric membranes, various phenomena can influence the effective permeability. For instance, plasticization may occur at high partial pressures, altering the diffusion coefficient and thus the overall transport. Additionally, both solubility and diffusivity are temperature-dependent, following an Arrhenius type law, which must be accounted for when modeling gas transport in polymer membranes.

Overall, the Solution-Diffusion model provides a robust framework for understanding these effects and predicting separation performance under different operating conditions.

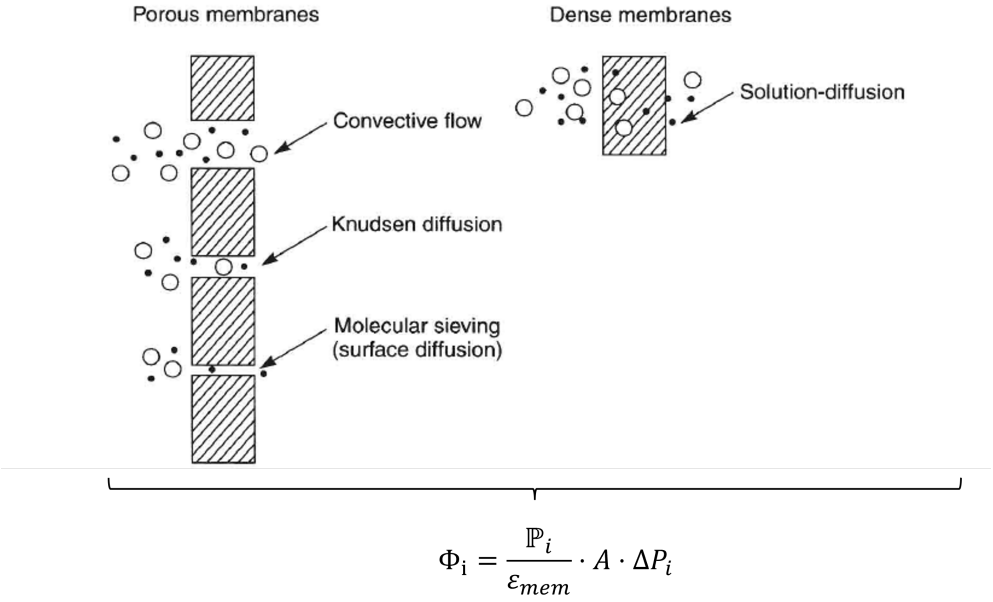


Figure 1.3 Tranpost mechanism in membrane. Left: Porous membrane; right: dense membrane [19].

In addition, it should be mentioned that porous membrane require different mechanism. As shown in Figure 1.3 on the left, transport behavior depends on the pore size relative to the gas molecules. Large pores allow mostly convective flow, with minimal separation. For smaller pores (less than 0.1 µm), Knudsen diffusion dominates, while molecular sieving becomes significant in pores around 5–20 Å. In these regimes, molecules interact more with the pore

walls than with each other, and separation arises from differences in molecular velocities or sizes. Such mechanisms are particularly relevant in inorganic materials, although industrial use remains limited [32].

Regardless of whether transport is described by the solution–diffusion model or by a pore-flow mechanism, it is often convenient at the process level to work with the permeance. Permeance incorporates both the intrinsic transport properties of the material and the geometric factor of membrane thickness, thereby providing a direct measure of the rate at which a species permeates under a given driving force. From a process perspective, the precise microscopic mechanism is less critical than obtaining an accurate value of permeance, since it ultimately governs the flux calculations and thus enables system design, scale-up, and optimization.

1.1.3 Materials

Synthetic membranes encompass a wide range of structures and materials tailored for specific separation applications. They can be classified as homogeneous or heterogeneous, and as isotropic or anisotropic, depending on their structural uniformity and manufacturing method. A schematic summary of these structural categories is provided in Figure 1.4.

A variety of materials are employed for gas permeation. Polymeric membranes dominate industrial use thanks to their low cost, mechanical flexibility, and ease of fabrication. However, newer and more complex options, such as zeolites, mixed-matrix membranes, and other hybrid structures, are emerging as commercially viable alternatives offering potentially superior performance.

Focusing on polymers, they are extensively used for separations such as air separation, H_2 recovery, condensed in Table 1.1. Their performance is constrained by the well-established permeability–selectivity trade-off, first quantified by Robeson in 1991 [33] and updated in 2008 [34]. Many materials development thus focus on surpassing this upper-bound [35, 30, 36]. Thin selective layers—about 1 μm thick and sometimes as thin as 50 nm, are necessary to achieve high fluxes while maintaining strength [9].

Inorganic membranes, particularly zeolites, are promising for gas separation because they can offer higher permeability and selectivity than polymers [37, 38]. Zeolites also exploit adsorption effects to enhance selectivity, making the permeability of some gases (e.g., CO_2) pressure-dependent.

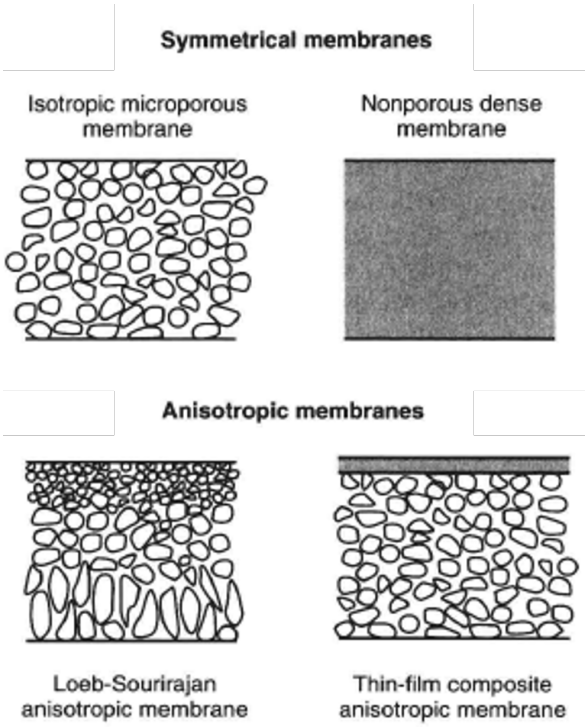


Figure 1.4 Classification of synthetic membranes according to structure and homogeneity [19].

Material	Target Separation	Reference
Cellulose acetate	CO_2/CH_4	[19, 9]
Silicone rubber	Organic vapor/air	[19, 9]
Polysulfone	H_2 recovery, air separation, CO_2 removal	[9]
Polyimides	H_2 recovery, air separation, CO_2 removal	[9]
Polyaramide	H_2 recovery, air separation, CO_2 removal	[9]
Polyphenylenoxide	Air separation	[9]

Table 1.1 Representative polymeric membranes and their typical gas separation applications.

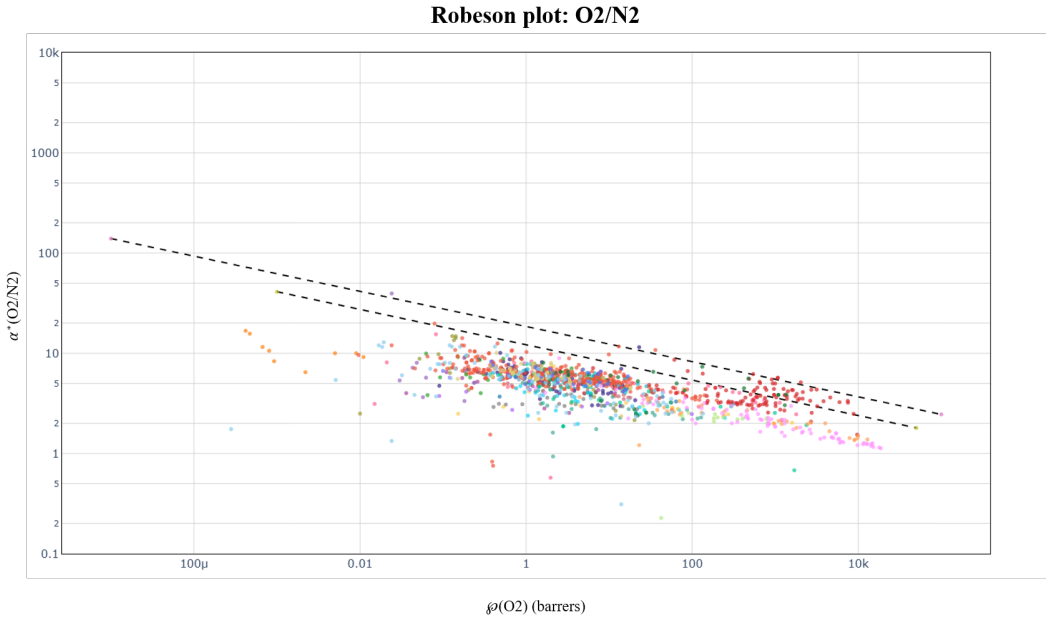


Figure 1.5 Robeson plots showing the upper-bound trade-off between permeability and selectivity for O_2/N_2. Data from [39]

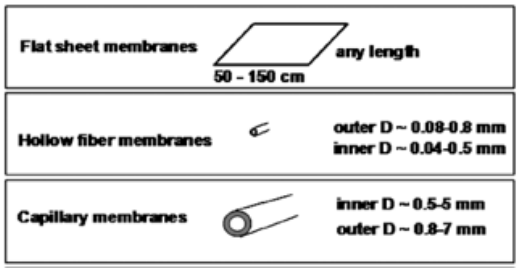
The relationship between permeability and selectivity is illustrated in Figure 1.5 for the O_2/N_2 pair and includes new materials development. Appendix A presents the same graph for CO_2/N_2 and CO_2/CH_4.

1.1.4 Membrane Modules and Flow Configurations models

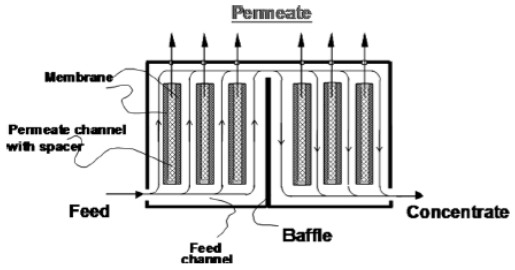
The performance of steady-state membrane separations depends strongly on the membrane surface area that can be packed into a module. Flat-sheet configurations, while simple, provide limited packing density [40]. To improve performance and scalability, several module types have been developed (Figure 1.6).

Industrial modules must withstand mechanical, thermal, and chemical stresses over long operating times. Selection criteria therefore include mechanical strength, thermal and chemical stability, uniform flow distribution, low pressure drop, ease of cleaning, and, importantly, high packing density (ratio of membrane area to module volume) [27]. Modules can also be arranged in series or multistage configurations to enhance overall separation efficiency (Figure 1.7).

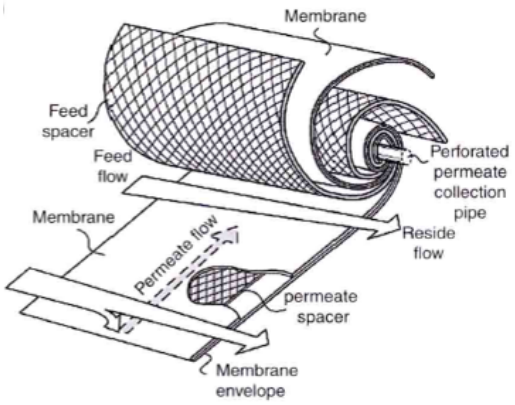
The main module types are [27]:



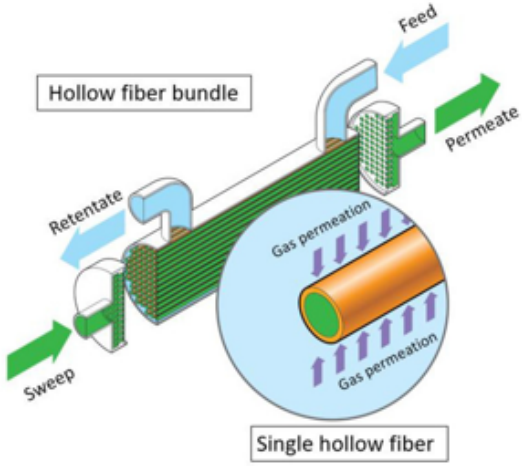
(a) Possible membrane format. Adapted from [19].



(b) Flat sheet module [27].



(c) Spiral wound module [19].



(d) Hollow-fibers module [41].

Figure 1.6 Examples of membrane module types.

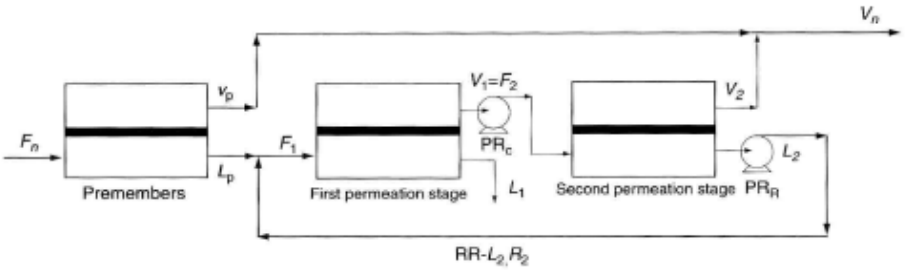


Figure 1.7 Multistage membrane separation process for carbon dioxide removal from natural gas [9]

- **Plate-and-frame (flat-sheet) modules**: The earliest design, with low packing density (30–500 $m^2\,m^{-3}$) and baffles to prevent bypassing. These are less used for gas separations, with a known use for Carbon Capture using the MTR process [42] but remain relevant for some liquid applications (e.g., OEA).
- **Spiral-wound modules**: Constructed by rolling flat membranes around a central tube with spacers. They tolerate high pressures (up to 150 bar), achieve moderate packing densities (200–1000 $m^2\,m^{-3}$), and account for about 20% of commercial gas separation modules .
- **Hollow-fiber modules**: Containing thousands of fine hollowed fibers, these modules offer very high packing densities (500–10 000 $m^2\,m^{-3}$), can tolerate pressures up to 150 bar, and can operate in either inside-out or outside-in configurations. They are the dominant choice for large-scale gas separations.

Within a chosen module geometry, the modelling of the flow pattern strongly influences separation performance (Figure 1.8). The main possibilities are:

- **Perfect mixing:** Both sides of the membrane are well-mixed, with uniform composition throughout.
- **Co-current:** Feed and permeate flow in the same direction along the membrane surface.
- **Counter-current:** Feed and permeate flow in opposite directions, typically yielding better separation efficiency.
- **Cross plug-flow:** One stream exhibits plug-flow behavior while the other is well-mixed or flows perpendicularly across it.

Among these configurations, the cross plug-flow arrangement is generally considered the most appropriate for modeling membrane systems. Consequently, it is adopted for the comparisons presented in this work, and its governing equations will be introduced as needed in the following sections 2.1.1.

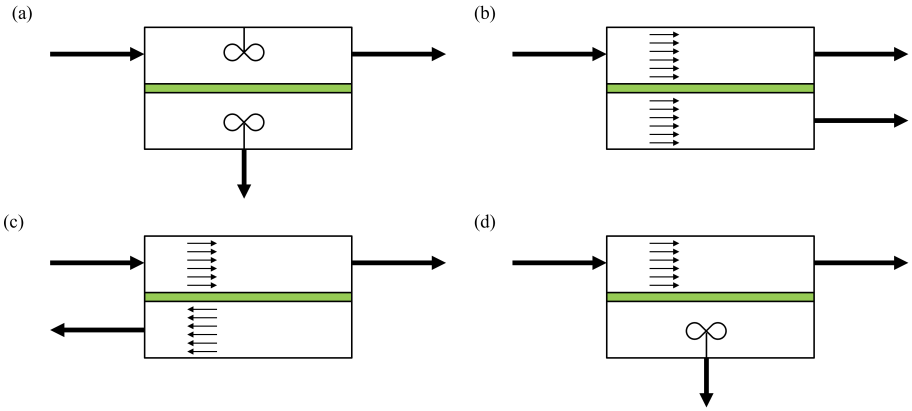


Figure 1.8 Schematic representation of common flow configurations in membrane modules adapted from [9].

1.2 Transient membrane separation

Usual membrane modules, presented up until now in this manuscript, adopt the steady-state mode. However, as it is done in many separation processes, such as adsorption with Pressure Swing Adsorption, introducing a time dependant element could be of interest. Thus, a few possibilities have been studied since the 70's and the emerging processes as well as their performances are detailed in this section. They started from the time-lag method, explained here as well, and used to measure membrane properties. A comprehensive review was conducted on transient membrane gas process in 2011 by Wang [16]. Since most of these processes differs greatly from this thesis objective, other than the fundamental work of Paul as well as the time-lag experiment description, the other works will not be repeated in detail here and the focus will be on the newer emerging processes.

1.2.1 Time-lag measurement

To obtain the permeability values used for the modeling, reliable experimental methods are essential. One widely used approach is the time-lag method, first introduced in 1920 by Daynes [43]. This classic technique determines both the diffusion coefficient and permeability

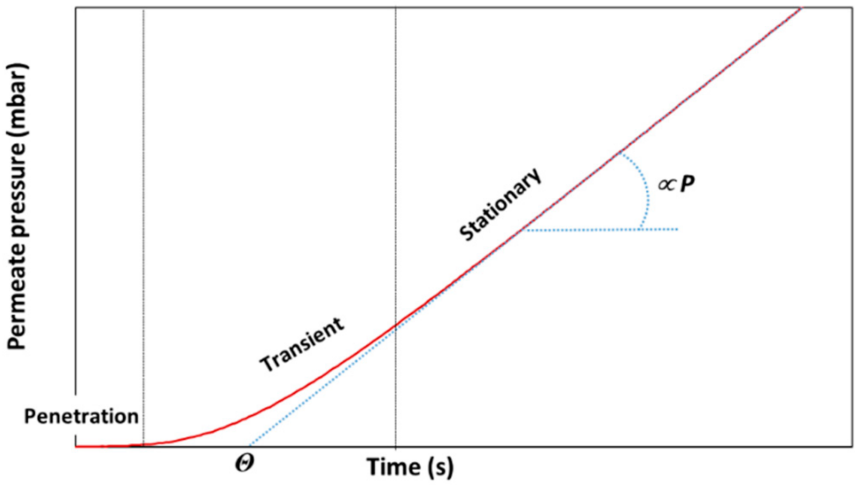


Figure 1.9 Time lag curve, operating under conditions where the permeate pressure is negligible relative to the feed pressure from [44]

of gases in dense membranes. In this method, a membrane separates two chambers: the upstream side is exposed to the test gas at a constant pressure, while the downstream side is initially under vacuum or swept by an inert carrier gas.

When the upstream gas contacts the membrane, permeation does not begin immediately. Instead, the gas molecules must first diffuse into and across the membrane. As a result, the downstream flux exhibits a characteristic delay, known as the time lag (Θ), before reaching steady-state permeation.

The downstream pressure (or detected flux) as a function of time typically follows an S-shaped curve. Extrapolating the linear portion of the steady-state region back to the time axis gives Θ. According to Fick's second law, for a homogeneous membrane of thickness ε_{mem}, the diffusion coefficient D is related to the time lag by:

$$\Theta = \frac{\varepsilon_{mem}^2}{6D}. \tag{1.9}$$

Once D is obtained, the permeability $\mathbb{P}$ can be determined using the steady-state flux and the known pressure difference. The solubility coefficient $\mathscr{S}$ is then calculated from $\mathbb{P} = D \cdot \mathscr{S}$. Time-lag measurements are widely used because they provide both kinetic (diffusion) and thermodynamic (solubility) information about gas–membrane interactions, making them essential for characterizing materials in gas separation applications.

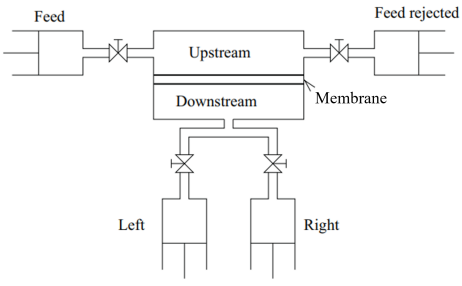
1.2.2 Paul's work: the Steady Cyclic Operation

Published in 1971 by D. R. Paul [10], this paper challenges the notion that membrane separation performance must be strictly limited by the intrinsic selectivity of a single material. Drawing on the definition of permeability from the Solution–Diffusion model (Section 1.1.2), the selectivity for a gas pair is expressed as:

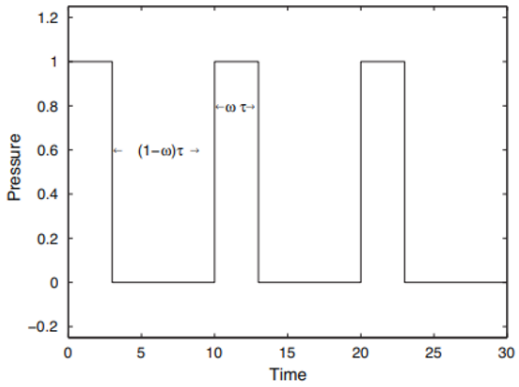
$$\alpha_{1/2} = \frac{D_1 \cdot \mathscr{S}_1}{D_2 \cdot \mathscr{S}_2} = \frac{\mathbb{P}_1}{\mathbb{P}_2} \tag{1.8}$$

Paul observed that, in many cases, the ratios $\frac{D_1}{D_2}$ and $\frac{S_1}{S_2}$ do not vary consistently for a given gas pair. In practice, an improvement in one ratio may be offset by a decrease in the other, a behavior strongly influenced by polymer structure.

To address this limitation, Paul proposed a novel Pulsed Membrane Operation, inspired by the time-lag experiment (Section 1.2.1). The concept involves pulsing the upstream pressure in square waves, as shown in Figure 1.10, to recover permeate enriched in the faster-diffusing component before the slower gas has sufficient time to permeate . The setup consists of two upstream tanks (Feed and Rejected Feed) and two downstream tanks (Left and Right), shown on Figure 1.10a.



(a) Schematic of Paul's apparatus.



(b) Pressure pulse applied to the upstream side.

Figure 1.10 Paul's pulsed membrane process and pressure cycle. τ is the cycle duration and w the fraction of the period at high pressure. [10]

The upstream pressure pulses are generated by synchronously opening and closing the Feed Reservoir and Rejected Feed, along with the Left and Right downstream tanks. By carefully selecting the cycle duration τ and the high-pressure fraction (w), the Left tank becomes enriched in the faster-diffusing component. Paul's analysis assumed:

- Constant upstream composition (due to a large upstream-to-downstream volume ratio),
- Fixed diffusivity (D_i) and permeability ($\mathbb{P}_i$) equal to their steady-state values,
- No mixing of downstream cuts when switching valves.

For a given membrane and gas pair, D_1 and D_2 are fixed. By adjusting the cycle period and pressure fraction, the selectivity can be greatly enhanced. Paul demonstrated that, for a He–CH_4 mixture and a short high-pressure fraction ($w = 0.1$), the effective selectivity α_H could be improved by nearly 79 times compared to steady-state selectivity α_{ss} if $D_1/D_2 = \infty$.

This approach showed significant selectivity gains for small w values and suggests potential for extension to multi-component mixtures or additional downstream cuts. However, Paul noted, and later Wang's reviews [16] confirmed, that the method's lower productivity and operational complexity compared to conventional steady-state processes likely explain its limited enthusiasm in membrane separation research and industry.

Corriou et al. noted that the chosen parameters, particularly the valve opening and closing times, were relatively simple [45]. Their work focused on optimizing these timings to enhance both selectivity and productivity. A thick membrane of 10 µm was required to ensure realistic minimum valve actuation times. By comparing steady-state and transient operations, the study examined the effects of synchronous, asynchronous, and symmetric modes, showing that synchronous operation defines the upper performance limit. Using a genetic algorithm and nonlinear programming, they observed a wide range of selectivity values (from 16 to 6,300), with productivity exhibiting an inverse trend. Despite optimization efforts, the fundamental trade-off remained and higher selectivity could only be achieved at the cost of lower productivity.

1.2.3 Pressure(-Vacuum) Swing Permeation

In 2000, Feng et al. presented a process largely inspired by the Pressure Swing Adsorption (PSA), that is called Pressure Swing Permeation (PSP) [11]. It offers the advantage of being continuous, using two hollow-fibers modules with the same membrane type at different pressure levels. Later, he proposed a new process, named Pressure-Vacuum Swing Permeation [12, 13] that necessitate only one module and one pump that switches between compression of the feed and vacuum pumping of the permeate. Both of these processes will be briefly described here.

Pressure Swing Permeation This process operates similarly to a PSA system, employing two or more membrane modules that function in a synchronized yet alternating manner

	Two Module Pressure Swing Permeation [11]		**Pressure-Vacuum Swing Permeation [12, 13]**
	Module A	*Module B*	
Step 1	Admission of feed gas and permeation	Reception of permeate from module A	Feed pressurization
Step 2	Withdrawal of residue from module	Pressurization with feed gas and product release	Feed admission / permeation
Step 3	Removal of residue remaining in gas line	Gas feeding stopped	Pump switching to vacuum mode
Step 4	Reception of permeate from module B	Admission of feed gas and permeation	Permeation and permeate evacuation
Step 5	Pressurization with feed gas and product release	Withdrawal of residue from module	Residue venting
Step 6	Gas feeding stopped	Removal of residue remaining in gas line	–

Table 1.2 Summary of the steps for Feng's processes.

presented in Figure 1.11a. The full steps are given by the first part of Table 1.2, and includes a permeation stage, permeate reception, permeate pressurization using the feed gas and product recovery. One of the major advantages of this process is the recovery of the permeate at high pressure. The experimental setup at bench scale was exploited and confirmed that the permeate could be recovered at a pressure close to the feed pressure, applied to a case of H_2/N_2 separation for the sake of demonstration. Operating conditions and results are summarized in Table 1.3. The PSP process demonstrated a clear improvement over conventional steady-state permeation, producing a hydrogen-enriched permeate at nearly feed pressure levels. Notably, the partial pressure of hydrogen in the permeate was about 32% higher than in the feed, a performance unattainable without recompression in conventional systems. This confirms that PSP can overcome the limitations of steady-state permeation in terms of both concentration and flow rate, and similar to Paul's process, its performance does not follow the typical trade-off between selectivity and permeance.

Pressure-Vacuum Swing Permeation Contrary to the Pressure Swing Permeation, this process only requires one membrane module but will nonetheless operates in a cycle, with

Table 1.3 Performance data for the Pressure Swing Permeation (PSP) process.

Parameter	Value	Notes
Feed gas	49.4 vol% H_2 in N_2	Demonstration case
Feed pressure	1590 kPa	–
Cycle time	13 s/module	Two modules operated alternately
Permeate composition	78.8 vol% H_2 at 1320 kPa	–
Recovery	29%	–
Partial pressure increase	+32% vs. feed	Cannot be achieved in steady-state
Steady-state comparison	54.9% H_2 (58.3% at 0 stage cut)	Lower concentration and flow rate
Key feature	High-pressure permeate recovery	Trade-off similar to Paul's process

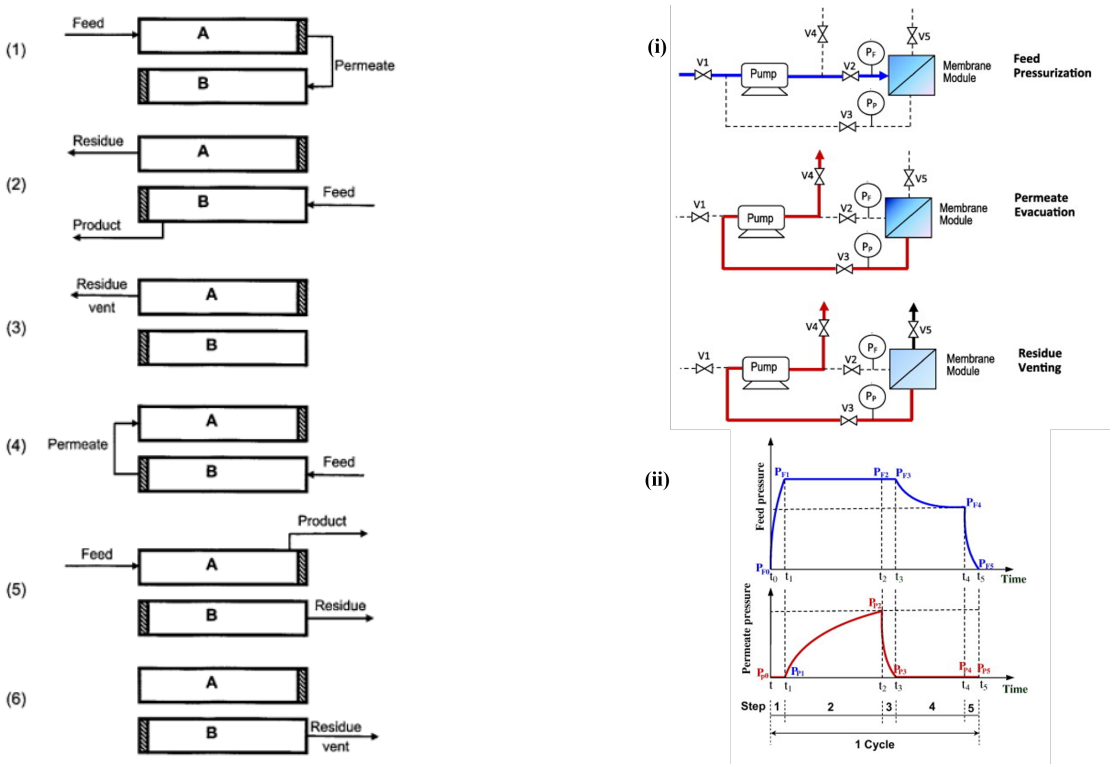
similar steps described in Table 1.2 and is shown on Figure 1.11b. Developed years later and based on the PSP process described previously, it uses a unique pump that is able to pressurize the feed if needed, and suction the permeate. A parametric study was conducted to evaluate the performances, the design impact and operating parameters:

- feed pressure
- A/V ratio
- permeate evacuation pressure
- feed to permeate volume ratio

The use of The parametric study on OEA production (Table 1.4) confirmed that increasing the feed-to-permeate volume ratio improves O_2 recovery at the expense of productivity, consistent with classical membrane behavior. Compared to steady-state operation, the unsteady PVSP process achieves higher recovery with comparable productivity, highlighting the advantage of using a single pump.

Table 1.4 Performance data for the Pressure–Vacuum Swing Permeation (PVSP) process – Oxygen-Enriched Air (OEA) case.

Parameter	Unsteady-State (PVSP)	Steady-State Comparison
Target product	40–45% O_2	same
Selectivity	6	same
Cycle time	138.3 s	–
Recovery	67.4–92.05% (up to +25%)	73.4%
Productivity	1.66–1.88 $molm^{-2}h^{-1}$	1.84 $molm^{-2}h^{-1}$
Energy consumption	2.79 $MJ\,cycle^{-1}$	4.88 MJh^{-1} (compressor)
Observations	Single pump system; higher recovery but lower productivity	Classical membrane operation



(a) Two Module Pressure Swing Permeation process [11]

(b) Pressure-Vacuum Swing Permeation [12, 13] (i) Process flow (ii) Pressure profiles

Figure 1.11 Feng's process schema and pressure cycle. τ is the cycle duration, w the fraction of period.

For a CO_2/N_2 separation from flue gas, aiming at 60% of CO_2 using a membrane with a selectivity of 20, with the biggest volumr ratio possible, this system reaches 85.7% recovery, with 13.51 MJ cycle^{-1} for 86 s cycle while the steady state requires 30.2 MJ h^{-1} with 25% recovery for a feed compression and 0.53 MJ h^{-1} for a 86.2% recovery using a vacuum pump. However the vacuum pump has a flow rate of product divided by 7 compared to the feed compression option.

Different case studies are realised, on air separation for oxygen enrichment in [12, 13], CO_2 separation from biogas and methane enrichment in [13]. The process allows for an enhanced separation, due to an increase transmembrane driving force. The feed to permeate volume ratio is an important parameters and it is essential to optimize the process to appropriately raise the performances regarding purity, recovery and, productivity.

The Pressure Swing Permeation (PSP) process laid the foundation for cyclic membrane separations by demonstrating enhanced permeate recovery and selectivity beyond steady-state limits. Its later evolution into the Pressure-Vacuum Swing Permeation (PVSP) simplified

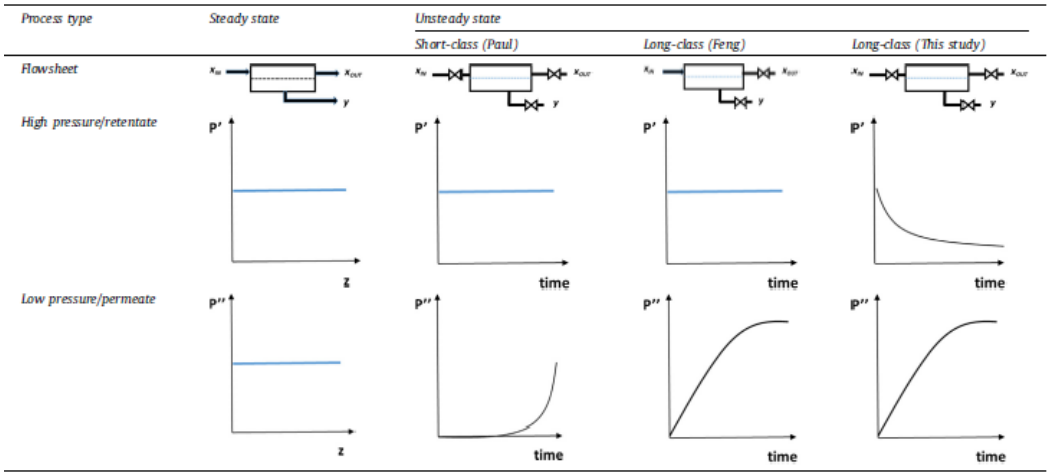
the setup to a single module and pump while further improving recoveries and maintaining comparable productivity. Across hydrogen, oxygen, and CO_2 separations, optimizing cycle parameters, especially the feed-to-permeate volume ratio, proved critical for maximizing purity, and recovery, highlighting the potential of unsteady-state operation to expand the flexibility and effectiveness of membrane processes. Although the energy requirements of these processes have been noted and compared to steady-state operation, they were not included in the optimization studies and are not the primary focus of this work.

1.2.4 Cyclic batch mode/Free diffusion

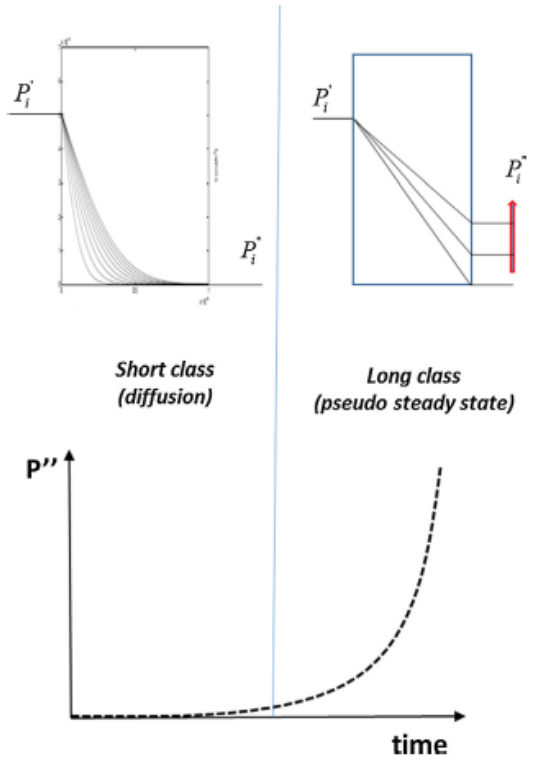
Wang presents a previously unexplored cyclic batch mode with no feed compensation as a new membrane process [15, 46]. This approach involves free permeation, where the compartment is completely closed, allowing both pressure and composition to evolve over time within a single module. The cycle consists of three main steps: free permeation, recovery of permeate and retentate separately, and regeneration of the module using a vacuum pump.

The study first identifies two main transient operation regimes for unsteady membrane separation. In the short-class period, like Paul's process, mass transfer is dominated by permeate diffusion and diffusivity selectivity, and generally yields very high purity for the faster-permeating component but negligible overall recovery. Upstream and downstream system conditions remain essentially constant, and unsteady behavior is confined primarily to the membrane. This mode is mainly useful for analytical purposes or when only trace amounts of high-purity product are required, though it demands very high valve frequencies and time-consuming regeneration.

In contrast, the long-class period begins when the partial pressure increases approximately linearly over time, with compound permeability and membrane selectivity becoming the key transport parameter. Here, membrane composition profiles remain nearly linear, while upstream and downstream compositions change significantly due to mass transfer, resulting in unsteady effects that are observed mainly in the gas compartments.



(a) Long and short class processes as defined by Wang.



(b) Differences between long and short class processes.

Figure 1.12 Long and short class processes for transient membrane separation [46].

The study compares three modes: the short-class (Paul-type [10]), which prioritizes purity over recovery; the long-class (Feng-type, using Pressure Swing Permeation [11]); and the novel long-class approach introduced in this work. These modes are analyzed using a composition path selectivity chart for four different cases. Inspired by distillation graphs, the composition paths are illustrated in Figure 1.13. For comparison, the steady-state case is modelled as a cross plug-flow system according to [47].

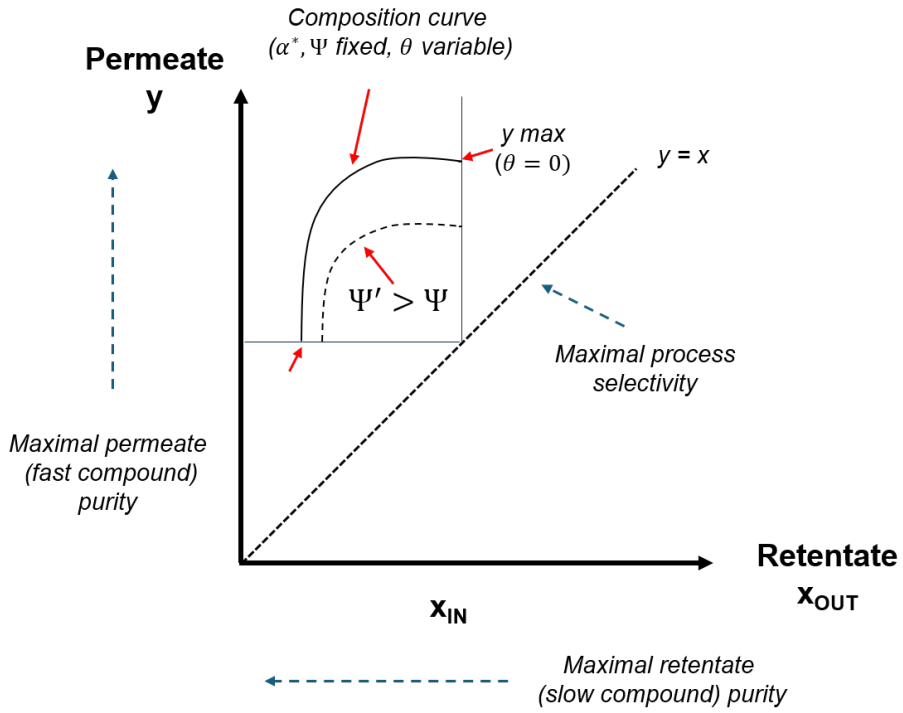


Figure 1.13 Composition path principle.

The cyclic batch concept was experimentally validated using a custom laboratory setup, confirming that the key assumptions hold: isothermal operation, constant permeability, perfectly mixed compartments, and negligible mass transfer resistance. The process was tested on several separations, including air separation, He/Kr with a high selectivity ($\alpha^* = 18$), and two H_2/CO_2 separations using polyimide or PEBAX membranes, with α^* values of 2.92 and 0.08, respectively.

Figure 1.14 presents the recovery and purity results for a CO_2 /O_2, compared to steady state (blue line). Using different options of volume ratio and sidestream, it is possible to improve at the same time the purity and the recovery ratio, corresponding to the area on the upper right side.

Results show that transient operation can enhance selectivity. While Paul's short-class process improves purity at the cost of productivity, the novel cyclic batch process also enhances selectivity. For the fast-permeating component, the purity/recovery trade-off was analysed across all four separations. It was found that, with an appropriate upstream-to-downstream volume ratio, unsteady-state operation can achieve purity and recovery levels unattainable under steady-state conditions.

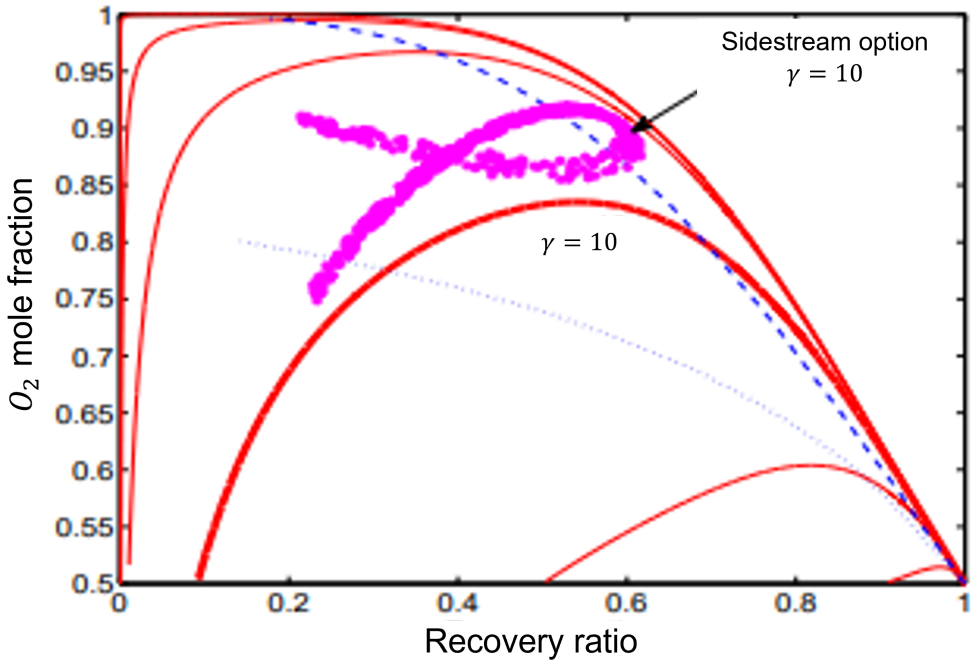


Figure 1.14 From [15]: O_2 recovery ratio of the O_2-enriched flux as a function of O_2 mole fraction in the same flux. Continued red lines: novel process using basic option with different volume ratios γ (0.1, 1, 10, 100, 1,000 and 10,000 from bottom to top, respectively). Bold continued red line: $\gamma = 10$. Dashed blue line: conventional operations using cross flow modules. Dotted blue line: conventional operations using perfectly stirred modules. Green stars: novel process using sidestream option with $\gamma = 10$ and the downstream flux is recycled.

The authors emphasized that the upstream-to-downstream pressure ratio is a critical factor in unsteady-state separation. However, they also noted that practical implementation is challenging: the vacuum must be nearly perfect to maintain performance, and precise valve timing is essential to avoid recovering any unwanted component.

1.2.5 Pulsed retentate separation

Trubyanov et al. proposed the Pulsed Retentate technique, a membrane separation process inspired by periodic withdrawal in batch distillation, specifically designed to remove fast-permeating impurities and recover a purified slow-permeating component [14, 48, 49].

The process operates in two steps, presented on Figure 1.15:

1. **Closed mode (enrichment phase):** the retentate valve is closed while feed is continuously supplied and permeate removed. During this step, a near-stationary concentration profile develops along the membrane module, resulting in maximum enrichment of the slow-permeant near the retentate outlet.
2. **Short-time withdrawal:** the retentate valve is briefly opened, and a small enriched fraction is withdrawn. This disturbs the established profile, which is then reformed in the next cycle.

This cyclic operation can be integrated with PSA processes and offers several advantages compared to other unsteady-state membrane methods:

- **No productivity loss (or even enhancement):** efficiency is improved without reducing throughput.
- **Universality:** relies on permselectivity (as in steady-state processes) rather than time-lag effects, enabling broad applicability.
- **Independence from membrane thickness:** suitable for industrial ultrathin membranes.
- **Constant transmembrane pressure:** avoids additional compression costs.
- **Simplicity:** implementation requires only one automatic valve at the retentate outlet.
- **Reduced contamination risk:** minimizes product mixing during flow switching.
- **Longer cycle times:** favorable for process stability and control.

Experimental validation was carried out using a radial counter-current membrane module (active volume ≈ 50 cm^3), equipped with SILAR^{TM} and later LESTOSIL^{TM} membranes. Binary mixtures of fast- and slow-permeating gases (e.g., N_2O/N_2, CO_2/CH_4, CH_4/N_2) were tested. Results confirmed an enhanced separation efficiency under unsteady operation,

particularly in the low-productivity regime ($L_{\text{ret}}/L_{\text{feed}} < 0.3$), with stronger improvements observed in mixtures of high effective selectivity (e.g., N_2O/N_2).

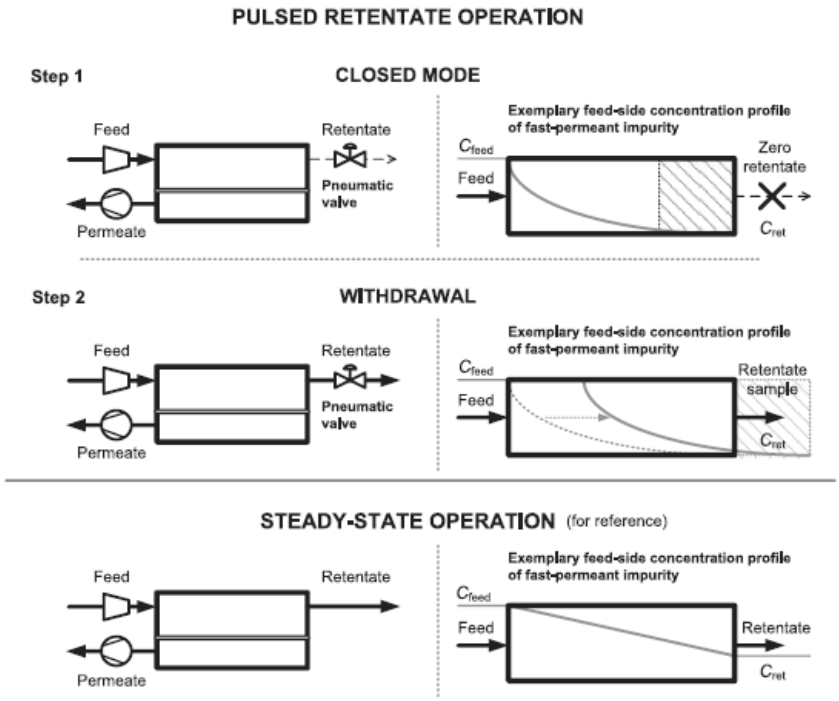


Figure 1.15 Pulsed Retentate Operation steps, compared to steady-state [14]

Mathematical modeling further elucidated the closed-mode dynamics, concentration profile establishment, and axial mixing effects [48, 49]. Optimization algorithms were developed to define optimal cycle parameters (e.g., withdrawal time, piston velocity, cycle duration), introducing a combined efficiency criterion balancing purity and productivity [50]. Extensions also considered multi-module configurations for further performance gains.

Overall, the pulsed retentate method represents a process intensification strategy, improving separation performance while maintaining acceptable productivity, by deliberately exploiting deviations from steady-state operation.

1.2.6 Summary of transient processes

Table 1.5 Summary of transient and cyclic membrane separation processes with operational descriptions

Author(s)	Process name	Process description (operation principle)	Main results / contributions
Daynes	Time-lag method	Two closed compartments separated by a flat dense membrane. A sudden pressure step is applied on the upstream side while the downstream side is initially evacuated and isolated. The transient pressure rise in the downstream compartment is monitored.	Introduced the time-lag concept to determine gas diffusivity and permeability; purely analytical method with no separation objective; reference framework for later transient membrane processes.
Paul	Steady Cyclic Operation	Two compartments separated by a flat membrane. Upstream side maintained at constant pressure and composition; downstream side initially evacuated and closed. Separation is achieved during the very early transient before steady state, exploiting differences in diffusion time lag.	Produces extremely high purity of the fast-permeating component due to diffusivity selectivity, but with negligible recovery and productivity; suitable mainly for trace separation; requires very short cycles and frequent regeneration.
Feng et al.	Pressure Swing Permeation (PSP)	Two membrane modules, each with feed and permeate compartments, operated alternately in a cyclic manner. Feed pressure is periodically increased and decreased, while permeate from one module is received and pressurized in the other.	Demonstrated high-pressure permeate recovery close to feed pressure; hydrogen partial pressure increased by about 32% compared to feed; exceeded steady-state limits in purity without recompression.

Continued on next page

Table 1.5 – continued from previous page

Author(s)	Process name	Process description (operation principle)	Main results / contributions
Feng et al.	Pressure–Vacuum Swing Permeation (PVSP)	Single membrane module with two compartments separated by a dense membrane. A reversible pump alternates between feed compression and permeate evacuation under vacuum, creating a cyclic pressure difference that enhances the transmembrane driving force.	Achieved higher recovery than steady-state operation with comparable productivity; simplified configuration (one module, one pump); validated for O_2 enrichment, CO_2/N_2 separation and biogas upgrading; performance strongly governed by feed-to-permeate volume ratio.
Wang	Cyclic batch mode / Free diffusion process	Single closed hollow fibers membrane module with fixed upstream and downstream volumes. Both compartments are isolated during permeation, allowing pressure and composition to evolve freely over time. The cycle includes free permeation, separate recovery of permeate and retentate, and vacuum regeneration.	Showed that unsteady operation can achieve simultaneous improvements in purity and recovery beyond steady-state limits; experimentally validated on multiple gas separations.

Continued on next page

Table 1.5 – continued from previous page

Author(s)	Process name	Process description (operation principle)	Main results / contributions
Trubyanov et al.	Pulsed retentate separation	Continuous feed membrane module operated at constant transmembrane pressure. The retentate outlet is periodically closed to allow concentration profile buildup, then briefly opened to withdraw a small enriched fraction of the slow-permeating component.	Enhanced separation of slow-permeating components without productivity loss; independent of membrane thickness; constant pressure operation; simple implementation using a single automatic valve; experimentally and theoretically validated.

In the processes discussed so far, the main focus was on separation performance, such as purity and recovery. Energy use was mentioned in some cases but never treated as a main objective. The next section looks at how these cyclic operations can also impact and improve energy efficiency.

1.3 Efficiency and steady-state membrane gas separation

In this thesis, the term energy efficient is somewhat of a misnomer, as it will not solely refer to a comparison with the theoretical minimum work (discussed in Chapter 5). A broader perspective aligns with dictionary definitions of efficiency, such as Merriam-Webster's description of "effective operation as measured by a comparison of production with cost (as in energy, time, and money)" and Cambridge's definition as "the quality of achieving the largest amount of useful work using as little energy, fuel, effort, etc. as possible". Since the analysis concerns a new process, efficiency is evaluated not only against its own thermodynamic minimum but also relative to an existing, steady-state operation.

1.3.1 Minimum work of separation

As every process operation incurs an energetic cost, reducing the energy required for a given process has long been an important objective. A classic thought experiment illustrating this idea is Maxwell's demon [51]. In this scenario, an imaginary being sorts gas molecules between two compartments by opening and closing a tiny door. By allowing only fast (hot) molecules to pass in one direction and slow (cold) molecules in the other, the demon appears to create two compartments at different temperatures without performing work or producing entropy. At first glance, this appears to defy the second law of thermodynamics, which holds that the entropy of an isolated system cannot decrease spontaneously and that real mass transfer processes are inherently irreversible.

However, real systems cannot achieve this idealized sorting. To separate components efficiently, the theoretical minimum work corresponds to using an infinitely selective membrane that produces perfectly pure components [52]. Such an idealized membrane represents a thermodynamic limit rather than a practical reality. Actual processes are not reversible: membranes, valves, or separation devices introduce irreversibilities, such as friction, mixing losses, and heat leaks. Irreversibilities are associated with the generation of entropy that occurs as a system evolves with time.

Unlike distillation, extraction, or absorption, where separation performance is bounded by phase-equilibrium relationships, membrane separations are governed by non-equilibrium mass transport through the membrane [53]. As an example, in conventional gas–liquid contactors, if the operation is stopped, the system will naturally evolve toward thermodynamic equilibrium, with each phase reaching its equilibrium composition. In contrast, in a membrane gas separation process, once the operation ceases, the two compartments will eventually reach the same pressure and composition, since the driving forces for mass transfer (pressure or concentration gradients) disappear. It is worth noting that Prigogine [52] theorised that for these non-equilibrium processes, a linear non-equilibrium system that cannot reach equilibrium settles into a stationary state with minimum entropy production. If no constraints prevent equilibrium, entropy production falls to zero.

W_{min} (i.e. minimum work of separation) is *usually* the theoretical minimum amount of energy required to reversibly and isothermally separate a gas mixture into its pure components at the same temperature and total pressure, which does not always correspond to the relevant separation. It represents the ideal thermodynamic limit, the work needed if the process were perfectly efficient and proceeded infinitely slowly, without any entropy generation or losses whereas W_{real} is the value taking into account all the irreversibilities. From this, the efficiency of a process can be defined as the ratio of both quantities:

$$\eta = \frac{W_{min}}{W_{real}} \tag{1.10}$$

with η the energy efficiency of the process and W the work.

The difference between the minimum work W_{min} and the real work W_{real} required arises precisely because of these irreversibilities. When designing or analyzing separation processes, it is therefore essential to account for non-ideal behavior to correctly estimate energetic costs and efficiency.

1.3.2 Improving energy efficiency

Comparative studies highlight that membranes are not universally the most efficient technology; for instance, nitrogen separation by membranes ($\eta \approx 0.04$) is less efficient than cryogenic distillation ($\eta \approx 0.1$) despite offering operational advantages [4]. Table 1.6 groups the efficiency of multiple processes.

To improve efficiency, several studies have explored the concept of equipartition as a design principle for minimizing entropy production and optimizing process performance. In this

Table 1.6 Comparison between minimum and real work of separation for various processes and process efficiency [4].

Mixture	**Process**	$W_{\mathbf{min}}$ (kJ·mol^{-1})	$W_{\mathbf{real}}$ (kJ·mol^{-1})	η (-)
Multiphase feed mixture				
Aqueous suspension	Microfiltration	–	0.007–2	–
Homogeneous feed mixture (gas or liquid)				
UF_6 isotopes (x = 0.004, y = 0.5)	Knudsen diffusion	13	2,000,000	6×10^{-6}
Liquids	Distillation	0.1–15	1–200	0.01–0.4
N_2 from air (x = 0.79, y = 0.9999)	Cryogeny	2	20	0.10
N_2 from air (x = 0.79, y = 0.98)	Membrane gas separation	1.5	40	0.04
Seawater desalination (x = 0.99)	Reverse osmosis	0.14	0.5	0.28
Seawater desalination (x = 0.99)	Evaporation	0.14	5.5	0.03

context, equipartition refers to maintaining uniform thermodynamic quantities throughout the system, which helps reduce energy losses and enhance overall efficiency. A brief overview includes:

- **Equipartition of Forces (EoF):** Sauar et al. [54] proposed EoF, suggesting that minimizing entropy production requires two process streams exchanging fluxes to maintain uniform driving forces across the transfer surface. Bedeaux et al. [] clarified that EoF holds only when transport paths are independent and all potential variations of process streams, including impractical ones, are considered. Kjelstrup et al. [55] further explained that EoF is valid only if the linear transport coefficients do not depend on fluxes or forces. Magnanelli et al. [56] confirmed that EoF may deviate from the numerical optimum when transport coefficients vary or driving forces cannot be independently controlled, but it can still serve as a reliable approximation .

- **Equipartition of Entropy Production (EoEP) [56]:** Tondeur and Kvaalen [] first introduced EoEP, proposing that the most effective process configuration is achieved when local entropy production is evenly distributed. Johannessen et al. [57] demonstrated that local entropy production must remain constant to minimize total entropy production, provided conservation equations are satisfied and linearity conditions apply. Sorin et al. [58] found that distributing entropy generation evenly produces results closest to the reference case in terms of overall exergy consumption .

- **Equal Thermodynamic Speed (ETS) and Equal Thermodynamic Length (ETL):** Originating from finite-time thermodynamics, ETS proposes that for processes with a

fixed number of relaxation steps, minimum entropy production occurs when thermodynamic speed remains constant. ETL states that for discrete processes, dissipation is minimized when the thermodynamic distance between successive steps is uniform. Magnanelli et al. [56] showed that ETS and EoEP can still approximate the optimal configuration effectively, even when independent control of driving forces is not possible.

- **Power of Separation:** Sorin et al. [58] introduced the concept of power of separation as an optimization objective. In their study of a pervaporation membrane network, they found that distributing the power of separation evenly across the system provided results closest to the reference case in terms of membrane surface area allocation, even though equipartition of entropy generation resulted in slightly lower total exergy consumption .

1.4 A few interrogations

In summary, membrane processes are most commonly operated under steady-state conditions. Only a few studies have explored the potential of transient or dynamic operation modes. These attempts generally aimed to enhance process efficiency through various configurations or operational adjustments, yet the improvements remained limited, as described above. Notably, previous research seldom considered energy consumption as a primary optimization objective.

This gap raises several important questions: How might a transiently operated membrane system, explicitly designed with energy reduction in mind, perform compared to classical steady-state configurations? Which parameters play a decisive role in this potential improvement? And fundamentally, what mechanisms govern any observed gains in performance or efficiency?

These questions naturally lead to the exploration of the Membrane Piston concept, a novel approach that leverages controlled transient behavior to enhance energy efficiency and process control within membrane systems.

1.5 Nomenclature

Roman symbols

A	Membrane surface area	m^2
D	Diffusion coefficient	$m^2\,s^{-1}$
L	Flowrate in Pulsed Permeate Retentate	$m^3_{STP}\,s^{-1}$
P	Pressure	Pa
P_i	Partial pressure of component i	Pa
$\mathscr{P}_i$	Permeance of component i	$mol\,m^{-2}\,s^{-1}\,Pa^{-1}$
$\mathbb{P}_i$	Permeability of component i	$mol\,m\,m^{-2}\,s^{-1}\,Pa^{-1}$
Q	Molar flowrate	$mol\,s^{-1}$
$\mathscr{S}$	Solubility coefficient	$mol\,m^{-3}\,Pa^{-1}$
w	High-pressure fraction in Paul's process	–
W	Work	J
$W_{\min}$	Minimum work required	J

Greek letters

α^*	Ideal selectivity (permeance ratio)	–
$\alpha_{ref/i}$	Selectivity of the reference component relative to i	–
ε_{mem}	Membrane thickness	m
η	Unit efficiency	–
γ	Volume ratio in cyclic batch operation	–
Φ_i	Molar flux of component i through the membrane	$mol\,s^{-1}$
ψ	Pressure ratio (P_{down}/P_{up})	–
θ	Stage cut	–
Θ	Time lag	s
τ	Cycle duration in Paul's process	s

Subscripts

$down$	Downstream membrane interface
$feed$	Feed side
i	Component i
I,II	Compartment I or II in the membrane piston
$perm$	Permeate side
ret	Retentate side
SS	Steady-state
up	Upstream membrane interface

Superscripts

$*$	Ideal or reference value
min	Minimum value

Acronyms

NEA	Nitrogen Enriched Air
OEA	Oxygen Enriched Air
PSA	Pressure Swing Adsorption
PSP	Pressure Swing Permeation

Chapter 2

Membrane Piston concept

The Membrane Piston concept has been explored in two published articles "Membrane gas separations and energy efficiency: Exploring the selective membrane-piston concept" [17] and "Reimagining gas separation: drastically improving energy efficiency with the Membrane-Piston concept" [18]. These articles both offered a similar description of the concept, synthesized for the Letters format, and thus, only the extended part is presented here. Additionally, an exploration of the model using dimensionless number was conducted and is added at the end.

2.1 Concept

The Membrane Piston concept comes from the target to reduce the energy requirement of gas permeation separation for a specified objective of separation and was recently introduced [17]. Nowadays in membrane separation, the energetic cost almost exclusively comes from the compression of the feed or the vacuum pumping of the permeate. Those solutions are effective but can be costly and difficult to implement, especially for vacuum operation [9]. A breakthrough concept allowing the combination of the two operations, compression and separation, while being technically possibly challenging to design and operate, could be of interest for energy efficiency purpose. Using a piston combined with a membrane would in fact allow the compression of a lower gas quantity and create a sufficient pressure difference to drive the separation. The resulting operation of such concept is expected to be less energy-consuming, which is a crucial point in separation techniques.
In the next section, the classical membrane separation process working in steady state, the baseline case, is introduced. The Membrane Piston concept, operating under unsteady condi-

tions, is then detailed.

2.1.1 Steady-state membrane process

A steady-state membrane process is a separation operation aimed at separating a gas feed using a pressure difference as driving force. The separation unit contains one inlet stream (the feed) and two outlet streams. The outlet stream enriched in the fastest components (the one crossing faster the membrane) is called *permeate*; the outlet stream enriched in the slowest components is called *retentate*. As the pressure ratio increases, the efficiency of the separation (i.e., the degree of purity of the fast and slow components increase in the permeate and retentate, respectively) increases. Therefore, the higher the difference pressure, the higher the separation efficiency.
The high pressure P_{up} in the retentate is generally controlled by a gas compressor before the membrane unit. Alternatively, a low pressure P_{down}, lower than the atmospheric pressure, is sometimes applied in the permeate compartment thanks to a vacuum pump.

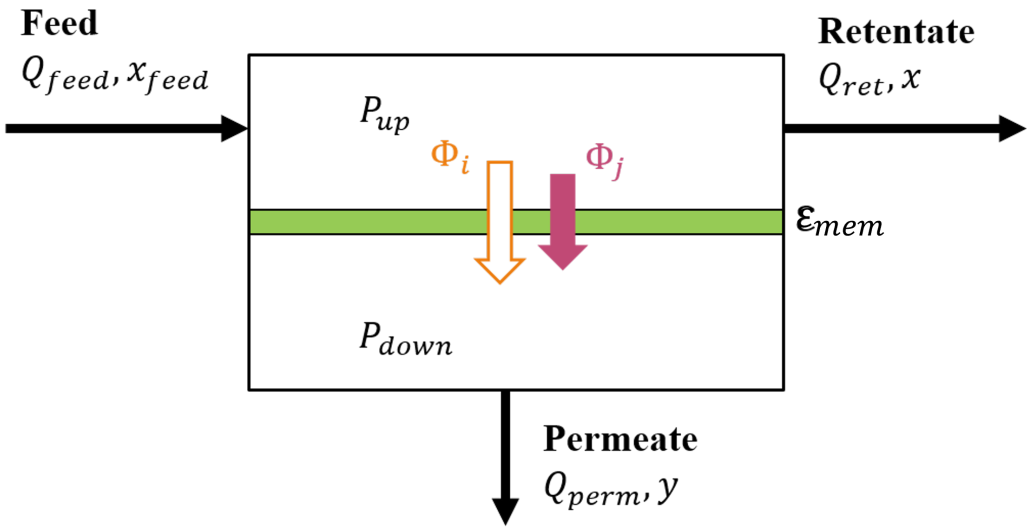


Figure 2.1 Steady-state membrane separation process. Q_{feed}, Q_{ret} and Q_{perm} denote the volumetric flowrates of the feed, retentate and permeate. x_{feed}, x and y are the molar fractions of the fast permeating component in the feed, retentate and permeate. Φ refers to the molar flux though the membrane, while ε_{mem} is the membrane thickness

To model the membrane separation unit for a binary system to be separated, the following set of dimensionless equations 2.1-2.9 is used, based on literature [47]. A cross plug flow

module is most often assumed.

Equation 2.1 expresses the global mass balance in the module.

$$\frac{d\theta}{dst} = \sum_j \Phi_j \tag{2.1}$$

$$\frac{dx_{ret,i}}{dst} = \frac{x_{ret,i}\sum_j \Phi_j - \Phi_i}{(1-\theta)} \tag{2.2}$$

with:

$$\Phi_i = \frac{1}{\alpha_{ref/i}}(x_{ret,i} - \psi y_{down,i}) \tag{2.3}$$

$$y_{down,i} = \frac{\Phi_i}{\sum_j \Phi_j} \tag{2.4}$$

$$y_{p,i} = \frac{x_{feed,i} - (1-\theta)x_{ret,i}}{\theta} \tag{2.5}$$

Where the selectivity $\alpha_{ref/i} = \frac{\mathscr{P}_{ref}}{\mathscr{P}_i}$ is the ratio of permeance, i.e., flux per unit transmembrane driving force of the reference component to component i [9]. The dimensionless area is denoted $st = \frac{A\mathscr{P}_{ref}P_{up}}{Q_{feed}}$ with A the total membrane area (m^2), the pressure ratio, $\psi = \frac{P_{down}}{P_{up}}$ and the stage cut,$\theta = \frac{Q_{permeate}}{Q_{feed}}$. The retentate composition for component i is written $x_{ret,i}$. The permeate flux composition, $y_{p,i}$, represents the composition of component i in the permeate stream as it exits the module and reflects the weighted average of the permeating species carried by the flux through the membrane. On the other hand, $y_{\text{down},i}$ denotes the composition of component i (permeate side) at the membrane interface (i.e., the downstream side), just before any bulk mixing occurs in the permeate channel.

Note that the energy requirement of the process is either the work required to compress the gas feed (Equation 2.6) or the work required to apply a vacuum in the permeate compartment (Equation 2.7) [9]. The study will focus on the molar work required to recover component i in the retentate.

$$W_{mol\ i,compression} = \frac{1}{x_{ret,i}(1-\theta)} \frac{\gamma}{\eta_{comp}(\gamma-1)} \left[\left(\frac{1}{\psi} \right)^{\frac{\gamma}{\gamma-1}} - 1 \right] \tag{2.6}$$

$$W_{mol\ i,vp} = \frac{\theta}{x_{ret,i}(1-\theta)} \frac{\gamma}{\eta_{vp}(\gamma-1)} \left[\left(\frac{1}{\psi} \right)^{\frac{\gamma}{\gamma-1}} - 1 \right] \tag{2.7}$$

The next section introduces the concept of a new separation process working in a transient mode.

2.1.2 Membrane piston

The key idea of the Membrane Piston process is to combine the steps of compression and separation within a single unit under non-steady state conditions.
The Membrane Piston contains the classic elements of a piston compressor: two compartments, separated by the head of the piston. The translation movement of the head reduces the volume of one compartment and increases the volume of the other. As an important difference between the present concept and the classical compression method, a membrane is inserted on the piston head. The membrane will move along the body of the piston, allowing a mass transfer between both compartments. Contrary to the steady-state compression, a dynamic separation process takes place in the Membrane Piston. While the piston moves, a pressure difference appears and increases between both compartments. Due to this pressure difference, a separation of the components occurs through the membrane.
Figure 2.2 illustrates graphically the concept of the Membrane Piston. Classically, the compartment where an enrichment in the fast component occurs is called permeate. The high pressure compartment is called retentate.

To fully understand how the module works, the separation process is described step by step. Figure 2.3 (a), (b),(c) represents the initial, intermediate and final states of the operation.

At $t = 0$, the piston head is close to one side (e.g., the left side in Figure 2.3) creating a small compartment (denoted compartment II) and a bigger one (compartment I) as shown in Figure 2.3(a). For sake of simplicity, it is considered that the two compartments have equal pressure, temperature, and composition at starting time.
During the operation, the piston starts moving, reducing the size of compartment I and

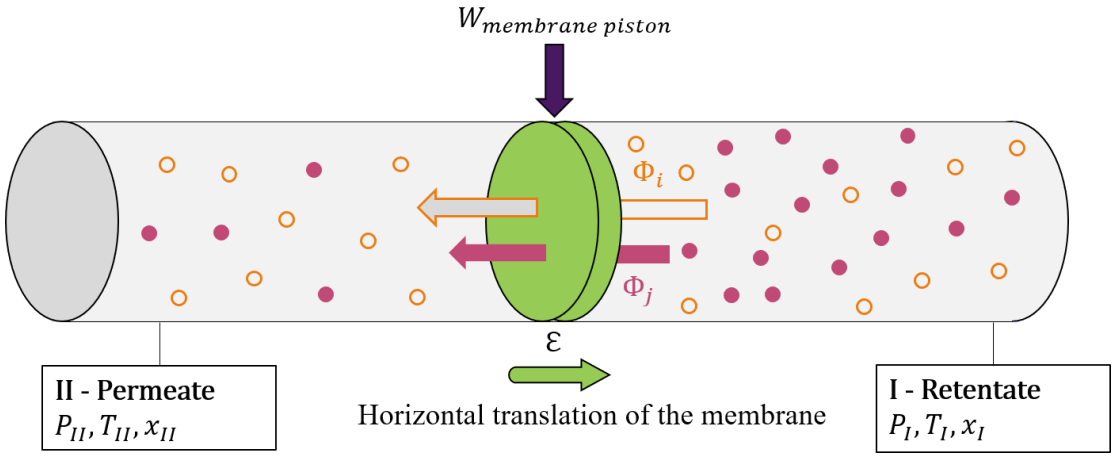


Figure 2.2 Membrane Piston system. The piston with the membrane acts as a wall between compartments I and II; $W_{membrane\ piston}$ denotes the necessary work for compression and separation, P the pressure, T the temperature and x the composition in the indicated compartment, ε_{mem} is the membrane thickness. i and j denotes the fast and slow components respectively

increasing the volume of compartment II. As mentioned above, with this volume change, the pressure increases in compartment I and decreases in the second compartment, creating a pressure difference between both sides of the membrane. This pressure difference will drive the operation and mass transfer will occur, leading to a separation effect. Note, however, that the Membrane Piston, similarly to the steady state membrane gas separation, may lead to non-isothermal conditions. As the volumes vary and the pressure difference increases during the operation, the molar quantities of both components in the compartments vary, causing temperature differences between the two compartments on the one hand, and a time variation of the temperatures in the compartments on the other. However, as will be shown subsequently, this temperature difference is mitigated by a heat transfer phenomenon through the membrane that tends to keep the temperatures uniform and constant in time.

The operation will stop when the Membrane Piston reaches the end at the final compression time $(t = t_{end})$ that is controlled by the Membrane Piston velocity and the volume available in compartment I.

Initially $(\text{at } t = 0)$, the atmospheric pressure is applied in both compartments. As expected, the pressure increases in compartment I (retentate) as its volume decreases (see the pressure-time curves in Figure 2.3). In compartment II (permeate), the volume is initially low and increases progressively causing an initial pressure drop. As a mixture essentially enriched in the fast compound fills the permeate, the pressure increases after reaching a minimum.

Note that at the final time t_{end}, the two mixtures resulting from the separation are both obtained at different pressures, the one in the retentate being high (with respect to the initial

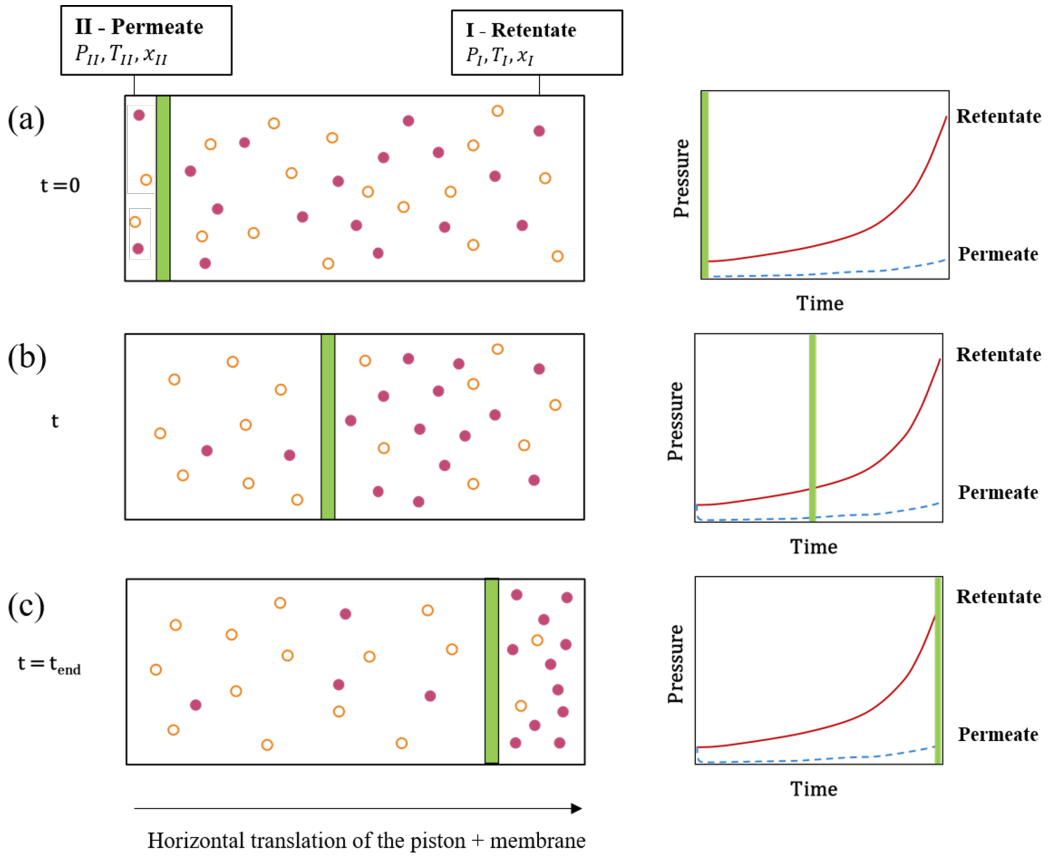


Figure 2.3 Membrane-Piston concept at the start of the operation, during the compression and at the end of the process with schematic pressure level associated (a,b,c). •: slow component, ○: fast component. Dotted line: pressure-time curve in the permeate. Continuous line: pressure-time curve in the retentate.

pressure) and the second in the permeate being (much) lower than that of the retentate. The energy input of the overall separation process is the work required to move the piston. After the compression, the piston is maintained at its end position for a relaxation period, until thermodynamic equilibrium is reached, leading to identical gas phase compositions in the two compartments. During the equilibration phase where the volumes of the compartments are kept fixed, mass and heat transfer are still possible. Due to the pressure difference between compartments I and II at t_{end}, a mass transfer persists through the membrane until pressure equilibration and temperature equilibration are reached. Once the thermodynamic equilibrium is reached, the system no longer evolves.
Figure 2.4 illustrated this final stage where a pressure equilibrium takes place in the module.

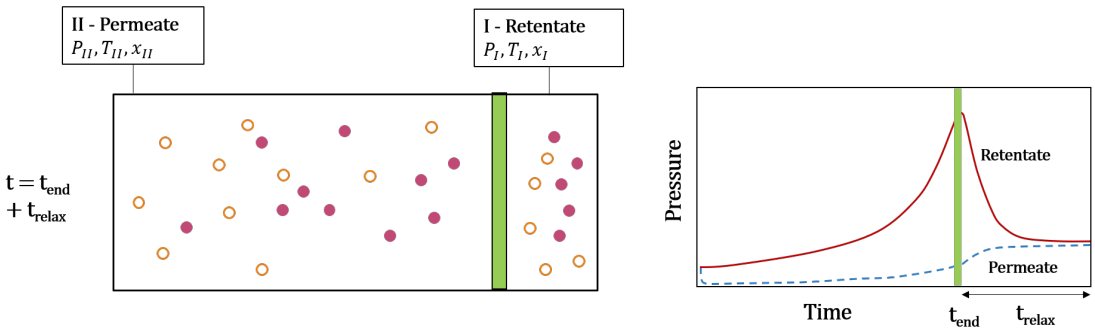


Figure 2.4 Membrane-Piston concept during the relaxation time with schematic pressure level associated. See caption of Figure 2.3 for the description of lines and symbols.

A second operation mode, called “open mode operation”, described by Figure 2.5, can be considered for the Membrane Piston concept. In this mode, one of the compartments (compartment II here) is open to an infinite external sink, such as the atmosphere or a much larger volume than compartment I of same initial composition as compartment I. This means that the pressure, temperature, and composition on the compartment II side of the membrane are fixed by the external environment (the “atmosphere”). It is assumed that the mass transfer occurring through the piston does not modify the atmosphere composition. The only recoverable flux in that case is the retentate mixture at high pressure. This mode is therefore interesting when only one of the 2 mixtures obtained after separation is of interest.

In Figure 2.5, the pressure-time curve of the retentate is similar to the curves shown in Figure 2.3 and 2.4 while the pressure-time curve of the permeate is constant (atmospheric conditions maintained throughout the separation process).

2.1.3 How could we compare the performances of the steady-state compression and the Membrane Piston?

To assess the performances of the separation process introduced in this paper, it is necessary to properly define what are considered to be the performance criteria. First, the separation objectives must be clearly defined. They can be expressed in terms of final concentrations of the compounds in the permeate and retentate and/or recovery ratios. Second, as energy aspects are considered, the energy requirement of the process must be quantified. To our opinion, these two criteria (separation and energy) are not enough to fully characterize the performance of the separation process and it is essential to involve in the analysis grid the thermodynamic state at which the final mixtures are obtained. Indeed, in terms of exergy,

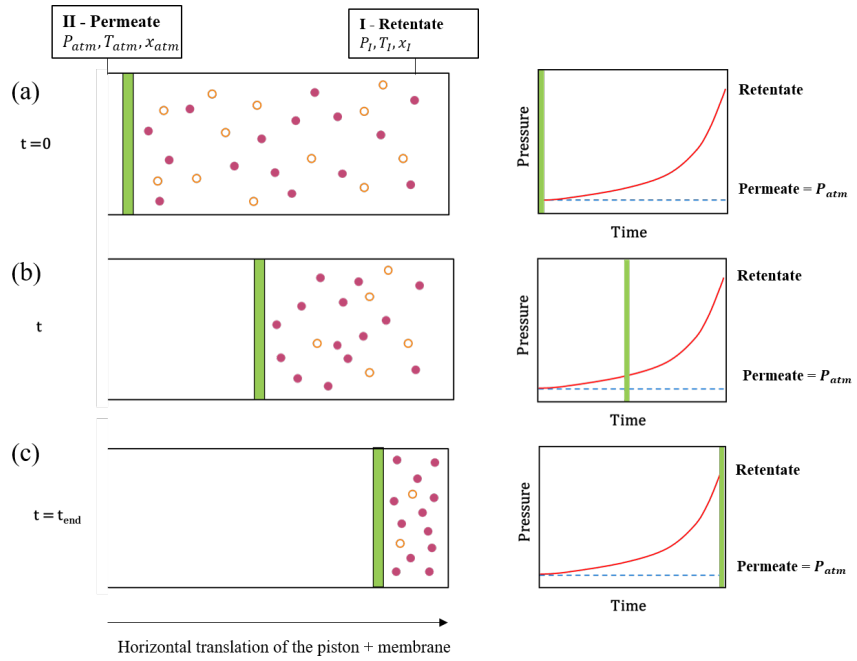


Figure 2.5 Membrane-Piston concept on open mode at the start of the operation, during the compression and at the end of the process with schematic pressure level associated. See caption of Figure 2.3 for the description of lines and symbols.

a mixture at given (temperature, composition) and at a high pressure contains more useful (mechanical) energy than a mixture at the same temperature and composition but at a low pressure. Therefore, it is considered that energy evaluation of the process should combine not only the work to pay to separate but also the exergy value of the mixtures after separation.

In addition, as the proposed membrane-piston process competes with the classical steady-state membrane process, it is desired to compare the performance of both processes in a fairly manner. Thus, it is compared for an identical membrane area. However, in terms of pressure levels, both systems behave differently:

- The gases in the membrane-piston system are initially at atmospheric pressure. In the final state, the pressure of the retentate is much above the atmospheric pressure P°. The pressure of the permeate is the atmospheric pressure when the system operates in open mode. Otherwise, the final permeate pressure depends on the operation conditions. It can be only stated that this pressure is much below the retentate pressure.

- In the steady-state membrane process, there are two modes enabling a high driving force in terms of pressure difference. The first option is to select the atmospheric pressure for the retentate, while the permeate pressure is set to a low pressure, well

below the atmospheric conditions, thanks to a vacuum pump. The second option is to compress the gas feed before the membrane separation and to set the permeate pressure to atmospheric conditions.

As the compression operation is much more expensive, in terms of energy requirement than the vacuum operation [46, 9], here the vacuum option is considered as the reference case.

To compare both processes, it is required to impose the same separation conditions. As the separations are driven by the pressure difference, the same pressure ratio $\psi = \frac{P_{down}}{P_{up}}$ will be imposed in both separation modules (in the transient membrane-piston process, the ψ ratio will be evaluated in final conditions, at t_{end}). Note however that the intrinsic values of the pressures will be different between both processes as in the classical membrane separation, one has $P_{up} = P^{\circ}$ and $P_{down} < P^{\circ}$, while for the membrane-piston: $P_{up} > P^{\circ}$ and $P_{down} < P_{up}$. Second, on exergy grounds, the final thermodynamic state (pressure, composition) of the

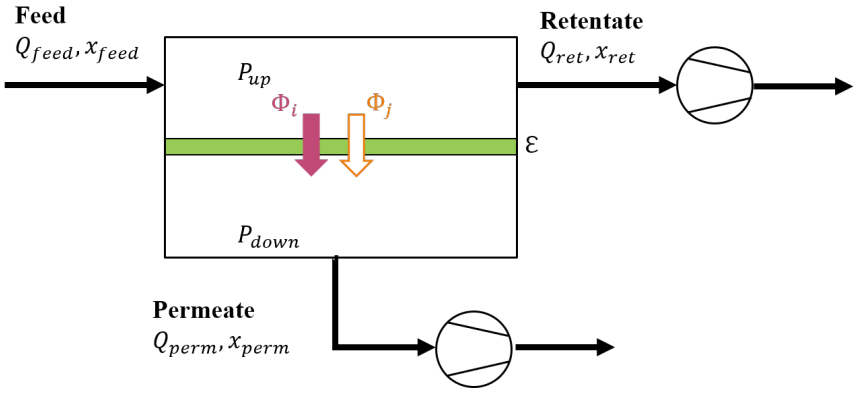


Figure 2.6 Reference steady-state for comparison purpose. See previous figures for symbols description.

resulting mixtures must be the same. Due to their own operation ways, the two types of operation units (Membrane Piston versus steady-state membrane) do not necessarily reach the same final conditions, which makes it very difficult to make a fair comparison between the both.

To circumvent this issue, it has been decided to impose the same final state conditions in both processes (in terms of pressure) in addition to the same separation conditions (expressed in terms of ψ). To ensure that the pressure conditions are the same in both types of separation processes, the gas mixtures exiting from the retentate of the steady-state unit will be compressed using a compressor in order to obtain a mixture in the retentate that shows the same exergy level as the retentate of the membrane-piston unit.

The reference case for the steady-state membrane compression is illustrated in Figure 2.6.

2.1.4 Synthesis

To provide a comprehensive overview of the different separation strategies considered in this work, Table 2.1 summarizes their main characteristics in terms of industrial use, energy and productivity performance, as well as typical applications. This comparative analysis highlights the strengths and limitations of each approach, and serves as a basis for evaluating the potential of the membrane-piston concept compared to more conventional processes.

Table 2.1 Comparison of separation approaches

	Feed compression	***Permeate vacuum pumping***	***Membrane Piston***
Industrial use	Classical solution	Most often discarded	Unexplored concept
Energy performance	High energy requirement	Minimal energy requirement	High energy efficiency expected
Advantages and limitations	Compressor cost dominates CAPEX. ERS can help to improve energy efficiency, but rarely applied due to extra cost	Vacuum pump limitations (leak issues, high footprint, low energy efficiency)	Integrated approach (compressor + membrane module in a single equipment)
Applications	Major markets: NEA, natural gas treatment, biogas upgrading, H_2 purification	VOC recovery (explosion hazards); Recently proposed as key solution for carbon capture	Potentially interesting for air gas separation or natural gas treatment

2.2 Membrane-piston modelling

In the following equations, the indices I and II refer to the corresponding compartment of the system, while *i* represents the different components (see Figure 2.2.

2.2.1 Gas model for pressure estimation

The modelling of the Membrane-Piston concept is realized with mass and energy balances as a first approach to evaluate the performance of the system. Thus, the simulations presented in this paper are at low pressure, which allows to use the perfect gas law as equation of state. It must be emphasized that this assumption can be considered as a weak hypothesis as long as the maximum pressure reached by the compressed gas remains below 15-20 bar and gases consist of small-size molecules ($N_2, O_2, CH_4 \ldots$). However, to convince the reader of the applicability of this hypothesis, the compressibility factor of the different mixtures of interest are provided in Appendix B.

2.2.2 Mass transfer

For a given component i of a p-component mixture, the mass transfer in compartment I is described by the mass balance in Equation (2.8) which expresses that the change in mole amount of i per unit of time in compartment I is the molar flow Φ_i of component i passing through the membrane.

$$\frac{dn_{I,i}}{dt} = -\Phi_i, \quad \text{for } i \in \{1, \ldots, p\} \tag{2.8}$$

Where $n_{k,i}$ is the mole amount of i in compartment k and t the the time variable. In the absence of transfer limitation in the gas phase, Equation (2.9) is commonly used for the molar flow, in agreement with literature [47, 9, 59]. The partial pressure difference between the compartment acts as the driving force. This model is generic and applies to any type of membrane material such as polymers or zeolites, as soon as the permeability's concept can be applied.

$$\Phi_i = \mathscr{P}_i A \left(x_{I,i} P_I - x_{II,i} P_{II} \right), \quad \text{for } i \in \{1, \ldots, p\} \tag{2.9}$$

Where $\mathscr{P}_i$ denotes the permeance of i through the membrane, A the membrane surface. $x_{k,i}$ is the mole fraction of i in compartment k Through the membrane, the mass transfer is usually considered to be in a quasi-stationary state (i.e., there is no accumulation of mass within the membrane). This assumption is well admitted by the scientific community in classical membrane separation [46, 11]. In the present case, this assumption is likely to apply since, intuitively, the very small volume membrane does not allow for a significant accumulation of mass. As the present article is aimed to discuss the general trends of the new separation device and to draw general conclusions about its potential interest for some applications, it is

decided to assume quasi-stationary conditions for the membrane. A finer modelling of the system including a precise description of the mass transfer in the membrane will be the topic of later studies. If the closed mode operation is considered, the matter leaving compartment I passes through the membrane and accumulates in compartment II. The mass balance in compartment II can be simply written as:

$$\frac{dn_{II,i}}{dt} = \Phi_i, \quad \text{for } i \in \{1,\ldots,p\} \tag{2.10}$$

If the open mode is selected, the matter leaving compartment I is released in the atmosphere (at ambient conditions, characterized by constant temperature and pressure).

At the gas/membrane interfaces, mass transfer limitation could arise due to diffusional boundary effects. In Equation (2.9), this transfer limitation was neglected. If this transfer is considered, boundary layers would appear, as introduced schematically in Figure 2.7. In such a case, transfer coefficient k_I and k_{II} of components in gases can be used to account for the mass transfer occurring in the boundary layers 1 and 3. The molar flow expressions of component i in these boundary layers (1 and 3) and in the membrane (2) are provided in Equations (2.11) to (2.13) that result in Equation (2.14) giving the expression of the global molar flow.

$$\Phi_i^1 = \frac{k_I}{RT_I} A \left(x_{I,i}P_I - y_{I,i}P_{II}\right) \tag{2.11}$$

$$\Phi_i^2 = \mathscr{P}_i A \left(y_{I,i}P_I - y_{II,i}P_{II}\right) \tag{2.12}$$

$$\Phi_i^3 = \frac{k_{II}}{RT_{II}} A \left(y_{II,i}P_I - x_{II,i}P_{II}\right) \tag{2.13}$$

$$\Phi_i = \frac{A}{\left(\frac{RT_I}{k_I} + \frac{1}{\mathscr{P}_i} + \frac{RT_{II}}{k_{II}}\right)} \left(x_{I,i}P_I - x_{II,i}P_{II}\right) \tag{2.14}$$

Coefficients k_I and k_{II}, characteristic for gas diffusion, are difficult to estimate accurately in the membrane-piston system and depend, among others, on the membrane characteristics such as the diffusivity and thickness of the boundary layer [60]. To fix ideas, these transfer coefficients are known to range in $[10^{-3}, 10^{-1}]$ m/s. To evaluate how important is the mass transfer limitation occurring from diffusional limitations, it was decided to assign arbitrary values to coefficients k_I and k_{II} that reflect usual orders of magnitude for such coefficients. Therefore, we imposed the equality $k_I = k_{II}$ (denoted k) and assigned three different values to k, based on characteristic values of diffusion for gases: $10^{-3}, 10^{-2}$ and 10^{-1} m/s. The impact

of the added limitation on the time evolution of temperature, pressure and composition is discussed in 2.3, which highlights that boundary layers around the membrane have a negligible effect on the Membrane Piston performance. Consequently, further results presented in this study do not take into account these transfer limitations.

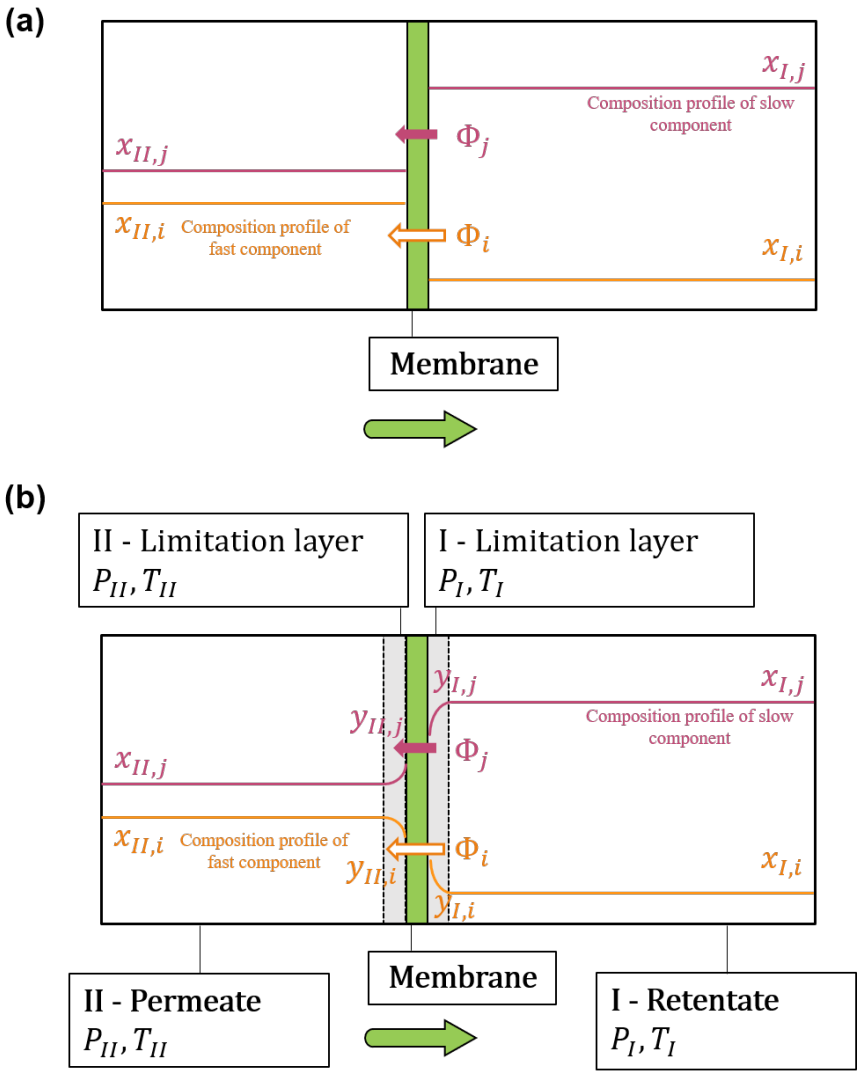


Figure 2.7 Illustration of mass transfer limitation in the Membrane Piston.

The permeability $\mathbb{P}$ of each membrane is temperature dependent. Therefore, if the temperature of the gas changes during the compression-separation process, the overall performance of the process can be affected. The impact of this assumption as well as the data used is discussed in 2.4, in which it appears that the gas temperatures are nearly uniform and close

to ambient conditions during the compression separation. This results from both the heat transfer through the membrane, denoted $\dot{Q}_{membrane}$, and thermal conduction through the piston body $\dot{Q}_{\text{piston wall}}$. These phenomena are detailed in Section 2.2.4 .

2.2.3 Volume variation of the two compartments within the system

The volume variation is related to the piston velocity, denoted $\dot{V}$ (m^3/s), and is governed by Equations (2.15)- (2.16). Note that $\dot{V}$ is defined as the product of the piston velocity (in m/s) by the piston surface. The volumetric velocity is a controlled key operating condition of the process.

$$\frac{dV_I}{dt} = -\dot{V} \tag{2.15}$$

If the closed mode operation is used, the volume of compartment II is governed by:

$$\frac{dV_{II}}{dt} = +\dot{V} \tag{2.16}$$

As mentioned above, the goal of this paper is to give insights about the physical phenomena taking place in the Membrane Piston system and to provide qualitative trends. For this reason, $\dot{V}$ is considered to be constant. In practice, this quantity changes in time (the piston speed increases initially, stabilizes, and starts decreasing just before the piston stops). It is assumed that the speed change does not affect the modelling of the system and the estimation of the energy work required for compression.

2.2.4 Energy balances

The application of an energy balance on the system {gas in compartment I} gives:

$$\frac{dU_I}{dt} = \dot{Q}_{\text{membrane}} + \dot{Q}_{\text{I, piston body}} + \dot{W}_{\text{volume change of compartment I}} - \dot{n}_I h_I \tag{2.17}$$

where $\dot{Q}_{\text{membrane}}$ denotes the heat transfer through the membrane from compartment I to compartment II (closed mode) or to the atmosphere (open mode). This heat transfer is assumed to be purely diffusional and is given by:

$$\dot{Q}_{\text{membrane}} = -\frac{\lambda A}{\varepsilon_{mem}}(T_I - T_{II}) \tag{2.18}$$

Symbol λ denotes the thermal conductivity of the membrane, ε_{mem} the membrane thickness. Note that if $T_I > T_{II}$, heat is released from compartment I to compartment II, explaining why $\dot{Q}_{\text{membrane}} < 0$ in such a case.

In addition to the heat transfer through the membrane, a heat loss through the lateral surfaces of the gas compartment is assumed. The conduction flux $\dot{Q}_{\text{piston body}}$through the lateral surface $S_{\text{I, ext}}$ of the piston body to the atmosphere can be written:

$$\dot{Q}_{\text{I, piston wall}} = -\frac{\lambda_{\text{piston}} S_{\text{I, ext}}}{\varepsilon_{\text{piston}}}(T_I - T_{atm}) \tag{2.19}$$

Where λ_{wall} is the thermal conductivity and $\varepsilon_{\text{piston}}$ the thickness of the piston body, referring specifically to the metal structure of the piston itself. The term $\dot{W}_{\text{volume change of compartment I}}$ quantifies the mechanical power associated with pressure forces acting on the system {gas in compartment I} and producing the volume change. Its expression is basically $-P_I \frac{dV_I}{dt} = +P_I \dot{V}$.

The term $-\dot{n}_I h_I$ expresses the energy rate of the matter leaving the system. It is the product of the molar flowrate of matter $\dot{n}_I$ by the molar enthalpy h_I of the gas in compartment I.

By expressing the internal energy U_I as the product of the molar internal energy u_I by the amount of matter n_I, Equation (2.17) can be written:

$$\begin{aligned} n_I \frac{du_I}{dt} + u_I \underbrace{\frac{dn_I}{dt}}_{-\sum_i \Phi_i} &= \underbrace{-\frac{\lambda A}{\varepsilon_{mem}}(T_I - T_{II})}_{\dot{Q}_{\text{membrane}}} + \underbrace{-\frac{\lambda_{\text{wall}} S_{\text{I, ext}}}{\varepsilon_{\text{piston}}}(T_I - T_{atm})}_{\dot{Q}_{\text{I, piston wall}}} \\ &+ \underbrace{P_I \dot{V}}_{\substack{\dot{W}_{\text{volume change}} \\ \text{of compartment I}}} - \underbrace{\dot{n}_I}_{\sum_i \Phi_i} h_I \end{aligned} \tag{2.20}$$

which simplifies to:

$$n_I \frac{du_I}{dt} = -\frac{\lambda A}{\varepsilon_{mem}}(T_I - T_{II}) - \frac{\lambda_{\text{wall}} S_{\text{I, ext}}}{\varepsilon_{\text{piston}}}(T_I - T_{atm}) + P_I \dot{V} - (h_I - u_I) \cdot \sum_i \Phi_i \tag{2.21}$$

For a perfect gas, $h_I - u_I$ is equal to RT_I. The final expression of the energy balance Equation (2.17) is:

$$n_I \cdot c_{v,I} \frac{dT_I}{dt} = -\frac{\lambda A}{\varepsilon_{mem}}(T_I - T_{II}) - \frac{\lambda_{\text{wall}} S_{\text{I, ext}}}{\varepsilon_{\text{piston}}}(T_I - T_{atm}) + P_I \dot{V} - RT_I \sum_i \Phi_i \tag{2.22}$$

In the perfect gas model assumption, the molar isochoric heat capacity $c_{v,I}$ of the gas mixture in compartment I is expressed as:

$$c_{v,I} = \sum_i x_{I,i} \cdot c_{v,\text{pure } i} \tag{2.23}$$

The same type of expression is used for $c_{v,II}$ involved in Equation (2.24) below.

If the closed mode is adopted, the energy balance applied to the {gas in compartment II} system can be written similarly:

$$n_{II} \cdot c_{v,II} \frac{dT_{II}}{dt} = +\frac{\lambda A}{\varepsilon_{mem}}(T_I - T_{II}) - \frac{\lambda_{\text{wall}} S_{\text{II, ext}}}{\varepsilon_{\text{piston}}}(T_{II} - T_{atm}) - P_{II} \dot{V} + RT_{II} \sum_i \Phi_i \tag{2.24}$$

2.2.5 Compression-Separation work

This calculation differs from the usual one used for the steady-state system comprising only a compression unit. To evaluate the compression power $\dot{W}_{\text{compression}}$ to be supplied to the system to perform the compression/separation operation, an energy balance is applied to the {membrane} system. Applied to this pseudo steady-state membrane (see assumption in section 2.2.2), the energy balance equates the energy inputs to the energy outputs:

$$\left(\begin{array}{c} \dot{W}_{\text{compression}} + \dot{Q}_{\text{membrane}} \\ + \dot{W}_{\substack{\text{volume change} \\ \text{of compartment I}}} + \underbrace{\dot{n}_I h_I}_{\substack{\text{energy of the matter} \\ \text{leaving compartment I}}} \end{array} \right) = \left(\begin{array}{c} \dot{Q}_{\text{membrane}} \\ + \dot{W}_{\substack{\text{volume change} \\ \text{of compartment II}}} \\ + \underbrace{\dot{n}_{II} h_{II}}_{\substack{\text{energy of the matter} \\ \text{leaving compartment II}}} \end{array} \right) \tag{2.25}$$

Through an algebraic rearrangement, the expression for $\dot{W}_{\text{compression}}$ is obtained:

$$\dot{W}_{\text{compression}} = -(P_{II} - P_I) \cdot \dot{V} - \sum_i \frac{dn_i}{dt} \left[h^{\bullet}_{i\ \text{pure}}(T_{II}) - h^{\bullet}_{i\ \text{pure}}(T_I) \right] \tag{2.26}$$

For diatomic molecules, it can be written as:

$$\dot{W}_{\text{compression}} = -(P_{II} - P_I) \cdot \dot{V} - (T_I - T_{II}) \sum_i c_{p,\text{pure } i} \cdot \Phi_i \tag{2.27}$$

The molar compression work is defined as:

$$W_{\text{mol i, compression}} = \frac{W_{\text{compression}}}{n_{I,i}} \tag{2.28}$$

Note that for perfect gases, the molar isobaric heat capacity $c_{p,\text{pure } i}$ is simply expressed as $c_{v,\text{pure } i} + R$, where R is the gas constant.

2.2.6 Summary: final expression of the model

For the closed mode operation, the global system is described by the following set of equations:

$$\begin{cases} \dfrac{dn_{I,i}}{dt} = -\Phi_i, \quad \text{for } i \in \{1,\dots,p\} \\ \dfrac{dn_{II,i}}{dt} = \Phi_i, \quad \text{for } i \in \{1,\dots,p\} \\ \dfrac{dV_I}{dt} = -\dot{V} \\ \dfrac{dV_{II}}{dt} = +\dot{V} \\ \underbrace{n_I}_{\sum_i n_{I,i}} \cdot c_{v,I} \dfrac{dT_I}{dt} = -\dfrac{\lambda A}{\varepsilon_{mem}}(T_I - T_{II}) - \dfrac{\lambda_{\text{wall}} S_{\text{I, ext}}}{\varepsilon_{\text{piston}}}(T_I - T_{atm}) + P_I \dot{V} - RT_I \sum_i \Phi_i \\ \underbrace{n_{II}}_{\sum_i n_{II,i}} \cdot c_{v,II} \dfrac{dT_{II}}{dt} = +\dfrac{\lambda A}{\varepsilon_{mem}}(T_I - T_{II}) - \dfrac{\lambda_{\text{wall}} S_{\text{II, ext}}}{\varepsilon_{\text{piston}}}(T_{II} - T_{atm}) - P_{II} \dot{V} + RT_{II} \sum_i \Phi_i \\ \dot{W}_{\text{compression}} = -(P_{II} - P_I) \cdot \dot{V} - \sum_i \dfrac{dn_i}{dt} \left[h_{i\,\text{pure}}^{\bullet}(T_{II}) - h_{i\,\text{pure}}^{\bullet}(T_I) \right] \\ P_I = \dfrac{n_I R T_I}{V_I} \\ P_{II} = \dfrac{n_{II} R T_{II}}{V_{II}} \end{cases} \tag{2.29}$$

In Equation (2.29), the quantities Φ_i are obtained from Equation (2.9) (if diffusional boundary layers are neglected) or (2.14) (otherwise); c_v is obtained from Equation (2.23). Apart from the expression for $\dot{W}_{\text{compression}}$, the model consists of $2p$+6 equations (where p is the number of compounds) relating $2p+7$ variables that are: $(n_{I,i})_{i=1,\dots,p}$, $(n_{II,i})_{i=1,\dots,p}$, T_I, T_{II}, P_I, P_{II}, V_I, V_{II}, $\dot{W}_{\text{compression}}$. The piston speed $\dot{V}$ and the initial conditions of the system variables are assumed to be known. Once the system is solved, it becomes possible to estimate $\dot{W}_{\text{compression}}$ at each time step from Equation (2.26). If the open mode is selected, the system is only described by the equations governing the gas in compartment I. Compartment II variables are then set to their values in the atmosphere conditions. The set of equations for open mode is given in Equation (2.30).

$$\begin{cases} \dfrac{dn_{I,i}}{dt} = -\Phi_i, \quad \text{for } i \in \{1,\dots,p\} \\ \dfrac{dV_I}{dt} = -\dot{V} \\ \underbrace{n_I}_{\sum_i n_{I,i}} \cdot c_{v,I} \dfrac{dT_I}{dt} = -\dfrac{\lambda A}{\varepsilon_{mem}}(T_I - T_{II}) - \dfrac{\lambda_{\text{wall}} S_{\text{I, ext}}}{\varepsilon_{\text{piston}}}(T_I - T_{atm}) + P_I\dot{V} - RT_I \sum_i \Phi_i \\ \dot{W}_{\text{compression}} = -(P_{II} - P_I)\cdot\dot{V} - \sum_i \dfrac{dn_i}{dt}\left[h^{\bullet}_{i\ \text{pure}}(T_{II}) - h^{\bullet}_{i\ \text{pure}}(T_I)\right] \\ P_I = \dfrac{n_I R T_I}{V_I} \end{cases} \tag{2.30}$$

The chosen system was subsequently solved using a custom-developed program written in Fortran 90. The first-order equation system was solved using DLSODA, a solver well-suited for both stiff and non-stiff systems.

2.3 Study of boundary limitations on flux

The issue of the boundary layer in the Membrane Piston system is challenging to address, as the membrane is a moving component. Its motion promotes mixing, and the boundary layer thickness depends on both the piston position and its velocity. Due to the lack of available correlations for such a dynamic configuration, a rough estimate of the mass transfer coefficient k is used to assess the potential impact of boundary layers on the overall transfer.

Following a common approach in the literature, k is estimated as:

$$k_{AB} = \frac{D_{AB}}{\delta} \tag{2.31}$$

where D_{AB} is the diffusion coefficient of gas A in gas B, and δ is the boundary layer thickness.

For the case of air separation, the diffusion coefficient of oxygen in nitrogen is taken as $D_{O_2/N_2} = 0.22\ cm^2/s$ [60]. The boundary layer thickness is assumed to lie within the range $[10^{-4}, 10^{-2}]\ m$, consistent with values reported in the literature [60]. As a result, the estimated range for the mass transfer coefficient is $k = [10^{-3}, 10^{-1}]\ m/s$. As mentioned in Section 2.2.2, the same value of k is assumed in both compartments, due to the lack of data and relevant literature specific to this type of system.

Figure 2.8 presents the results for a separation using an ideal membrane with $\alpha^* = 8$ and $\mathscr{P}_0 = 11\ GPU$, identical to the base case of the air separation study.

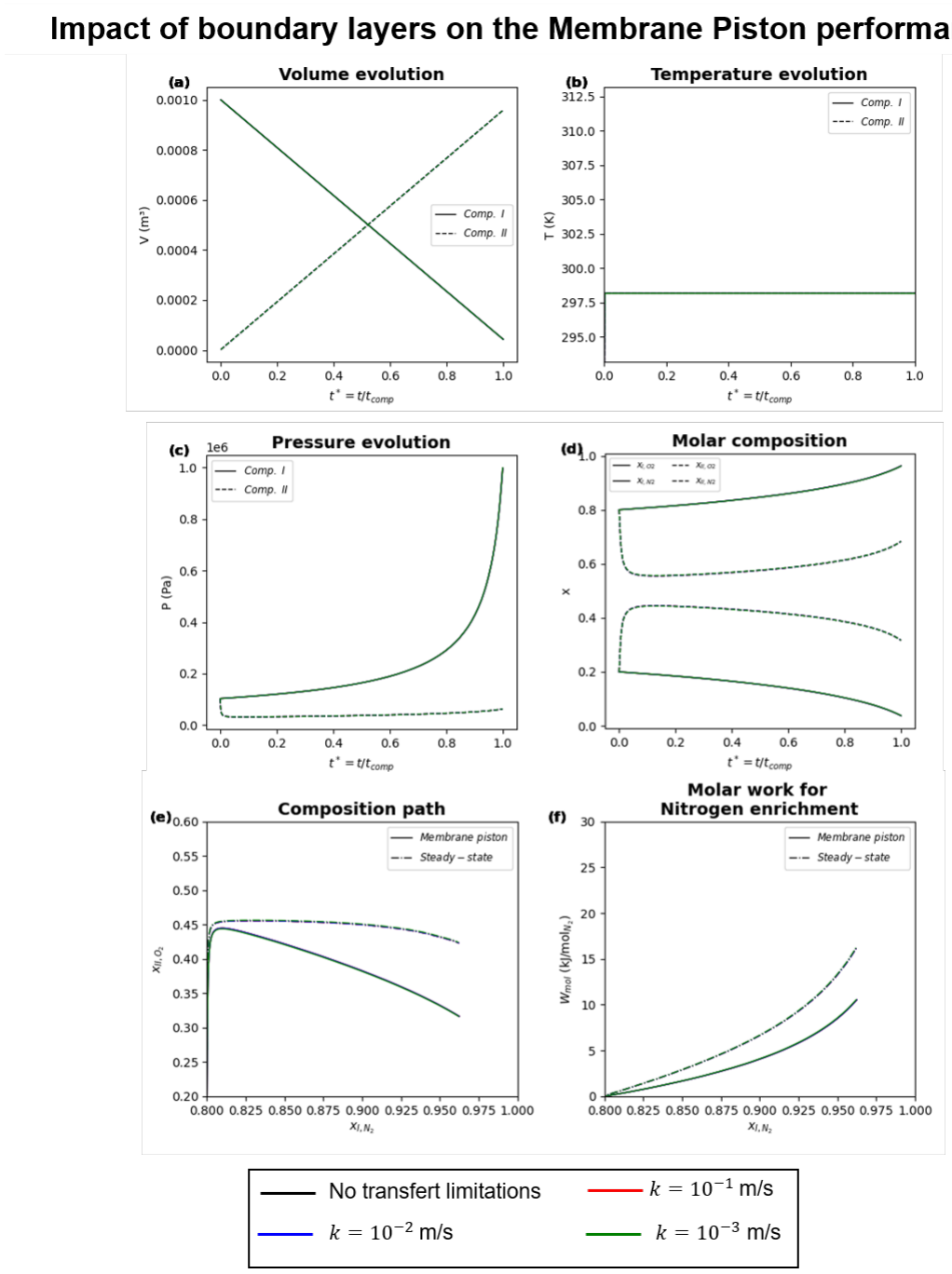


Figure 2.8 Impact of boundary layers on Membrane Piston performance. (a) Volume evolution versus time (b) Temperature evolution versus time. In both cases, curves are overlayed (c) Pressure evolution versus time (d) Molar composition (e) Composition path (f) Molar work for nitrogen production. Black: No mass transfert limitations; Red curves: $k = 10^{-1} m/s$; Blue curves: $k = 10^{-2} m/s$; Green curves: $k = 10^{-3} m/s$.

As shown in the figure, the impact of even the highest value of k on the performance of the Membrane Piston is negligible. This confirms that, at least as a first approximation, it is reasonable to neglect boundary layer effects in the model. It is nonetheless important to highlight that the absence of detailed geometry in the current model limits its ability to capture flow-induced non-idealities, especially under non-laminar conditions typical of high-speed or confined geometries. In practical membrane modules, turbulence and channel design can significantly affect both heat and mass transfer. Although the piston motion in the Membrane Piston configuration inherently promotes mixing, a more detailed characterization, via CFD (out of the scope of this paper) could be necessary to fully understand the impact of geometry and flow regime on mass balances.

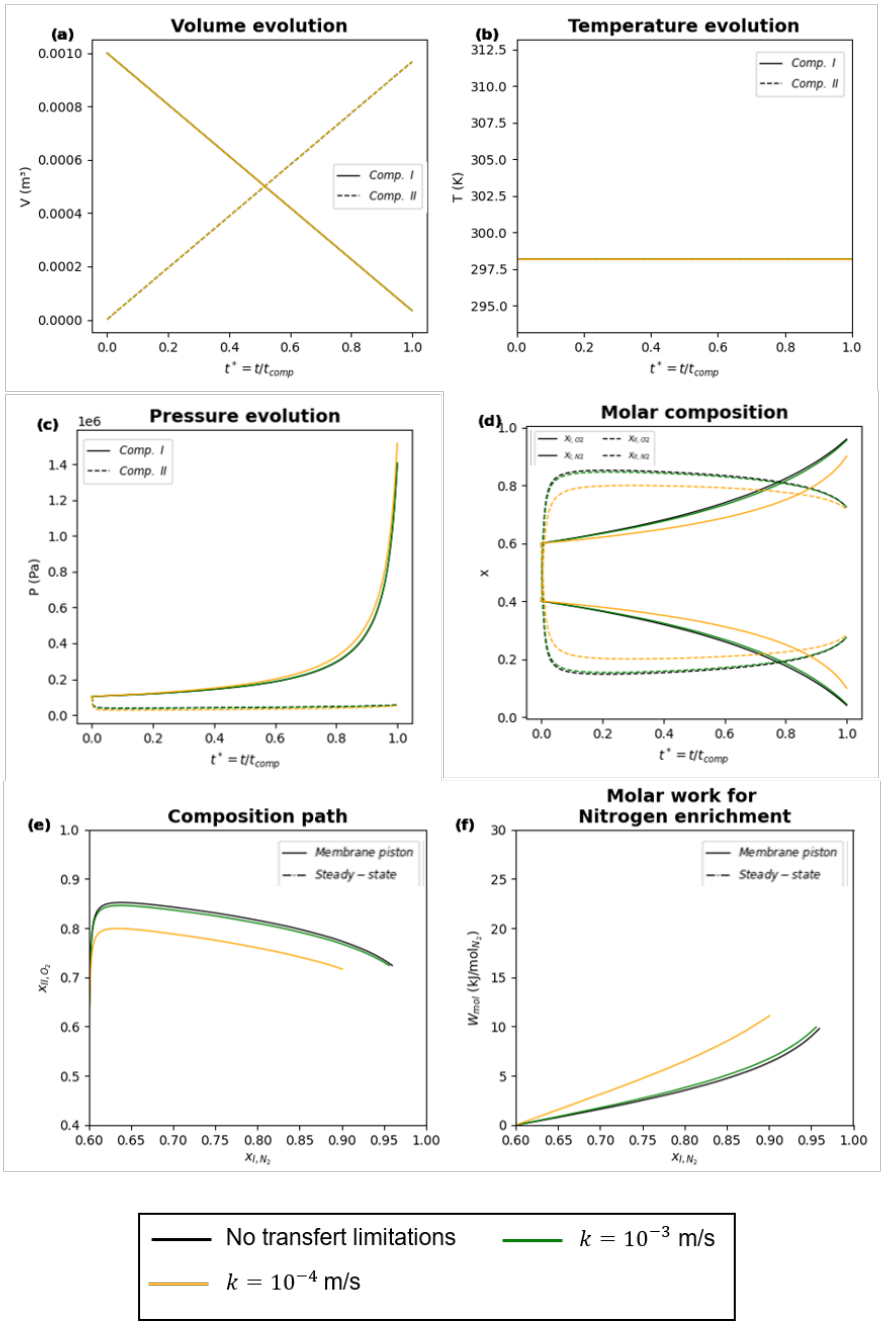


Figure 2.9 Impact of boundary layers on Membrane Piston performance. (a) Volume evolution versus time (b) Temperature evolution versus time. In both cases, curves are overlayed (c) Pressure evolution versus time (d) Molar composition (e) Composition path (f) Molar work for nitrogen production. Black: No mass transfer limitations; Green curves: $k = 10^{-3} m/s$; Orange curves: $k = 10^{-4} m/s$.

A complementary case study shown on Figure 2.9 was carried out for CO_2/CH_4 separation using an ideal membrane with a selectivity of 40 and a relatively large boundary layer thickness (δ between 0.01 and 0.1 m), to evaluate whether the previous conclusions for O_2/N_2 remain valid. These conditions correspond to a mass transfer coefficient k in the range of 10^{-3} to 10^{-4} m/s, close to those assumed in the air separation case. The simulation results indicate that for $k = 10^{-3}$ m/s, the effect of the boundary layer remains minor, with negligible impact on overall performance. However, when k is decreased to 10^{-4} m/s, representing a very thick and poorly mixed boundary layer, a notable degradation in separation performance is observed. While this latter scenario helps to outline the sensitivity of the system, it is considered extreme and not representative of realistic operating conditions. As such, the assumption of negligible boundary layer resistance remains a valid first approximation for modelling the Membrane Piston system, even in the context of CO_2/CH_4 separation.

2.4 Study of temperature dependency of selectivity

One of the main concerns when using polymeric membranes for gas separation is the relationship between selectivity and temperature, since $\alpha^*(T)$ tends to decrease as the temperature increases [61].

In Figure 2.10, three scenarios for air separation are illustrated, each based on different assumptions. The first scenario, represented by the black and blue curves, reflects the parameters used throughout this paper. It assumes heat transfer through the piston body and an ideal membrane. The second scenario, shown by the red and magenta curves, incorporates laboratory data on membrane permeability and its temperature dependence following an Arrhenius law such as $\mathbb{P} = \mathbb{P}_0 \exp(-E_a/RT)$. The third scenario, depicted with cyan and green curves, builds upon the second but assumes the Membrane Piston is adiabatic, with no heat transfer. Each gas retains the same permeance across the compared cases at $t = 0$.

Table 2.2 Activation energy and pre-exponential permeability factor for N_2 and O_2 from laboratory data.

Gas	**Activation Energy E_a (kJ/mol)**	$ln(\mathbb{P}_0)$
N_2	15.60	7.56
O_2	14.76	9.20

As can be seen, if the Membrane Piston system is not adiabatic (which is the assumption retained in the present article), heat is transferred through the metallic piston body (aluminium for example, or stainless steel). As a noticeable result, this heat transfer through the piston body creates a nearly isothermal process, maintaining the temperature close to ambient conditions. Note that this observation of a nearly uniform temperature profile persists even if the thermal conductivity of the membrane is decreased up to surrealistic values such as $10^{-6}\ W.m^{-1}.K^{-1}$. As a result, the impact of temperature change on separation performance is minimal as long as any thermal flux exists between compartments and towards the exterior.

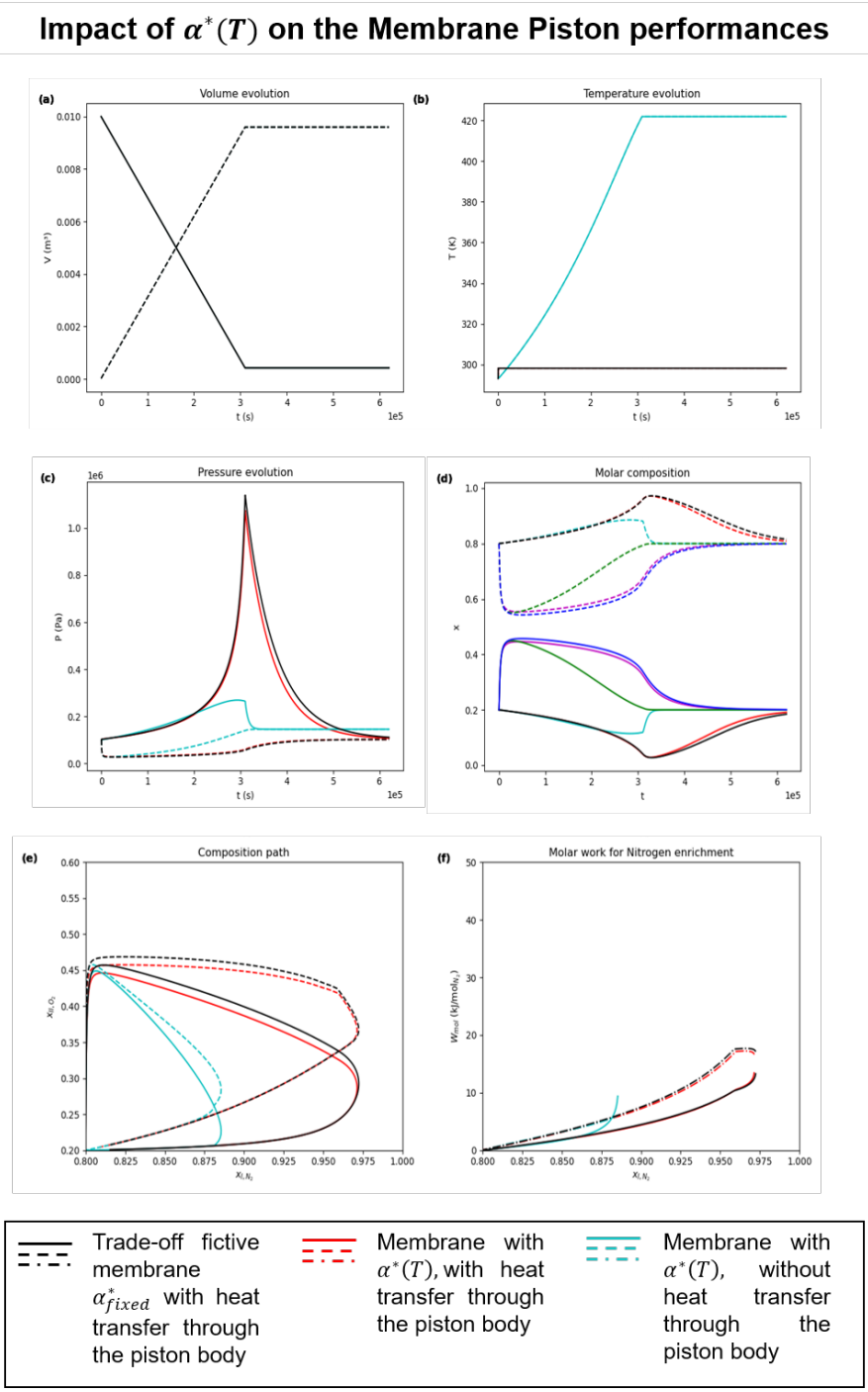


Figure 2.10 Impact of $\alpha(T)$ on Membrane Piston performance: O_2/N_2 separation in the Membrane Piston process. (a) Volume evolution versus time (b) Temperature evolution versus time. In both cases, curves are overlayed (c) Pressure evolution versus time (d) Molar composition (e) Composition path (f) Molar work for nitrogen production. Black and blue curves: $\alpha^* = 7.3$ and conduction through the piston walls; red and magenta curves: $\alpha(T)$ for the same membrane and conduction through the piston walls; cyan and green curves: $\alpha(T)$ for the same membrane and NO conduction through the piston walls. (a)-(d): Continuous line: Compartment I. Dashed line: Compartment II. (e)-(f): Continuous line: Membrane Piston. Dash-dotted line: steady-state results.

However, when the adiabatic assumption is made, it becomes clear that the performance reduction is drastic. The selectivity is decreased from 7.3 at $t = 0$ to 6.5 at $t = t_{end}$ and permeability goes from $\mathscr{P}_{O_2} = 2.32 \times 10^{-15}$ mol m^{-1} s^{-1} Pa^{-1} to $\mathscr{P}_{O_2} = 1.472 \times 10^{-14}$ mol m^{-1} s^{-1} Pa^{-1}. The mass transfer, in this specific case, is faster than the compression and leads to lower maximal pressure, which in turns, leads to poor separation performances.

2.5 Dimensionless numbers for the Membrane Piston

2.5.1 Model & numbers

Steady-state membrane modelling requires dimensionless numbers, such as α^*, θ, Ψ, detailed in Section 2.1.1. Essentially, every required equations can be transformed into dimensionless parameters. Thus, it seemed logical to try and apply the same principle to the Membrane Piston, using a dimensionless time t^* that will allow easier comparison between cases.

$$t^* = \frac{t}{t_0}, \text{with } t_0 = \frac{V_{I,0}}{\dot{V}_0} \tag{2.32}$$

Where $\dot{V}_0$ is the initial velocity of the piston and $V_{I,0}$ the initial volume of compartment I. Based on the system described in Section 2.2, in order to display other dimensionless number, t^* was introduced. Then the different variables are standardized using their initial value, i.e. $P_I^* = P_I/P_{I,0}$, $V_I^* = V_I/V_{I,0}$,$T_I^* = T_I/T_{I,0}$ etc... available in Table 2.3.

The rearranged equations are:

$$\frac{dn_{I,i}}{dt} = -\Phi_i \quad \Longrightarrow \quad x_{I,i0}\frac{dn_{I,i}^*}{dt^*} = -\Pi_{\text{perm},0}\left(P_I^* x_{I,i} - P_{II}^* \frac{P_{II,0}}{P_{I,0}} x_{II,i}\right) = -\Phi_i^* \tag{2.33}$$

$$\frac{dn_{II,i}}{dt} = \Phi_i \quad \Longrightarrow \quad x_{II,i,0}\frac{n_{I,0}}{n_{II,0}}\frac{dn_{II,i}^*}{dt^*} = \Pi_{\text{perm},0}\left(P_I^* x_{I,i} - P_{II}^* \frac{P_{II,0}}{P_{I,0}} x_{II,i}\right) \tag{2.34}$$

$$\frac{dV_I}{dt} = -\dot{V} \quad \Longrightarrow \quad \frac{dV_I^*}{dt^*} = -\dot{V}^* \tag{2.35}$$

$$\frac{dV_{II}}{dt} = \dot{V} \quad \Longrightarrow \quad \frac{V_{II,0}}{V_{I,0}}\frac{dV_{II}^*}{dt^*} = \dot{V}^* \tag{2.36}$$

Dimensionless Groups and Ratios			
$\Pi_{\text{perm},0}$	$A\mathscr{P}_i P_{I,0}/(\rho_{\text{mol},I,0}\dot{V}_0)$	$\Pi_{\text{therm},0}$	$(\lambda/\varepsilon_{mem})AT_{I,0}\,/\,(P_{I,0}\dot{V}_0)$
$x_{I,i}$	$n_{I,i}/n_{I,\text{tot}}$	$x_{II,i}$	$n_{II,i}/n_{II,\text{tot}}$
ψ	P_{II}/P_I	K	$V_{I,0}/V_{II,0}$
c_v^*	c_v/R	$c_{p,\text{pure }i}^*$	$c_{p,\text{pure }i}/R$
Standardize Variables			
t^*	t/t_0	$\dot{V}^*$	$\dot{V}/\dot{V}_0$
n_I^*	$n_I/n_{I,0}$	n_{II}^*	$n_{II}/n_{II,0}$
$n_{I,i}^*$	$n_{I,i}/n_{I,i0}$	$n_{II,i}^*$	$n_{II,i}/n_{II,i0}$
P_I^*	$P_I/P_{I,0}$	P_{II}^*	$P_{II}/P_{II,0}$
V_I^*	$V_I/V_{I,0}$	V_{II}^*	$V_{II}/V_{II,0}$
T_I^*	$T_I/T_{I,0}$	T_{II}^*	$T_{II}/T_{II,0}$
W^*	$W/(n_{I,0}RT_{I,0})$		

Table 2.3 Dimensionless numbers organized by similarity across phases.

$$n_I \cdot c_{v,I}\frac{dT_I}{dt} = -\frac{\lambda A}{\varepsilon_{mem}}(T_I - T_{II}) - \frac{\lambda_{\text{wall}} S_{\text{I, ext}}}{\varepsilon_{\text{piston}}}(T_I - T_{atm}) + P_I\dot{V} - RT_I\sum_i \Phi_i \tag{2.22}$$

$$\Downarrow$$

$$\begin{aligned} n_I^* c_v^* \frac{dT_I^*}{dt^*} &= -\Pi_{\text{therm},0}\left(T_I^* - T_{II}^*\frac{T_{II,0}}{T_{I,0}}\right) + P_I^*\dot{V}^* - T_I^*\sum_i \Phi_i^* \\ &\quad - \frac{\lambda_{wall} S_{I,ext} T_{I,0}}{\varepsilon_{piston} P_{I,0}\dot{V}^*}\cdot\left(T_I^* - \frac{T_{ext}}{T_{I,0}}\right) \end{aligned} \tag{2.37}$$

$$n_{II} \cdot c_{v,II}\frac{dT_{II}}{dt} = +\frac{\lambda A}{\varepsilon_{mem}}(T_I - T_{II}) - \frac{\lambda_{\text{wall}} S_{\text{II, ext}}}{e_{\text{wall}}}(T_{II} - T_{atm}) - P_{II}\dot{V} + RT_{II}\sum_i \Phi_i \tag{2.24}$$

$$\Downarrow$$

$$\begin{aligned} n_{II}^* c_{v,II}^* \frac{dT_{II}^*}{dt^*} &= \Pi_{\text{therm},0}\left(T_I^*\frac{T_{I,0}}{T_{II,0}} - T_{II}^*\right)\frac{n_{I,0}}{n_{II,0}} - P_{II}^*\dot{V}^*\frac{V_{I,0}}{V_{II,0}} + T_{II}^*\frac{n_{I,0}}{n_{II,0}}\sum_i \Phi_i \\ &\quad - \frac{\lambda_{wall} S_{II,ext} T_{II,0}}{\varepsilon_{piston} P_{I,0}\dot{V}^*}\cdot\left(T_{II}^* - \frac{T_{ext}}{T_{I,0}}\right) \end{aligned} \tag{2.38}$$

$$\dot{W}_{\text{compression}} = -(P_{II} - P_I) \cdot \dot{V} - (T_I - T_{II}) \cdot \sum_i c_{p,\text{pure } i} \cdot \Phi_i \tag{2.26}$$

$$\Downarrow$$

$$\dot{W}^* = -P_I^* \cdot (\psi - 1) \cdot \dot{V}^* - \left(T_I^* - T_{II}^* \frac{T_{II,0}}{T_{I,0}} \right) \sum_i \left(c_{p,\text{pure } i}^* \cdot \Phi_i^* \right) \tag{2.39}$$

A few interesting factors appear in the equation for mass transfer and heat transfer, that have been named Π_{perm} and Π_{therm}. They respectively represent the ratio of mass transfer to piston momentum and heat transfer to compressing force.

$$\Pi_{\text{perm},0} = \frac{A \cdot \mathscr{P}_i \cdot P_{I,0}}{\rho_{\text{mol},I,0} \cdot \dot{V}_0} = \frac{\text{Mass transfer}}{\text{Piston momentum}} \tag{2.40}$$

$$\Pi_{\text{therm},0} = \frac{(\lambda / \varepsilon_{mem}) \cdot A \cdot T_{I,0}}{P_{I,0} \dot{V}_0} = \frac{\text{Heat transfer}}{\text{Compressing force}} \tag{2.41}$$

2.5.2 Results

In order to assess whether the chosen dimensionless numbers are indeed sufficient to represent the system, their values were kept fixed while the dimensional variables composing them were varied. The study was carried out for air separation under a compression ratio of 90 %, with an initial volume V_I ranging between 0.01 m^3 and 1 m^3, while V_{II} was set to $V_I/500$. The temperature was varied between 273.15 K and 323.15 K, which corresponds to piston velocity $\dot{V}$ ranging from $1 \times 10^{-6}\,\text{m}^3\,\text{s}^{-1}$ to $1 \times 10^{-3}\,\text{m}^3\,\text{s}^{-1}$. The permeability was varied within $\left[1.89 \times 10^{-13}, 2.24 \times 10^{-10}\right]$, with $\alpha = 8$ and λ varying in a range where the membrane is still permeable. The duration of operation was kept fixed throughout the analysis. Two possibilities are studied: one considering an adiabatic piston, with no exchange with the exterior environment, while the second one take into account the heat transfer through the piston wall, which is the hypothesis used in the rest of the thesis.

The aim was to see if a defined set of dimensionless number could predict the performances of the system separation and ernegy-wise.

Adiabatic system

When the Membrane Piston operates under fully adiabatic conditions, i.e. with no heat transfer through the piston wall ($\lambda_{\text{wall}} = 0\,\text{W}\,\text{m}^{-1}\,\text{K}^{-1}$), the system exhibits distinct behaviors. As shown in Figure 2.11(b), the evolution of the gas composition in both compartments collapses onto a single master curve, confirming that the chosen dimensionless numbers are sufficient to characterize separation performance. However, Figure 2.11(a) highlights a key limitation: while the composition dynamics remain consistent, the energy required for separation is strongly affected by the initial temperature of the system. This dependence indicates that, in an adiabatic configuration, the dimensionless framework alone cannot fully predict the energetic cost of the process.

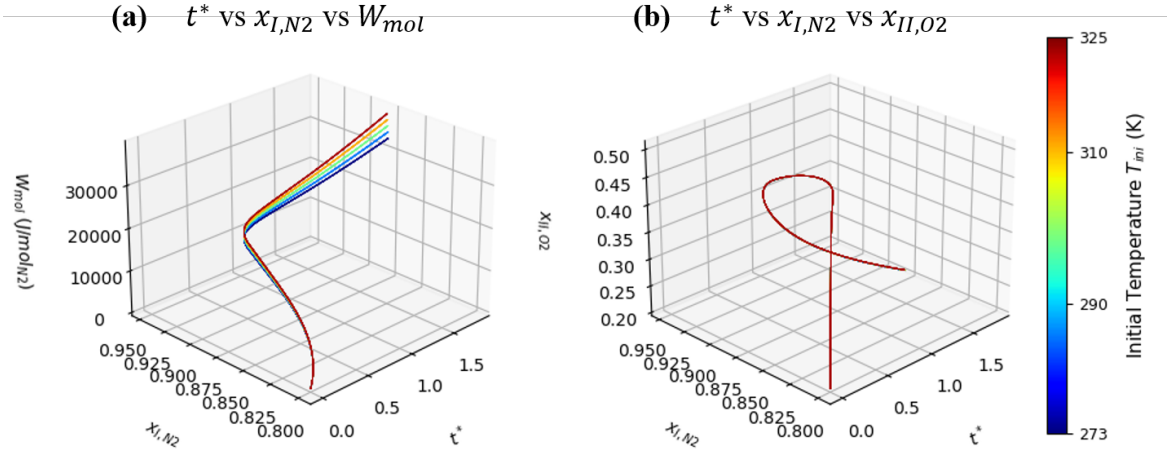


Figure 2.11 Master curves for the adiabatic system (a) Dimensionless time t^* vs $x_{I,N2}$ vs W_{mol} (b) Dimensionless time t^* vs $x_{I,N2}$ vs $x_{II,O2}$

Heat-transfer through the piston - Closed mode

When heat transfer through the piston wall is taken into account, the system becomes influenced by its thermal interaction with the surrounding environment, as illustrated in Figure 2.12(b). In this case, the gas temperature rapidly equilibrates with the ambient temperature and remains essentially constant thereafter. As a result, the separation work W no longer exhibits significant variation, aside from a brief transient associated with the short equilibration time (typically only a few seconds). Nevertheless, because temperature effects are suppressed, the mass transfer process differs from the adiabatic case: it is now governed primarily by pressure-driven mechanisms, leading to subtle but noticeable deviations in the observed behavior.

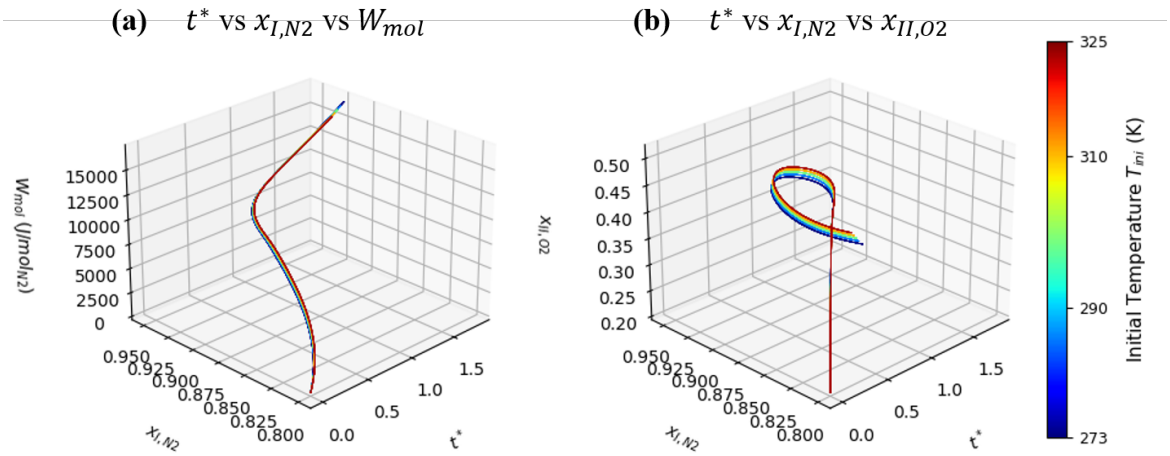


Figure 2.12 Master curves for the closed system with heat transfer through the piston wall (a) Dimensionless time t^* vs $x_{I,N2}$ vs W_{mol} (b) Dimensionless time t^* vs $x_{I,N2}$ vs $x_{II,O2}$

Heat-transfer through the piston - Open mode

In open-mode operation, where both heat and mass are exchanged with the surroundings, the master curves obtained in the closed cases are no longer valid. Several competing phenomena come into play, as illustrated in Figure 2.13(a), where the curves progressively diverge rather than collapsing onto a single trajectory. The analysis presented in Figures 2.13(b1) and (b2) further indicates that the initial temperature and pressure strongly influence the system's evolution. These parameters, in turn, affect the final composition of the compartments, revealing a more complex dependence than in the adiabatic or conductive closed cases.

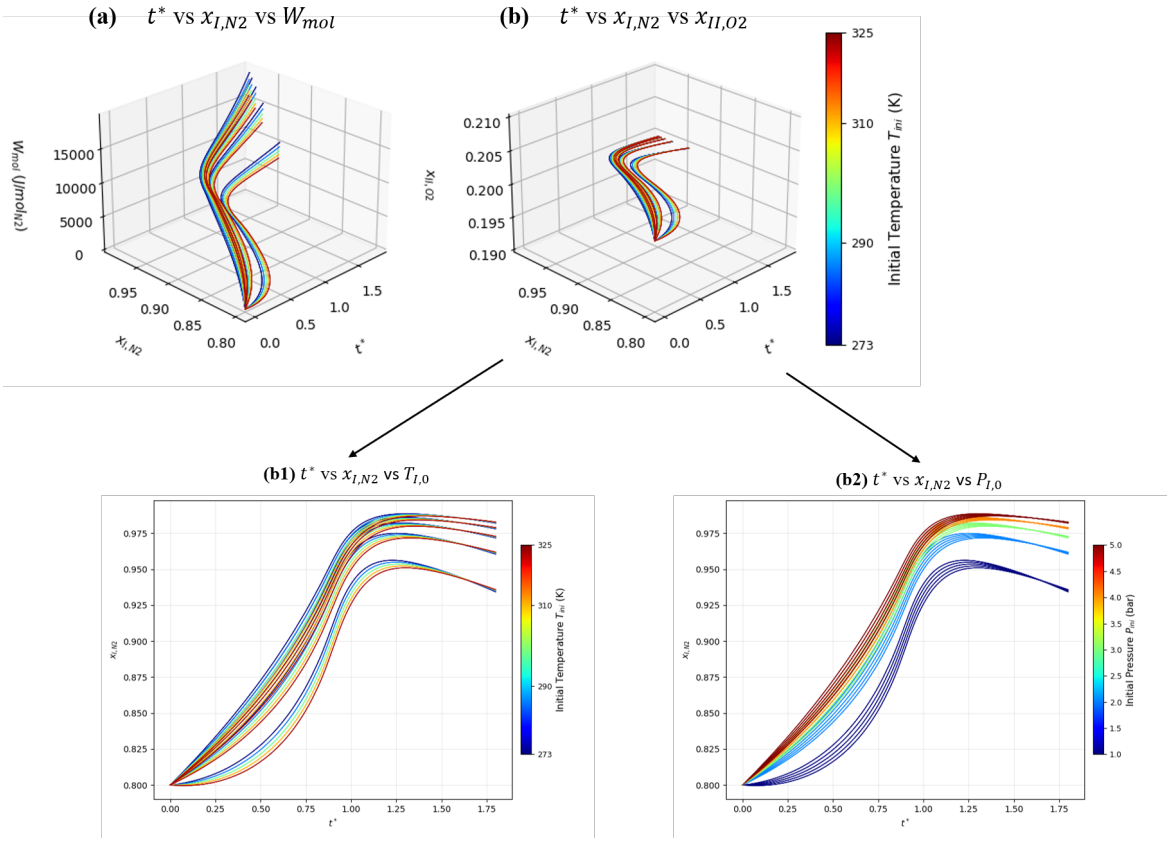


Figure 2.13 Master curves for the open system (a) Dimensionless time t^* vs $x_{I,N2}$ vs W_{mol} (b) Dimensionless time t^* vs $x_{I,N2}$ vs $x_{II,O2}$

2.6 Conclusion

The Membrane Piston concept is a new approach to gas permeation separation, designed to reduce energy consumption while achieving specific separation objectives. The key innovation of the Membrane Piston comes from the integration of compression and separation within a single, non-steady state module. It combines the elements of a classic piston compressor with a membrane encased on a piston head, allowing for simultaneous compression and separation. Based on several assumptions, such as ideal gas behavior, a model is proposed to study this system with special attention is given to the effects of boundary layers and selectivity in order to simplify the model. A method is also presented to compare this system with a conventional module. A dimensionless study is initiated and presents the noteworthy dimensionless number obtained for the system as well as mastercurves.

2.7 Nomenclature

Roman symbols

A	Membrane surface area	m^2
c_p	Molar heat capacity at constant pressure	$\mathrm{J\,mol^{-1}\,K^{-1}}$
c_v	Molar heat capacity at constant volume	$\mathrm{J\,mol^{-1}\,K^{-1}}$
D	Diffusion coefficient	$\mathrm{m^2\,s^{-1}}$
E_a	Activation energy in Arrhenius law	$\mathrm{kJ\,mol^{-1}}$
h	Molar enthalpy	$\mathrm{J\,mol^{-1}}$
k	Mass transfer coefficient in boundary layer	$\mathrm{m\,s^{-1}}$
n	Amount of substance	mol
$\dot{n}$	Molar flow rate	$\mathrm{mol\,s^{-1}}$
P	Pressure	Pa
P°	Atmospheric pressure	Pa
$\mathscr{P}_i$	Permeance of component i	$\mathrm{mol\,m^{-2}\,s^{-1}\,Pa^{-1}}$
$\mathbb{P}_i$	Permeability of component i	$\mathrm{mol\,m\,m^{-2}\,s^{-1}\,Pa^{-1}}$
$\dot{Q}$	Heat flow rate	W
R	Ideal gas constant	$\mathrm{J\,mol^{-1}\,K^{-1}}$
$S_{k,\mathrm{ext}}$	Lateral surface area of the piston body in compartment k	$\mathrm{m^2}$
st	Dimensionless area $st = AP_{up}\mathscr{P}_{ref}/Q_{feed}$	–
t	Time	s
T	Temperature	K
U	Total internal energy	J
u	Molar internal energy	$\mathrm{J\,mol^{-1}}$
V	Volume	$\mathrm{m^3}$
$\dot{V}$	Volumetric piston velocity	$\mathrm{m^3\,s^{-1}}$
W_{mol}	Molar work	$\mathrm{J\,mol^{-1}}$
x, y	Compositions	-
y_down	Composition at the permeate membrane interface before bulk mixing	

y_p	Permeate composition	

Greek letters

α^*	Ideal selectivity (permeance ratio)	–
δ	Boundary layer thickness	m
ε_{mem}	Membrane thickness	m
ε_{piston}	Piston wall thickness	m
η	Unit efficiency	–
γ	Laplace coefficient	–
λ	Thermal conductivity of the membrane	$\mathrm{W\,m^{-1}\,K^{-1}}$
λ_{wall}	Thermal conductivity of the piston body	$\mathrm{W\,m^{-1}\,K^{-1}}$
Φ_i	Molar flux of component i through the membrane	$\mathrm{mol\,s^{-1}}$
ψ	Pressure ratio (P_{down}/P_{up})	–
θ	Stage cut	–

Subscripts

$comp$	Compressor
$down$	Downstream membrane interface
$feed$	Feed side
i	Component i
I, II	Compartment I or II in the membrane piston
$perm$	Permeate side
pure i	Pure component i
ret	Retentate side
SS	Steady-state
up	Upstream membrane interface
vp	Vacuum pump

Superscripts

$*$	Dimensionless or ideal quantity
$\bullet$	Perfect gas

Acronyms

CAPEX	Capital expenditure
ERS	Energy Recovery System
NEA	Nitrogen Enriched Air
OEA	Oxygen Enriched Air
VOC	Volatile Organic Compound

Chapter 3

Numerical investigation of Membrane-Piston behavior

This chapter presents the results of simulation studies on the Membrane-Piston system, which have been published and are compiled here [17, 18]. Additionally, a section on CO_2 separation using a reverse-selective membrane is included, corresponding to a future article, highlighting another potential application of the Membrane-Piston system.

3.1 Case study on Air separation

As a foundation for the Membrane Piston analysis presented in this chapter, the air separation case study from (Lafont et al.) [17] is presented below. This work provides valuable context and a tangible example of the concept in action, helping to frame the discussion of further results.

In order to explore the potential interest of the membrane piston concept, a case study focusing on air separation, an important application of gas separation using membranes [3], is discussed here. One membrane is selected on the trade-off [34] with a selectivity of 7, typical of current commercial membranes for NEA (Nitrogen Enriched Air). Figure 2.3 presents the comparison with steady-state process of equal driving force and final thermodynamic state. The input parameters as well as the important results are summarized in Table 3.1.

Figure 3.1(a) showcases the volume evolution in the Membrane Piston system: compartment I has a fixed decrease of volume, based on the velocity selected and proportional to com-

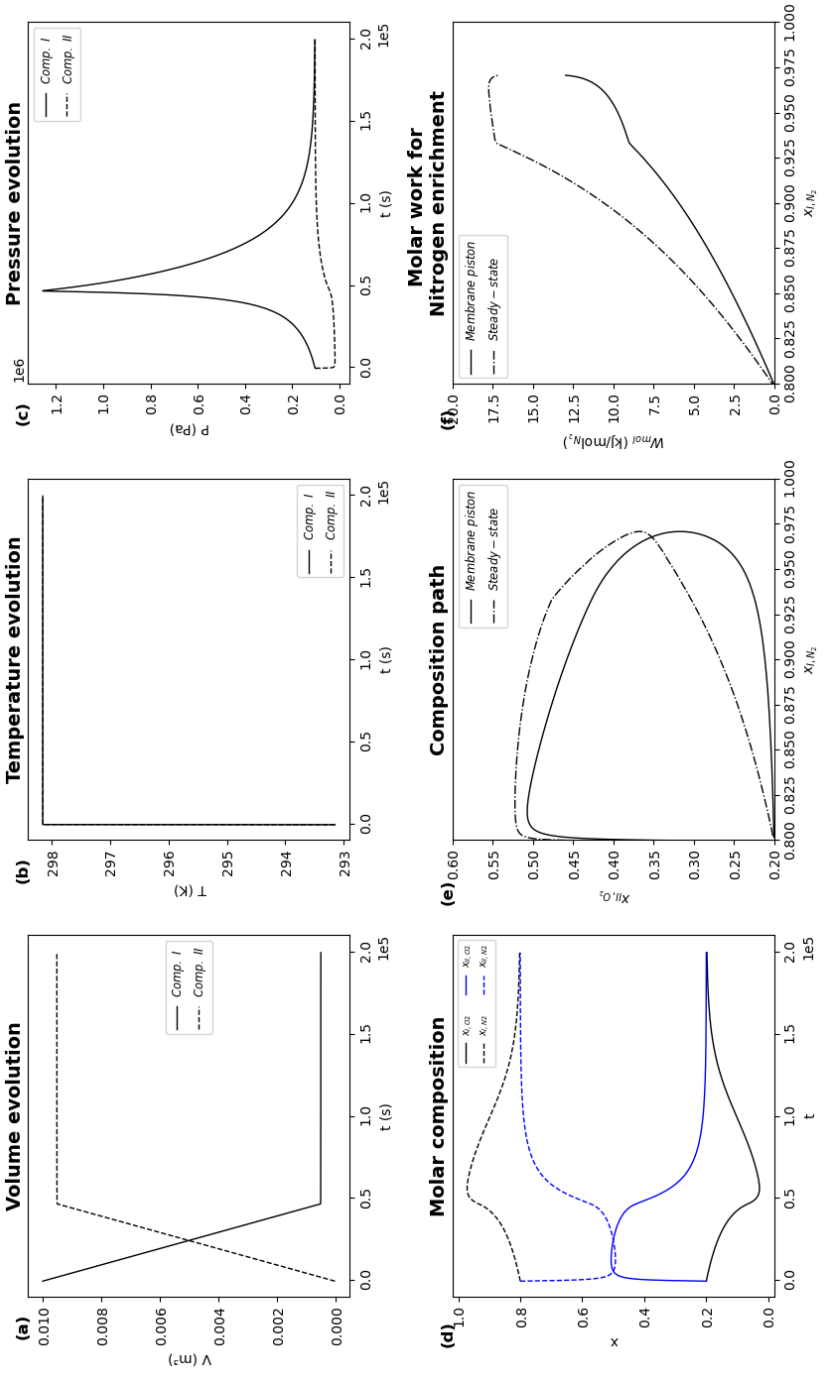


Figure 3.1 O_2/N_2 separation in the Membrane Piston process, using inputs from Table 1. Continuous line: Compartment I. Dashed line: Compartment II. Dash-dotted line: steady-state results (a) Volume evolution versus time (b) Temperature evolution versus time. In both cases, curves are overlayed (c) Pressure evolution versus time (d) Molar composition (e) Composition path (f) Molar work for nitrogen production.

partment II increasing volume. A short period of slow-down is considered at the end of the compression. The final pressure, presented on Figure 3.1(c), of 12 bar is reached at the end of the operation. This maximum validates the use of the perfect gas law here. The maximum is reached after t_{end}, delay caused by the difference of stiffness in the pressure increase. Figure 3.1(b) shows that the heat transfer through the membrane is sufficient to equate the temperature in both compartments. Moreover, the transfer through the side of the aluminium piston body tends to create an isothermal process. In this example, the piston gradually slows down, causing a slight continuation of the separation onto the relaxation period. This explains the improvement in purity after the end of the compression seen on Figure 2.3(d-e). The slight bump visible on Figure 3.1(e-f) comes from the beginning of the relaxation period, modifying the dynamics of the system. In steady-state membrane gas separation, the composition path typically exhibits two maxima depending on stage-cut, for each component. In the unsteady-state piston-driven process, the mass transfer dynamics significantly differs. Thus, the usual maxima found in the compared steady-state are not always reached. Regarding the separation performances, the Membrane Piston system, with the same pressure ratio and retentate composition as a steady-state process, is not able to produce a permeate as enriched in O_2 as the classical system. Nevertheless, the enrichments in N_2, of 97.1% is relevant for many inerting application [3] or as an economic pre-concentration brick in an integrated system. In this case, the steady-state is computed with the method from Figure 2.6, since the feed compression is here always more energy demanding. Isentropic efficiency of both compressor and vacuum are available in Table 3.1. Using a membrane with a selectivity of $\alpha^* = 7$ and assuming no temperature dependence due to minimal temperature variation, the unsteady process achieves a 45% reduction in molar work required to produce 95% pure nitrogen from air. For higher purities, the molar work needed to reach $x_{I,N2}^{max}$ is 24% lower compared to the steady-state process. These results represent significant improvements in energy efficiency, highlighting the potential of the unsteady process for reducing operational energy demands.

To further improve the separation performances, one must understand the different transport phenomena at play here. The system is highly constricted by the piston velocity, and increasing any parameter, such as the selectivity, implies an adjustment to stay into a feasible domain.

Note: The compression times are evaluated for a fixed system geometry and are intrinsically linked to the piston velocity. Under the current conditions, the system's operating speed seems too low for industrial application.

Table 3.1 Input parameters and results for a O_2/N_2 separation using the Membrane Piston system and comparison to the steady-state with permeate vacuum and retentate compression

Input	**Value**
Selectivity α^*	7
Velocity $\dot{V}$ (m^3/s)	2.02×10^{-7}
Compression period (s)	47000
Relaxation period (s)	200000
Piston body	Aluminium, $\lambda_{\text{piston}} = 240W.m^{-1}.K^{-1}$
Isentropic efficiency of compressor, η_{comp}	0.85
Isentropic efficiency of vacuum pump, η_{vp} [21]	$0.1058 \cdot \ln\left(\frac{P_{\text{down}}}{P_{\text{atm}}}\right) + 0.8746$
Output	
$P_I^{\max}$ (bar)	12.4
$x_{I,\text{N}_2}^{\max}$ (%)	97.1%
$W_{\text{mol,N}_2}(x_{I,\text{N}_2}^{\max})$ ($\text{kJ/mol}_{\text{N}_2}$)	12.96
$W_{\text{mol,N}_2}^{\text{steady-state}}(x_{I,\text{N}_2}^{\max})$ ($\text{kJ/mol}_{\text{N}_2}$)	17.15
$W_{\text{mol,N}_2}(x_{I,\text{N}_2} = 95\%)$ ($\text{kJ/mol}_{\text{N}_2}$)	9.74
$W_{\text{mol,N}_2}^{\text{steady-state}}(x_{I,\text{N}_2} = 95\%)$ ($\text{kJ/mol}_{\text{N}_2}$)	17.61

3.2 Sensitivity analysis on case studies

Following this case study, it was decided to expand the examination and include a sensitivity analysis, while still focusing on industry relevant gas separation, which has been the object of the second publication [18].

To gauge the realm of possible performances for the Membrane Piston system, a study on the piston velocity, membrane permeance and selectivity is performed. Note that selectivity is defined $\alpha^* = \frac{\mathscr{P}_{\text{fast component}}}{\mathscr{P}_{\text{slow component}}}$. The idea is to explore what energy efficiency performances the Membrane Piston can really achieve, through a generic simulation set. A previous study on air separation for Nitrogen Enriched Air was conducted and showcased the results obtainable from the simulations at a single velocity [17]. This study now extends those findings by solving the system presented above (Eq. 2.29) for different piston velocity conditions. The specifications of interest are compiled on Figure 3.2.

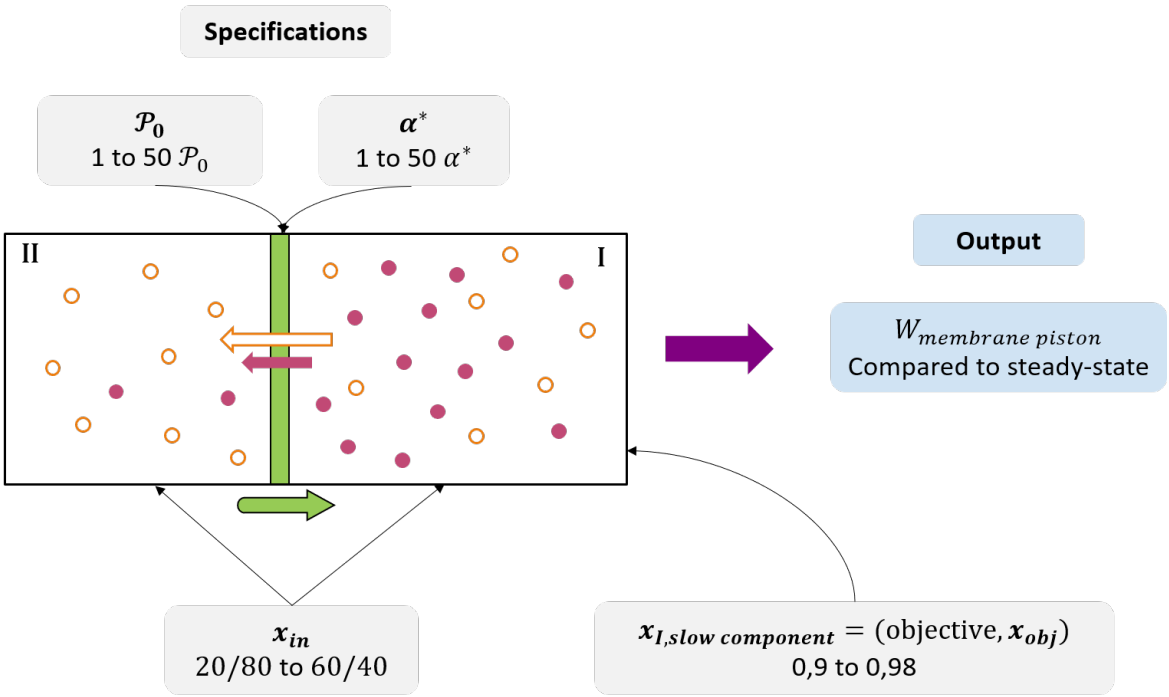


Figure 3.2 Recap of the parameters of interest in the parametric study.

Thus, five studies are performed to assess the impact of piston velocity on system performances for a fixed geometry and for different gas mixtures (see Table 3.2): the base one on the trade-off from [34], two with higher selectivity α^* at the same permeance of the fastest component $\mathscr{P}_{\text{fast component}} = \mathscr{P}_0$ and two with higher permeance and equal selectivity. This allows a broad range of possible membrane materials to be explored.

Only velocities allowing a composition in Compartment I higher than an objective composition x_{obj} equal to 0.95 of the slow component are kept. Then, following the protocol explained in section 2.1.3, a similar separation is simulated in the a steady-state module, conserving equal pressure ratio, $x_{ret,N_2} = x_{I,N_2} = 0.95$ and ensuring identical final conditions as in the previous simulation. For representation purposes, the results are plotted for each simulation corresponding to a specific piston velocity.

This part studies a set range of piston velocity variations, as too large variation fails to yield noteworthy results. It is important to note that piston velocity is necessarily in a defined range, with a low and high limit. When the piston velocity is too high, the compression and separation processes no longer occur simultaneously. This condition approaches the situation of a classical compression with impermeable walls. Conversely, at too low velocities, separation does not take place due to the too slow compression process, resulting in a series

Table 3.2 Model input parameters

Velocity range $\dot{V}$ (m^3/s)	$[1\times10^{-10},\ 1\times10^{-5}]$	
A/V ratio	0.7	
Piston body	Aluminum, $\lambda_{wall} = 240\ W\cdot m^{-1}\cdot K^{-1}$	
Isentropic efficiency (I.E.) for the compressor: η_{comp}	0.85	
I.E. for the vacuum pump: η_{vp}, from [62]	$0.1058\cdot\ln\left(\frac{P_{down}}{P_{atm}}\right)+0.8746$	
Gas mixture	O_2/N_2	CO_2/CH_4
Initial composition	20/80	40/60
Base $(\alpha^*, \mathscr{P}_0)$ (-,GPU)	$(8, 11)$	$(40, 155)$
$\frac{\alpha^*}{\alpha^*_{\text{base case}}}$	[1, 5, 50]	[1, 5, 50]
$\frac{\mathscr{P}_0}{\mathscr{P}_{0,\text{ base case}}}$	[1, 5, 50]	[1, 5, 50]

of equilibrium states instead. So, in the two cases, no separation takes place when the piston exceeds the velocity limits.

3.2.1 Air separation for Nitrogen Enriched Air

Closed mode

Figure 3.3(a) shows a significant impact of the piston velocity on the required work for unsteady-state separation: for all combinations of selectivity and permeance, the required molar work to achieve an industrially relevant nitrogen purity of $x_{N_2} = 0.95$ presents a minimum that depends on the piston velocity. This set of results shows that, for a given system geometry, it is possible to determine an optimal piston velocity for minimal work of separation. It can also be observed that this minimum is generally lower than the work required in the classical separation case used as a reference, indicating that a properly optimized unsteady-state separation could lead to substantial energy savings. Table 3.3 presents the minimum work required by the Membrane–Piston system and the lowest ratio of this work to that needed for an equivalent separation under steady-state conditions obtained across all piston velocities considered in this case study.

Selectivity has a clear influence on the quantity $\min(W_{\text{mol}}^{x_{N_2}=0.95})$, reducing the required work. This is because higher selectivity allows achieving the same final purity with lower pressure

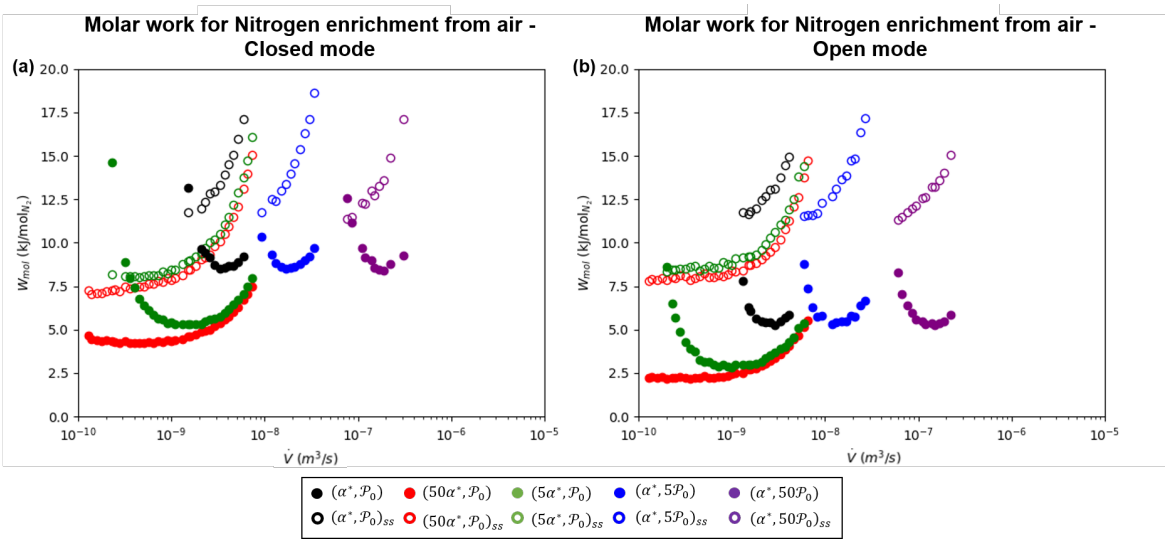


Figure 3.3 Impact of velocity, selectivity and permeability on energy requirement of the Membrane Piston for Nitrogen Enrichment. (a) Closed mode (b) Open mode. Full symbol: Membrane piston system; Hollow symbol: Steady-state following the reference process ; black: base case; red: $50\alpha^*$, green: $5\alpha^*$; blue: $5\mathscr{P}_{\text{fast component}}$; purple: $50\mathscr{P}_{\text{fast component}}$.

Table 3.3 Velocity, selectivity and permeance impact on required molar work for air separation in closed mode. SS = steady-state, referring to the classical compression then membrane module unit.

Case	$(50\alpha^*, \mathscr{P}_0)$	$(5\alpha^*, \mathscr{P}_0)$	$(\alpha^*, \mathscr{P}_0)$	$(\alpha^*, 5\mathscr{P}_0)$	$(\alpha^*, 50\mathscr{P}_0)$
$\dot{V}$ **at min**$(W_{\mathbf{mol}}^{x_{N_2}=0.95})(m^3/s)$	5.1e-10	1.6e-9	3.3e-9	1.7e-8	1.9e-7
min$(W_{\mathbf{mol}}^{x_{N_2}=0.95})(kJ/mol_{N_2})$	4.21	5.29	8.52	8.49	8.40
min$(W_{\mathbf{mol}}^{x_{N_2}=0.95}/W_{\mathbf{mol,SS}}^{x_{N_2}=0.95})$	0.5	0.49	0.54	0.52	0.54

differences. The optimal separation velocity also tends to decrease with increasing selectivity, as the molar flux is reduced, which could negatively affect the productivity of an integrated process. Moreover, as the selectivity increases, the parabola opens up and the region near the minimum broadens, offering similar performances and reducing the impact of slight velocity changes on the work. For the separation at $50\alpha^*$, the minimum is less distinct than in other cases, as the lower velocities are outside the studied range.

However, the permeance of the materials tested here shows little effect on $\min(W_{\text{mol}}^{x_{N_2}=0.95})$. In fact, for a given selectivity α^* the minimum remains relatively stable around 8.5 kJ/mol_{N_2}, suggesting that the minimal compression-separation work depends primarily on membrane selectivity. Permeance does, however, logically influence the piston velocity required to

reach the desired purity, increasing it by a factor of 60. Therefore, depending on productivity goals and available materials, it is possible to find a suitable compromise without sacrificing the advantage of the reduced energy requirements brought by the Membrane Piston. Contrary to the selectivity impact, as the permeance increases, the minimum region becomes narrower, and the work becomes more sensitive to velocity changes, amplifying the impact of even slight deviations.

It is also to be noted that the minimum ratio of Membrane–Piston molar work to the work required in steady-state operation (SS) at the same final state is consistently achieved at the highest feasible piston velocity for each case study. Conversely, lower velocities tend to result in higher energy consumption than their steady-state counterparts. This suggests that, when aiming to minimize energy requirements, increasing the piston velocity may be advantageous. This behaviour can be attributed to the influence of piston velocity on the peak pressure reached: at higher velocities, the final pressure is high, thereby increasing the energy demand in steady-state operation. In contrast, lower velocities lead to reduced end pressures, which makes steady-state operation comparatively more favourable in those conditions. This minimum is around 0.5 for all the studied cases here. This shows that the Membrane Piston system can enable a very significant reduction in energy requirement compared to the steady state operation.

Open mode

For the open mode operation, presented on Figure 3.3(b) and Table 3.4, similar trends to the closed mode can be observed: a minimum in the molar work of the Membrane Piston, a reduction of this minimum along the selectivity increase, a velocity increase as the permeance grows.

Table 3.4 Velocity, selectivity and permeance impact on required molar work for air separation in open mode. SS = Steady-state.

Case	$(50\alpha^*, \mathscr{P}_0)$	$(5\alpha^*, \mathscr{P}_0)$	$(\alpha^*, \mathscr{P}_0)$	$(\alpha^*, 5\mathscr{P}_0)$	$(\alpha^*, 50\mathscr{P}_0)$
$\dot{V}$ **at min**$(W_{\mathbf{mol}}^{x_{N_2}=0.95})(m^3/s)$	3.6e-10	1.e-9	2.9e-9	1.2e-8	1.5e-7
min$(W_{\mathbf{mol}}^{x_{N_2}=0.95})(kJ/mol_{N_2})$	2.15	2.82	5.24	5.31	5.28
min$(W_{\mathbf{mol}}^{x_{N_2}=0.95}/W_{\mathbf{mol,SS}}^{x_{N_2}=0.95})$	0.27	0.32	0.39	0.39	0.39

The main distinction between closed and open mode operations lies in the minimum molar work required. In the base case, $\min(W_{\mathrm{mol}}^{x_{N_2}=0.95})$ is 37% lower in open mode compared to

closed mode operation. This difference comes from the evolution of the driving force in both systems: in the closed mode, pressure builds up in both compartments, reducing the effective driving gradient over time.

In contrast, when compartment II is open to the atmosphere, the pressure increases only in compartment I, resulting in a more favourable pressure difference for the Membrane–Piston system at identical final states. This configuration can be particularly advantageous in applications where permeate recovery is not required, such as nitrogen enriched air, suggesting that with proper optimization of piston size and velocity, energy requirement could be significantly reduced.

3.2.2 Biogas separation

Closed mode

Biogas separation is another high-interest application for membrane processes. As for the nitrogen enrichment case, the Membrane–Piston system demonstrates promising performance, achieving 95% CH_4 enrichment with lower energy requirements, as shown in Figure 3.4. The minimum work values are summarized in Table 3.5 and exhibit trends similar to those observed in the previous case study, suggesting that this behaviour is largely independent of the feed gas composition. However, the system does not perform equally well across all material types, particularly for high permeance levels.

Table 3.5 Velocity, selectivity and permeability impact on required molar work for biogas separation in closed mode. SS = Steady-state.

Case	$(50\alpha^*, \mathscr{P}_0)$	$(5\alpha^*, \mathscr{P}_0)$	$(\alpha^*, \mathscr{P}_0)$	$(\alpha^*, 5\mathscr{P}_0)$	$(\alpha^*, 50\mathscr{P}_0)$
$\dot{V}$ **at min**$(W_{\mathbf{mol}}^{x_{N_2}=0.95})(m^3/s)$	3.7e-9	1.2e-8	2.7-8	1.4e-7	N/A
min$(W_{\mathbf{mol}}^{x_{N_2}=0.95})(kJ/mol_{N_2})$	6.59	7.38	9.04	9.02	N/A
min$(W_{\mathbf{mol}}^{x_{N_2}=0.95}/W_{\mathbf{mol,SS}}^{x_{N_2}=0.95})$	0.43	0.44	0.48	0.47	N/A

As illustrated in Figure 3.4(a), when the configuration $(\alpha^*, 5\mathscr{P}_0)$ is used, only three piston velocities within the studied range achieve the target specification of $x_{\mathrm{I},CH_4} = 0.95$, and none do so with $(\alpha^*, 50\mathscr{P}_0)$. While the velocity range considered here was intentionally broad to evaluate system performance under various operating conditions, this lack of feasible solutions in certain configurations indicates that proper system sizing remains essential, and must be tailored to membrane characteristics and feed composition. However, the energetic

performances of the Membrane-Piston system are improved compared to the classical steady-state, with a reduction of half of the molar work required to reach the purification specification in the base case. As seen previously, the minimal ratio of the Membrane-Piston molar work to its steady-state counterpart is slightly improved at higher velocity.

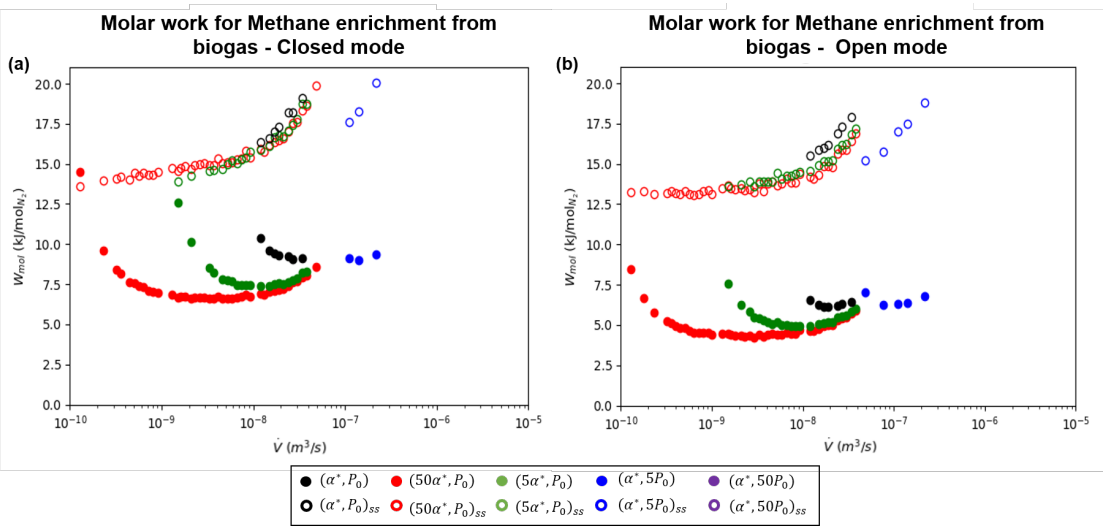


Figure 3.4 Impact of velocity, selectivity and permeability on energy requirement of the Membrane Piston for Biogas separation. (a) Closed mode (b) Open mode. See Fig 3.3 for description.

Open mode

The implementation of the open mode for biogas requires some adaptation, as the separated CO_2 needs to be confined still in an atmosphere and not vented. Therefore, the Membrane-Piston system must operate within a much larger enclosed volume that serves as an infinite sink, where the CO_2 can be contained. This volume should be large enough that the addition of the released gas does not significantly alter the molar fraction on the open side of the system. The results for such a case are presented in Figure 3.4(b) and Table 3.6. As observed in the case of air separation, the open mode offers an attractive option for reducing the minimum molar work required for separation. Specifically, it lowers the baseline case $(\alpha^*, \mathscr{P}_0)$ from 9.04 kJ/mol$_{CH_4}$ to 6.11 kJ/mol$_{CH_4}$ when achieving a methane purity of 95%. Furthermore, this mode of operation consistently requires less work compared to a steady-state process with the same final specifications. The ratio $\min(W_{\text{mol}}^{x_{N_2}=0.95}/W_{\text{mol,SS}}^{x_{N_2}=0.95})$ averages around 0.34 across the wide range of materials considered. This represents a significant improvement over the traditional steady-state system.

The trends previously observed remain evident in this case, although the reduction of the

minimum in the base case brings it closer to the minima of the other cases. As a result, the distinction is less visually apparent in Figure 3.4(b) compared to Figure 3.4(a).

Table 3.6 Velocity, selectivity and permeability impact on required molar work for biogas separation in open mode. SS = Steady-state.

Case	$(50\alpha^*, \mathscr{P}_0)$	$(5\alpha^*, \mathscr{P}_0)$	$(\alpha^*, \mathscr{P}_0)$	$(\alpha^*, 5\mathscr{P}_0)$	$(\alpha^*, 50\mathscr{P}_0)$
$\dot{V}$ **at min**$(W_{\mathbf{mol}}^{x_{N_2}=0.95})(m^3/s)$	2.9e-9	7.4e-9	1.9e-8	7.6e-8	N/A
min$(W_{\mathbf{mol}}^{x_{N_2}=0.95})(kJ/mol_{N_2})$	4.25	4.93	6.11	6.23	N/A
min$(W_{\mathbf{mol}}^{x_{N_2}=0.95}/W_{\mathbf{mol,SS}}^{x_{N_2}=0.95})$	0.32	0.34	0.36	0.36	N/A

3.3 Global parametric analysis

3.3.1 Minimal work requirement for velocity, permeance & selectivity study

From the two case studies presented before, two main conclusions arise: the permeance has little impact on the minimal work required for the separation, but only on the optimal velocity and an increasing selectivity leads to a decrease of the minimum work and of the optimal velocity. The study was thus extended to a broader range of selectivity and permeance data, ranging from $\alpha^* = 8$ to $\alpha^* = 800$, and $\mathscr{P}_0 = 5.5$ to $\mathscr{P}_0 = 1102.5$. Following the previous modus operandi, simulations on the velocity range of $[1 \times 10^{-10},\ 1 \times 10^{-5}]$ were realised for all the sets $(\alpha^*, \mathscr{P}_0)$, and the minimal value of the required molar work for an enrichment in the slow component at 95% (more enrichment objective are available in C) is noted for each set. When a sufficient number of data points are collected in a set, smoothing is applied to the minimum values to reduce sensitivity to outliers and to minimize the impact of small fluctuations arising from data processing and case selection.

On the top of Figure 3.5, an annotated version of Figure 3.3 highlights the previously discussed trends, with the minimum of each case clearly marked. These minima are then plotted on the bottom part, illustrating how the earlier cases are incorporated into this figure. For instance, the minimum for the base case discussed in Section 3.2.1, which occurs at 8.52 kJ/mol_{N_2} for a flow rate of 3.3×10^{-9} m^3/s, can be seen at the same location in Figure 3.5.

Figure 3.5 shows that the observable tendencies seen on the case studies are confirmed when expanding the ranges for both the selectivity and permeance. Initially, keeping a fixed selectivity and varying the permeance results in straight isoselectivity curves, represented by the solid lines on Figure 3.5. This means that the minimum molar work for a specified selectivity does not depend on permeance for a specified feed gas. It is accompanied by an increased piston velocity following the increase of permeance, which will impact the productivity and duration of the compression, which are not considered here.

Moreover, when the permeances are held constant and the selectivity is increased, the minimum decreases but tends to level off at high selectivity values. This suggests that, beyond a certain selectivity threshold, the membrane plays a dominant role on the separation work, reducing the contribution from piston movement and thus leading to lower velocities. For instance, doubling the selectivity from 40 to 80 results in a 10% decrease in $\min(W_{\text{mol}}^{x_{N_2}=0.95})$, whereas doubling it from 400 to 800 yields only a 2.5% reduction. This is expected as the

pressure ratio tends to be the limiting factor for high selectivity.
This work proposes a grid-like graphical tool that enables the estimation of the required energy input for a given feed composition, depending on the membrane characteristics, thus offering a wide range of possible configurations, with different output composition requirement available in Appendix C. The use of the ideal gas assumption enables generalization to all small molecules, extending the relevance of the approach to a wide range of potential industrial applications.

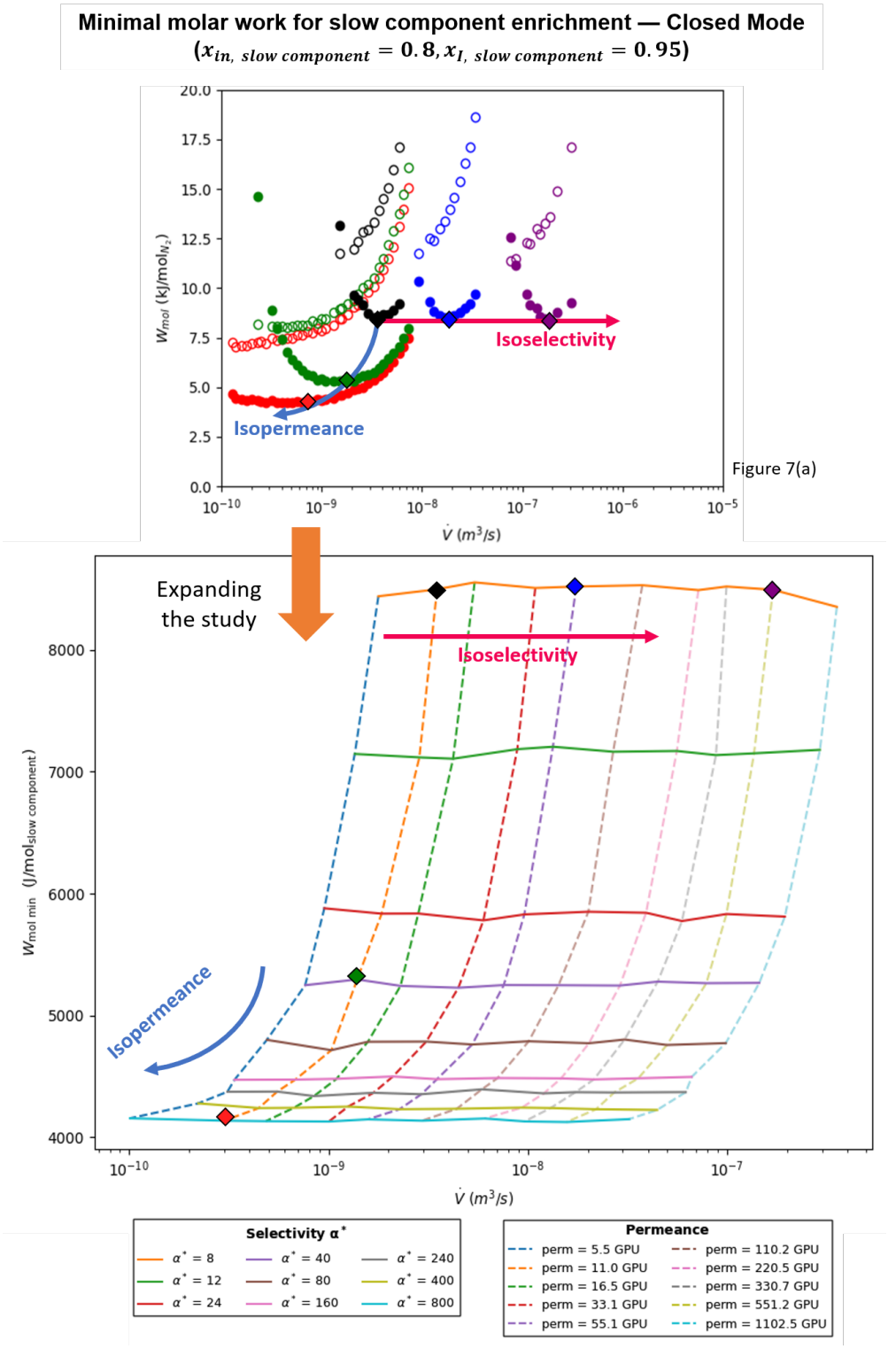


Figure 3.5 Minimal molar work for slow component enrichment in closed mode, with $x_{\text{in, slow component}} = 0.8$ & $x_{\text{I, slow component}} = 0.95$, from 5 cases to a broad range of possible materials

3.3.2 Comparison of molar work necessary for slow component enrichment to the steady-state

While observing the evolution of the minimum value of $\min(W_{\text{mol}}^{x_{N_2}=x_{obj}})$ leads to interesting performances, the most interesting challenge lies in the improvement compared to the steady-state. In the previous case studies, it was observed that the minimal $W_{\text{mol}}^{x_{N_2}=x_{obj}}/W_{\text{mol,SS}}^{x_{N_2}=x_{obj}}$ does not correspond to the velocity where $\min(W_{\text{mol}}^{x_{N_2}=x_{obj}})$ is obtained, but to a higher one. To clarify this point, two cases where selected from the ranges presented in the previous section, $(\alpha^* = 8, \mathscr{P}_0 = 11 \text{ GPU})$ and $(\alpha^* = 40, \mathscr{P}_0 = 220.5 \text{ GPU})$. Figure 3.5 recaps minimal ratio obtained for each case at different input compositions and output purities, with values available in Table 3.7. First of all, the open mode, simulated only on the case with $x_{\text{in, slow component}} = 0.8$ that corresponds to the air separation where the compartment II content can be realised to the atmosphere, can reach equivalent separation performances to its closed counterpart but with a lower ratio when compared to the steady-state, for reasons previously stated, going from around 0.5 to 0.32 when $\alpha^* = 40$ and $x_{\text{obj}} = 0.95$.

However, the Membrane–Piston system struggles when the initial concentration of the slow component is low. For instance, no solution is found at $\alpha^* = 8$ when $x_{\text{in, slow component}} = 0.4$, and even with a selectivity of 40, well beyond the typical performance of current air separation membranes [34], the system can only achieve the 90% target. Performance improves as the feed becomes richer in the slow component. However, for important concentration increases starting from low initial values, the transient system would require further optimization, particularly for parameters such as the membrane area-to-volume ratio. A multi-stage configuration, as it is usually done for classical membrane gas permeation could enhance separation performances. The Membrane–Piston system still demonstrated lower energy consumption compared to the steady-state model across a range of separation specifications, ranging in the presented case from 0.63 and going as low as 0.19 in open mode, showing the potential of this new process.

Table 3.7 Comparison of minimal molar work ratio $W_{\text{mol}}^{x_{\text{slow}}}$ for two membrane configurations

		x_{obj} for $(\alpha^* = 8, \mathscr{P}_0 = 11 \text{ GPU})$				x_{obj} for $(\alpha^* = 40, \mathscr{P}_0 = 220.5 \text{ GPU})$			
Mode	x_{slow}^{in}	0.90	0.95	0.98	0.99	0.90	0.95	0.98	0.99
Closed	0.95	–	–	0.478	0.634	–	–	0.524	0.519
Closed	0.80	0.483	0.540	–	–	0.505	0.504	0.518	–
Closed	0.60	0.591	–	–	–	0.465	0.479	–	–
Closed	0.40	–	–	–	–	0.459	–	–	–
Open	0.80	0.283	0.391	–	–	0.192	0.321	0.370	–

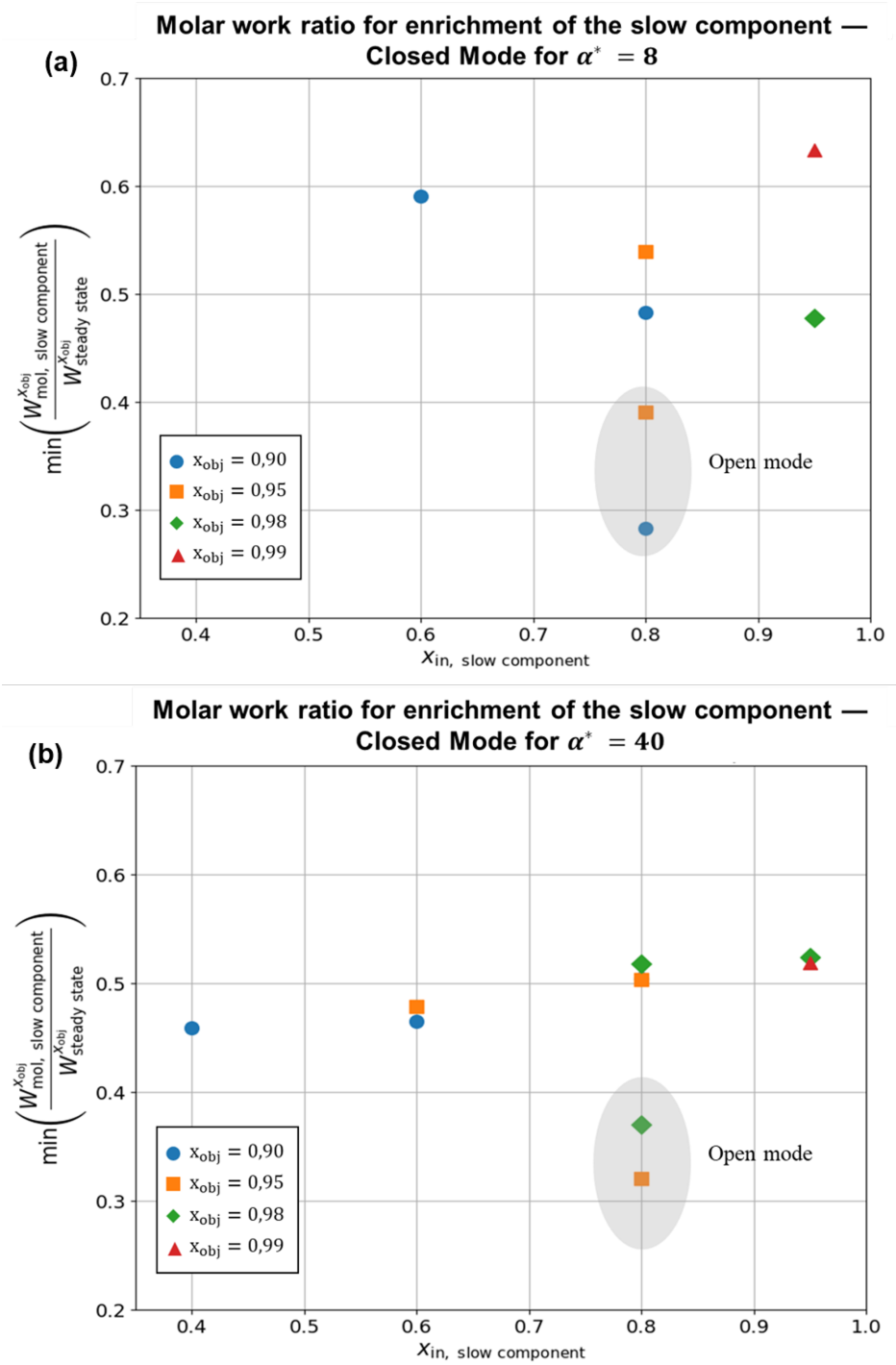


Figure 3.6 Minimal molar work ratio for different initial compositions $x_{\text{in, slow component}}$, with $x_{I,\text{slow component}} = x_{\text{obj}}$. Blue •: $x_{\text{obj}} = 0.9$; yellow ■: $x_{\text{obj}} = 0.95$; green ♦: $x_{\text{obj}} = 0.98$; red ▲: $x_{\text{obj}} = 0.99$. (a) $\alpha^* = 8$ case, (b) $\alpha^* = 40$ case.

3.4 Prospective impact of the Membrane-Piston

Until this point, the potential of the Membrane-Piston in two of the major gas permeation industry has been investigated, showing promising results for the recovery of the slow permeating component. A significant sector had not yet been given full consideration, on account of the fact that the component of interest is recovered at the permeate level: carbon capture. However, the development of new materials, reported to be N_2-selective instead of CO_2-selective, would be a game changer. This prospective analysis, comparing the transient concept to actual performances of membranes in the domain and situating both in the landscape of carbon capture, is detailed here and to be submitted.

Carbon capture has been identified as a key lever to achieve energy transition and limit global warming [63, 64]. In the midst of the multiple options possible to tackle the issue, it has been noted that post-combustion carbon capture is an interesting possibility [42, 65, 66]. While examining the overall process of CCS, carbon capture is actually the most expensive part. The various carbon capture technologies have been investigated for decades, and nowadays the consensus is that the BAT (Best Available Technology) is chemical absorption using amines [65, 67].

In the industry, the most important key performance indicator is the energy efficiency. Currently, carbon capture processes require around 2.5 GJ per tonne of CO_2 [68], through solvent formulation and process improvements [69, 70]. It seems difficult to significantly improve this energy requirement level, despite tremendous efforts [71–73]. Among the second generation technologies, post-combustion capture using membrane shows promising performances, with no chemical degradation, waste production or emission issues. The state of the art process is based on a two stages design with a recycling loop [42] with an energy requirement around 250 kWh per tonne of CO_2 for a feed containing 12% CO_2, and specifications on recovery and purity (85-95%). Despite important efforts in high performance membrane material development, no breakthrough in energy efficiency seems foreseen.

It is interesting to note that, even though the heat (from the amines absorption) to electrical power (for gas compression or vacuum in membrane technologies) conversion is subject to caution, the two processes globally reach similar energy efficiency performances (i.e. 100 kWh approximately corresponds to 1 GJ).

Historically, membrane development remained limited to CO_2 selective materials for a long time, which imply that the captured CO_2 is recovered on the low pressure side of the membrane (permeate). Since vacuum pumping is needed to respect the energy requirement constraints, an extra compression step is required subsequently for the transport and storage [42, 74]. In the recent years, N_2 selective materials, systematically based on inorganic structures have been reported. This novelty could offer interesting perspectives for energy requirement purpose [75, 76], but the impact remains to be estimated through further rigorous process simulation and optimisation studies, though it has been studied for coal-fired power plant, considering fictional membranes [76, 77].

The objective of this study is to explore the possibility to achieve drastic improvements in energy efficiency for CO_2 capture through the combined use of novel N_2 selective materials and Membrane Piston concept [17, 18]. The starting idea is to simultaneously achieve compression and separation in a single unit, so that the compression force is gradually applied to a decreasing quantity of gas. Through the use of a nitrogen selective material, CO_2 is finally recovered under pressure, which can be of major interest in a CCUS framework.

3.4.1 Results

Membrane-based processes for carbon capture often employ Polaris membranes, characterized by a selectivity CO_2/N_2 of $\alpha^* = 50$ [42]. When energy efficiency is considered as the primary optimization criterion, the most effective configuration involves the use of a vacuum pump. In this setup, the captured CO_2 is recovered on the permeate side at low pressure, as illustrated in Figure 3.7(a). The corresponding performance metrics are summarized in Table 3.8, which presents the results required to achieve a permeate stream containing approximately 80% CO_2. Under these conditions, the process exhibits an energy consumption of about 216 kWh/t_{CO2} for an 80% recovery when operating under vacuum. Notably, the use of compressors is of limited interest in this context, as CO_2 would not be effectively recovered at higher pressures due to its permeation through the membrane, while incurring a significantly higher energy cost exceeding 500 kWh/t_{CO2}.

To our knowledge, the use of reverse selectivity membrane is barely explored in literature from a process point of view [77–79]. The study benchmarks potential membrane performance, assuming permeance and selectivity targets likely attainable in the near future to propose alternatives to established capture methods, informed by existing literature on N_2 selective membranes (Appendix D). A selectivity $\alpha^* = 80$ was chosen, with multiple configurations:

- 1 stage or 2 stages

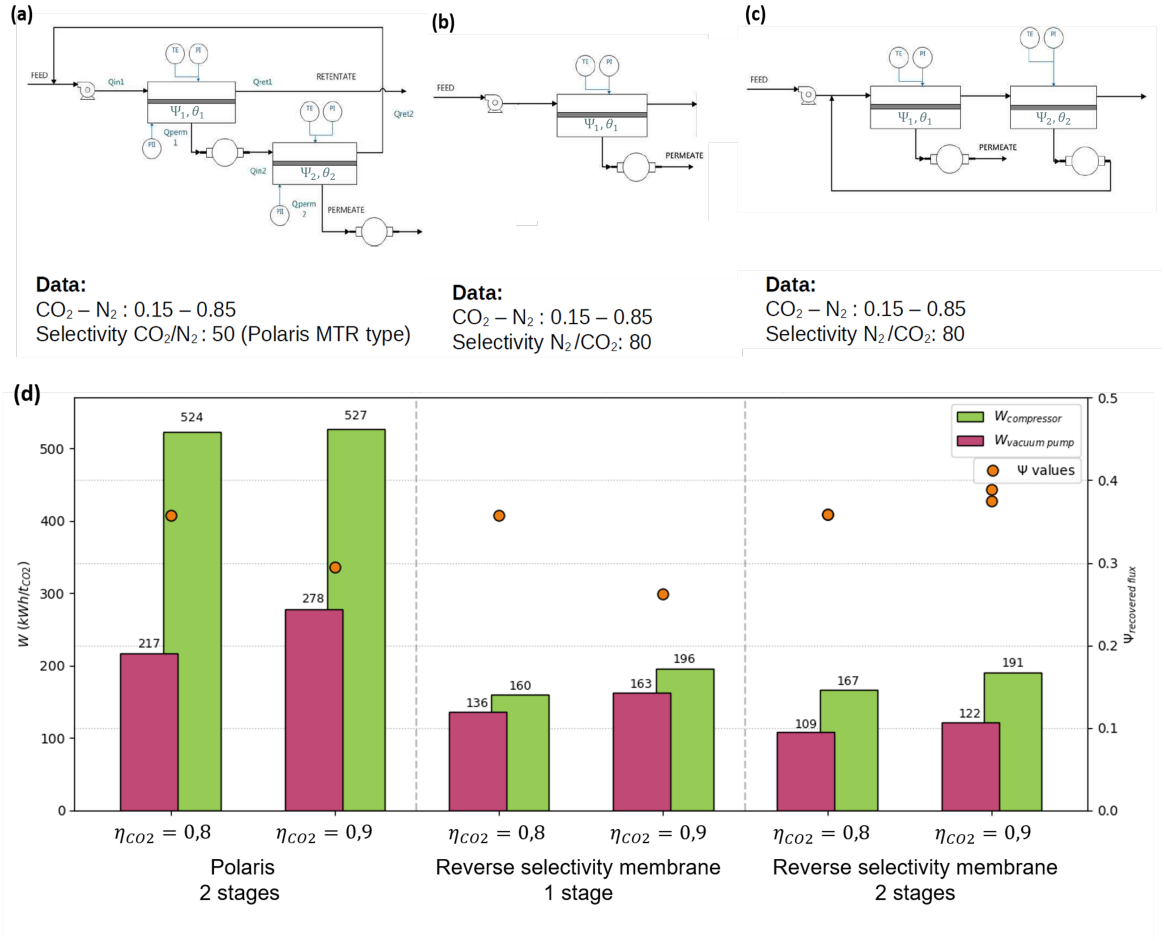


Figure 3.7 Steady-state membrane separation (a) Using Polaris Membrane with two stages (b) Using a reverse selectivity membrane with one stage (c) Using a reverse selectivity membrane with two stages (d) Final molar work for two $\eta = 0.8$ and $\eta = 0.9$ for all three cases presented. $\Psi_{recovered}$ corresponds to the pressure ratio of the stage where the CO_2 is recovered.

- Objective of CO_2 recovery of 80% or 90%
- Optimized for vacuum pumping or feed compression

Figure 3.7(b-c) shows the process diagrams for these possibilities. As in the classic Polaris case presented previously, two operations are presented in all cases, i.e. using either compressors or a vacuum pump at the same exact (Ψ, θ) for both. It emerges from this study that using two stages is more efficient, reducing the required energy to 108 kWh/t_{CO_2}, nearly half of the actual requirement of carbon capture using membrane. Using compressors, while technically being slightly less efficient at 166 kWh/t_{CO_2}, would allow the recovery of the CO_2 at the retentate and directly at a higher pressure, between 2.5 and 2.8 bar for the

described cases. Figure 3.7(d) and Table 3.8 present the condensed results of the steady-state study, with a clear improvement in energy requirement when using the reverse selectivity membrane.

Table 3.8 Performance metrics for different configurations in steady-state

	2 stages Polaris type		1 stage Reverse type		2 stages Reverse type			
$x_{recovered,CO_2}$	0.80	0.80	0.80	0.80	0.80	0.80	0.80	0.80
η_{CO_2}	0.80	0.90	0.80	0.90	0.80	0.80	0.90	0.90
ψ_1	0.12	0.11	0.36	0.26	0.67	0.60	0.68	0.61
ψ_2	0.36	0.30	-	-	0.36	0.36	0.39	0.38
θ_1	0.24	0.30	0.85	0.83	0.71	0.66	0.68	0.65
θ_2	0.56	0.48	-	-	0.57	0.59	0.62	0.63
Case: Vacuum pump only W_{vp} (kWh/t_{CO_2})	216.44	277.24	135.70	162.65	108.14	-	121.22	-
Case: Compressor only W_{comp} (kWh/t_{CO_2})	523.42	526.11	159.64	195.66	-	166.42	-	190.19

The Membrane Piston (MP) concept integrates compression and membrane separation within a single device, offering promising potential for improving the energy efficiency of carbon capture processes. The computational model follows the framework described previously and builds on earlier studies [17, 18]. In this work, the Membrane Piston operates in Open Mode, with a sink volume on the permeate side that remains unaffected by N_2 emission.

Note: Here, u defines the piston velocity in m/s, such as $u = \dot{V}/A$.

For a fixed geometry and material, the performances of the system are governed mainly by the piston velocity, as seen on Figure 3.8. Using the same ideal N_2-selective membrane as for the steady-state, the piston velocity can be optimized to reach a minimum or to respect CO_2-recovery condition. In both cases, for a recovery of 80 or 90%, the system offers a better energy efficiency, using 59 kWh/t_{CO_2} and 73 kWh/t_{CO_2} respectively. This also offers the advantage of getting the CO_2 directly at a higher pressure (5.1 and 6.2 bar respectively for 2.5 to 2.8 bar using the steady-state process). However, the operation is relatively slow, requiring piston velocities of 6.5×10^{-5} and 1.5×10^{-4} $\mathrm{m\,s^{-1}}$ to achieve 98% compression.

What about future materials improvement?

In order to anticipate the possibilities of the next materials development of N_2-selective membrane for carbon capture, since this sector is developing fast, a wider range of perfor-

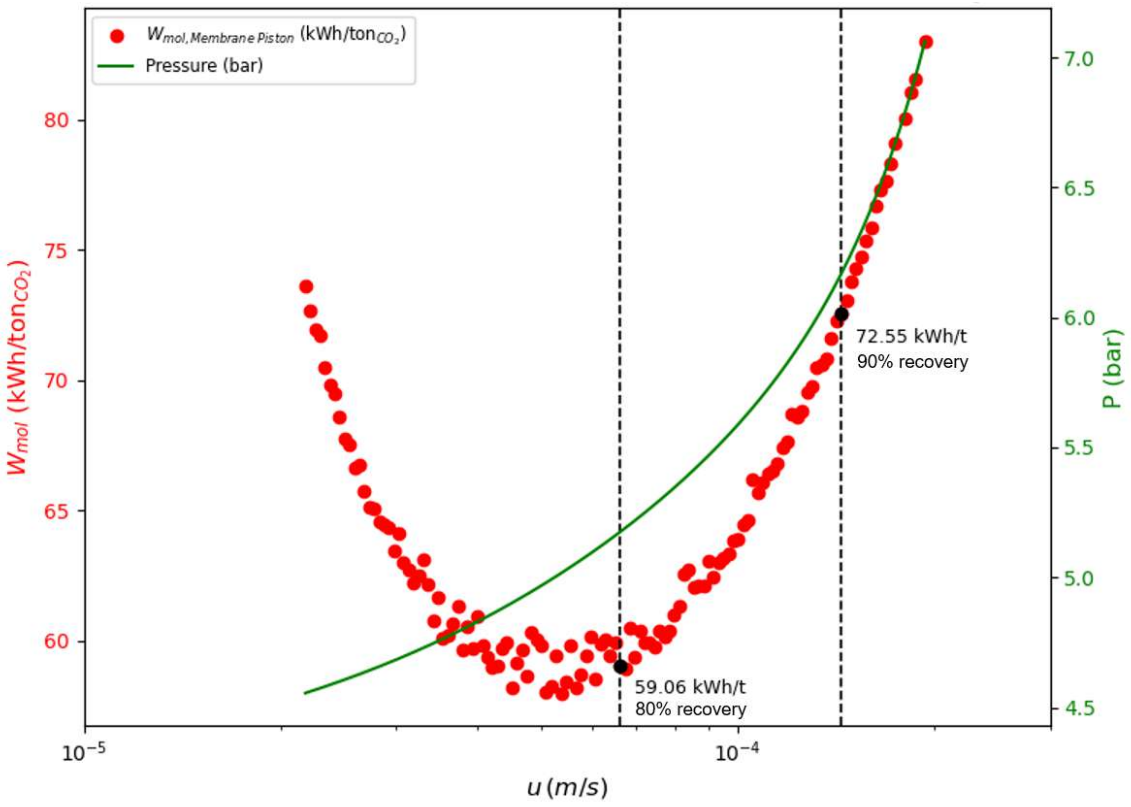


Figure 3.8 Membrane piston performances to reach 80% purity of CO_2 including the required molar work (red) to end pressure in the process (green)

mances have been envisioned for the Membrane Piston to gauge the potential and maybe guide the research on materials in a specific direction. This approach has been used in a previous paper [18], and showed consistent improvement compared to a classic steady-state process. In the cases studied here, the Membrane Piston reached equivalent performances to the two previous steady-state study, with 80 or 90% of CO_2-recovery for a purity of $x_{recovered,CO_2} = 0.8$. The selectivity and permeance in GPU were multiplied by 2.5 and 5, following the sequence of $(\alpha, \mathscr{P}_{N_2}$ (GPU)): $(400, 550)$, $(200, 550)$, $(80, 550)$ (base case presented previously), $(80, 1375)$ and $(80, 2750)$, with results represented on Figure 3.9 and Table 3.9. For higher selectivity than the one initially chosen, it is possible to both minimize the energy requirement and increase the recovery over 80%. Otherwise, it is necessary to use more than the minimum to reach the appropriate recovery. However, if the membrane are too permeable, it is not possible to reach the targeted recovery of 90% any more. In all cases where it is feasible to meet the specifications, the use of unsteady-state can lead to huge energy improvement compared to actual processes, with a requirement of 44 to

59 kWh/ton_{CO_2} compared to the 108 kWh/ton_{CO_2} at best for the steady-state at pressure between 4 and 6 bar.

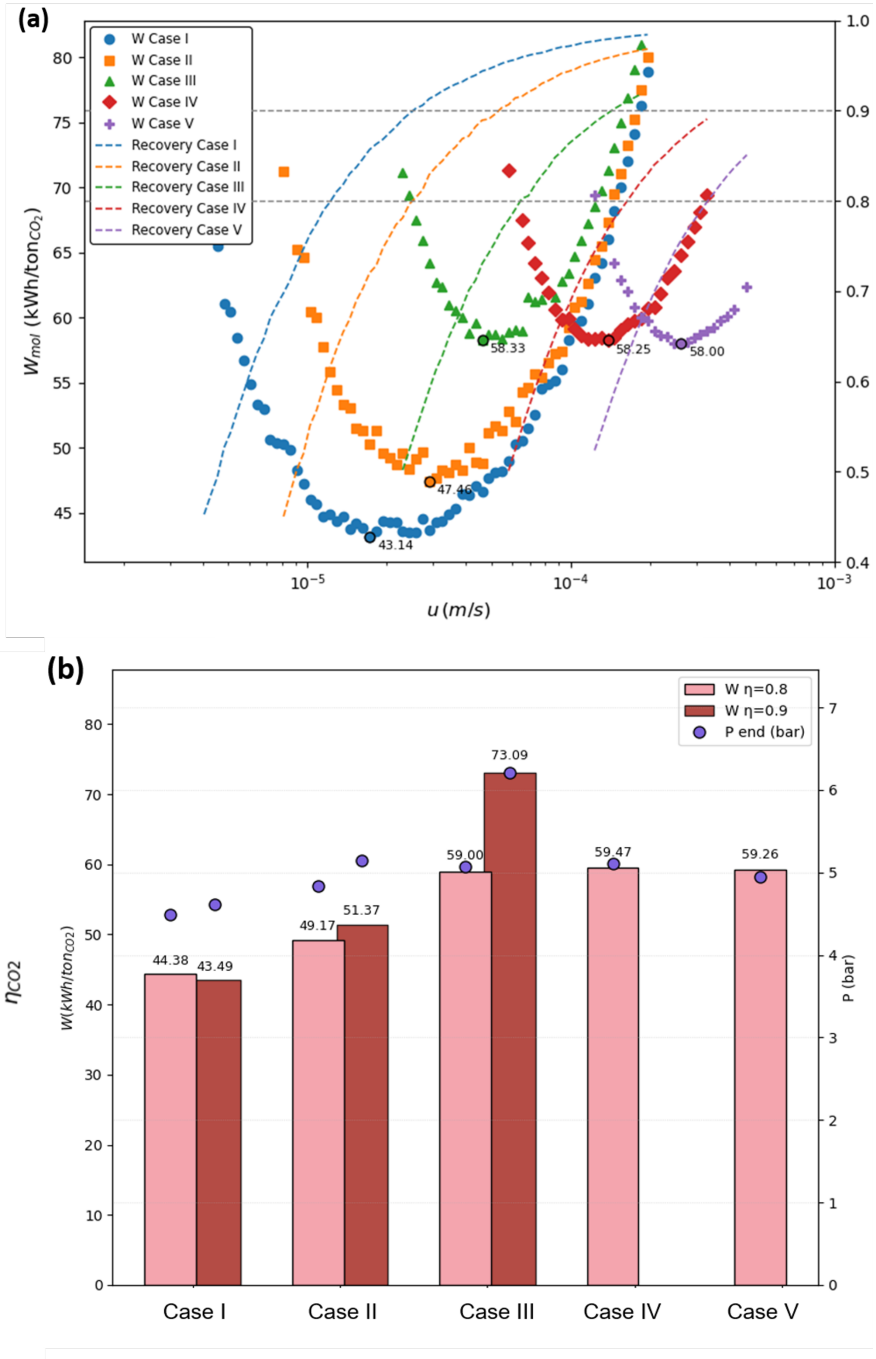


Figure 3.9 Membrane piston performances for five cases of selectivity and permeance (a) Molar work evolution compared to piston velocity with respective recovery. Label at min(W). (b) Molar work for targeted recovery compared to end pressure in the system.

Table 3.9 Performance parameters for five membrane type cases using the Membrane Piston. Upper part of the table: parameters and performances at minimum work; lower part: performances for 80 and 90% recovery

	Case I		Case II		Case III		Case IV		Case V	
$(\alpha, \mathscr{P}_{N_2}$ (GPU))	(400,550)		(200,550)		(80,550)		(80,1375)		(80,2750)	
u (m/s)	1.72E-05		2.90E-05		4.60E-05		1.38E-04		2.61E-04	
min(W) (kWh/t_{CO_2})	43.11		47.46		58.32		58.26		58.00	
η_{CO2} atmin(W)	0.86		0.83		0.73		0.77		0.76	
$P_{\min(W)}$ (bar)	4.48		4.60		4.82		4.89		4.78	
η_{CO_2}	0.81	0.90	0.80	0.90	0.80	0.90	0.80	-	0.81	-
u (m/s)	1.29E-05	2.58E-05	2.58E-05	5.48E-05	6.52E-05	1.46E-04	1.64E-04	-	3.49E-04	-
$x_{recovered,CO_2}$	0.80	0.80	0.81	0.81	0.80	0.80	0.81	-	0.80	-
P (bar)	4.49	4.61	4.84	5.15	5.07	6.21	5.11	-	4.94	-
W (kWh/t_{CO_2})	44.38	43.50	49.17	51.37	59.00	73.09	59.47	-	59.26	-

3.4.2 Discussion & Conclusion

The use of reverse selectivity membrane would allow a impressive step up in energy efficiency when focusing on Carbon Capture with membrane processes. Adding the development of new processes, such as the Membrane Piston, will help propel the use of membranes in the industry as well as make tremendous progress towards decarbonization.

The introduction of better materials is essential and relies on the expertise of materials scientists to achieve it. This will already allow for 30 to 50 % reduction of the energy requirement compared to actual membrane technologies when considering vacuum pump, and up to 69.5% if the system only uses compressors, with the added benefit of producing CO_2 at approximately 2.5 bar already. The Membrane Piston concept is an original process, out-of-the-box gas permeation system that challenges the actual glass ceiling in energetic performances. The selectivity in the process will govern minimal energy requirement, together with the optimal pressure increase velocity (piston velocity here). This process capacity logically depends on membrane permeance and specific surface area and the combined part is a huge advantage.

3.5 Conclusion

While the Membrane Piston still needs improvement, the preliminary results obtained probably call for a complete revision of compressor design. Theoretically, the concept can be extended to steady-state compressors and the energy efficiency improvement is expected to apply to any membrane gas separation process. Besides physical separation systems, the combined compression/separation approach could also be of interest for reacting systems, especially endothermic reactions showing a decreasing mole number variation. In that case, the temperature increase due to compression, the increased pressure and continuous product removal achieved by the membrane should be favorable and provide synergetic effects. The transposition of the concept to a real technological object addresses a formidable challenge, especially for post combustion capture where very large flowrates have to be treated. The major target of this study is however to draw attention to the appealing perspectives to combine compression and separation when energy efficiency improvements are aimed.

3.6 Nomenclature

Roman symbols

A	Membrane surface area	m^2
$\mathscr{P}_i$	Permeance of component i	$mol\,m^{-2}\,s^{-1}\,Pa^{-1}$
t	Time	s
u	Piston velocity ($u = \dot{V}/A$)	$m\,s^{-1}$
$\dot{V}$	Volumetric piston velocity	$m^3\,s^{-1}$
W_{mol}	Molar work	$J\,mol^{-1}$
x, y	Compositions	–

Greek letters

α^*	Ideal selectivity (permeance ratio)	–
η	Unit efficiency	–
η_{CO_2}	CO_2 recovery	–
λ_{wall}	Thermal conductivity of the piston body	$W\,m^{-1}\,K^{-1}$
ψ	Pressure ratio (P_{down}/P_{up})	–
θ	Stage cut	–

Subscripts

$comp$	Compressor
$down$	Downstream membrane interface
i	Component i
I, II	Compartment I or II in the membrane piston
up	Upstream membrane interface
vp	Vacuum pump

Acronyms

BAT	Best Available Technology
CCUS	Carbon Capture Utilisation and Storage
NEA	Nitrogen Enriched Air

Chapter 4

Experimental validation

This chapter presents the results of the experimental proof-of-concept that was built in the labortory in order to verify the model of the Membrane Piston. It includes the results obtained by two interns, Rebeca Costisor and Maxime Sturmer.

4.1 Aim of the experimental set-up

The membrane cylinder concept offers good perspective results on paper, but needs to be validated experimentally. An in-house system was constructed and operated in the lab in order to try and validate the model and the assumption made for different gas mixture of CO_2/N_2.

The difficulty of conception was the moving part. As described in Chapter 2, the original idea was to have a moving membrane that acts like a permeable wall between two compartments, with one of these that can be open or closed. However, it was not possible to create such pieces in laboratory and workshop without creating an uncertainty regarding the seal around the membrane, and thus being unable to distinguish between a leak and mass transfer between the compartments. Thus, it was decided to validate the model mainly in open mode, following the idea shown in Figure 4.1. The core concept of compression would be realised using a piston, while the membrane would be fixed at the end of this piston. This would allow the representation of one compartment with reducing volume and a permeable wall.

In the set-up, the controlled parameters are the feed composition, initial pressure and piston velocity. The model validation is focused on two variables, the pressure profile $P(t)$ and the composition. Since the composition cannot be measured at all times without creating disturbances, it will be analyzed at a defined time t.

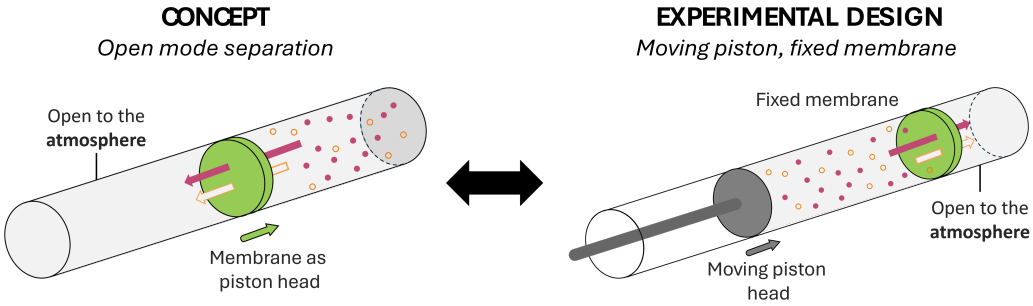


Figure 4.1 Membrane piston, from concept to experiental design

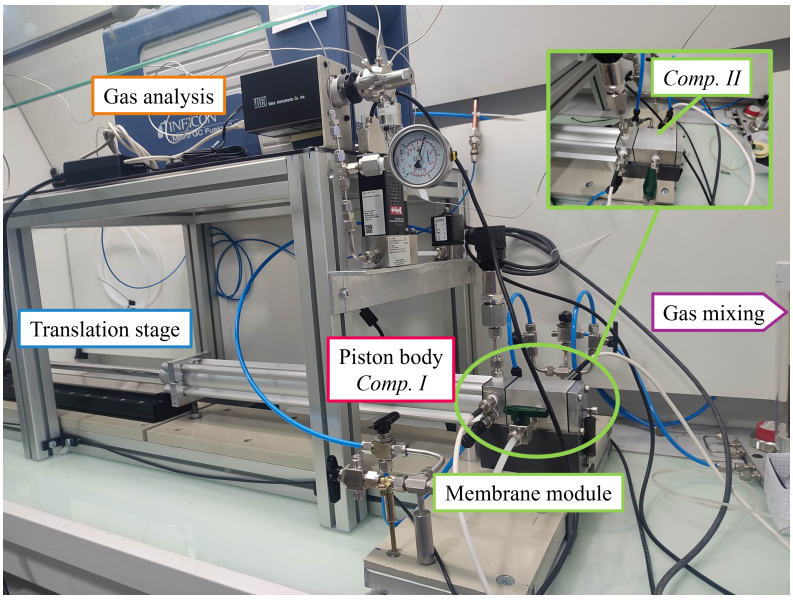
4.2 Materials

4.2.1 Experimental set-up description

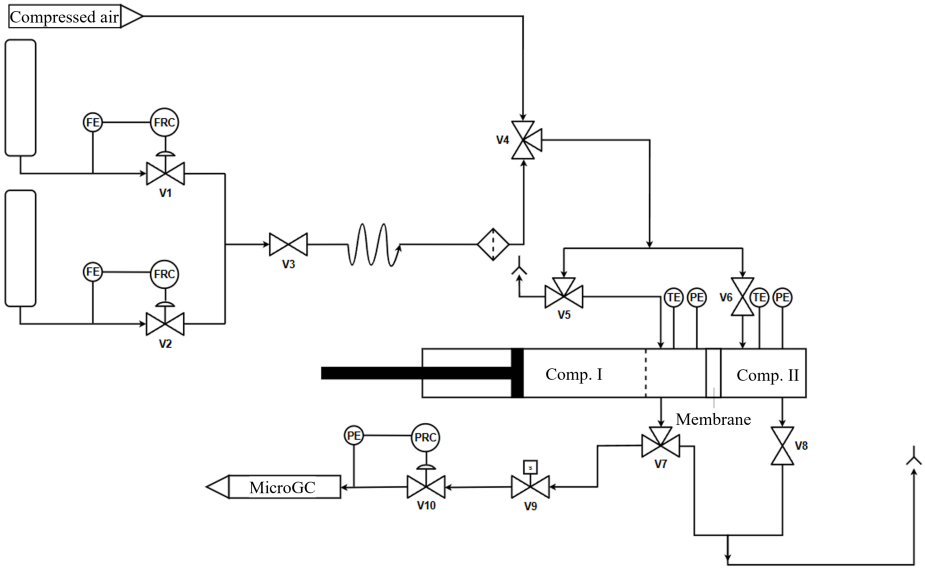
Due to the constraint explained before, the Membrane piston proof of concept is designed mainly for the open mode. To maintain the fixed composition and pressure required on the permeate side, a second compartment of fixed volume is incorporated and continuously flushed with a gas mixture identical to the feed. This approach ensures better homogenization than would be achieved under the fume hood.

Figure 4.2 presents the experimental set-up globally as well as the Process Flow Diagram. The gas coming from bottles are mixed via flow meters, and passed through a coil before being introduced on both sides of the membrane, allowing the definition of a $t = 0$ condition where no transfer occurs.

Both compartments can be fully isolated using valves V5 to V8. Compartment I is connected to a micro-GC through an electromechanical valve and a pressure–flow regulator, which controls the inlet to the analyser, while the excess gas is vented to the hood. A compressed-air feed, available via valve V4, enables leak testing without excessive consumption of pure gases.



(a) Experimental set-up picture

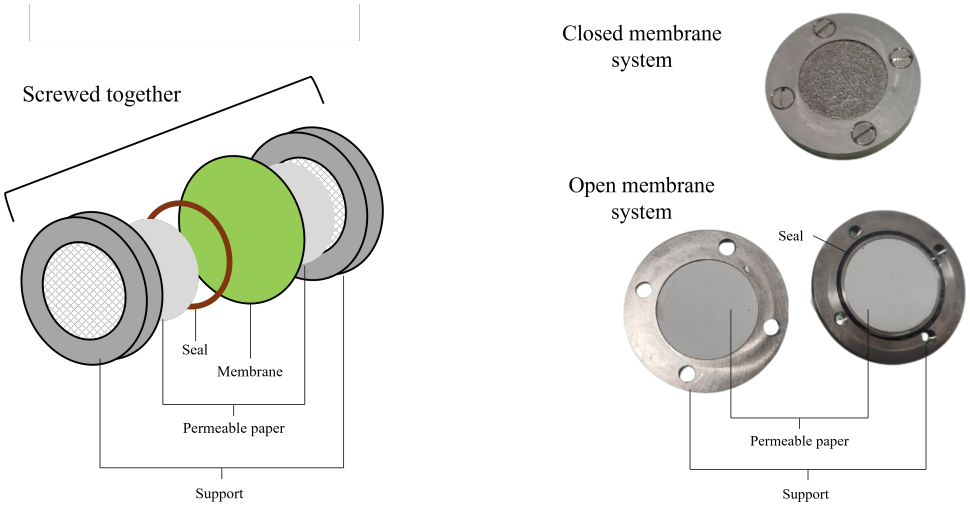


(b) Experimental set-up diagram

Figure 4.2 Experimental set-up

4.2.2 Membrane

With the membrane design fixed, the primary challenge was to develop a system capable of providing a seal that was both sufficiently robust and easy to remove and replace.



(a) Design of the membrane holder system (b) Picture of the membrane system

Figure 4.3 Membrane system

To support the membrane, two layers of permeable paper were placed over the metallic support. While the supports are fully permeable to gases, they can induce indentations in the membrane due to the alternating pressure applied on each side, which pushes the membrane back and forth. The permeable papers limits this issue.

The membrane was cut with high precision to match the geometry of the system illustrated in Figure 4.3, extending just beyond the sealing interface to ensure proper engagement and secure fastening, with a membrane diameter of 2.2 cm.

Permeance tests were conducted on the PolyActive membrane prior to performing gas mixture separations, in order to verify that its properties were still consistent with database values and to update simulations with recent measurements. In the vacuum method, used here as an example, both compartments of the membrane piston were first filled with the pure test gas to 2 bar. A vacuum pump was then connected to compartment II, creating the driving pressure difference across the membrane, while the pressure decay in compartment I was recorded over time. The permeance $\mathscr{P}_i$ was determined from the flux equation for pure gases, $\Phi_i = \mathscr{P}_i A(P_I - P_{II}) = \frac{dn}{dt}$, combined with the ideal gas law, leading to $\ln(P_I) = f(t)$ for $P_{II} \approx 0$. Prior to testing, both compartments were flushed with the target gas to ensure purity

and avoid contamination. Multiple measurement methods (vacuum, closed, and flushed compartment 2) were applied to validate the results.

Table 4.1 Permeance comparison of the PolyActive with different measurement methods compared to the lab database

Gaz	Vacuum (GPU)	Flush (GPU)	Closed (GPU)	Database (GPU)
CO_2	729.88	717.32	750.56	930
N_2	110.34	/	/	63
O_2	84.83	/	/	28

Permeance measurements were repeated on the new PolyActive^{TM} membrane, which, although aged, was tested using the three methods and compared to database values (Tables 4.1 and 4.2). An increase in permeance for CO_2, N_2, and O_2 was observed with the membrane replacement. The CO_2 permeance approached its database value, while N_2 and O_2 deviated further. This resulted in improved selectivity for the CO_2/N_2 mixture and decreased selectivity for O_2/N_2. Despite the replacement, selectivity values remained different from those in the database, indicating that the observed discrepancies are likely due to membrane aging, which altered its separation properties. Subsequent results are therefore reported using the permeance and selectivity values of the membrane after replacement.

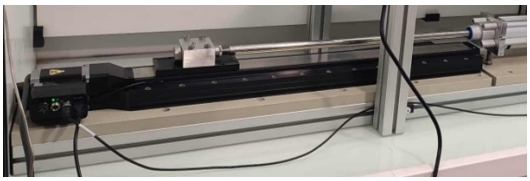
Table 4.2 Selectivity comparison of the PolyActive compared to the lab database

Gaz mixture	Vacuum	Database (GPU)
CO_2/N_2	6.6	33
O_2/N_2	1.3	2.3

4.2.3 Piston

A motorized translation stage (model [001-X-LRT0500AL-C-KX14NF]) was used to provide precise linear motion over a travel range of 500 mm. The stage operates at speeds of up to 45 $mm\,s^{-1}$ and as low as 0.000076 $mm\,s^{-1}$ and can support a maximum centered load of 500 kg. Motion control is fully managed via computer interface, enabling accurate and repeatable positioning during experiments.

An aluminium piston body, selected for its favourable heat transfer properties, with a diameter of 4 cm, was mounted on the translation stage. The piston head was subsequently modified to



(a) Translation stage



(b) MicroGC

Figure 4.4 Experimental apparatus

incorporate two successive seals and guiding rings, in order to improve alignment and ensure reliable sealing, as maintaining airtightness in moving components is inherently challenging.

Leakage in the system can be influenced by:

- Piston position (misalignment increases leakage),
- Pressure,
- Compression time.

An experimental study was conducted with an initial pressure of 1 bar (gauge) in both compartments, testing various piston positions. Results show that leakage starts when the piston reaches 300 mm.

To account for this, a loss coefficient k_{loss} was added to the original mass balance equation, which initially only considered membrane flow:

$$\frac{dn_{I,i}}{dt} = \Phi_{\text{membrane}} + \Phi_{\text{leak}} = \mathscr{P}_i A \left(P_I x_i - P_{II} x_i\right) + k_{\text{loss}} \left(P_I - P_{\text{atm}}\right) \tag{4.1}$$

The loss coefficient was determined by tuning, minimizing manually the difference between experimental data and simulation: $k_{\text{loss}} = 2.5 \times 10^{-12}\,\text{mol}\,\text{s}^{-1}\,\text{Pa}^{-1}$.

Comparisons between experimental data and simulations (e.g., with CO_2 at $0.05\,\text{mm}\,\text{s}^{-1}$) show good agreement, with similar results for different speeds and gases, including N_2 which has a lower permeance, see section 4.4.1.

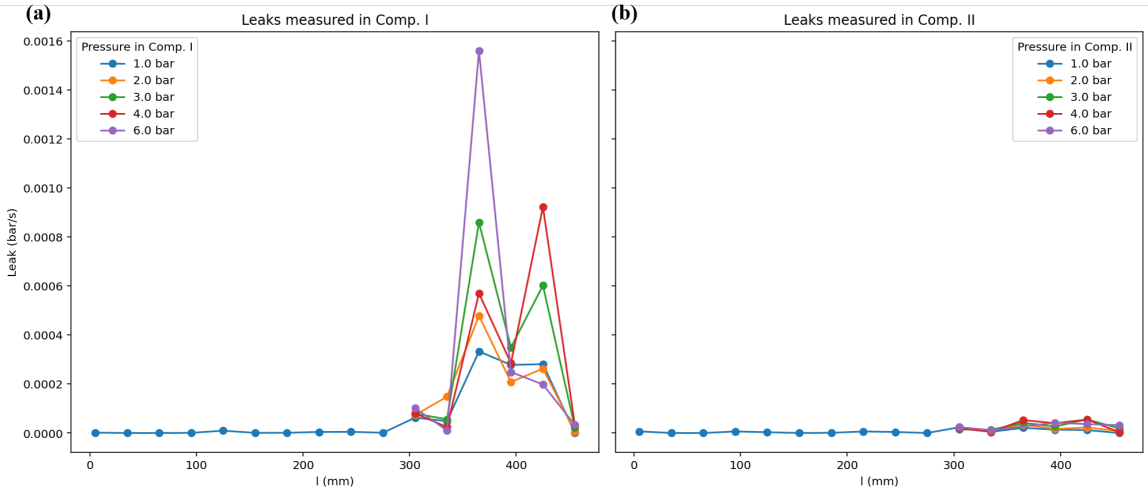


Figure 4.5 Leaks in compartments (a) I and (b) II at pressure from 1 to 6 bar gauge

4.2.4 Gas Chromatography

A micro gas chromatograph (Micro GC, Figure 4.4b) was employed for the analysis of vapors and non-condensable gases. Its operating principle is similar to that of a conventional gas chromatograph but implemented on a miniaturized platform, enabling compact and rapid measurements. The instrument separates gases according to their retention times in dedicated columns and, through prior calibration, identifies the individual components and quantifies their concentrations in the mixture. The Micro GC used in this study is equipped with two analysis modules: Module A detects O_2, N_2, CH_4, Ar, and He, while Module B measures CO_2, C_2, C_3, and other light hydrocarbons. Gas samples are introduced at pressures below 2 bar and temperatures below 100 °C, while the carrier gas (purity $\geq$ 5.5) is supplied at a constant pressure of approximately 5.5 bar. The device allows continuous monitoring via an integrated pump and is controlled directly from a computer, with data acquisition and export possible.

4.3 Methods

4.3.1 Pressure and temperature measurements

Pressure is measured directly in both compartments using pressure sensors, and recorded every second. As soon as the piston starts moving, the recording starts and a pressure history curve can be obtained.

Temperature sensosr are similarly implemented in both compartments. It is worth noting that the temperature sensor in Compartment I is situated towards the end of compartments I, close to the membrane. While this assures that the temperature of the membrane is low enough, this prevents measures in the center of the compartment, or closer to the piston head.

4.3.2 Composition measurements

Composition tests for a CO_2 and N_2 mixture in compartment I during piston displacement were carried out in the Membrane-Piston system. These tests followed the same principle as the pressure–displacement measurements, but with the piston stopped at specific positions (5 mm, 325 mm, and 380 mm). At each stop, the gas mixture was sampled and sent to the Micro GC by opening valves V7 and V9, while maintaining the loop pressure at 0.5 bar gauge through valve V10. The Micro GC provided the molar fractions of both species, which were recorded and compared with the simulations. For each displacement distance, the piston was refilled at the initial position to ensure representative compositions.
Measurements were first performed in closed mode and then in open mode, following the same operating principle described earlier.

4.3.3 Simulation framework for comparison

The equations used for simulations and comparison with the experimental set-up are based on the system presented in Section 2.2 for the Open or Closed mode, only considering a fixed volume for V_{II}.

Closed mode

$$\begin{cases} \dfrac{dn_{I,i}}{dt} = -\Phi_{membrane,i}, \quad \text{for } i \in \{1,\dots,p\} \\ \dfrac{dn_{II,i}}{dt} = \Phi_{membrane,i}, \quad \text{for } i \in \{1,\dots,p\} \\ \dfrac{dV_I}{dt} = -\dot{V} \\ \dfrac{dV_{II}}{dt} = 0 \\ \underbrace{n_I}_{\sum_i n_{I,i}} \cdot c_{v,I} \dfrac{dT_I}{dt} = -\dfrac{\lambda A}{\varepsilon_{mem}}(T_I - T_{II}) - \dfrac{\lambda_{\text{wall}} S_{\text{I, ext}}}{\varepsilon_{\text{piston}}}(T_I - T_{atm}) + P_I\dot{V} - RT_I \sum_i \Phi_{membrane,i} \\ \underbrace{n_{II}}_{\sum_i n_{II,i}} \cdot c_{v,II} \dfrac{dT_{II}}{dt} = +\dfrac{\lambda A}{\varepsilon_{mem}}(T_I - T_{II}) - \dfrac{\lambda_{\text{wall}} S_{\text{II, ext}}}{\varepsilon_{\text{piston}}}(T_{II} - T_{atm}) - P_{II}\dot{V} + RT_{II} \sum_i \Phi_{membrane,i} \\ P_I = \dfrac{n_I R T_I}{V_I} \\ P_{II} = \dfrac{n_{II} R T_{II}}{V_{II}} \end{cases} \tag{4.2}$$

Open mode

$$\begin{cases} \dfrac{dn_{I,i}}{dt} = -\Phi_{membrane,i}, \quad \text{for } i \in \{1,\dots,p\} \\ \dfrac{dV_I}{dt} = -\dot{V} \\ \underbrace{n_I}_{\sum_i n_{I,i}} \cdot c_{v,I} \dfrac{dT_I}{dt} = -\dfrac{\lambda A}{\varepsilon_{mem}}(T_I - T_{II}) - \dfrac{\lambda_{\text{wall}} S_{\text{I, ext}}}{\varepsilon_{\text{piston}}}(T_I - T_{atm}) + P_I\dot{V} - RT_I \sum_i \Phi_{membrane,i} \\ P_I = \dfrac{n_I R T_I}{V_I} \end{cases} \tag{2.30}$$

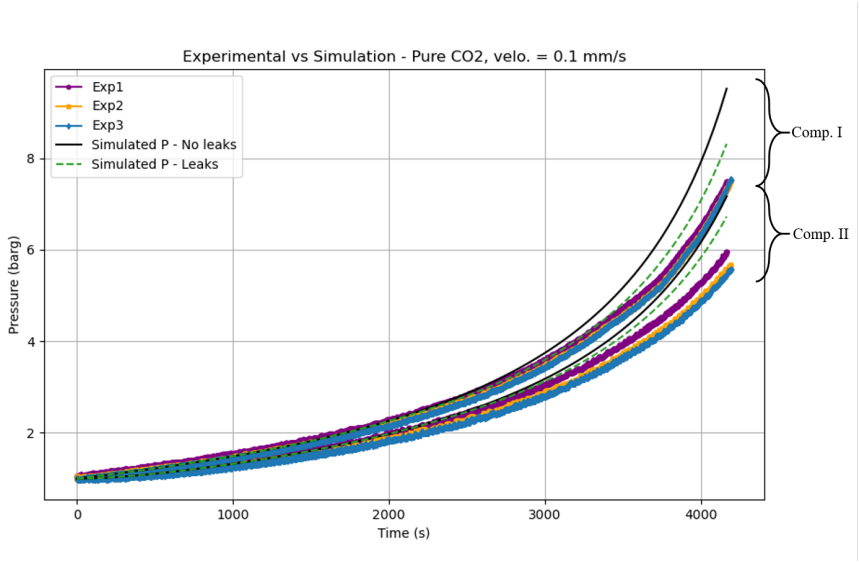
4.4 Results and discussion

4.4.1 Pressure evaluation

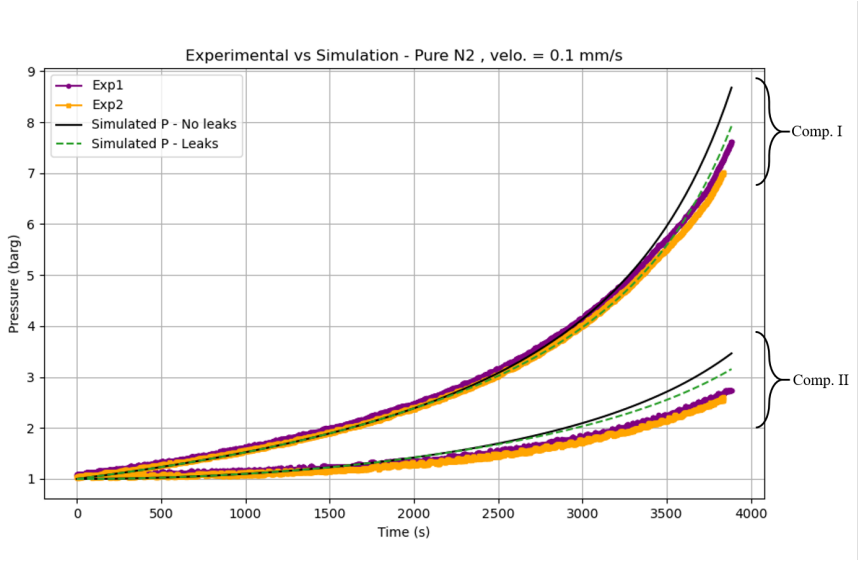
Pure Gas

As indicated in section 4.2.3, the pressure measurement simulation of the system was fitted using a leak coefficient using the closed mode. This was tested on both pure gas that were used in experimentation. Following the previously detailed methods, Figure 4.6 presents the results of experiments as well as simulation for CO_2 and N_2 .

The system shows good reproducibility for one velocity, despite the presence of leaks, with a consistently similar end pressure for multiple iterations. The leak coefficient was fitted using only compartment I on the slowest velocity (0.05 mm), since pressure measurements in compartment II indicated minimal, though still existing, leakage. At a different velocity, it can be seen that simulation and experiment are in accordance up until the system reaches $\tilde{5}$ bar gauge, corresponding also to the zone where the leaks is variable, according to 4.5.



(a) Experimental vs simulation results for pure CO_2 at piston velocity of 0.1 mm



(b) Experimental vs simulation results for pure N_2 at piston velocity of 0.1 mm

Figure 4.6 Comparison of experimental and simulation pressure values vs time for pure gas with and without leaks. Symbols: experimental data (●, ■, and ♦); solid lines: simulations without leaks; dashed lines (–): simulations with leaks.

The results for different velocities for CO_2 are displayed on Figure 4.7. Results for N_2 are available in Appendix E.

In this analysis, the system was operated in closed mode with multiple velocities, which allowed for improved monitoring of its behavior in both compartments. Two reference moments were considered: the first when the piston reached a displacement of 300 mm,

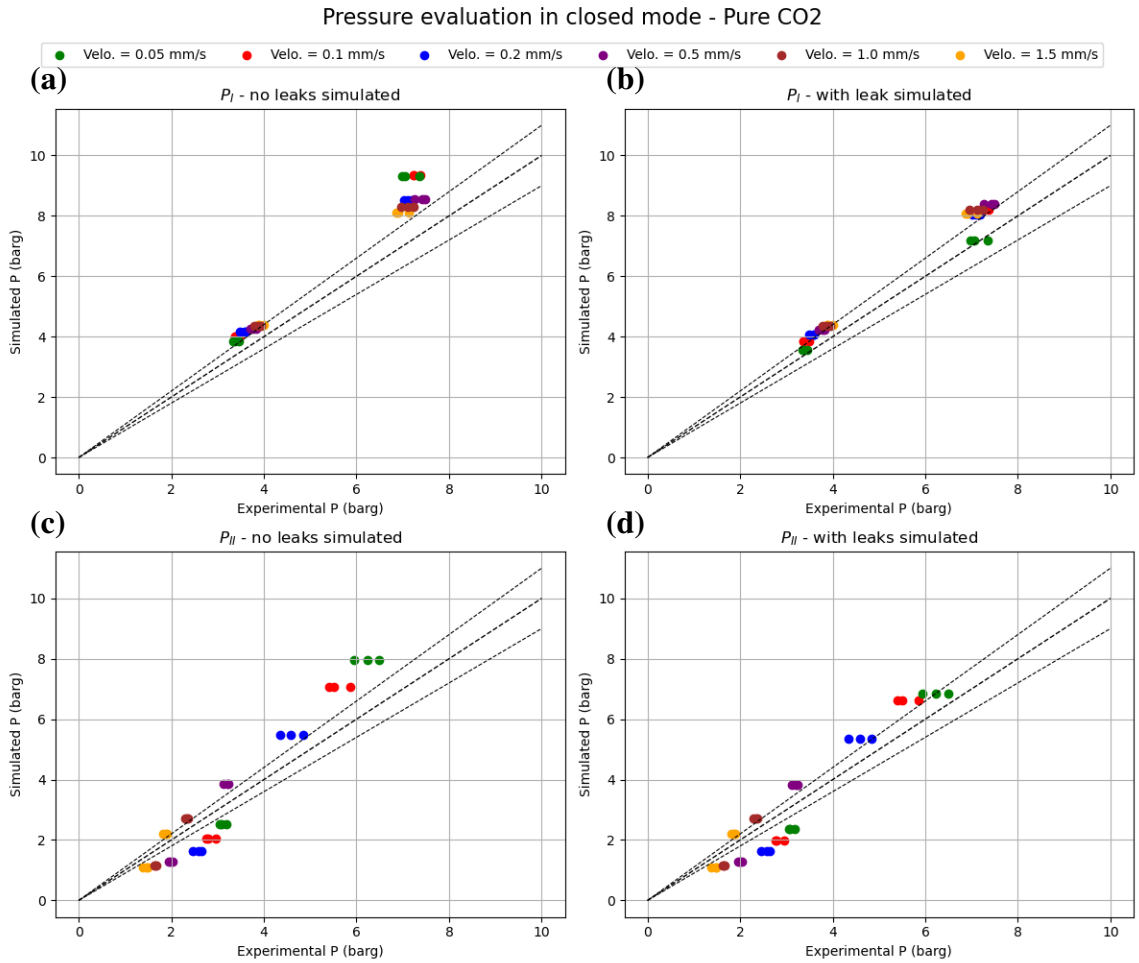


Figure 4.7 Parity plot experimental vs simulated values pressure in the Membrane Piston system at 300 mm (before the leaks) and at $t^* = 1$ (end of compression). Green: 0.05 mm s^{-1}; red: 0.1 mm s^{-1}; blue: 0.2 mm s^{-1}; purple: 0.5 mm s^{-1}; brown: 1 mm s^{-1}; yellow: 1.5 mm s^{-1} (a) Compartment I, no leaks simulated (b) Compartment I with leaks in the simulation (c) Compartment II with no simulated leaks in compartment I (d) Compartment II with leaks simulated in compartment I

corresponding to lower pressure points (around 3-4 bar gauge), and the second at the end of the experiment, at the end of compression, i.e. at the dimensionless time $t^* = 1$. This dimensionless time does not always correspond to the same end length, but rather to the moment where the system reached its maximal pressure for materials constraints. The leak coefficient reduces the error to approximately 10%. Given the detailed discussion of leakage issues previously presented, this level of error was considered acceptable for the studied system. Furthermore, the results demonstrated good reproducibility, as evidenced by the clustering of points according to color, which represents multiple trials of the same velocity.

A slightly larger error was observed in compartment P_{II}. This can be explained by the absence of a fitted leak coefficient in this region, since it was originally designed to operate in flush/open mode and little physical leaks were detected during testing.

Mixture

Two mixtures were considered: 30% CO_2/70% N_2 and 50% CO_2/50% N_2, for a range of velocities from 0.08 mm s^{-1} to 0.8 mm s^{-1}.

As seen on Figure 4.8 and consistent with the observations for the pure gas case, the measured pressures in compartment I for both mixtures remained within a 10% error interval at the two reference moments.

In compartment I, most data points remained close to the target values, indicating good reproducibility. In compartment II under closed-mode operation, some deviations were observed, which can be attributed to the absence of correction factors in this compartment. These deviations, although noticeable, can be traced back to multiple sources, as it is also important to consider experimental uncertainties in the permeance measurements, which are not directly quantifiable and tend to be more significant for gas mixtures.

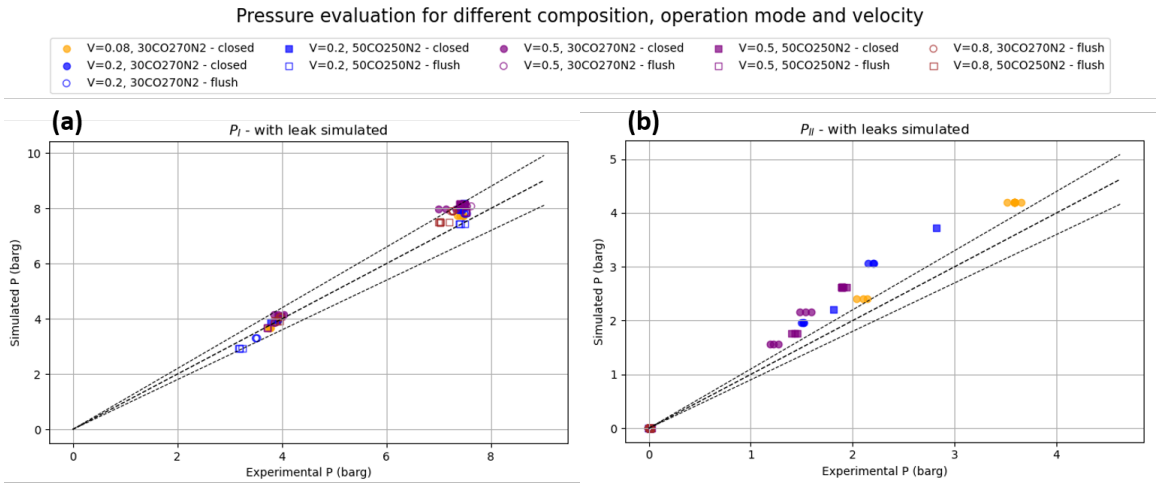


Figure 4.8 Parity plot experimental vs simulated values pressure in the Membrane Piston system at 300 mm (before the leaks) and at $t^* = 1$ (end of compression). Yellow: 0.08 mm s^{-1}; blue: 0.2 mm s^{-1} ; purple: 0.5 mm s^{-1} ; brown: 0.8 mm s^{-1}. Empty marker: flush/open mode; filled marker: closed mode. • & ○: initial composition 30%CO_2/70%N_2; ■ & □: initial composition 50%CO_2/50%N_2. (a) Compartment I with leaks in the simulation (b) Compartment II with leaks simulated in compartment I

4.4.2 Composition evaluation

Focus on one result in flush mode

Following the methods described in Section 4.3.2, the composition within the system was measured at different velocities. The requirement to reproduce each measurement multiple times, along with the need to pause the operation to perform the readings, made the acquisition of a large number of data points challenging. For this reason, the values reported here correspond to the average composition at each position, which were each calculated from three to four readings obtained with the Micro GC.

A closer examination of the flush operation shown on Figure 4.9 indicates that the observed variations in composition remain within an acceptable range of error, consistent with the behavior previously noted for the pressure measurements.

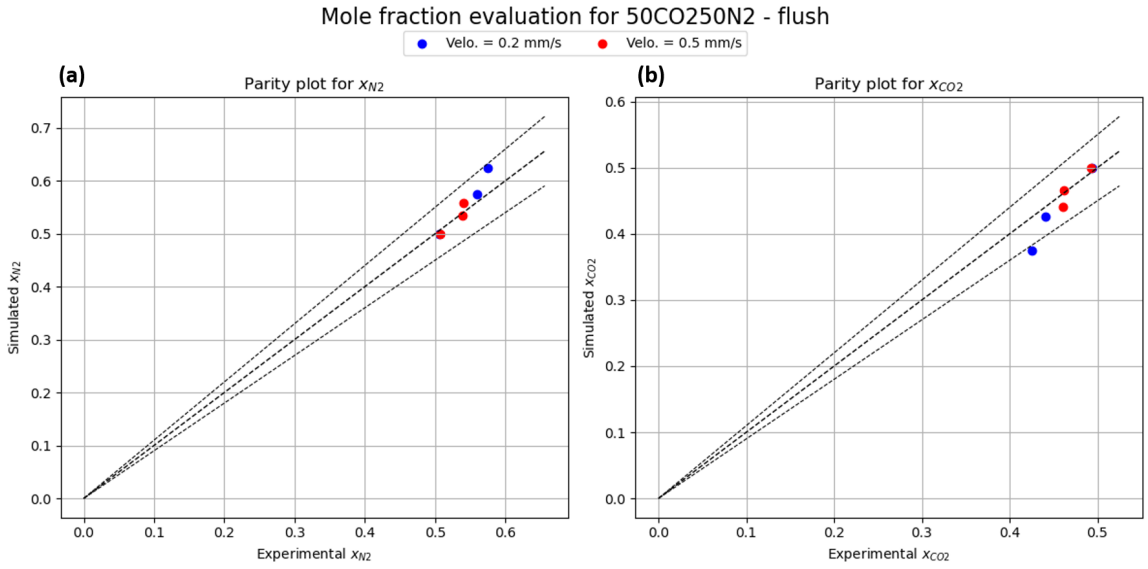


Figure 4.9 Parity plot experimental vs simulated values for molar fraction in compartment I in the Membrane Piston system at 320 mm (before the leaks) and at 375 mm (end of compression). Blue: 0.2 $mm\,s^{-1}$; red: 0.5 $mm\,s^{-1}$. (a) Composition in N_2 (b) Composition in CO_2

All composition measurement

The composition study previously described was repeated for the two initial mixtures, 30% CO_2/70% N_2 and 50% CO_2/50% N_2, at two different velocities, in both flush and closed modes. The results are presented in Figure 4.10, which summarizes all composition

measurements obtained throughout the system. The observed values remain within the expected error margins, providing encouraging support for the validity of the model, given the assumptions and limitations adopted in the modeling approach.

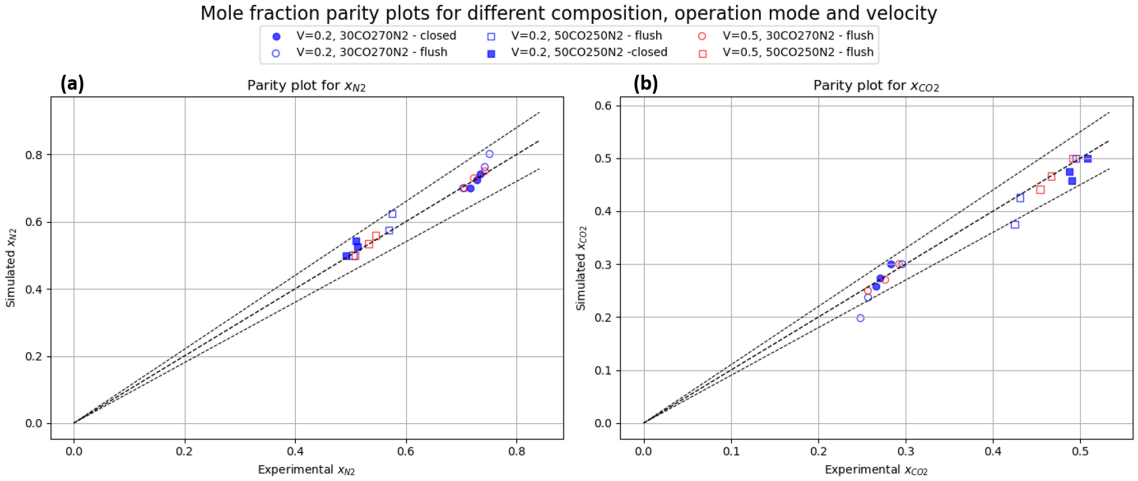


Figure 4.10 Parity plot experimental vs simulated values for molar fraction in compartment I in the Membrane Piston system at 320 mm (before the leaks) and at 375 mm (end of compression). Blue: 0.2 $\mathrm{mm\,s^{-1}}$; red: 0.5 $\mathrm{mm\,s^{-1}}$. Empty marker: flush/open mode; filled marker: closed mode. ● & ○: initial composition 30%CO_2/70%N_2; ■ & □: initial composition 50%CO_2/50%N_2. (a) Composition in N_2 (b) Composition in CO_2

Relevance of the composition measurements an possible bias

It is worth noting that the difference between the initial and final compositions, x_{ini} and x_{end}, remains small in all cases, including the simulations, with a maximum change of approximately 0.1. Consequently, it is difficult to assess the actual relevance of the measured values. The system was originally designed to operate with membranes of higher selectivity, which could not be obtained within the timeframe of the experiments. In addition, the observed leak rates were higher than anticipated. At lower velocities, the flux through the membrane becomes comparable to the flux from the leaks, limiting the ability to slow the process and resulting in only modest improvements in composition.

The challenges in obtaining accurate data are also related to the measurement procedure. When the piston reaches a given position, it is stopped, and the operator opens the necessary valves to direct the content of compartment I to the Micro GC. However, it is not possible to completely flush the connecting pipes, so residual material can influence the measurement. Moreover, due to the batch nature of the system, the measurement must be

performed promptly, preventing thorough flushing of the pipes with the compartment content. Meanwhile, pressure differences between compartments persist, and both mass transfer and leaks continue during the Micro GC analysis, causing the composition to vary.

Membrane aging, which can significantly reduce selectivity, remains poorly quantified. Although the available measurements align reasonably well with simulation results, the possibility of ongoing degradation cannot be excluded. Accurately monitoring this effect would require regular permeance measurements, which were not feasible within the timeframe of this study. Additionally, assessing the mechanical wear of the various seals proved challenging, as they underwent multiple assembly and repair cycles during the system's operation.

4.5 Conclusion

The Membrane Piston is a challenging system to implement due to its moving parts and the presence of leaks at multiple locations, which are difficult to quantify. This issue was mitigated as effectively as possible by using a fitted leak coefficient, which was verified for multiple gases and mixtures.

Pressure measurements at two positions within the piston show good agreement with the simulations in compartment I, whereas deviations exceeding 10% are observed in compartment II, likely due to non quantifiable leaks. Similar trends are observed in the evolution of the molar fraction in compartment I. To improve the agreement and fully validate the model, potential next steps include realigning the piston to reduce leaks and using membranes with higher selectivity to enhance measurable differences in composition.

Despite these limitations, as a proof of concept and the first of its kind, the operation partially validates the model, providing reasonable predictions of composition and pressure for the tested mixtures. However, as discussed in Section 4.4.2, these results should be interpreted with caution, as multiple sources of bias may influence the measurements.

4.6 Nomenclature

Roman symbols

A	Membrane surface area	m^2
d	Membrane diameter	m
k_{loss}	Leak coefficient	$mol\,s^{-1}\,Pa^{-1}$
n	Amount of substance	mol
P	Pressure	Pa
$\mathscr{P}_i$	Permeance of component i	$mol\,m^{-2}\,s^{-1}\,Pa^{-1}$
t	Time	s
x, y	Compositions	–

Greek letters

α	Selectivity (permeance ratio)	–
Φ_i	Molar flux of component i through the membrane	$mol\,s^{-1}$

Subscripts

$feed$	Feed side
i	Component i
I, II	Compartment I or II in the membrane piston
vp	Vacuum pump

Superscripts

$*$	Dimensionless or ideal quantity

Chapter 5

Efficiency analysis

Energy efficiency plays a central role in modern processes, where reducing losses is a key objective. In this chapter, the Membrane Piston is examined through the classical lens of efficiency. An entropy-based analysis provides deeper insight into the system's mechanisms and enables optimization with piston velocity as a key parameter. The results of this study is the basis of an article soon to be submitted.

5.1 Theoretical framework

From a thermodynamic perspective, the concepts of entropy generation and the minimum work of separation arise from the irreversible loss of useful (noble) energy when two distinct energy sources are brought into equilibrium. Energy is emitted when a form of energy passes from a high energetic potential to a low energetic potential (e.g., from high to low electric potential, from high to low altitude, from high to low pressure etc.). An ideal converter captures this energy and converts it into another form of energy used by an energy receptor to increase its energetic potential (e.g., the second form of energy passes from low to high electric potential or low to high altitude, low to high pressure etc.). For instance, in a hydroelectric power plant, potential energy associated with a difference of altitude (Δz) is released, $\Delta E_p = mg\Delta z$, is captured by the conversion system (turbine + alternator) and converted into electrical energy (electric charges pass then from low to high electric potential thus resulting in an electric tension ΔV_e). However, in the presence of irreversibilities, the energy derived from this Δz can only be partially converted in electricity, with the remainder dissipated as heat in the environment characterized by a uniform temperature.
Energy is called *noble* when it is associated with 2 sources and therefore 2 energy potentials.

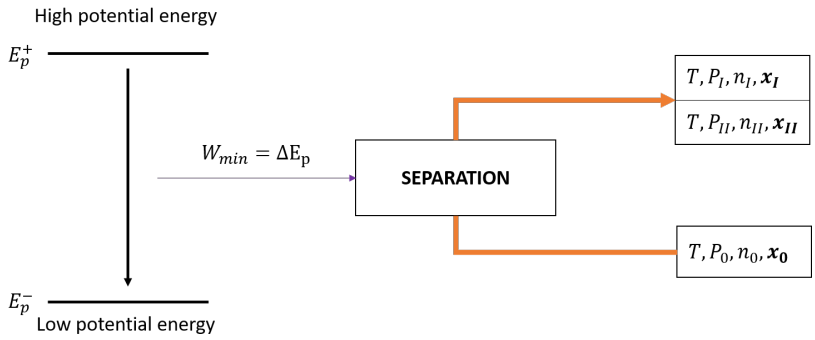


Figure 5.1 Schematic representation of the minimum work for a separation

However, when energy is converted into thermal energy at the unique temperature of the environment, it is considered as *degraded energy*.

At fixed separation objectives, as illustrated in Figure 5.1, the minimum work of separation corresponds to the quantity of noble energy required to separate an initial mixture defined by $(T, P_0, n_0, \mathbf{x_0})$ into two distinct mixtures, $(T, P_I, n_I, \mathbf{x_I})$ and $(T, P_{II}, n_{II}, \mathbf{x_{II}})$, under reversible conditions (i.e., the generated / created entropy S_c is zero).

In membrane-based separations, the transport of species is driven by a difference in partial pressures across the membrane. During this transfer, part of the driving energy is consumed and degraded, introducing irreversibilities in the process. Thus, it seems logical to try to destroy the less exergetic potential during the separation to have the less work required afterwards.

5.1.1 Estimation of the thermodynamic properties of perfect-gas mixtures

In this paragraph, we remind the expressions for the enthalpy and entropy of a perfect gas mixture. These expressions will be useful for all the developments that follow. The symbol $\bullet$ is used to indicate a perfect gas.

For a perfect-gas mixture at temperature T, pressure P and composition $\mathbf{x}$ (vector of molar fractions), the molar enthalpy is expressed as:

$$h^{\bullet}(T, \mathbf{x}) = \sum_{\text{all components } i} x_i \cdot h^{\bullet}_{\text{pure } i}(T) \tag{5.1}$$

Note that this property is pressure independent.
Similarly, the expression of the molar internal energy is:

$$u^{\bullet}(T,\mathbf{x}) = \sum_{\text{all components } i} x_i \cdot u^{\bullet}_{\text{pure } i}(T) \tag{5.2}$$

The expression of the molar entropy is given by:

$$s^{\bullet}(T,P,\mathbf{x}) = \sum_{\text{all components } i} x_i \cdot s^{\bullet}_{\text{pure } i}(T,P) \quad - R \sum_{\text{all components } i} x_i \cdot \ln x_i \tag{5.3}$$

In addition, it is recalled that the molar entropy of a pure perfect-gas at (T,P) can be expressed with respect to its molar entropy at (T,P_0):

$$s^{\bullet}_{\text{pure } i}(T,P) = s^{\bullet}_{\text{pure } i}(T,P_0) - R \cdot \ln\left(\frac{P}{P_0}\right) \tag{5.4}$$

Eventually:

$$s^{\bullet}(T,P,\mathbf{x}) = \sum_{\text{all components } i} x_i \cdot \left[s^{\bullet}_{\text{pure } i}(T,P_0) - R \cdot \ln\left(\frac{P}{P_0}\right)\right] \quad - R \sum_{\text{all components } i} x_i \cdot \ln x_i \tag{5.5}$$

5.1.2 Minimum work required for membrane separation

As mentioned in section 1.3.1, process efficiency is based on the calculation of the estimation of the minimum work of separation corresponding to a reversible process. For a binary mixture of known composition, the minimal work of separation depends on the separation considered:

- **Perfect separation:** A binary mixture, assumed to be a perfect gas at (T,P), with a total molar flow rate of $\dot{n}$ and a composition $(x, 1-x)$, feeds the separation process. At the output of this process, two pure material streams are recovered: the first stream, denoted I, contains the first pure ideal gas component at (T,P), while the second stream, denoted II, contains the second pure ideal gas component at (T,P).

  According to molar balance equations, the flow rates of streams I and II are resp. $\dot{n}_I = \dot{n} \cdot x$ and $\dot{n}_{II} = \dot{n} \cdot (1-x)$. In this separation process, the removal rate of the component of interest, defined as the ratio of the flow rate of component 1 in stream I over its flow rate in the feed, is thus equal to 1.

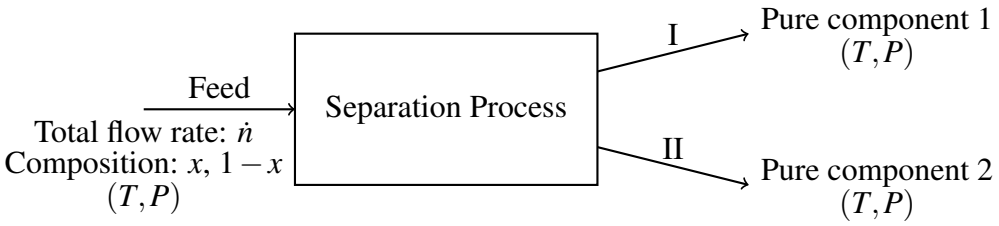


Figure 5.2 Perfect separation.

As defined, this separation process is both isothermal and isobaric. The minimum work of separation will be theoretically obtained if the separation process operates in reversible conditions. The expression of the minimal work to be provided per mole of component of interest is defined as $W_{min}^{isobaric} = \dot{W}/(\dot{n}\cdot x)$ (with $\dot{W}$, the minimal power to be provided for the separation) and has the following expression:

$$W_{min}^{isobaric} = -RT\frac{x\cdot\ln(x)+(1-x)\cdot\ln(1-x)}{x} \tag{5.6}$$

Short proof:

• Energy balance for the isothermal process:

$$\dot{W}+\dot{Q} = \dot{n}x\cdot h^{\bullet}_{\text{pure 1}}(T)+\dot{n}(1-x)\cdot h^{\bullet}_{\text{pure 2}}(T)-\dot{n}h^{\bullet}_{\text{feed}}$$

The expression of the molar enthalpy of the perfect-gas feed is: $h^{\bullet}_{\text{feed}} = x\cdot h^{\bullet}_{\text{pure 1}}(T)+(1-x)\cdot h^{\bullet}_{\text{pure 2}}(T)$. Thus, the final expression for the energy balance is: $\dot{W}+\dot{Q}=0$.

• Entropy balance for the reversible process:

$$\frac{\dot{Q}}{T} = \dot{n}x\cdot s^{\bullet}_{\text{pure 1}}(T,P)+\dot{n}(1-x)\cdot s^{\bullet}_{\text{pure 2}}(T,P)-\dot{n}s^{\bullet}_{\text{feed}}$$

The molar entropy of the perfect gas feed stream is:

$$s^{\bullet}_{\text{feed}} = x\cdot s^{\bullet}_{\text{pure 1}}(T,P)+(1-x)\cdot s^{\bullet}_{\text{pure 2}}(T,P)-Rx\cdot\ln(x)-R(1-x)\cdot\ln(1-x)$$

Finally: $\dot{W} = -\dot{Q} = -\dot{n}\cdot RT\,[x\ln(x)+(1-x)\ln(1-x)]$.

The expression for $\dot{W}/(\dot{n}\cdot x)$ can now be obtained and leads to Eq. (5.6).

- **Perfect separation with partial recovery rate of a pure stream of the component of interest:** As described previously, a binary mixture, assumed to be a perfect gas at (T,P), with a total molar flow rate $\dot{n}$ and a composition $(x,1-x)$, enters the separation

process. The molar flow rate of the component of interest is given by $\dot{n}_1 = \dot{n} \cdot x$, while the molar flow rate of the second component is $\dot{n}_2 = \dot{n} \cdot (1-x)$.
At the output of this process, two streams at (T,P) are recovered: the first stream, denoted I, consists of the component of interest in a pure perfect gas state, with a molar flow rate of $\dot{n}_1 \cdot \eta = \dot{n} \cdot x \cdot \eta$, where η represents the *recovery rate* of the component of interest. The second stream, denoted II, is a mixture composed of the remaining portion of the first component, i.e., the partial molar flow $\dot{n}_1 \cdot (1-\eta) = \dot{n} \cdot x \cdot (1-\eta)$, and the partial molar flow of the second component, $\dot{n}_2 = \dot{n} \cdot (1-x)$.

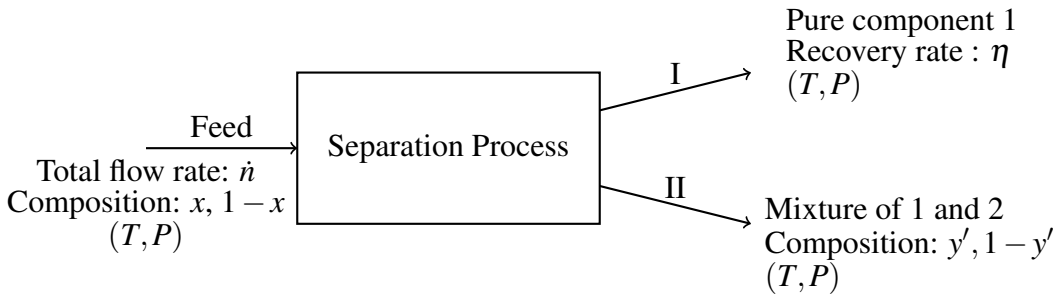


Figure 5.3 Perfect separation with partial recovery rate of a pure stream of the component of interest.

The expression of the minimal work to be provided per mole of component of interest is:

$$W_{min}^{isobaric} = -RT\left(\frac{\ln(x)}{\eta} + \frac{1-x}{x\cdot\eta}\cdot\ln(1-x\cdot\eta) + \frac{1-\eta}{\eta}\cdot\ln\left(\frac{1-x\eta}{x(1-\eta)}\right)\right) \tag{5.7}$$

Short proof:
The properties h_{feed} and s_{feed} retain the same expressions as before.
• Energy balance on the isothermal process:

$$\begin{aligned}\dot{W}+\dot{Q} &= \dot{n}_I h_I^\bullet + \dot{n}_{II} h_{II}^\bullet - \dot{n} h_{\text{feed}}^\bullet \\ &= \left[\dot{n}x\eta\cdot h_{\text{pure 1}}^\bullet(T)\right] + \left[\dot{n}x(1-\eta)\cdot h_{\text{pure 1}}^\bullet(T) + \dot{n}(1-x)\cdot h_{\text{pure 2}}^\bullet(T)\right] - \dot{n}h_{\text{feed}}^\bullet \\ &= 0\end{aligned}$$

• Entropy balance on the reversible process:

$$\frac{\dot{Q}}{T} = \dot{n}_I \cdot s_I^\bullet + \dot{n}_{II}\cdot s_{II}^\bullet - \dot{n}s_{\text{feed}}^\bullet$$

The expression of the minimal work to be provided per mole of component of interest is the ratio of the power $\dot{W}$ over the flowrate of component 1 recovered ($\dot{n}x\eta$):

$$W_{min}^{isobaric} = \frac{-\dot{Q}}{\dot{n}\eta x} = -T\frac{\dot{n}_I \cdot s_I^{\bullet} + \dot{n}_{II} \cdot s_{II}^{\bullet} - \dot{n}s_{\text{feed}}^{\bullet}}{\dot{n}\eta x}$$

with: $\dot{n}_I \cdot s_I^{\bullet} = \dot{n}x\eta \cdot s_{\text{pure 1}}^{\bullet}(T,P)$ (pure component 1 is recovered in stream I). In the stream II, the total molar flowrate is $\dot{n}_{II} = \dot{n}(1-\eta x)$. The molar fractions of components 1 and 2 in stream II are resp.: $y' = \frac{(1-\eta)x}{1-\eta x}$ and $1-y' = \frac{1-x}{1-\eta x}$. The flux of entropy of the perfect gas II is: $\dot{n}_{II} \cdot s_{II}^{\bullet} = \dot{n}x(1-\eta)s_{\text{pure 1}}^{\bullet}(T,P) + \dot{n}(1-x)s_{\text{pure 2}}^{\bullet}(T,P) - R\dot{n}x(1-\eta)\ln y' - R\dot{n}(1-x)\ln(1-y')$. The entropy flux of the feed is: $\dot{n}s_{\text{feed}}^{\bullet} = \dot{n}xs_{\text{pure 1}}^{\bullet}(T,P) + \dot{n}(1-x)s_{\text{pure 2}}^{\bullet}(T,P) - R\dot{n}x\ln(x) - R\dot{n}(1-x)\ln(1-x)$
Finally:

$$W_{min}^{isobaric} = -RT\frac{\ln x - x(1-\eta)\ln y' - (1-x)\ln(1-y') + x\ln x + (1-x)\ln(1-x)}{\eta x}$$

After some calculations, Eq. (5.7) is obtained.

- **Perfect separation with partial recovery rate of a non-pure stream of the component of interest:** The feed of the separation process is still the feed.
  At the output of this process, two streams at (T,P) are recovered: the first stream, denoted I, essentially contains the component of interest. In this stream, the molar fractions in components 1 and 2 are resp. y and $1-y$. The *recovery rate* of the component of interest is denoted η. The flow rate of component 1 in stream I is thus: $\dot{n}_{1,I} = \eta x\dot{n}$. This molar flow rate can also be expressed as $\dot{n}_{1,I} = y\dot{n}_I$. Consequently, $\dot{n}_I = \eta x\dot{n}/y$.
  The second stream, denoted II, is composed of the remaining partial molar flow rates of compounds 1 and 2, that are $\dot{n}_{1,II} = \dot{n}_1(1-\eta) = \dot{n}x(1-\eta)$ for component 1 and $\dot{n}_{2,II} = \dot{n}_2 - (1-y)\dot{n}_I = \dot{n}\cdot(1-x) - (1-y)\eta x\dot{n}/y$ for component 2. The molar fraction y' of component 1 in stream II is:

$$y' = \frac{\dot{n}_{1,II}}{\dot{n}_{1,II} + \dot{n}_{2,II}} = \frac{\dot{n}x(1-\eta)}{\dot{n}x(1-\eta) + \dot{n}\cdot(1-x) - (1-y)\eta x\dot{n}/y} = \frac{yx(1-\eta)}{y-\eta x}$$

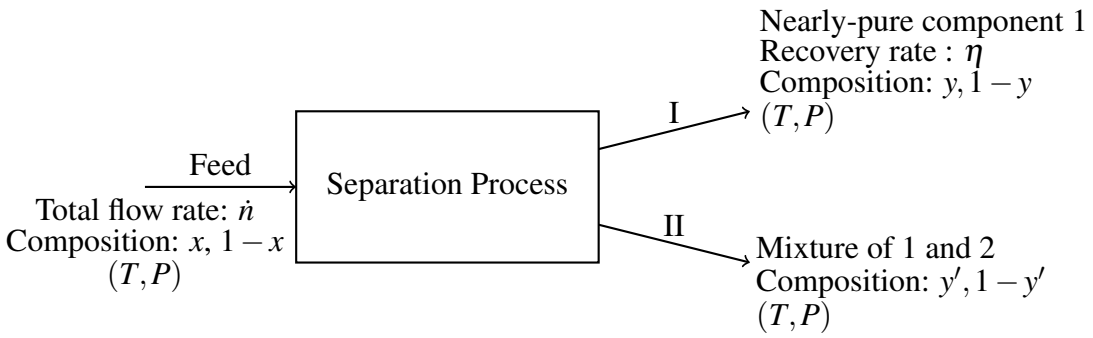


Figure 5.4 Perfect separation with partial recovery rate of a non-pure stream of the component of interest.

The expression of the minimal work to be provided per mole of component of interest is:

$$\begin{aligned} W_{min}^{isobaric} = & -RT\frac{x\ln(x)+(1-x)\ln(1-x)}{x\eta} \\ & +RT\frac{y\ln(y)+(1-y)\ln(1-y)}{y} \\ & +RT\frac{1-\frac{x\eta}{y}}{x\eta}\left(y'\ln y'+(1-y')\ln(1-y')\right) \end{aligned} \tag{5.8}$$

Short proof:
As before, the combination of the energy and entropy balances leads to:

$$W_{min}^{isobaric} = \frac{-\dot{Q}}{\dot{n}\eta x} = -T\frac{\dot{n}_I\cdot s_I+\dot{n}_{II}\cdot s_{II}-\dot{n}s_{\text{feed}}}{\dot{n}\eta x}$$

with:

- $\dot{n}_I\cdot s_I^\bullet = \dot{n}_I[y\cdot s^\bullet_{\text{pure 1}}(T,P)+(1-y)\cdot s^\bullet_{\text{pure 2}}(T,P)-Ry\ln y-R(1-y)\ln(1-y)]$, and $\dot{n}_I=\eta x\dot{n}/y$.
- $\dot{n}_{II}\cdot s_{II}^\bullet = \dot{n}_{II}[y'\cdot s^\bullet_{\text{pure 1}}(T,P)+(1-y')\cdot s^\bullet_{\text{pure 2}}(T,P)-Ry'\ln y'-R(1-y')\ln(1-y')]$, and: $\dot{n}_{II}=\dot{n}_{1,II}+\dot{n}_{2,II}=\dot{n}(1-\eta x/y)$.

The combination of all the above expressions leads to Eq. (5.8).

Similarly, for the Membrane Piston, the system path from the initial state to the final state using the minimum of work possible can be obtained through balances on mass, entropy and energy combined on the system described by Figure 5.5.

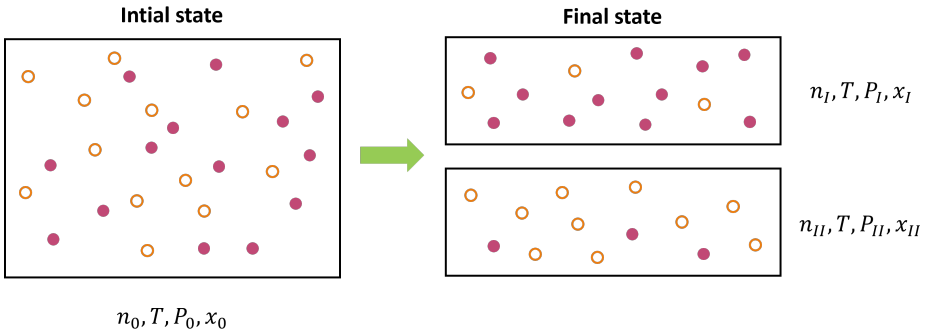


Figure 5.5 Initial and final state for separation using the Membrane Piston process

The material balance describes the distribution of the total moles between phases I and II:

Material balance

The global material balance is simply written: $n_0 = n_I + n_{II}$. Applied to component i, the material balance is :

$$n_0 x_{0,i} = n_I x_{I,i} + n_{II} x_{II,i} \tag{5.9}$$

By coupling these two equations, one obtains:

$$\begin{cases} n_I = n_0 \dfrac{x_{0,i} - x_{II,i}}{x_{I,i} - x_{II,i}} \\ n_{II} = n_0 - n_I \end{cases} \tag{5.10}$$

Energy balance

The system described in Figure 5.5 is closed. In a closed system, the energy balance involves a difference in internal energy ΔU (instead of a difference in enthalpy, as was the case for the previous systems which were assumed to be open and in steady-state).

$$W_{\min} + Q = U^{\bullet}_{\text{final state}} - U^{\bullet}_{\text{initial state}} \tag{5.11}$$

$$W_{\min} + Q = n_I u^{\bullet}_I + n_{II} u^{\bullet}_{II} - n_0 u^{\bullet}_0 \tag{5.12}$$

$$W_{\min} + Q = \sum_i u^{\bullet}_{\text{pure } i}(T) \underbrace{(n_I x_{I,i} + n_{II} x_{II,i} - n_0 x_{0,i})}_{\text{0 (material balance)}} \tag{5.13}$$

$$W_{\min} = -Q \tag{5.14}$$

with, under the perfect-gas assumption:

$$n_{I \text{ or } II} u^{\bullet}_{I \text{ or } II} = \sum_i n_{i,I \text{ or } II} \cdot u^{\bullet}_{\text{pure } i}(T) = \sum_i n_{I \text{ or } II} x_{I \text{ or } II,i} \cdot u^{\bullet}_{\text{pure } i}(T)$$

Similarly: $n_0 u^{\bullet}_0 = \sum_i n_{0,i} \cdot u^{\bullet}_{\text{pure } i}(T)$

Entropy balance

The entropy balance considers contributions from mixing, temperature, and pressure differences. The separation process is assumed to be reversible; consequently, the entropy balance does not include a term for entropy generation.

$$0 = \frac{Q}{T} + S^{\bullet}_0 - (S^{\bullet}_I + S^{\bullet}_{II}) \tag{5.15}$$

$$0 = \frac{Q}{T} + \sum_i \underbrace{n_0 x_{0,i}}_{=n_I x_{I,i} + n_{II} x_{II,i}} \left(s^{\bullet}_{\text{pure } i}(T, P_0) - R \ln x_{0,i} \right) - \sum_i n_I x_{I,i} \left(s^{\bullet}_{\text{pure } i}(T, P_I) - R \ln x_{I,i} \right) - \sum_i n_{II} x_{II,i} \left(s^{\bullet}_{\text{pure } i}(T, P_{II}) - R \ln x_{II,i} \right) \tag{5.16}$$

$$0 = \frac{Q}{T} + \sum_i \underbrace{n_I x_{I,i}}_{n_{I,i}} \left(s^{\bullet}_{\text{pure } i}(T, P_0) - s^{\bullet}_{\text{pure } i}(T, P_I) \right) - R \sum_i \underbrace{n_I x_{I,i}}_{n_{I,i}} \ln \left(\frac{x_{0,i}}{x_{I,i}} \right) + \sum_i \underbrace{n_{II} x_{II,i}}_{n_{II,i}} \left(s^{\bullet}_{\text{pure } i}(T, P_0) - s^{\bullet}_{\text{pure } i}(T, P_{II}) \right) - R \sum_i \underbrace{n_{II} x_{II,i}}_{n_{II,i}} \ln \left(\frac{x_{0,i}}{x_{II,i}} \right) \tag{5.17}$$

Using $\left(s^{\bullet}_{\text{pure } i}(T, P_0) - s^{\bullet}_{\text{pure } i}(T, P) \right) = -R \ln(\frac{P_0}{P})$, Equation 5.17 is rearraraged to obtain Equation 5.19.

$$Q = RT \left[\sum_i n_{I,i} \ln \left(\frac{P_0 x_{0,i}}{P_I x_{I,i}} \right) + \sum_i n_{II,i} \ln \left(\frac{P_0 x_{0,i}}{P_{II} x_{II,i}} \right) \right] \tag{5.18}$$

$$Q = RT \left[\sum_i \underbrace{(n_{I,i} + n_{II,i})}_{n_{0,i}} \ln(P_0 x_{0,i}) - \sum_i n_I x_{I,i} \ln(P_I x_{I,i}) - \sum_i n_{II} x_{II,i} \ln(P_{II} x_{II,i}) \right] \tag{5.19}$$

Note that, unlike the previous expressions for W_{min}, this expression accounts for the facts that (1) the initial and final pressures are different, and (2) in the final state, the two compartments are at distinct pressures. For this reason, this expression of W_{min} is now denoted $W_{min}^{\text{non isobaric}}$.

Finally,

$$\boxed{W_{min}^{\text{non isobaric}} = -RT\left[\sum_i n_{0,i}\ln(P_0 x_{0,i}) - \sum_i n_I x_{I,i}\ln(P_I x_{I,i}) - \sum_i n_{II} x_{II,i}\ln(P_{II} x_{II,i})\right]} \quad (5.20)$$

5.1.3 Entropy analysis of the Membrane Piston

The Membrane Piston concept has been investigated through heat and mass balances under strong simplifying assumptions, such as neglecting friction during membrane movement. In principle, the system could be divided into three subsystems: compartment I, compartment II, and the membrane. However, the presence of boundary layers on both sides of the membrane complicates this picture, as their compositions differ. These layers cannot be characterized reliably, since no correlation exists to estimate the actual thickness of a moving mass-transfer boundary, nor is it possible to quantify the associated heat losses. For this reason, the analysis is performed on a larger system that encompasses the membrane together with both boundary layers.

Accordingly, all limitations are attributed to the membrane itself. This results in the consideration of three systems in total, as illustrated at the top of Figure 5.6, two of which are uniform. Entropy generation therefore arises exclusively from the membrane. Furthermore, the membrane is modelled under a quasi-steady-state regime, such that During a time step dt, the amount of substance i entering the membrane is equal to the amount leaving it: $\delta n_i^{\text{in}} = \delta n_i^{\text{out}}$. Under these conditions, the composition of the matter is the same at the inlet and outlet of the membrane in steady state.

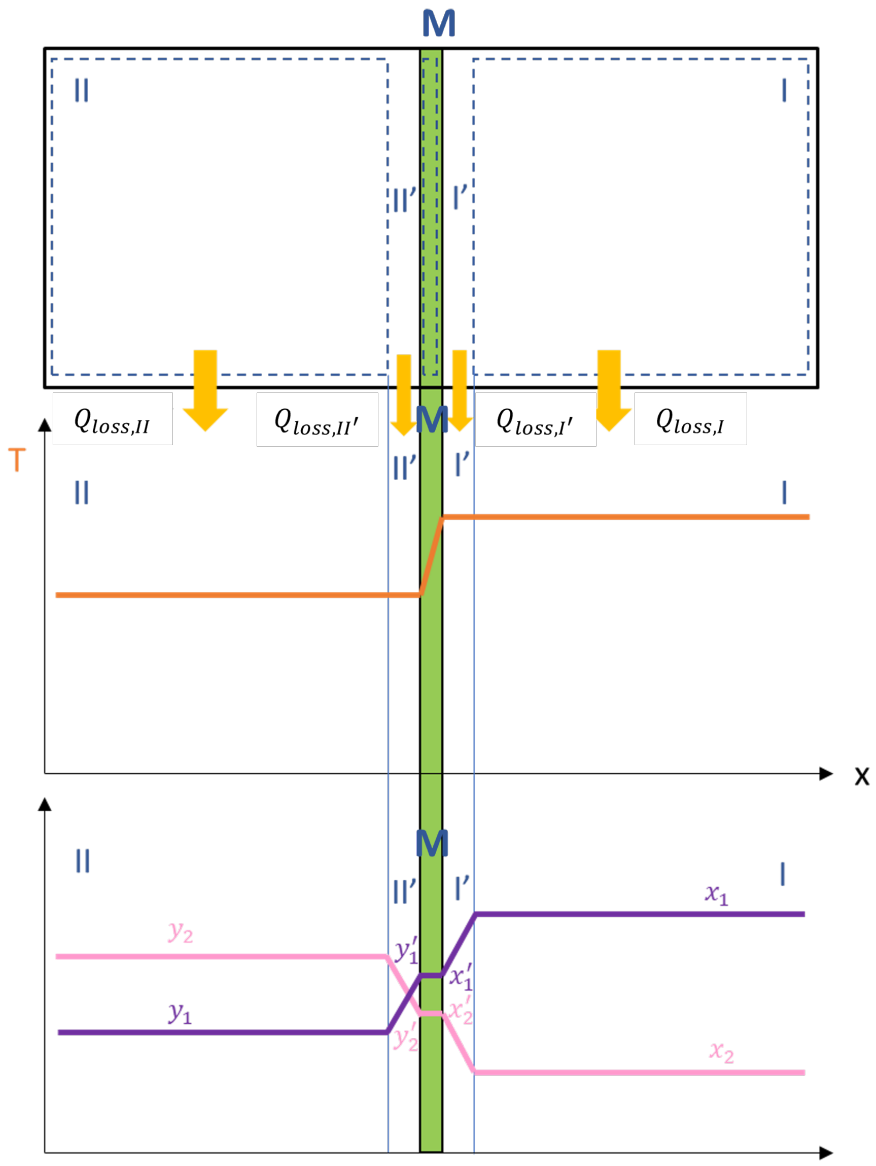


Figure 5.6 System boundaries for the entropy analysis.

Thus, for compartments I and II, which are considered uniform for a time step:

$$\frac{dS_I}{dt} = \frac{\dot{Q}_{loss,I}}{T_I} + \underbrace{\dot{S}_{c,I}}_{\substack{=0 \\ \text{uniform system}}} - \dot{n}_I \cdot s_I^{\bullet} \tag{5.21}$$

$$\frac{dS_{II}}{dt} = \frac{\dot{Q}_{loss,II}}{T_{II}} + \underbrace{\dot{S}_{c,II}}_{\substack{=0 \\ \text{uniform system}}} + \dot{n}_I \cdot s_I^{\bullet} \tag{5.22}$$

Where $\dot{n}_I \cdot s_I^\bullet$ represents the entropy flux convected by matter, leaving compartment I and entering compartment II.
In the previous chapters, we highlighted the near uniformity of temperature in the system when the membrane is assumed to be non-adiabatic. It is thus assumed that: $T_I = T_{II}$, denoted T.
The partial molar flow rate is denoted of a substance i is denoted $\dot{n}_i$. When focusing on the system $M' = M + I' + II'$ (membrane + boundary layers around it):

$$\underbrace{\frac{dS_{M+I'+II'}}{dt} = 0}_{\text{quasi-steady-state regime}} = \sum_i \dot{n}_i \left(s_i^\bullet(T,P_I) - R\ln x_{I,i}\right) - \sum_i \dot{n}_i \left(s_i^\bullet(T,P_{II}) - R\ln x_{II,i}\right) + \dot{S}_c \quad (5.23)$$

$$= \sum_i \dot{n}_i \left[s_i^\bullet(T,P_I) - s_i^\bullet(T,P_{II})\right] - R\sum \dot{n}_i \ln\left(\frac{x_{I,i}}{x_{II,i}}\right) + \dot{S}_c \quad (5.24)$$

$$= \sum_i \dot{n}_i \left[-R\ln\left(\frac{P_I}{P_{II}}\right)\right] - R\sum \dot{n}_i \ln\left(\frac{x_{I,i}}{x_{II,i}}\right) + \dot{S}_c \quad (5.25)$$

The final expression of the total flux of entropy created $\dot{S}_{c,\mathrm{TOT}}$ in the Membrane Piston is given by:

$$\boxed{\dot{S}_{c,\mathrm{TOT}} = -R\sum_i \dot{n}_i \ln\left(\frac{P_{II}x_{II,i}}{P_I x_{I,i}}\right)} \quad (5.26)$$

It does correspond to the expression of entropy given by Hwang for binary gas separation [53].

5.1.4 Optimization framework

In order to optimize the efficiency of the Membrane Piston, the velocity profile is treated as a control parameter. The objective of this optimization is to minimize the entropy generation function derived above in Equation 5.26 as well as the molar work, by appropriately adjusting the piston velocity during compression in order to compare the improvement in the system.

As a first approach, the piston is divided into several sections of equal length. Within each section i, the velocity (defined as the volume displaced by the piston per unit time) is assumed constant, forming a plateau described by:

$$\dot{V}_i = c_i \cdot \dot{V}_{ini} \quad (5.27)$$

where $\dot{V}_{ini}$ is the initial velocity and c_i is a scaling coefficient applied to section i. Five potential coefficients $(1/3,\ 1/2,\ 1,\ 2,\ 3)$ were selected as a first approach in order to introduce significant variations in the piston velocity and assess their influence on system performance. This discretization provides an initial approximation of the velocity profile that can later be refined. $\dot{V}_{ini}$ is selected within the realm of velocity allowing to reach a sufficient purity in nitrogen at 95% and is independently discussed in each study.

Consequently, the total compression time depends on the velocities $\dot{V}_i$ of all sections i of the velocity profile and is expressed as:

$$t_{comp} = \sum_i t_i = \sum_i \frac{l \cdot A}{\dot{V}_i} = \sum_i \frac{l \cdot A}{c_i \cdot \dot{V}_{ini}} \tag{5.28}$$

with l the section length and A the piston cross-sectional area.

In the following studies of an Air separation, the piston geometry, membrane properties and process variables are fixed and described in Table 5.1:

Table 5.1 Fixed parameters and geometry for the piston optimization study.

Parameter	Value
Initial volume V_I	1.0×10^{-3} m^3
Piston diameter d	0.05 m
Membrane selectivity (trade-off [34])	8
Gas mixture	Air separation (20 % O_2 / 80 % N_2)
Temperature T	293.15 K
Initial pressure P_I	101325 Pa

5.2 Results and discussion

5.2.1 Membrane Piston efficiency

Traditionally, the computation of $W_{\min}$ is performed for an isobaric process using Equation 5.8. This equation has the drawback of not accounting for the fact that the mixtures produced by the separation process are not at atmospheric pressure and have a higher exergy value because they are under pressure. We consider the minimum separation work to be the work required both to separate the mixture and to produce mixtures under pressure. For this reason, we will use equation 5.20 to express the minimum separation work. The separation efficiency is defined as $\eta_{eff} = W_{\min}/W_{\text{mol}}$.

Figure 5.7 presents the results obtained for the studied case, comparing the molar work of separation and the corresponding efficiencies, $\eta_{eff}^{\text{isobaric}}$ and $\eta_{eff}^{\text{non-isobaric}}$. For an identical product purity ($x_{I,\text{N}_2} = 0.95$), the efficiency relative to the non-isobaric reversible separation ranges between 0.25 and 0.5, which is significantly higher than typical steady-state membrane separations (approximately 0.04 [4]). Conversely, when the molar work is compared to $W_{\text{min}}^{\text{isobaric}}$, the efficiency returns to the expected range of 0.03–0.05. Regarding the molar work, and consistent with the observations discussed previously in Section 3.2, the piston velocity must be optimized to achieve the targeted performance. The screening was carried out for velocities ranging from $1 \times 10^{-9}\,\text{m}^3\,\text{s}^{-1}$ to $1 \times 10^{-5}\,\text{m}^3\,\text{s}^{-1}$, although only a subset of these velocities reaches $x_{N2} = 0.95$. The minimum molar work is obtained at a velocity of approximately $1 \times 10^{-8}\,\text{m}^3\,\text{s}^{-1}$. The data points are not perfectly aligned because the system occasionally reaches a slightly higher nitrogen purity (e.g., $x_{\text{N}_2} = 0.950$ versus 0.951), depending on the chosen step size.

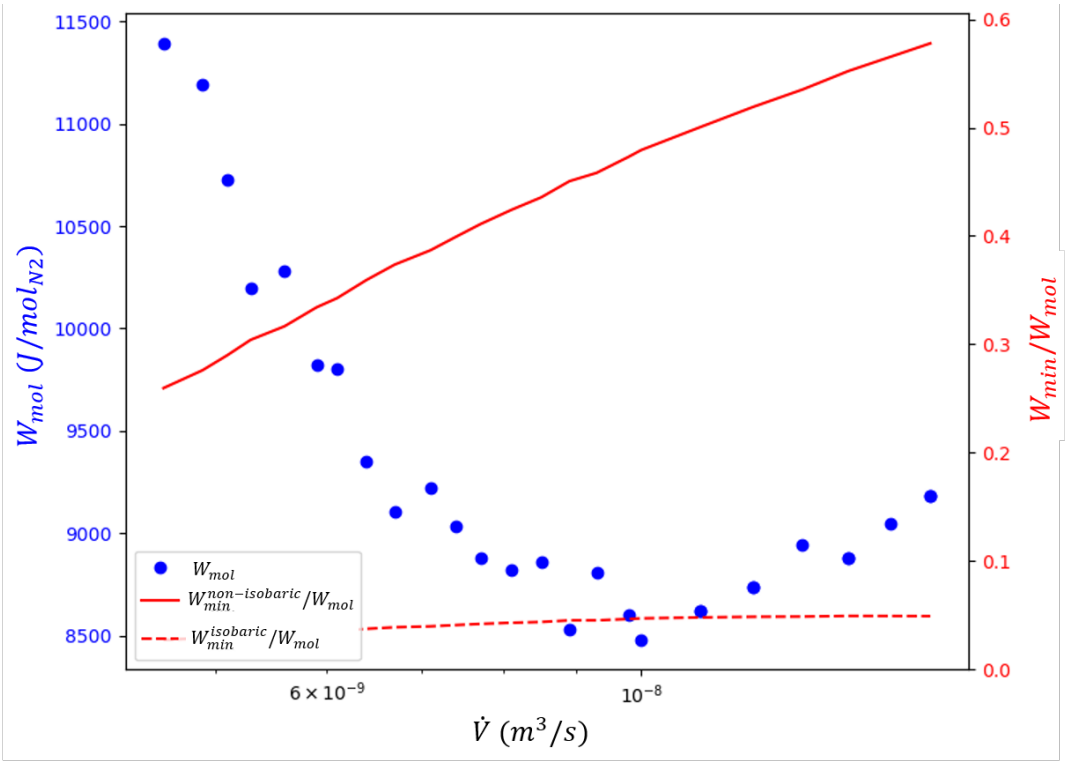


Figure 5.7 Molar work and Membrane Piston efficiency for multiple velocities for a fixed output of $x_{I,N_2} = 0.95$ for air separation

As the piston velocity increases, the recovery also rises for a fixed outlet composition, which in turn affects the minimum work required to achieve these specifications.

5.2.2 Optimization of the system

The optimization of the piston was considered first in terms of increasing and decreasing the velocity compared to the initial velocity, to gauge the impact of this variation on the system.

Impact of velocity variations

This study investigates the impact on entropy generation, work, and the recovery of N_2 of the possible velocity profiles within a fixed-length section, namely:

- Constant velocity (which was done up until now)
- Acceleration
- Deceleration
- Acceleration followed by a deceleration, i.e. a velocity pulse

Each velocity profile influences the flow differently, affecting the energy transfer, dissipation, and overall efficiency of nitrogen recovery in the section. By analysing these cases, the effects of velocity variations on entropy generation and work can be systematically understood.

Figure 5.8 helps to outline the main trends according to the piston speed profile. This figure presents the results of the study, showing three simple cases designed to evaluate the impact of the velocity profile on performance. It is important to note that both acceleration and deceleration significantly affect entropy and the work required for the separation. This is attributed to the large differences in compression time associated with these operations, which lead to a reduction in separation performance. As illustrated in Figure 5.8(d), these two cases (acceleration and deceleration, see the blue and red lines) do not reach the $x_{I,N_2} = 0.95$ threshold used in the previous study as a standard. This behavior is linked to the prior optimization of the constant velocity case, which serves as a reference case with optimized performance. Additionally, the oxygen composition in compartment II as well as the nitrogen recovery in (Figure 5.8(f)) are both increased when the piston accelerates.

As a first conclusion, it appears that, for a given initial velocity, the increase in generated entropy is correlated with the increase in molar work across all velocity profiles as clearly evidences by Figure 5.9. Acceleration seems to be the most favorable approach when starting from the optimized velocity, as it minimizes both entropy generation and work. However, as mentioned previously, this also leads to a reduction in separation performance. Further

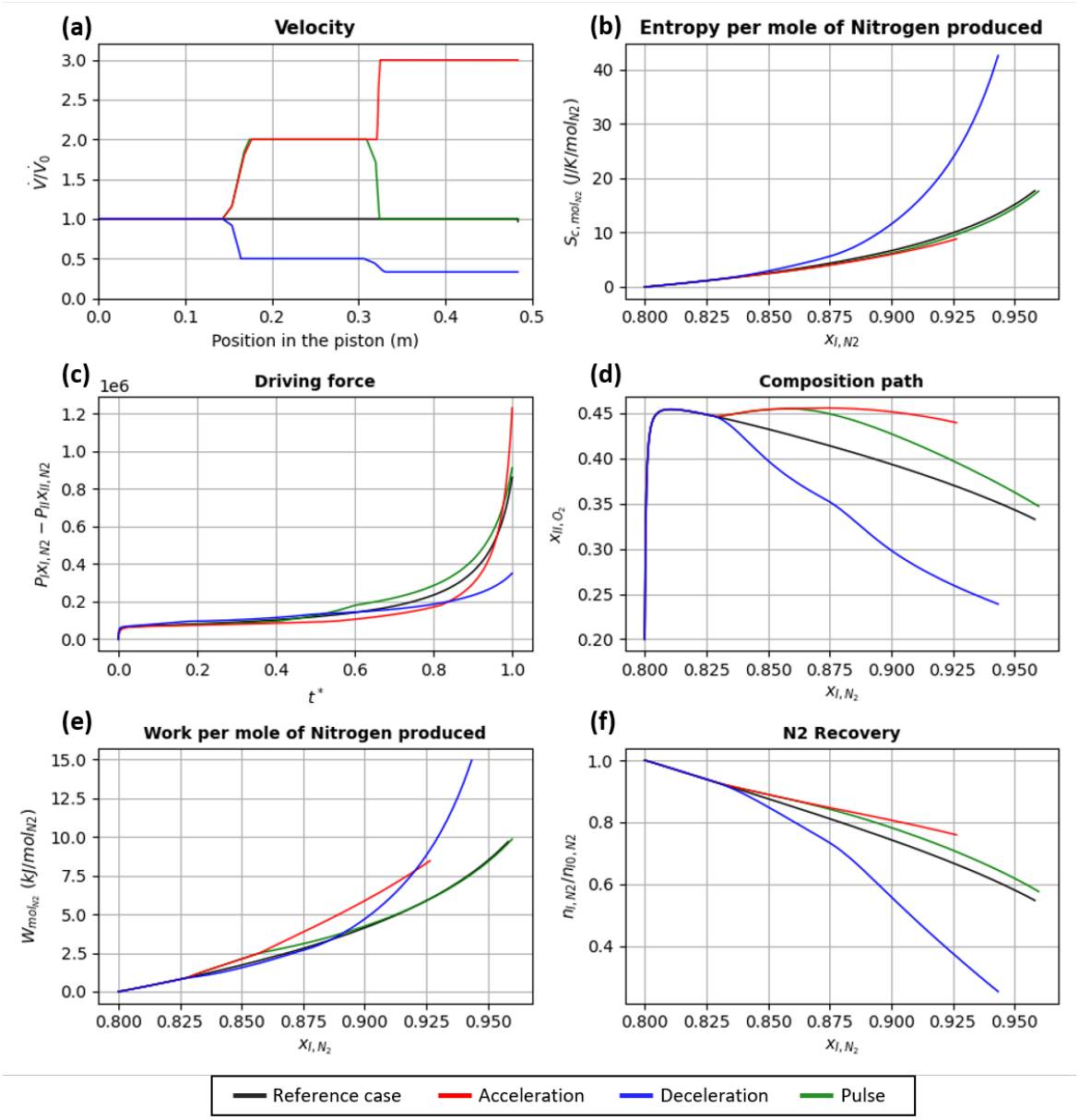


Figure 5.8 Impact of the velocity variation on the separation performances (a) Velocity depending on position in the piston (b) Entropy per mole of nitrogen produced (c) Pressure ratio evolution (d) Composition path (e) Work per mole of nitrogen produced (f) Nitrogen recovery. Black: reference case; blue: slow down; red: speed up; green: pulse.

optimization is therefore required to find the best compromise between these trends and therefore, to improve the overall efficiency.

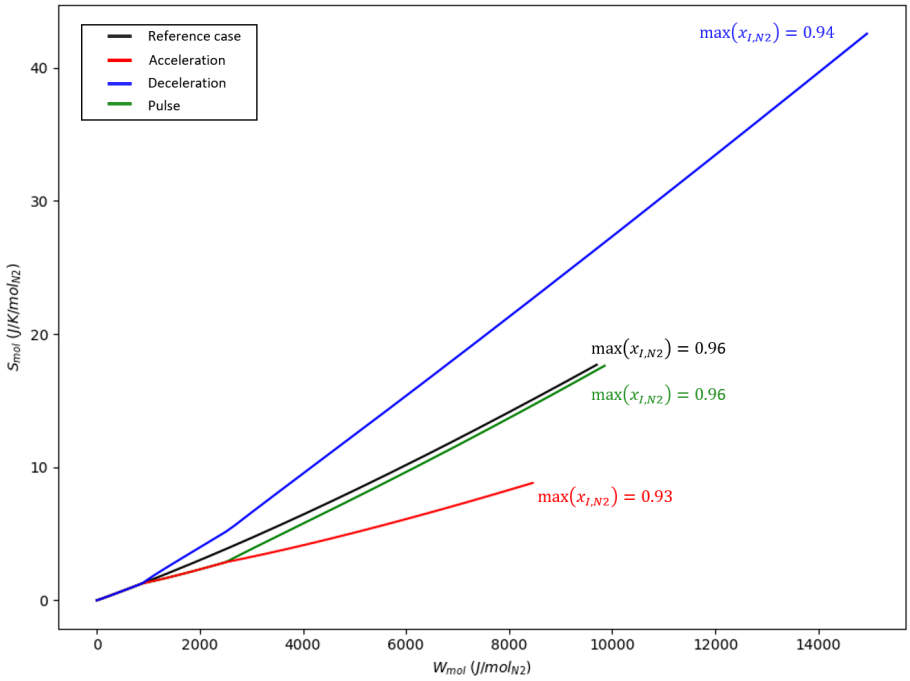


Figure 5.9 Impact of the velocity variation on the separation performances: zoom on entropy versus work. Labels indicate the maximum of x_{N_2} reached.

Optimized velocity profile on three sections

Based on the analysis of the different possible piston velocity profiles, the preliminary optimization was carried out by systematically testing all combinations and isolating the minimum of the function of interest (molar entropy or molar work). The selected configuration was obtained by dividing the piston length into three sections.

With the piston divided into three sections, the two previously defined optimization objectives are considered: minimizing entropy generation and minimizing molar work, the latter being directly related to the energy cost of separation. The results obtained from these optimizations are compared with those of the reference case, in which the velocity is kept constant and equal to the initial one.

In Table 5.2, Case 1 corresponds to the scenario with the optimal constant velocity, for which the molar work is minimized. Starting from this velocity and exploring all possible combinations of coefficients, the observed improvements in both molar work and molar entropy remain negligible, with a reduction of less than 1 $\mathrm{J\,K^{-1}\,mol^{-1}}$ in entropy and a variation of less than 1% in the work.

Considering all possible velocity profiles for three sections and five velocity levels, the two optimizations lead to different results. When minimizing entropy, as shown in Figure 5.10, and called Case 3 for $\dot{V} = 4.4 \times 10^{-9}$ $m^3 s^{-1}$ in Table 5.2, the system reaches similar nitrogen purity levels but achieves a significant improvement in oxygen purity in the second compartment, which could then be valorized. Furthermore, the entropy decreases from approximately 30 $J K^{-1} mol^{-1}$ to about 13 $J K^{-1} mol^{-1}$, while the molar work also diminishes. The corresponding velocity profile features an acceleration during the second part of the piston motion and provides better performance than using only the initial velocity or maintaining a uniformly higher speed throughout.

Table 5.2 Summary of piston configurations and corresponding thermodynamic results.

Parameter	**Case 1**	**Case 2**	**Case 3**	**Case 4**
Scaling coefficient c_i (Eq. 5.27)	(1,1,1)	(1,3,1)	(1,3,3)	(1,3,3)
Corresponding figure	5.7	-	5.10	5.11
Number of sections	3	3	3	3
Velocity ($m^3 s^{-1}$)	1.0×10^{-8}	1.0×10^{-8}	4.4×10^{-9}	3.3×10^{-9}
W_{mol} (kJ/mol_{N_2})	8.48	8.42	8.59	8.26
S_c ($J/K/mol_{N_2}$)	15.12	14.41	13.21	14.42

When the molar work is chosen as the optimization variable, the results deviate from those obtained by minimizing entropy. The optimal initial velocity is lower, at $3.3 \times 10^{-9} m^3 s^{-1}$, called Case 4, while the overall velocity profile remains similar, with the piston accelerating over approximately two-thirds of its travel length. However, in contrast to the entropy-minimized case, the increase in oxygen purity is accompanied by a slightly larger decrease in nitrogen recovery, directly reflecting the trade-off between separation sharpness and overall yield (from 0.6 to 0.5). This reduction in recovery is likely associated with the lower initial velocity, which limits the available driving force for mass transfer as seen on Figure 5.11.

Additionally, the configuration with a constant velocity does not satisfy the targeted N_2 purity specification, from 0.95 expected to 0.925 obtained, further emphasizing the importance of velocity optimization in achieving the desired separation performance.

Thus, it appears that selecting an appropriate velocity profile can significantly enhance the overall performance of the membrane piston process at a given velocity. Both optimization strategies demonstrate that the control of piston motion influences not only the separation efficiency but also the energy requirements of the system. These results highlight the potential

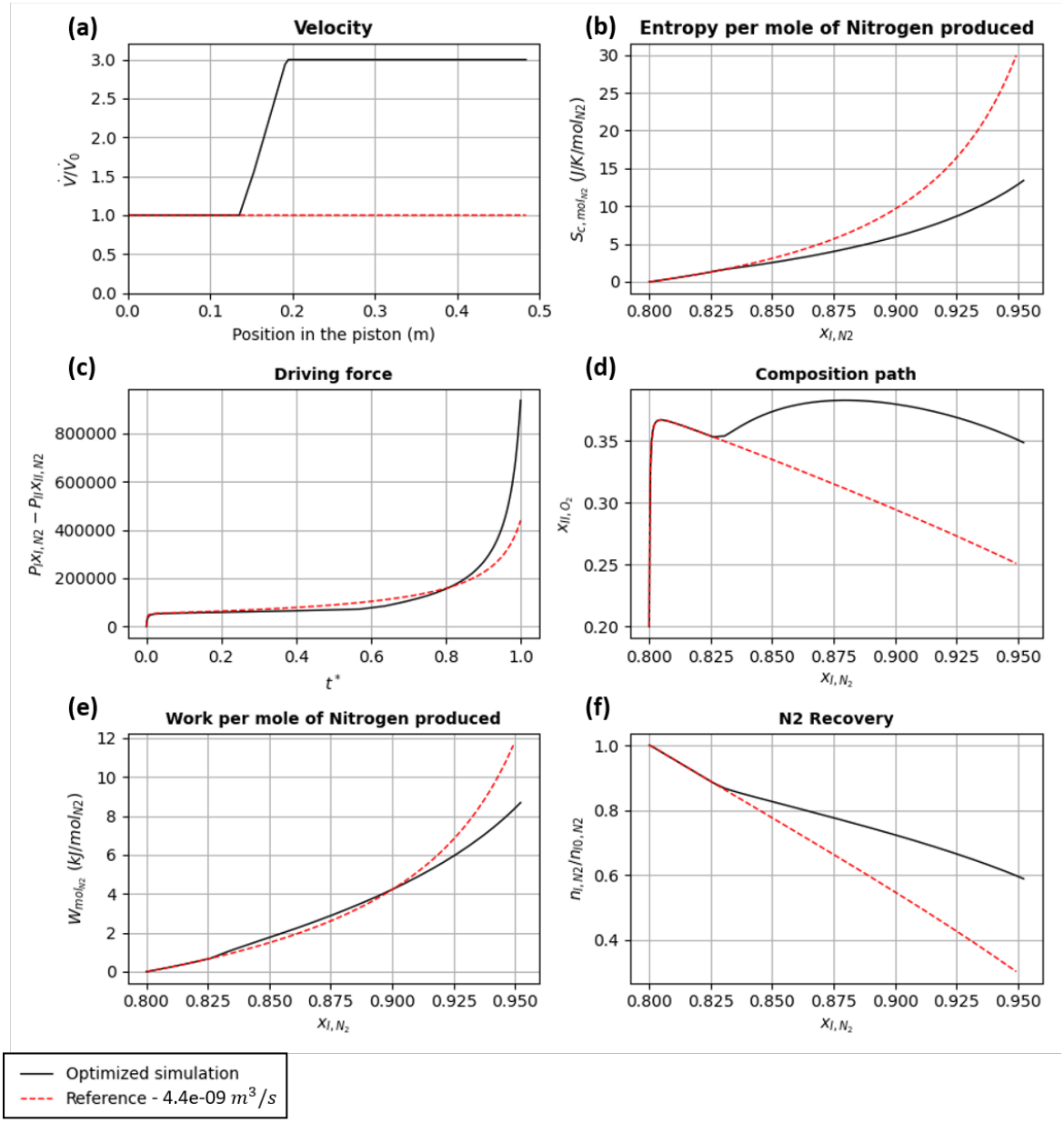


Figure 5.10 Velocity profile minimizing S_c (a) Velocity depending on position in the piston (b) Entropy per mole of nitrogen produced (c) Pressure ratio evolution (d) Composition path (e) Work per mole of nitrogen produced (f) Nitrogen recovery. Black: optimized case; red: reference case at $\dot{V} = 4.4 \cdot 10^{-9} \mathrm{m}^3\,\mathrm{s}^{-1}$.

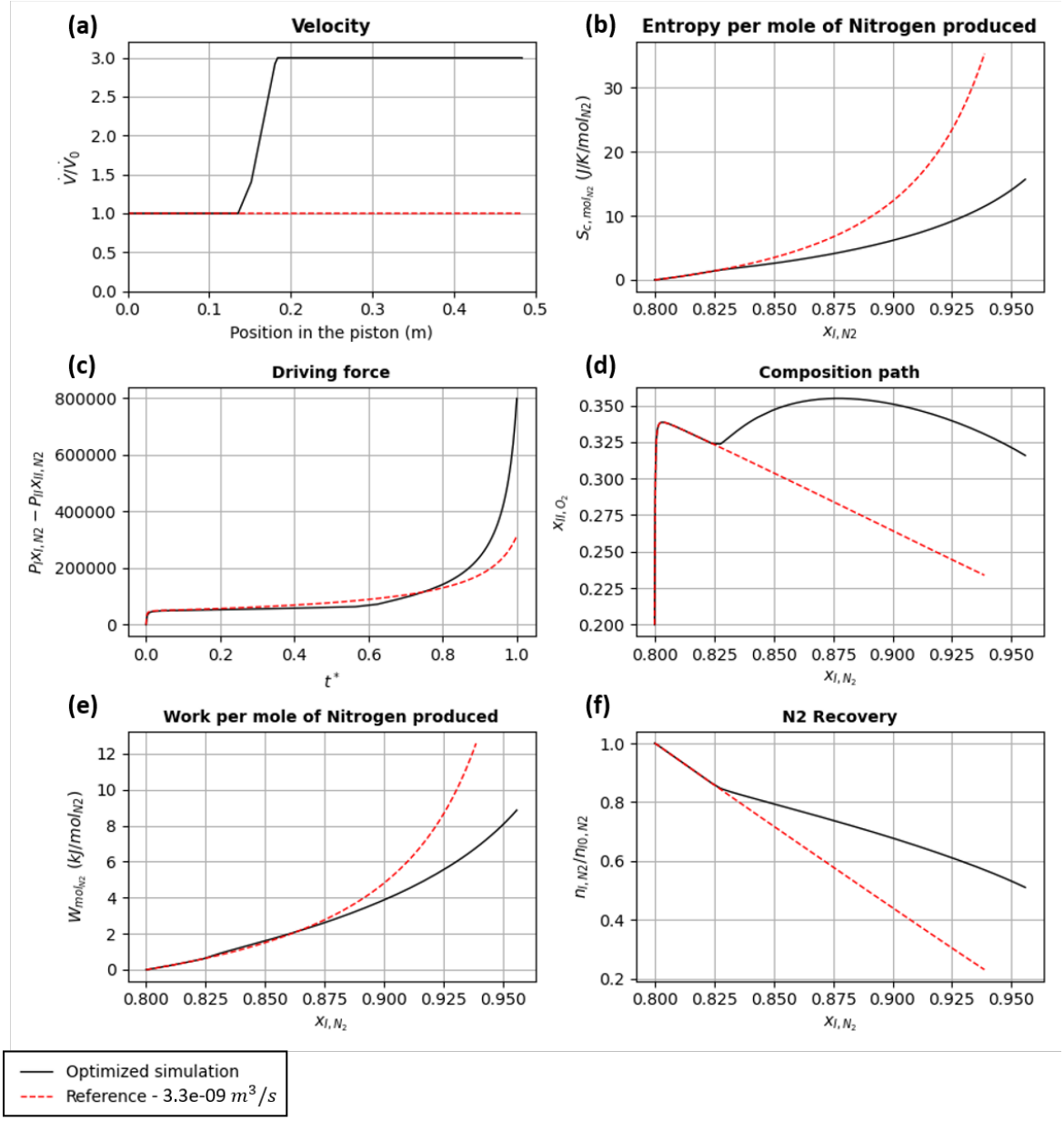


Figure 5.11 Velocity profile minimizing W (a) Velocity depending on position in the piston (b) Entropy per mole of nitrogen produced (c) Pressure ratio evolution (d) Composition path (e) Work per mole of nitrogen produced (f) Nitrogen recovery. Black: optimized case; red: reference case at $\dot{V} = 3.3 \cdot 10^{-9} \mathrm{m}^3\,\mathrm{s}^{-1}$.

of dynamic operation to approach reversible-like separations while maintaining practical energy consumption levels. However, as shown in Table 5.2, the improvement relative to the optimized constant velocity case remains modest. Further optimization efforts should therefore aim to refine the velocity profile continuously rather than in discrete sections, in order to fully exploit the benefits of dynamic control.

5.3 Conclusion

Energy efficiency is closely linked to the performance of the Membrane Piston system, as it directly limits the amount of irreversibilities occurring during operation. The calculation of $W_{min}^{non-isobaric}$ and W_{mol} indicates that the system is significantly more efficient than conventional separation processes, with efficiency increasing as the piston velocity rises. The analysis of different piston velocity profiles demonstrates that variations in acceleration and deceleration significantly influence both entropy generation and molar work, directly affecting the separation performance. While acceleration generally reduces molar entropy and molar work when starting from the optimized velocity, it also impacts the recovery and composition path taken, giving a window for a possible optimization on the velocity profile. The preliminary optimization showed that dividing the piston motion into multiple sections allows for improved control of the flow behavior and thermodynamic performance. In particular, configurations featuring acceleration during the second part of the stroke provided a good compromise between reduced entropy, lower work, and enhanced oxygen purity. Overall, further optimization is required to refine the velocity profiles and achieve an optimal balance between efficiency, work input, and product purity. Finally, it is important to highlight that this study is conducted for only one geometry, and this added parameters (d,V) will probably impact the obtained profiles.

It is important to note that the created entropy is a challenging function to obtain in this situation. Although many precautions were taken, accurately evaluating the phenomena involved, such as mixing and the actual composition of the flux, remains difficult. This has not been taken into account and can be improved.

5.4 Nomenclature

Roman symbols

c_i	Scaling coefficient	–
d	Membrane diameter	m
E_p	Potential energy	J
g	Gravitational acceleration	$\mathrm{m\,s^{-2}}$
h	Molar enthalpy	$\mathrm{J\,mol^{-1}}$
l	Section of the piston's length	m
m	Mass	kg
n	Amount of substance	mol
$\dot{n}$	Molar flow rate	$\mathrm{mol\,s^{-1}}$
P	Pressure	Pa
$\dot{Q}$	Heat flow rate	W
R	Ideal gas constant	$\mathrm{J\,mol^{-1}\,K^{-1}}$
s	Molar entropy	$\mathrm{J\,mol^{-1}\,K^{-1}}$
S	Entropy	$\mathrm{J\,K^{-1}}$
S_c	Entropy created	$\mathrm{J\,K^{-1}}$
t	Time	s
T	Temperature	K
u	Molar internal energy	$\mathrm{J\,mol^{-1}}$
U	Total internal energy	J
V_e	Electric potential	V
$\dot{V}$	Volumetric piston velocity	$\mathrm{m^3\,s^{-1}}$
W_{min}	Minimal molar work	$\mathrm{J\,mol^{-1}}$
$\dot{W}$	Power	W
x, y	Compositions	–

Greek letters

α^*	Ideal selectivity (permeance ratio)	–
η	Recovery	–
η_{eff}	Separation efficiency	–
Φ_i	Molar flux of component i through the membrane	$\text{mol}\,\text{s}^{-1}$

Subscripts

0	At initial time $t = 0$
i	Component i
I, II	Compartment I or II in the membrane piston
pure i	Pure component i

Superscripts

$*$	Dimensionless or ideal quantity
$\bullet$	Perfect gas

Conclusion & Perspectives

Conclusions

Membrane separations are a key technology for the energy transition. Their advantages, such as the absence of solvents, no phase changes, and the possibility of component recovery, make them attractive for sustainable processes. These systems are typically operated in steady-state, which simplifies operation but also limits performance due to the constraints of available materials. Several alternative processes have been proposed to overcome these limitations, notably by Paul, inspired by the solution-diffusion model of permeability. However, such transient processes remain largely theoretical and are still insufficiently explored in the literature.

The Membrane Piston concept offers an innovative approach to meeting the growing demand for energy-conscious separation processes. It combines compression and separation to selectively target the component of interest. With the membrane acting as a permeable, moving wall between compartments, the driving force for separation evolves differently than in conventional membrane systems. In the open-mode configuration, performance is evaluated for one compartment while considering the other as an infinite sink. Modeling is performed using first-order mass and energy balances with ideal gases, as the systems studied mostly involve binary mixtures at pressures between 5 and 15 bar. Dimensionless numbers have been defined to facilitate sizing and performance estimation.

The study results indicate that the Membrane Piston can achieve industrially relevant performance for air separation while significantly reducing energy requirements for a given geometry. Parametric studies show that the molar work can be minimized for a fixed geometry and a given $(\alpha^*, \mathscr{P})$ set. Selectivity influences the minimum work achievable, while permeance affects the velocity at which this minimum occurs. For air separation and biogas

applications, the open mode shows promising results, outperforming the closed mode and achieving 30–60% lower energy consumption than conventional steady-state systems for equivalent performance. The potential application to carbon capture is also significant; however, as the system favors recovery of the slower-permeating component, current membranes are not yet suitable. Emerging materials with reversed selectivity could address this limitation. Studies with realistic hypothetical membranes show that the Membrane Piston can achieve around 80% CO_2 purity at 5 bar, with energy requirements significantly lower than classical systems using the same membrane.

Experimental validation of the system proved challenging due to the difficulty of making the moving parts leak-proof. Quantification of these leaks allowed for more realistic simulations and showed pressure differences between estimated and measured values around 10%, which is acceptable for this system. However, due to membrane performance limitations and remaining leaks, the measured compositions, while consistent with simulations, showed little variation from the initial mixture and must therefore be interpreted cautiously.

Finally, to further improve energy efficiency, an entropy analysis was conducted. This approach allows evaluation of the system efficiency in the classical sense, i.e., $W_{\text{min}}/W_{\text{real}}$, and demonstrates that the Membrane Piston is significantly more efficient than conventional systems. Optimization of the piston velocity profile, either to minimize entropy generation or molar work, further improves performance. While the results differ slightly depending on the optimization criterion, both approaches show that accelerating the piston is an effective strategy, enhancing both efficiency metrics and even achieving higher purity compared to constant-velocity operation. However, a complex profile seems to only have a slight impact on the required energy when comparing to the optimized constant velocity, indicating that further optimization is required on that part.

Perspectives

Future work will focus on several key directions to further develop and validate the Membrane Piston concept.

Short-term objectives:

- The work initiated in Chapter 5 on the optimization of the velocity profile will be pursued to obtain a more complex profile. The aim is to determine whether minimizing entropy generation or minimizing the molar work still lead to similar results, and focus on the impact of initial velocity on the optimized profile and the use of continuous velocity profile instead of discrete fixed levels of velocity.
- Computational Fluid Dynamics (CFD) simulations, currently being developed in collaboration with Dr. François Lesage, will aim to reproduce the Open Mode separation for several representative cases. The objective is to compare these simulations with the analytical model presented in this thesis, thereby validating key assumptions such as perfect mixing and uniform temperature.

Long-term objectives:

- Once the optimization of the piston dynamics for a single stage is completed, the next step will be to investigate the potential of a multi-stage Membrane Piston configuration. The goal will be to assess its relevance in terms of energy efficiency and separation performance. This study will require defining the optimal geometry, operational complexity, timing, and performance objectives. As in conventional steady-state membrane separation processes, where multi-stage operation is typically employed to improve efficiency, a similar approach could prove beneficial for the Membrane Piston concept. Therefore, this comparison may provide valuable insights into the potential advantages and trade-offs associated with multi-stage operation.
- Finally, collaboration with industrial partners specialized in compressors and pressure-generation systems will be sought to evaluate the practical implementation of the concept. Such partnerships will help identify the main operational challenges and potential areas for improvement that have not yet been explored from a process engineering perspective.

In the spirit of continuous improvement, other innovative process configurations will also be explored, using other pressure-generating devices and membrane coupling to enhance overall performance and broaden the scope of potential applications.

Bibliography

[1] Heinz-Wolfgang Häring. *Industrial gases processing*. Wiley-VCH, Weinheim, 2008. ISBN 978-3-527-31685-4.

[2] Richard W. Baker. Future Directions of Membrane Gas Separation Technology. *Industrial & Engineering Chemistry Research*, 41(6):1393–1411, March 2002. ISSN 0888-5885, 1520-5045. doi: 10.1021/ie0108088. URL https://pubs.acs.org/doi/10.1021/ie0108088.

[3] K. Scott. *Handbook of industrial membranes*. Elsevier Advanced Technology, Oxford, 1st ed edition, 1995. ISBN 978-1-85617-233-2.

[4] Christophe Castel and Eric Favre. Membrane separations and energy efficiency. *Journal of Membrane Science*, 548:345–357, February 2018. ISSN 03767388. doi: 10.1016/j.memsci.2017.11.035. URL https://linkinghub.elsevier.com/retrieve/pii/S0376738817315831.

[5] P. Bernardo, E. Drioli, and G. Golemme. Membrane Gas Separation: A Review/State of the Art. *Industrial & Engineering Chemistry Research*, 48(10):4638–4663, May 2009. ISSN 0888-5885, 1520-5045. doi: 10.1021/ie8019032. URL https://pubs.acs.org/doi/10.1021/ie8019032.

[6] G.G. Haselden. Gas separation fundamentals. *Gas Separation & Purification*, 3(4):209–215, December 1989. ISSN 09504214. doi: 10.1016/0950-4214(89)80007-6. URL https://linkinghub.elsevier.com/retrieve/pii/0950421489800076.

[7] William J. Koros. Evolving beyond the thermal age of separation processes: Membranes can lead the way. *AIChE Journal*, 50(10):2326–2334, October 2004. ISSN 0001-1541, 1547-5905. doi: 10.1002/aic.10330. URL https://aiche.onlinelibrary.wiley.com/doi/10.1002/aic.10330.

[8] David S. Sholl and Ryan P. Lively. Seven chemical separations to change the world. *Nature*, 532(7600):435–437, April 2016. ISSN 0028-0836, 1476-4687. doi: 10.1038/532435a. URL https://www.nature.com/articles/532435a.

[9] E. Favre. Polymeric Membranes for Gas Separation. In *Comprehensive Membrane Science and Engineering*, pages 155–212. Elsevier, 2010. ISBN 978-0-08-093250-7. doi: 10.1016/B978-0-08-093250-7.00020-7. URL https://linkinghub.elsevier.com/retrieve/pii/B9780080932507000207.

[10] Donald R. Paul. Membrane Separation of Gases Using Steady Cyclic Operation. *Industrial & Engineering Chemistry Process Design and Development*, 10(3):375–379, July 1971. ISSN 0196-4305, 1541-5716. doi: 10.1021/i260039a016. URL https://pubs.acs.org/doi/abs/10.1021/i260039a016.

[11] Xianshe Feng, Chuen Y. Pan, and John Ivory. Pressure swing permeation: Novel process for gas separation by membranes. *AIChE Journal*, 46(4):724–733, April 2000. ISSN 00011541, 15475905. doi: 10.1002/aic.690460407. URL https://onlinelibrary.wiley.com/doi/10.1002/aic.690460407.

[12] Yiwei Chen, Darren Lawless, and Xianshe Feng. Pressure–vacuum swing permeation: A novel process mode for membrane separation of gases. *Separation and Purification Technology*, 125:301–310, April 2014. ISSN 1383-5866. doi: 10.1016/j.seppur.2014.01.053. URL https://www.sciencedirect.com/science/article/pii/S1383586614000872.

[13] Prodip K. Kundu, Amit Chakma, and Xianshe Feng. Unsteady state cyclic pressure-vacuum swing permeation for low pressure niche gas separation applications. *Chemical Engineering Research and Design*, 109:505–512, May 2016. ISSN 0263-8762. doi: 10.1016/j.cherd.2016.02.033. URL https://www.sciencedirect.com/science/article/pii/S0263876216300016.

[14] Maxim M. Trubyanov, Pavel N. Drozdov, Artem A. Atlaskin, Stanislav V. Battalov, Egor S. Puzanov, Andrey V. Vorotyntsev, Anton N. Petukhov, Vladimir M. Vorotyntsev, and Ilya V. Vorotyntsev. Unsteady-state membrane gas separation by novel pulsed retentate mode for improved membrane module performance: Modelling and experimental verification. *Journal of Membrane Science*, 530:53–64, May 2017. ISSN 0376-7388. doi: 10.1016/j.memsci.2017.01.064. URL https://www.sciencedirect.com/science/article/pii/S0376738816322517.

[15] Lei Wang. *Séparation Membranaire de Composés Gazeux en Régime Cyclique*. Thèse de doctorat, Université de Lorraine, 2012.

[16] Lei Wang, Jean-Pierre Corriou, Christophe Castel, and Eric Favre. A critical review of cyclic transient membrane gas separation processes: State of the art, opportunities and limitations. *Journal of Membrane Science*, 383(1-2):170–188, November 2011. ISSN 03767388. doi: 10.1016/j.memsci.2011.08.052. URL https://linkinghub.elsevier.com/retrieve/pii/S0376738811006417.

[17] Mathilde Lafont, Christophe Castel, Romain Privat, and Eric Favre. Membrane gas separations and energy efficiency: Exploring the selective membrane-piston concept. *Journal of Membrane Science Letters*, 5(1):100091, June 2025. ISSN 27724212. doi: 10.1016/j.memlet.2024.100091. URL https://linkinghub.elsevier.com/retrieve/pii/S2772421224000254.

[18] Mathilde Lafont, Romain Privat, Christophe Castel, and Eric Favre. Reimagining gas separation: drastically improving energy efficiency with the Membrane-Piston concept. *Chemical Engineering Science*, page 122535, September 2025. ISSN 00092509. doi: 10.1016/j.ces.2025.122535. URL https://linkinghub.elsevier.com/retrieve/pii/S0009250925013569.

[19] Richard William Baker. *Membrane technology and applications*. Wiley, Chichester, 2nd ed edition, 2004. ISBN 978-0-470-85445-7.

[20] J.A. Nollet. *Leçons de physique expérimentale*. 1784.

[21] Adolph Fick. V. *On liquid diffusion. The London, Edinburgh, and Dublin Philosophical Magazine and Journal of Science*, 10(63):30–39, July 1855. ISSN 1941-5982, 1941-5990. doi: 10.1080/14786445508641925. URL https://www.tandfonline.com/doi/full/10.1080/14786445508641925.

[22] Sidney Loeb and Srinivasa Sourirajan. *Saline Water Conversion—II*, volume 38 of *Advances in Chemistry*. AMERICAN CHEMICAL SOCIETY, WASHINGTON, D. C., January 1963. ISBN 978-0-8412-0039-5 978-0-8412-2204-5. doi: 10.1021/ba-1963-0038. URL https://pubs.acs.org/doi/book/10.1021/ba-1963-0038.

[23] E. Drioli, Giuseppe Barbieri, and Adele Brunetti, editors. *Membrane engineering for the treatment of gases*. Royal Society of Chemistry, Croydon [England], 2nd edition edition, 2018. ISBN 978-1-78262-896-5 978-1-78262-874-3 978-1-78262-875-0.

[24] R Barrer, J Barrie, and N Raman. Solution and diffusion in silicone rubber I—A comparison with natural rubber. *Polymer*, 3:595–603, 1962. ISSN 00323861. doi: 10.1016/0032-3861(62)90108-8. URL https://linkinghub.elsevier.com/retrieve/pii/0032386162901088.

[25] R Barrer, J Barrie, and N Raman. Solution and diffusion in silicone rubber II—The influence of fillers. *Polymer*, 3:605–614, 1962. ISSN 00323861. doi: 10.1016/0032-3861(62)90109-X. URL https://linkinghub.elsevier.com/retrieve/pii/003238616290109X.

[26] Jay M. S. Henis and Mary K. Tripodi. A Novel Approach to Gas Separations Using Composite Hollow Fiber Membranes. *Separation Science and Technology*, 15(4):1059–1068, May 1980. ISSN 0149-6395, 1520-5754. doi: 10.1080/01496398008076287. URL http://www.tandfonline.com/doi/abs/10.1080/01496398008076287.

[27] Giuseppe Barbieri and E. Drioli, editors. *Membrane engineering for the treatment of gases: Volume 1: Gas-separation problems with membranes*. Royal Society of Chemistry, Cambridge, 2011. ISBN 978-1-84973-171-3 978-1-84973-347-2. doi: 10.1039/9781849733472.

[28] Tim C. Merkel, Meijuan Zhou, and Richard W. Baker. Carbon dioxide capture with membranes at an IGCC power plant. *Journal of Membrane Science*, 389:441–450, February 2012. ISSN 03767388. doi: 10.1016/j.memsci.2011.11.012. URL https://linkinghub.elsevier.com/retrieve/pii/S0376738811008283.

[29] Adolfo Iulianelli and Enrico Drioli. Membrane engineering: Latest advancements in gas separation and pre-treatment processes, petrochemical industry and refinery, and future perspectives in emerging applications. *Fuel Processing Technology*, 206:106464, September 2020. ISSN 03783820. doi: 10.1016/j.fuproc.2020.106464. URL https://linkinghub.elsevier.com/retrieve/pii/S0378382020307554.

[30] Oğuz Orhun Teber, Anil Kuban, Vahid Vatanpour, and Ismail Koyuncu. Advancing O2/N2 separation with thin film coatings on hollow fiber membranes: A review. *Journal of Industrial and Engineering Chemistry*, page S1226086X25005180, August 2025. ISSN 1226086X. doi: 10.1016/j.jiec.2025.07.064. URL https://linkinghub.elsevier.com/retrieve/pii/S1226086X25005180.

[31] Benny D. Freeman. Basis of Permeability/Selectivity Tradeoff Relations in Polymeric Gas Separation Membranes. *Macromolecules*, 32(2):375–380, January 1999. ISSN 0024-9297, 1520-5835. doi: 10.1021/ma9814548. URL https://pubs.acs.org/doi/10.1021/ma9814548.

[32] Ch. Baerlocher, D. Brouwer, B. Marler, and L.B. McCusker. Database of Zeolite Structure. URL https://www.iza-structure.org/databases/.

[33] Lloyd M. Robeson. Correlation of separation factor versus permeability for polymeric membranes. *Journal of Membrane Science*, 62(2):165–185, October 1991. ISSN 03767388. doi: 10.1016/0376-7388(91)80060-J. URL https://linkinghub.elsevier.com/retrieve/pii/037673889180060J.

[34] Lloyd M. Robeson. The upper bound revisited. *Journal of Membrane Science*, 320 (1-2):390–400, July 2008. ISSN 03767388. doi: 10.1016/j.memsci.2008.04.030. URL https://linkinghub.elsevier.com/retrieve/pii/S0376738808003347.

[35] Ali Hayek, Yasser A. Shalabi, and Abdulkarim Alsamah. Sour mixed-gas upper bounds of glassy polymeric membranes. *Separation and Purification Technology*, 277: 119535, December 2021. ISSN 13835866. doi: 10.1016/j.seppur.2021.119535. URL https://linkinghub.elsevier.com/retrieve/pii/S1383586621012430.

[36] Yuewen Jia, Kelvin Wong, Can Zeng Liang, Ji Wu, Tai-Shung Chung, and Sui Zhang. Recent development of membranes for carbon capture: From materials to asymmetric membranes. *Progress in Materials Science*, 146:101324, December 2024. ISSN 00796425. doi: 10.1016/j.pmatsci.2024.101324. URL https://linkinghub.elsevier.com/retrieve/pii/S0079642524000938.

[37] Nikolay Kosinov, Jorge Gascon, Freek Kapteijn, and Emiel J. M. Hensen. Recent developments in zeolite membranes for gas separation. *Journal of Membrane Science*, 499:65–79, February 2016. ISSN 0376-7388. doi: 10.1016/j.memsci.2015.10.049. URL https://www.sciencedirect.com/science/article/pii/S0376738815302805.

[38] Omar Abdul Majid. *Computational Fluid Dynamics (CFD) simulations in membrane gas separation processes: Application to biogas upgrading with zeolite membranes*. PhD thesis, Université de Lorraine, 2024.

[39] A. W. Thornton, B. D. Freeman, and L. M. Robeson. Membrane Database – Polymer Gas Separation Membranes, 2012. URL https://research.csiro.au/virtualscreening/membrane-database-polymer-gas-separation-membranes/.

[40] M. Scholz, M. Wessling, and J. Balster. Chapter 5. Design of Membrane Modules for Gas Separations. In *Membrane Engineering for the Treatment of Gases: Gas-separation Problems with Membranes*, pages 125–149. The Royal Society of Chemistry, 2011. doi: 10.1039/9781849733472-00125. URL https://books.rsc.org/books/monograph/1386/chapter-abstract/1169534/.

[41] Marcos Da Conceicao, Leo Nemetz, Joanna Rivero, Katherine Hornbostel, and Glenn Lipscomb. Gas Separation Membrane Module Modeling: A Comprehensive Review. *Membranes*, 13(7):639, June 2023. ISSN 2077-0375. doi: 10.3390/membranes13070639. URL https://www.mdpi.com/2077-0375/13/7/639.

[42] Tim Merkel, Richard Baker, Pingjiao Hao, Jay Kniep, Zhenjie He, Ivy Huang, and Witopo Salim. Carbon Capture with Membranes: An Opportunity Revisited. *Journal of Membrane Science*, page 124829, October 2025. ISSN 03767388. doi: 10.1016/j.memsci.2025.124829. URL https://linkinghub.elsevier.com/retrieve/pii/S0376738825011421.

[43] H. A. Daynes. The process of diffusion through a rubber membrane. *Proceedings of the Royal Society of London. Series A, Containing Papers of a Mathematical and Physical Character*, 97(685):286–307, June 1920. ISSN 0950-1207, 2053-9150. doi: 10.1098/rspa.1920.0034. URL https://royalsocietypublishing.org/doi/10.1098/rspa.1920.0034.

[44] Alessio Fuoco, Marcello Monteleone, Elisa Esposito, Rosaria Bruno, Jesús Ferrando-Soria, Emilio Pardo, Donatella Armentano, and Johannes Carolus Jansen. Gas Transport in Mixed Matrix Membranes: Two Methods for Time Lag Determination. *Computation*, 8(2):28, April 2020. ISSN 2079-3197. doi: 10.3390/computation8020028. URL https://www.mdpi.com/2079-3197/8/2/28.

[45] Jean-Pierre Corriou, Christian Fonteix, and Eric Favre. Optimization of a pulsed operation of gas separation by membrane. *AIChE Journal*, 54(5):1224–1234, May 2008. ISSN 0001-1541, 1547-5905. doi: 10.1002/aic.11443. URL https://aiche.onlinelibrary.wiley.com/doi/10.1002/aic.11443.

[46] Christophe Castel, Lei Wang, Jean Pierre Corriou, and Eric Favre. Steady vs unsteady membrane gas separation processes. *Chemical Engineering Science*, 183:136–147, June 2018. ISSN 0009-2509. doi: 10.1016/j.ces.2018.03.013. URL https://www.sciencedirect.com/science/article/pii/S0009250918301313.

[47] Sol Weller and Waldo A. Steiner. Separation of Gases by Fractional Permeation through Membranes. *Journal of Applied Physics*, 21(4):279–283, April 1950. ISSN 0021-8979, 1089-7550. doi: 10.1063/1.1699653. URL https://pubs.aip.org/jap/article/21/4/279/159280/Separation-of-Gases-by-Fractional-Permeation.

[48] Maxim M. Trubyanov, Sergei Y. Kirillov, Andrey V. Vorotyntsev, Tatyana S. Sazanova, Artem A. Atlaskin, Anton N. Petukhov, Yuri P. Kirillov, and Ilya V. Vorotyntsev. Dynamic behavior of unsteady-state membrane gas separation: Modelling of a closed-mode operation for a membrane module. *Journal of Membrane Science*, 587:117173, October 2019. ISSN 0376-7388. doi: 10.1016/j.memsci.2019.117173. URL https://www.sciencedirect.com/science/article/pii/S0376738819310853.

[49] Artem A. Atlaskin, Maxim M. Trubyanov, Sergei Y. Kirillov, Tatyana S. Sazanova, Sergey S. Kryuchkov, Andrey V. Vorotyntsev, Anton N. Petukhov, Yuri P. Kirillov, Jakub Peter, and Ilya V. Vorotyntsev. Transient dynamics in a membrane module with a pulsed change of retentate: Modeling and experimental study of an unsteady-state mode of membrane gas separation process. *Separation and Purification Technology*, 259:118201, March 2021. ISSN 1383-5866. doi: 10.1016/j.seppur.2020.118201. URL https://www.sciencedirect.com/science/article/pii/S1383586620326745.

[50] S. V. Battalov, T. S. Sazanova, M. M. Trubyanov, E. S. Puzanov, V. M. Vorotyntsev, P. N. Drozdov, and I. V. Vorotyntsev. Modeling of Fast-Permeant Component Removal from Gas Mixture in a Membrane Module with Pulsed Retentate. *Petroleum Chemistry*, 58(9):806–814, November 2018. ISSN 1555-6239. doi: 10.1134/S0965544118090049. URL https://doi.org/10.1134/S0965544118090049.

[51] Dilip Kondepudi and Ilya Prigogine. *Modern Thermodynamics: From Heat Engines to Dissipative Structures*. Wiley, 1 edition, November 2014. ISBN 978-1-118-37181-7 978-1-118-69872-3. doi: 10.1002/9781118698723. URL https://onlinelibrary.wiley.com/doi/book/10.1002/9781118698723.

[52] Ilya Prigogine and Jacques Chanu. *Introduction à la thermodynamique des processus irréversibles*. J. Gabay, Paris, reprod. en fac-sim. edition, 1996. ISBN 978-2-87647-169-6.

[53] Sun-Tak Hwang. Nonequilibrium thermodynamics of membrane transport. *AIChE Journal*, 50(4):862–870, April 2004. ISSN 0001-1541, 1547-5905. doi: 10.1002/aic.10082. URL https://aiche.onlinelibrary.wiley.com/doi/10.1002/aic.10082. Publisher: Wiley.

[54] Erik Sauar, Signe Kjelstrup Ratkje, and Kristian M. Lien. Equipartition of Forces: A New Principle for Process Design and Optimization. *Industrial & Engineering Chemistry Research*, 35(11):4147–4153, January 1996. ISSN 0888-5885, 1520-5045. doi: 10.1021/ie9507078. URL https://pubs.acs.org/doi/10.1021/ie9507078. Publisher: American Chemical Society (ACS).

[55] Signe Kjelstrup, Dick Bedeaux, and Erik Sauar. Minimum Entropy Production by Equipartition of Forces in Irreversible Thermodynamics. *Industrial & Engineering Chemistry Research*, 39(11):4434–4436, November 2000. ISSN 0888-5885, 1520-5045. doi: 10.1021/ie0006920. URL https://pubs.acs.org/doi/10.1021/ie0006920. Publisher: American Chemical Society (ACS).

[56] Elisa Magnanelli, Eivind Johannessen, and Signe Kjelstrup. Entropy Production Minimization as Design Principle for Membrane Systems: Comparing Equipartition Results to Numerical Optima. *Industrial & Engineering Chemistry Research*, 56(16):4856–4866, April 2017. ISSN 0888-5885, 1520-5045. doi: 10.1021/acs.iecr.7b00493. URL https://pubs.acs.org/doi/10.1021/acs.iecr.7b00493. Publisher: American Chemical Society (ACS).

[57] Eivind Johannessen, Lars Nummedal, and Signe Kjelstrup. Minimizing the entropy production in heat exchange. *International Journal of Heat and Mass Transfer*, 45(13):2649–2654, June 2002. ISSN 0017-9310. doi: 10.1016/s0017-9310(01)00362-3. URL https://linkinghub.elsevier.com/retrieve/pii/S0017931001003623. Publisher: Elsevier BV.

[58] M. Sorin, E. Ayotte-Sauvé, F. Sadeghi, and F. Rheault. Thermodynamic equipartition and energy efficient membrane networks. *International Journal of Thermodynamics*, 2010.

[59] Patricia Luis. *Fundamental modelling of membrane systems: membrane and process performance*. Elsevier, Cambridge, MA, 1st edition edition, 2018. ISBN 978-0-12-813483-2.

[60] E. L. Cussler. *Diffusion: mass transfer in fluid systems*. Cambridge Univ. Press, Cambridge, 3. ed., 4. printing edition, 2011. ISBN 978-0-521-87121-1.

[61] Brandon W. Rowe, Lloyd M. Robeson, Benny D. Freeman, and Donald R. Paul. Influence of temperature on the upper bound: Theoretical considerations and comparison with experimental results. *Journal of Membrane Science*, 360(1-2):58–69, September 2010. ISSN 03767388. doi: 10.1016/j.memsci.2010.04.047. URL https://linkinghub.elsevier.com/retrieve/pii/S0376738810003686.

[62] M. Bozorg, Álvaro A. Ramírez-Santos, B. Addis, V. Piccialli, C. Castel, and E. Favre. Optimal process design of biogas upgrading membrane systems: Polymeric vs high performance inorganic membrane materials. *Chemical Engineering Science*, 225: 115769, November 2020. ISSN 00092509. doi: 10.1016/j.ces.2020.115769. URL https://linkinghub.elsevier.com/retrieve/pii/S0009250920303018.

[63] Katherine Calvin and et al. IPCC, 2023: Climate Change 2023: Synthesis Report. Contribution of Working Groups I, II and III to the Sixth Assessment Report of the Intergovernmental Panel on Climate Change [Core Writing Team, H. Lee and J. Romero (eds.)]. IPCC, Geneva, Switzerland. Technical report, Intergovernmental Panel on Climate Change (IPCC), July 2023. URL https://www.ipcc.ch/report/ar6/syr/. Edition: First.

[64] Energy Transitions Comission. Carbon capture, utilisation & storage in the energy transition: vital but limited. 2022.

[65] Luísa Marques, Miguel Monteiro, Charles Cenci, Maria Mateus, and José Condeço. Review of Post-Combustion Carbon Capture in Europe: Current Technologies and Future Strategies for Largest CO2-Emitting Industries. *Energies*, 18(13):3539, July 2025. ISSN 1996-1073. doi: 10.3390/en18133539. URL https://www.mdpi.com/1996-1073/18/13/3539.

[66] A.G. Olabi, Tabbi Wilberforce, Khaled Elsaid, Enas Taha Sayed, Hussein M. Maghrabie, and Mohammad Ali Abdelkareem. Large scale application of carbon capture to process industries – A review. *Journal of Cleaner Production*, 362:132300, August 2022. ISSN 09596526. doi: 10.1016/j.jclepro.2022.132300. URL https://linkinghub.elsevier.com/retrieve/pii/S0959652622019047.

[67] Cong Chao, Yimin Deng, Raf Dewil, Jan Baeyens, and Xianfeng Fan. Post-combustion carbon capture. *Renewable and Sustainable Energy Reviews*, 138:110490, March 2021. ISSN 13640321. doi: 10.1016/j.rser.2020.110490. URL https://linkinghub.elsevier.com/retrieve/pii/S1364032120307760.

[68] Gary T. Rochelle. Amine scrubbing for c02 capture. *Science*, 325(5948):1652–1654, 2009. ISSN 00368075, 10959203. URL http://www.jstor.org/stable/40301873.

[69] Thibaut Neveux, Yann Le Moullec, Jean-Pierre Corriou, and Eric Favre. A Rigorous Optimization Method of Operating Parameters for Amine-Based CO2 Capture Processes. *Energy Procedia*, 37:1821–1829, 2013. ISSN 18766102. doi: 10.1016/j.egypro.2013.06.060. URL https://linkinghub.elsevier.com/retrieve/pii/S1876610213003032.

[70] Thibaut Neveux, Yann Le Moullec, Jean Pierre Corriou, and Eric Favre. Energy Performance of CO2 Capture Processes: Interaction Between Process Design and Solvent. *Chemical Engineering Transactions*, 35:337–342, 2013. doi: 10.3303/CET1335056. URL https://edf.hal.science/hal-01831760.

[71] Matthew E. Boot-Handford, Juan C. Abanades, Edward J. Anthony, Martin J. Blunt, Stefano Brandani, Niall Mac Dowell, José R. Fernández, Maria-Chiara Ferrari, Robert Gross, Jason P. Hallett, R. Stuart Haszeldine, Philip Heptonstall, Anders Lyngfelt, Zen Makuch, Enzo Mangano, Richard T. J. Porter, Mohamed Pourkashanian, Gary T. Rochelle, Nilay Shah, Joseph G. Yao, and Paul S. Fennell. Carbon capture and storage update. *Energy Environ. Sci.*, 7(1):130–189, 2014. ISSN 1754-5692, 1754-5706. doi: 10.1039/C3EE42350F. URL https://xlink.rsc.org/?DOI=C3EE42350F.

[72] Kurt Zenz House, Antonio C. Baclig, Manya Ranjan, Ernst A. Van Nierop, Jennifer Wilcox, and Howard J. Herzog. Economic and energetic analysis of capturing CO_2 from ambient air. *Proceedings of the National Academy of Sciences*, 108(51):20428–20433, December 2011. ISSN 0027-8424, 1091-6490. doi: 10.1073/pnas.1012253108. URL https://pnas.org/doi/full/10.1073/pnas.1012253108.

[73] Mai Bui, Claire S. Adjiman, André Bardow, Edward J. Anthony, Andy Boston, Solomon Brown, Paul S. Fennell, Sabine Fuss, Amparo Galindo, Leigh A. Hackett, Jason P. Hallett, Howard J. Herzog, George Jackson, Jasmin Kemper, Samuel Krevor, Geoffrey C. Maitland, Michael Matuszewski, Ian S. Metcalfe, Camille Petit, Graeme Puxty, Jeffrey Reimer, David M. Reiner, Edward S. Rubin, Stuart A. Scott, Nilay Shah, Berend Smit, J. P. Martin Trusler, Paul Webley, Jennifer Wilcox, and Niall Mac Dowell. Carbon capture and storage (CCS): the way forward. *Energy & Environmental Science*, 11(5):1062–1176, 2018. ISSN 1754-5692, 1754-5706. doi: 10.1039/C7EE02342A. URL https://xlink.rsc.org/?DOI=C7EE02342A.

[74] Eric Favre. Membrane Separation Processes and Post-Combustion Carbon Capture: State of the Art and Prospects. *Membranes*, 12(9):884, September 2022. ISSN 2077-0375. doi: 10.3390/membranes12090884. URL https://www.mdpi.com/2077-0375/12/9/884.

[75] William J. Koros and Chen Zhang. Materials for next-generation molecularly selective synthetic membranes. *Nature Materials*, 16(3):289–297, March 2017. ISSN 1476-1122, 1476-4660. doi: 10.1038/nmat4805. URL https://www.nature.com/articles/nmat4805.

[76] Eric Favre, Denis Roizard, Roda Bounaceur, and William J. Koros. CO_2 /N_2 Reverse Selective Gas Separation Membranes: Technological Opportunities and Scientific Challenges. *Industrial & Engineering Chemistry Research*, 48(7):3700–3701, April 2009. ISSN 0888-5885, 1520-5045. doi: 10.1021/ie801923w. URL https://pubs.acs.org/doi/10.1021/ie801923w.

[77] Li-Xuan Ren, Feng-Ling Chang, Dun-Yen Kang, and Cheng-Liang Chen. Hybrid membrane process for post-combustion CO2 capture from coal-fired power plant. *Journal of*

Membrane Science, 603:118001, May 2020. ISSN 03767388. doi: 10.1016/j.memsci.2020.118001. URL https://linkinghub.elsevier.com/retrieve/pii/S0376738820305809.

[78] S. Sreenath and Ashish Alex Sam. N2 selective membrane based hybrid cryogenic carbon capture process for coal-fired power plants: A techno-economic case study. *Chemical Engineering Research and Design*, 213:25–41, January 2025. ISSN 02638762. doi: 10.1016/j.cherd.2024.11.027. URL https://linkinghub.elsevier.com/retrieve/pii/S0263876224006580.

[79] Arshad Hussain, Sarah Farrukh, and Fozia T. Minhas. Two-Stage Membrane System for Post-combustion CO_2 Capture Application. *Energy & Fuels*, 29(10):6664–6669, October 2015. ISSN 0887-0624, 1520-5029. doi: 10.1021/acs.energyfuels.5b01464. URL https://pubs.acs.org/doi/10.1021/acs.energyfuels.5b01464.

[80] E. W. Lemmon, I. H. Bell, M. L. Huber, and M. O. McLinden. NIST Standard Reference Database 23: Reference Fluid Thermodynamic and Transport Properties-REFPROP, Version 10.0, National Institute of Standards and Technology, 2018.

[81] Xiaoheng Jin, Tobias Foller, Xinyue Wen, Mohammad B. Ghasemian, Fei Wang, Mingwei Zhang, Heriberto Bustamante, Veena Sahajwalla, Priyank Kumar, Hangyel Kim, Gwan-Hyoung Lee, Kourosh Kalantar-Zadeh, and Rakesh Joshi. Effective Separation of CO_2 Using Metal-Incorporated rGO Membranes. *Advanced Materials*, 32(17): 1907580, April 2020. ISSN 0935-9648, 1521-4095. doi: 10.1002/adma.201907580. URL https://onlinelibrary.wiley.com/doi/10.1002/adma.201907580.

[82] Parveen Kumar, Sangil Kim, Junichi Ida, and Vadim V. Guliants. Polyethyleneimine-Modified MCM-48 Membranes: Effect of Water Vapor and Feed Concentration on N_2 /CO_2 Selectivity. *Industrial & Engineering Chemistry Research*, 47(1):201–208, January 2008. ISSN 0888-5885, 1520-5045. doi: 10.1021/ie070700d. URL https://pubs.acs.org/doi/10.1021/ie070700d.

[83] Hyung-Ju Kim, Watcharop Chaikittisilp, Kwang-Suk Jang, Stephanie A. Didas, Justin R. Johnson, William J. Koros, Sankar Nair, and Christopher W. Jones. Aziridine-Functionalized Mesoporous Silica Membranes on Polymeric Hollow Fibers: Synthesis and Single-Component CO_2 and N_2 Permeation Properties. *Industrial & Engineering Chemistry Research*, 54(16):4407–4413, April 2015. ISSN 0888-5885, 1520-5045. doi: 10.1021/ie503781u. URL https://pubs.acs.org/doi/10.1021/ie503781u.

[84] Yong Wang, Qingyuan Yang, Chongli Zhong, and Jinping Li. Graphene-like Poly(triazine imide) as N_2 -Selective Ultrathin Membrane for Postcombustion CO_2 Capture. *The Journal of Physical Chemistry C*, 120(50):28782–28788, December 2016. ISSN 1932-7447, 1932-7455. doi: 10.1021/acs.jpcc.6b08529. URL https://pubs.acs.org/doi/10.1021/acs.jpcc.6b08529.

[85] Su-Young Moon, Eunkyung Jeon, Jae-Sung Bae, Minseon Byeon, and Ji-Woong Park. Polyurea networks via organic sol–gel crosslinking polymerization of tetrafunctional amines and diisocyanates and their selective adsorption and filtration of carbon dioxide. *Polymer Chemistry*, 5(4):1124, 2014. ISSN 1759-9954, 1759-9962. doi: 10.1039/c3py01593a. URL https://xlink.rsc.org/?DOI=c3py01593a.

[86] Endashaw Tilahun Gizaw, Hsin-Hung Yeh, Jinn P. Chu, and Chien-Chieh Hu. Fabrication and characterization of nitrogen selective thin-film metallic glass/polyacrylonitrile composite membrane for gas separation. *Separation and Purification Technology*, 237:116340, April 2020. ISSN 13835866. doi: 10.1016/j.seppur.2019.116340. URL https://linkinghub.elsevier.com/retrieve/pii/S1383586619338389.

[87] Gengsheng Xu, Jianfeng Yao, Kun Wang, Li He, Paul A. Webley, Chu-sheng Chen, and Huanting Wang. Preparation of ZIF-8 membranes supported on ceramic hollow fibers from a concentrated synthesis gel. *Journal of Membrane Science*, 385-386: 187–193, December 2011. ISSN 03767388. doi: 10.1016/j.memsci.2011.09.040. URL https://linkinghub.elsevier.com/retrieve/pii/S0376738811007289.

[88] Chunjuan Zhang, Yuanlong Xiao, Dahuan Liu, Qingyuan Yang, and Chongli Zhong. A hybrid zeolitic imidazolate framework membrane by mixed-linker synthesis for efficient CO_2 capture. *Chem. Commun.*, 49(6):600–602, 2013. ISSN 1359-7345, 1364-548X. doi: 10.1039/C2CC37621K. URL https://xlink.rsc.org/?DOI=C2CC37621K.

[89] Zhaoxiang Zhong, Jianfeng Yao, Rizhi Chen, Zexian Low, Ming He, Jefferson Zhe Liu, and Huanting Wang. Oriented two-dimensional zeolitic imidazolate framework-L membranes and their gas permeation properties. *Journal of Materials Chemistry A*, 3 (30):15715–15722, 2015. ISSN 2050-7488, 2050-7496. doi: 10.1039/C5TA03707G. URL https://xlink.rsc.org/?DOI=C5TA03707G.

[90] Hui Li, Li Han, Jingwei Hou, Jindun Liu, and Yatao Zhang. Oriented Zeolitic imidazolate framework membranes within polymeric matrices for effective N2/CO2 separation. *Journal of Membrane Science*, 572:82–91, February 2019. ISSN 03767388. doi: 10.1016/j.memsci.2018.10.086. URL https://linkinghub.elsevier.com/retrieve/pii/S0376738818317198.

[91] Jie Shen, Guozhen Liu, Yufan Ji, Quan Liu, Long Cheng, Kecheng Guan, Mengchen Zhang, Gongping Liu, Jie Xiong, Jian Yang, and Wanqin Jin. 2D MXene Nanofilms with Tunable Gas Transport Channels. *Advanced Functional Materials*, 28(31):1801511, August 2018. ISSN 1616-301X, 1616-3028. doi: 10.1002/adfm.201801511. URL https://onlinelibrary.wiley.com/doi/10.1002/adfm.201801511.

[92] Fatemeh A. Nezhad, Ning Han, Zhangfeng Shen, Yun Jin, Yangang Wang, Naitao Yang, and Shaomin Liu. Experimental and theoretical exploration of gas permeation mechanism through 2D graphene (not graphene oxides) membranes. *Journal of Membrane Science*, 601:117883, March 2020. ISSN 03767388. doi: 10.1016/j.memsci.2020.117883. URL https://linkinghub.elsevier.com/retrieve/pii/S0376738819333150.

[93] Shuwen Yu, Ben Qin, Fan Yang, Meiying Xie, Liyan Xue, Zhigang Zhao, and Kaixian Wang. Unlocking the limits of diffusion and adsorption of metal-crosslinked reduced graphene oxide membranes for gas separation. *Applied Surface Science*, 586: 152868, June 2022. ISSN 01694332. doi: 10.1016/j.apsusc.2022.152868. URL https://linkinghub.elsevier.com/retrieve/pii/S0169433222004445.

[94] Wanbin Li, Guoliang Zhang, Congyang Zhang, Qin Meng, Zheng Fan, and Congjie Gao. Synthesis of trinity metal–organic framework membranes for CO_2 capture. *Chem. Commun.*, 50(24):3214–3216, 2014. ISSN 1359-7345, 1364-548X. doi: 10.1039/C3CC49815H. URL https://xlink.rsc.org/?DOI=C3CC49815H.

[95] Wan-Zhong Lang, Jie-Xia Ouyang, Ya-Jun Guo, and Lian-Feng Chu. Synthesis of Tubular Faujasite X-Type Membranes with Mullite Supports and their Gas Permeances for N_2 /CO_2 Mixtures. *Separation Science and Technology*, 46(11):1716–1725, July 2011. ISSN 0149-6395, 1520-5754. doi: 10.1080/01496395.2011.572940. URL https://www.tandfonline.com/doi/full/10.1080/01496395.2011.572940.

[96] Run Li, Shaohan Lian, Zezhou Zhang, Shuai Deng, and Chunfeng Song. Simulation of a novel hybrid membrane-cryogenic process for post-combustion carbon capture. *Carbon Capture Science & Technology*, 5:100075, December 2022. ISSN 27726568. doi: 10.1016/j.ccst.2022.100075. URL https://linkinghub.elsevier.com/retrieve/pii/S277265682200046X.

Appendix A

Robeson plot for O_2/N_2, CO_2/N_2 and CO_2/CH_4

Figure A.1 Permeability–selectivity relationship for O_2/N_2.

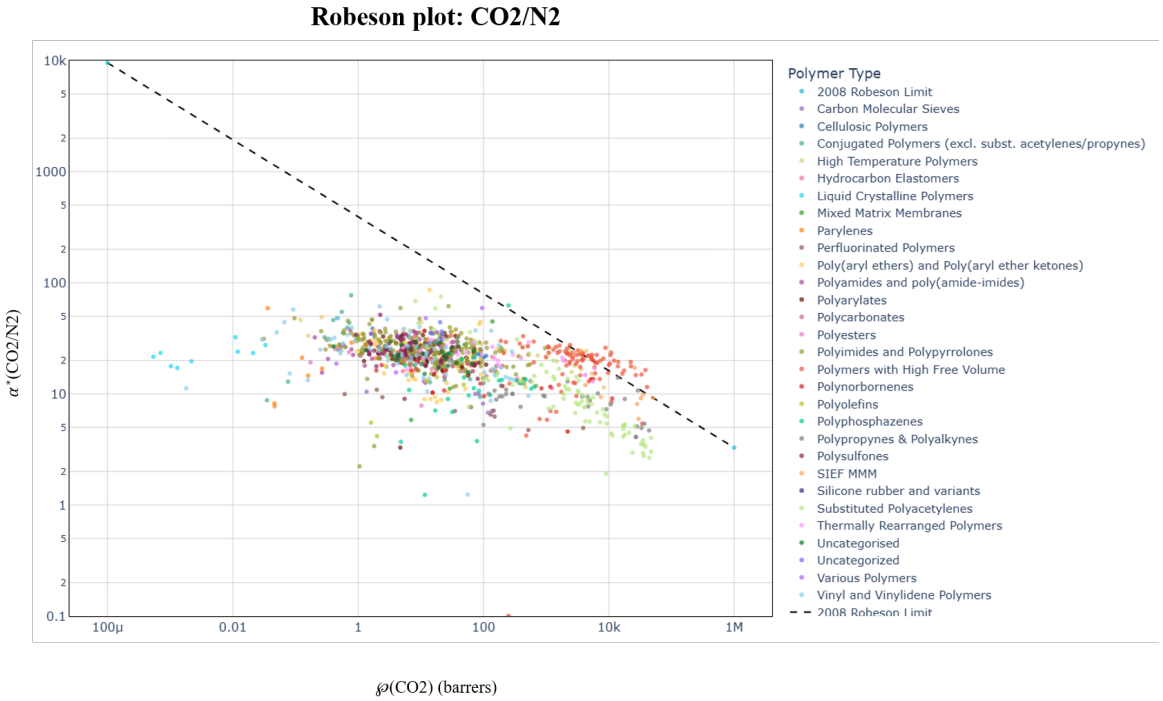


Figure A.2 Permeability–selectivity relationship for CO_2/N_2.

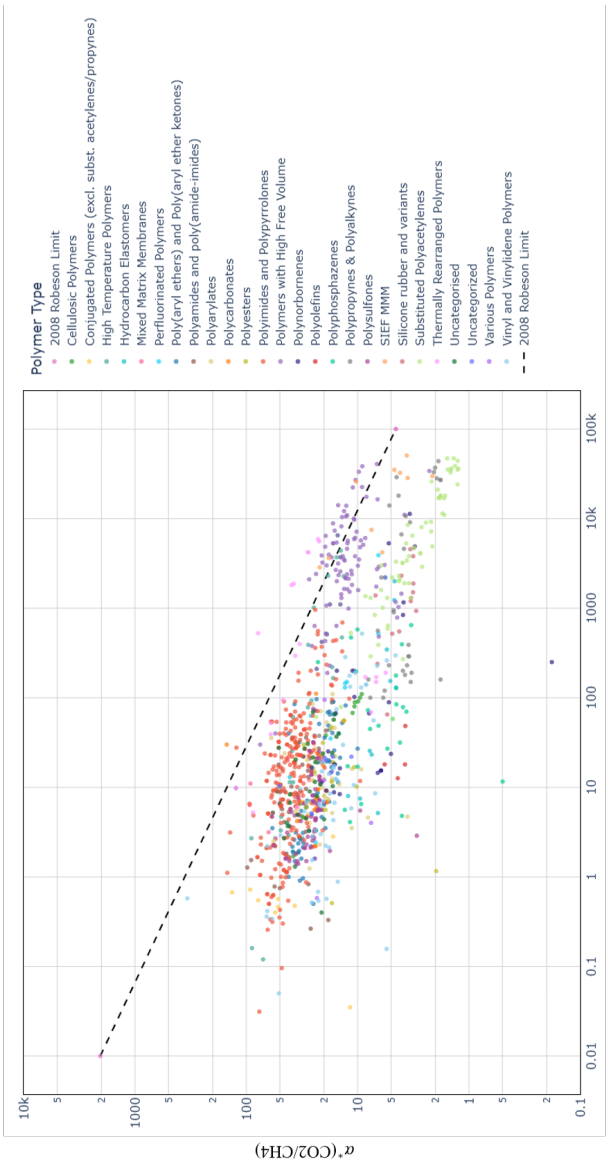


Figure A.3 Permeability–selectivity relationship for CO_2/CH_4.

Appendix B

Compressibility factor

Compression coeff Figure B.1 and B.2 reports isotherms of real gases in the Compressibility factor vs pressure plane for two mixtures of interest, obtained using the Span-Wagner equation of state [80]. Calculations were performed using the Refprop software. The temperature range from 270K to 470K and the pressure between 0.5 to 50 bar covers all conditions considered in the present study.

The first mixture studied in this paper is close to air, with $20\%O_2$ and $80\%N_2$. As can be seen, this mixture always exhibits a compressibility factor close to 1 and therefore it can be claim that this mixture behaves similarly to a perfect gas.

The second mixture is composed of $40\%CO_2$ and $60\%CH_4$, close to biogas composition. The compressibility factor changes are more important towards the highest pressures $Z \in [0.8, 1]$, but in the scope of this study, where the Membrane Piston tends to reach pressure around 15 bar max at the very end of the compression by the piston, the hypothesis of perfect gases can be considered as acceptable as it will not be prejudicial to the general trends and conclusions of the study.

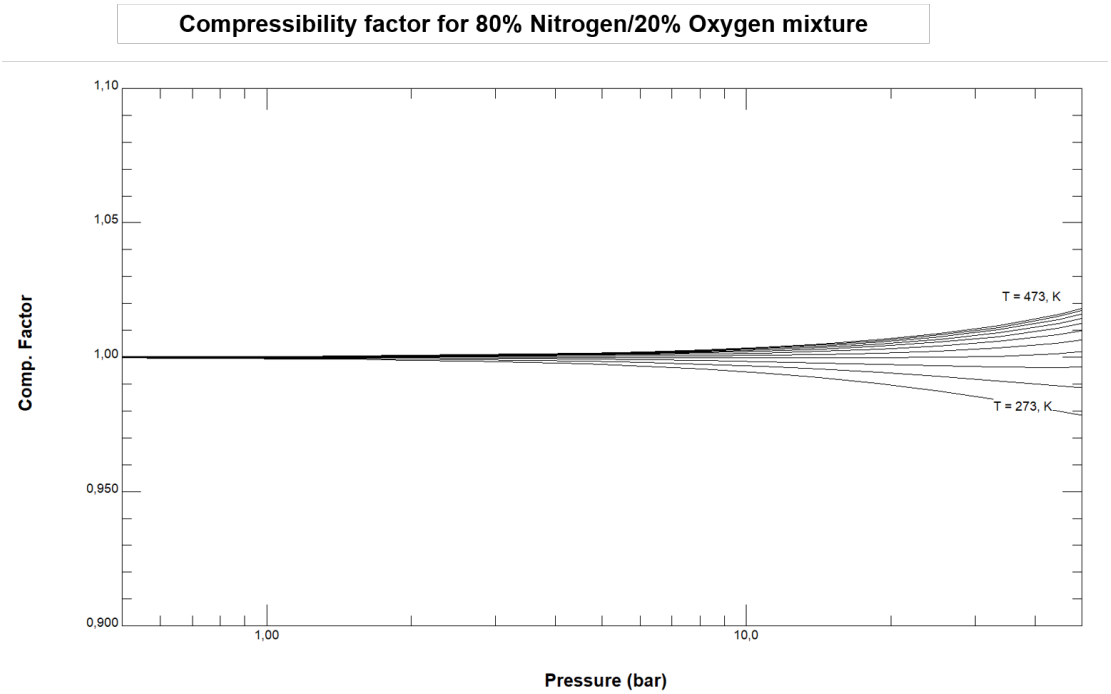


Figure B.1 Compressibility factor for a $20\%O_2/80\%N_2$ mixture

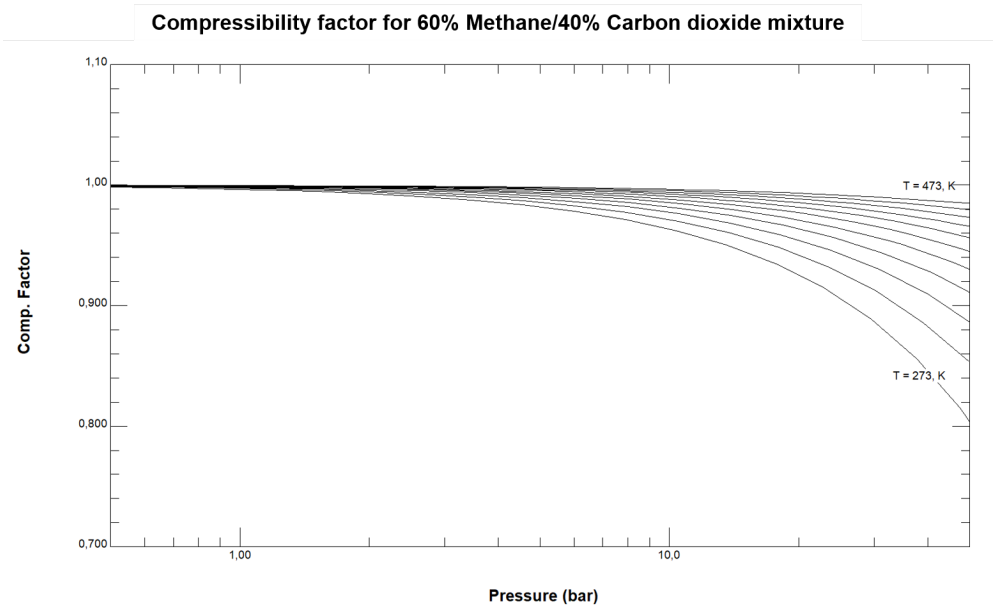


Figure B.2 Compressibility factor for a $40\%CO_2/60\%CH_4$ mixture

Appendix C

Minimal molar work for multiple $(\alpha^*, \mathscr{P}_0)$ at different $x_{\text{in, slow component}}$ and $x_{\text{I, obj}}$

C.1 $x_{\text{in, slow component}} = 0.95$

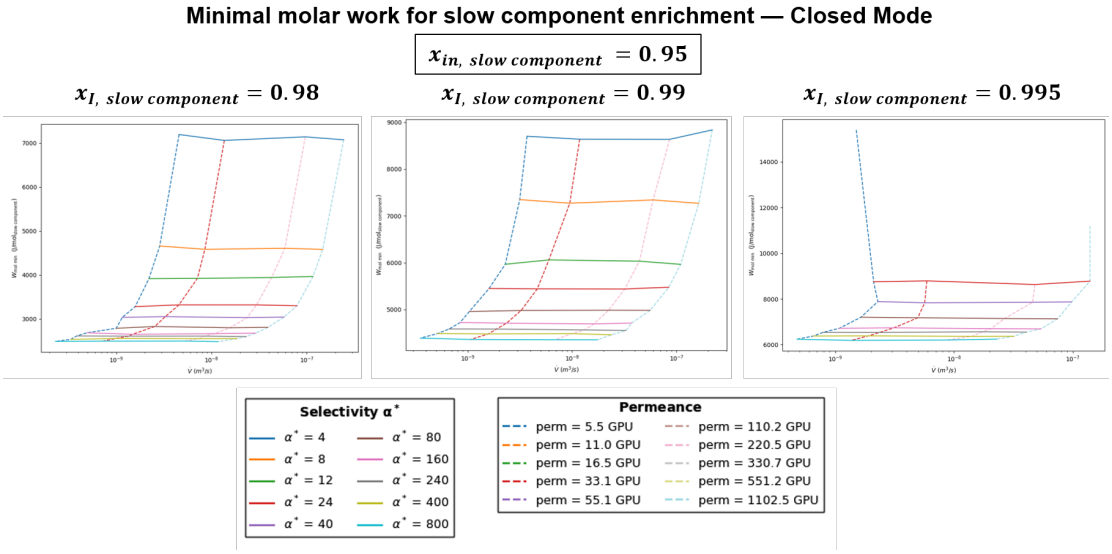


Figure C.1 $x_{\text{in, slow component}} = 0.95$

C.2 $x_{\text{in, slow component}} = 0.80$

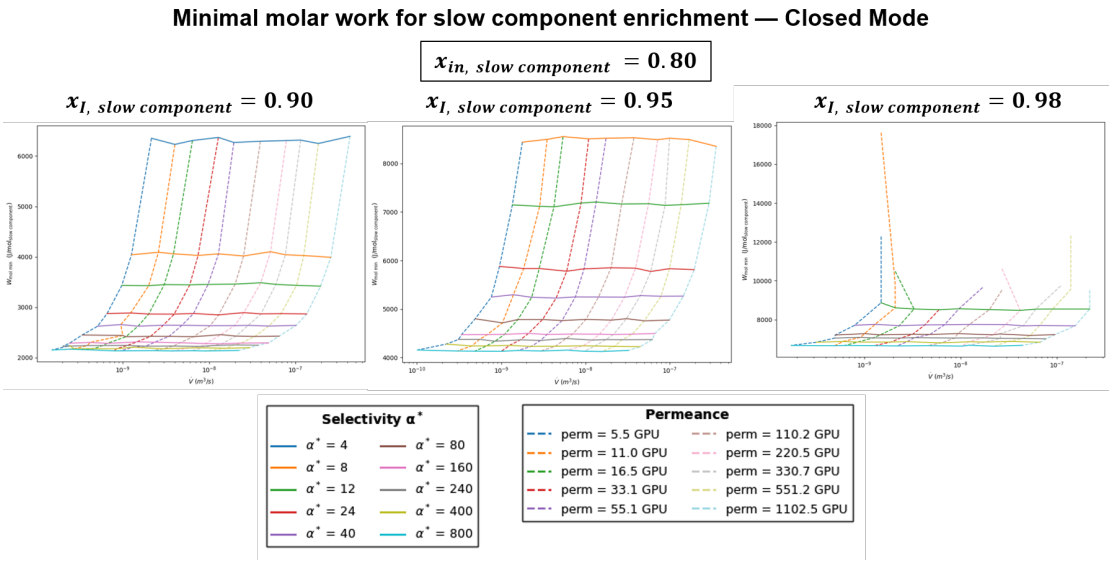


Figure C.2 $x_{\text{in, slow component}} = 0.80$ - Closed mode

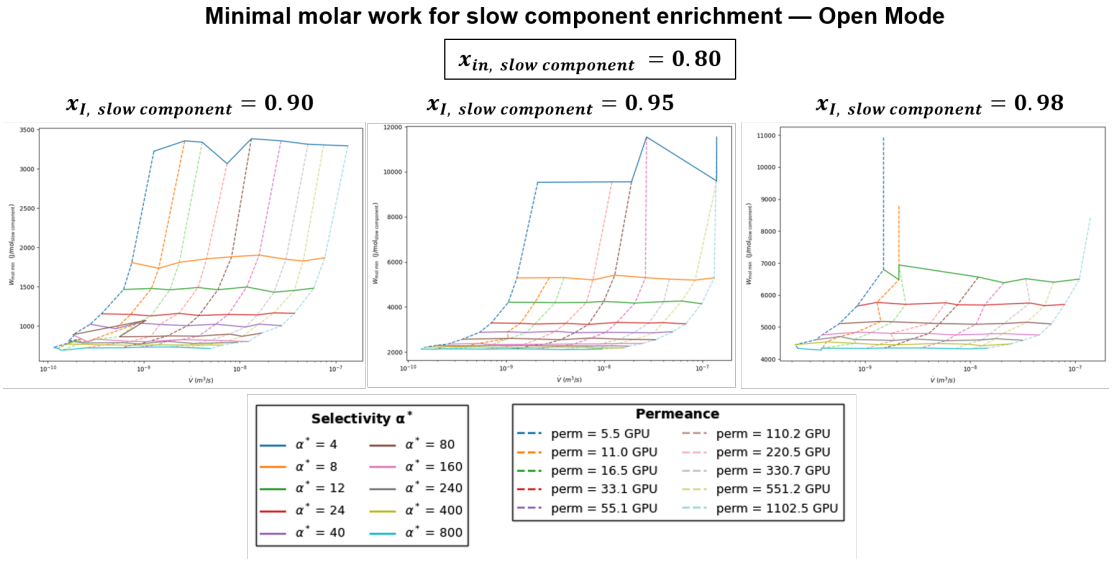


Figure C.3 $x_{\text{in, slow component}} = 0.80$ - Open mode

C.3 $x_{\text{in, slow component}} = 0.6$

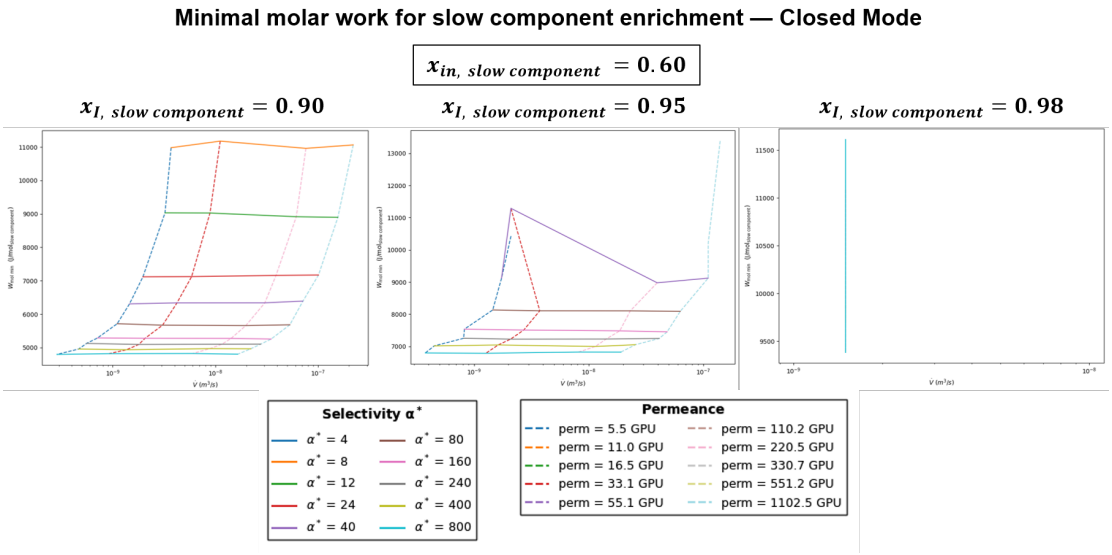


Figure C.4 $x_{\text{in, slow component}} = 0.60$

C.4 $x_{\text{in, slow component}} = 0.4$

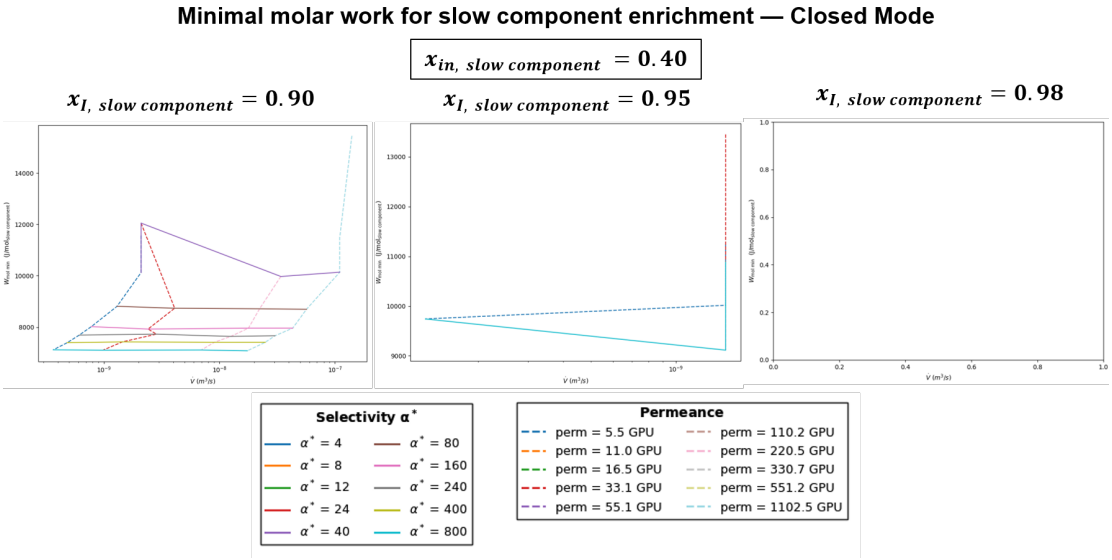


Figure C.5 $x_{\text{in, slow component}} = 0.40$

C.5 Summary

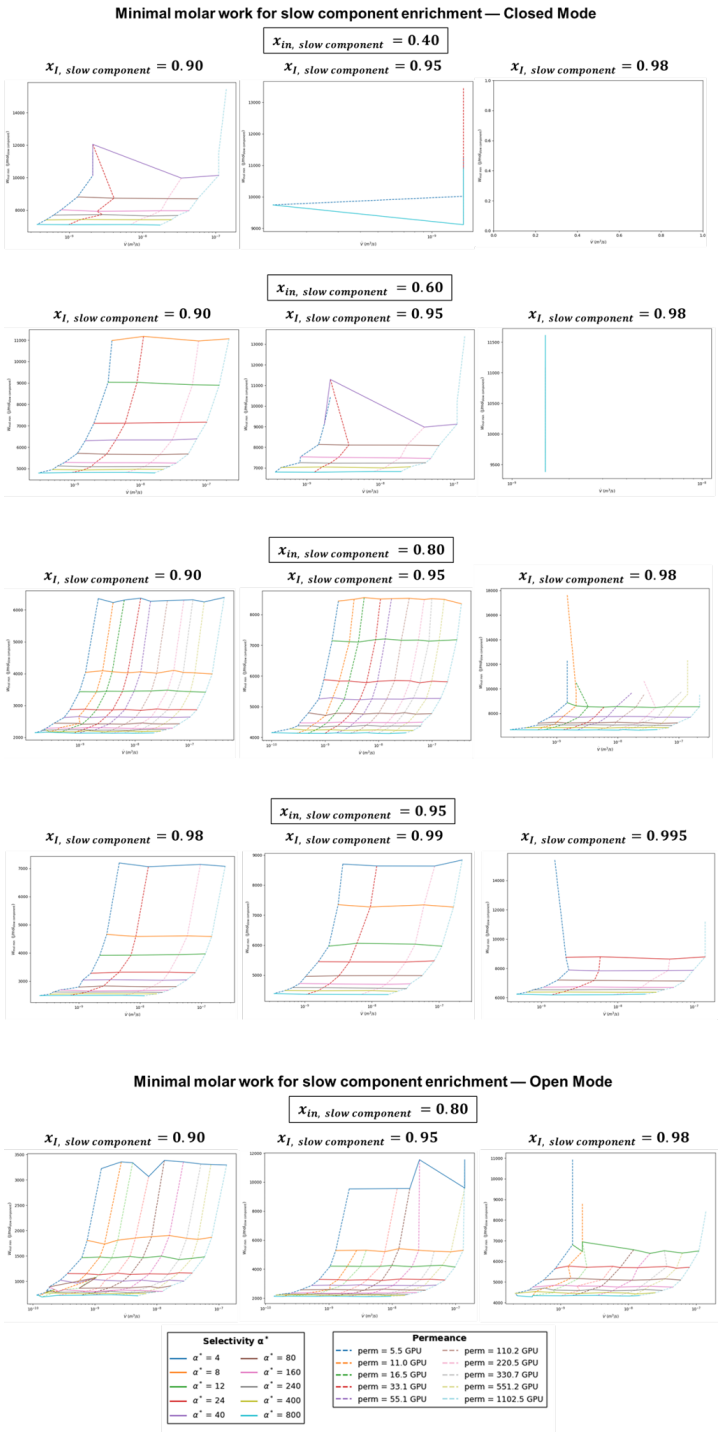


Figure C.6 Summary of all $x_{\text{in, slow component}}$ and $x_{\text{ret, slow component}}$

Appendix D

N2 selective membranes literature review

Table D.1 Performances of N_2-selective membranes

Membrane	$\mathscr{P}_{N_2}$ (GPU)	Selectivity $\alpha_{N2/CO2}$	Year	Source
Fe-rGOM	1136	67	2020	[81]
Fe-rGOM	1798	4.1	2020	[81]
Ca/SiCL	1904.6	22	2015	[79]
PEI modified MCM48	86.5	1.2	2007	[82]
PEI modified MCM48 + water vapor	27.0	3.0	2007	[82]
HAS	12.2	6.8	2014	[83]
HAS+water vapor	3.3	0.4	2014	[83]
PTI	3.7×10^6	273	2016	[84]
TAPM-HDI	0.022	2.8	2014	[85]
TFMG/PAN	4288	1.95	2020	[86]
ZIF-8	–	12.9	2011	[87]
ZIF-9-67	11385	2.41	2013	[88]
2D ZIF-L	–	3.0	2015	[89]
ZIF-L	174	51.9	2019	[90]
MXene	328	4.7	2018	[91]
2D graphene	60.3	2.9	2020	[92]
rGO	3.9	4.7	2022	[93]

Table D.1 Performances of N_2-selective membranes (continued)

Membrane	$\mathscr{P}_{N_2}$ (GPU)	Selectivity $\alpha_{N2/CO2}$	Year	Source
rGO-Th-2-1	540	5.4	2022	[93]
rGO-La-2-1	90.2	11.4	2022	[93]
Th4+rGO	31450	1.2	2022	[93]
Trinity MOF	500	7.23	2014	[94]
FAU X-type	981	7.85	2011	[95]
PEI-modified MCM-48 (363K)	98.5	1.32	2008	[82]
PEI-modified MCM-48 (363K + vapor)	101.5	1.26	2008	[82]
S200P10 - fictive	3698.2	200	2020	[77]
S200P0.6 - fictive	221.9	200	2020	[77]
S50P10 - fictive	3698.2	50	2020	[77]
S50P0.6 - fictive	221.9	50	2020	[77]
Fictive	1850	37	2022	[96]
Fictive based on [96]	–	–	2025	[78]

Appendix E

Supplementary experimental data

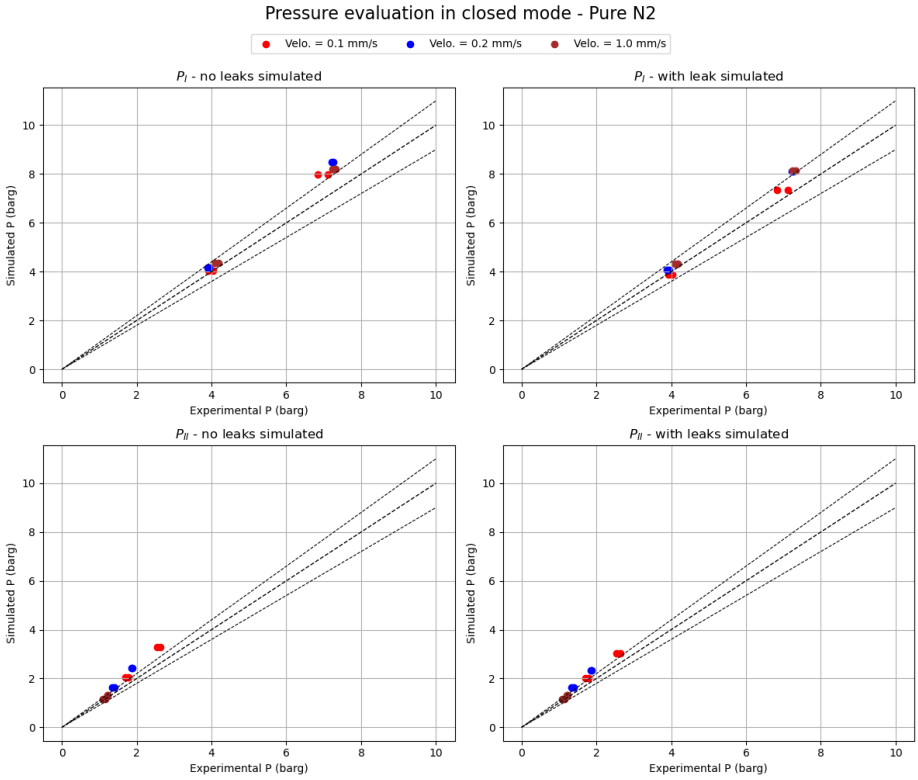


Figure E.1 Parity plot experimental vs simulated values pressure in the Membrane Piston system at 300 mm (before the leaks) and at $t^* = 1$ (end of compression). Green: 0.05 mm s^{-1}; red: 0.1 mm s^{-1}; blue: 0.2 mm s^{-1}; purple: 0.5 mm s^{-1}; brown: 1 mm s^{-1}; yellow: 1.5 mm s^{-1} (a) Compartment I, no leaks simulated (b) Compartment I with leaks in the simulation (c) Compartment II with no simulated leaks in compartment I (d) Compartment II with leaks simulated in compartment I

List of Figures

1.1 Gas permeation history [19] 7

1.2 Schematic representation of a gas separation membrane module. The feed mixture is separated into permeate and retentate streams [18]. 9

1.3 Tranpost mechanism in membrane. Left: Porous membrane; right: dense membrane [19]. 11

1.4 Classification of synthetic membranes according to structure and homogeneity [19]. 13

1.5 Robeson plots showing the upper-bound trade-off between permeability and selectivity for O_2/N_2. Data from [39] 14

1.6 Examples of membrane module types. 15

1.7 Multistage membrane separation process for carbon dioxide removal from natural gas [9] 16

1.8 Schematic representation of common flow configurations in membrane modules adapted from [9]. 17

1.9 Time lag curve, operating under conditions where the permeate pressure is negligible relative to the feed pressure from [44] 18

1.10 Paul's pulsed membrane process and pressure cycle. τ is the cycle duration and w the fraction of the period at high pressure. [10] 19

1.11 Feng's process schema and pressure cycle. τ is the cycle duration, w the fraction of period. 23

1.12 Long and short class processes for transient membrane separation [46]. . . . 25

1.13 Composition path principle. 26

1.14 From [15]: O_2 recovery ratio of the O_2-enriched flux as a function of O_2 mole fraction in the same flux. Continued red lines: novel process using basic option with different volume ratios γ (0.1, 1, 10, 100, 1,000 and 10,000 from bottom to top, respectively). Bold continued red line: $\gamma = 10$. Dashed blue line: conventional operations using cross flow modules. Dotted blue line: conventional operations using perfectly stirred modules. Green stars: novel process using sidestream option with $\gamma = 10$ and the downstream flux is recycled. 27

1.15 Pulsed Retentate Operation steps, compared to steady-state [14] 29

2.1 Steady-state membrane separation process. Q_{feed}, Q_{ret} and Q_{perm} denote the volumetric flowrates of the feed, retentate and permeate. x_{feed}, x and y are the molar fractions of the fast permeating component in the feed, retentate and permeate. Φ refers to the molar flux though the membrane, while ε_{mem} is the membrane thickness 40

2.2 Membrane Piston system. The piston with the membrane acts as a wall between compartments I and II; $W_{membrane\ piston}$ denotes the necessary work for compression and separation, P the pressure, T the temperature and x the composition in the indicated compartment, ε_{mem} is the membrane thickness. i and j denotes the fast and slow components respectively 43

2.3 Membrane-Piston concept at the start of the operation, during the compression and at the end of the process with schematic pressure level associated (a,b,c). •: slow component, ○: fast component. Dotted line: pressure-time curve in the permeate. Continuous line: pressure-time curve in the retentate. 44

2.4 Membrane-Piston concept during the relaxation time with schematic pressure level associated. See caption of Figure 2.3 for the description of lines and symbols. 45

2.5 Membrane-Piston concept on open mode at the start of the operation, during the compression and at the end of the process with schematic pressure level associated. See caption of Figure 2.3 for the description of lines and symbols. 46

2.6 Reference steady-state for comparison purpose. See previous figures for symbols description. 47

2.7 Illustration of mass transfer limitation in the Membrane Piston. 51

2.8 Impact of boundary layers on Membrane Piston performance. (a) Volume evolution versus time (b) Temperature evolution versus time. In both cases, curves are overlayed (c) Pressure evolution versus time (d) Molar composition (e) Composition path (f) Molar work for nitrogen production. Black: No mass transfert limitations; Red curves: $k = 10^{-1} m/s$; Blue curves: $k = 10^{-2} m/s$; Green curves: $k = 10^{-3} m/s$. 58

2.9 Impact of boundary layers on Membrane Piston performance. (a) Volume evolution versus time (b) Temperature evolution versus time. In both cases, curves are overlayed (c) Pressure evolution versus time (d) Molar composition (e) Composition path (f) Molar work for nitrogen production. Black: No mass transfer limitations; Green curves: $k = 10^{-3} m/s$; Orange curves: $k = 10^{-4} m/s$. 60

2.10 Impact of $\alpha(T)$ on Membrane Piston performance: O_2/N_2 separation in the Membrane Piston process. (a) Volume evolution versus time (b) Temperature evolution versus time. In both cases, curves are overlayed (c) Pressure evolution versus time (d) Molar composition (e) Composition path (f) Molar work for nitrogen production. Black and blue curves: $\alpha^* = 7.3$ and conduction through the piston walls; red and magenta curves: $\alpha(T)$ for the same membrane and conduction through the piston walls; cyan and green curves: $\alpha(T)$ for the same membrane and NO conduction through the piston walls. (a)-(d): Continuous line: Compartment I. Dashed line: Compartment II. (e)-(f): Continuous line: Membrane Piston. Dash-dotted line: steady-state results. 63

2.11 Master curves for the adiabatic system (a) Dimensionless time t^* vs $x_{I,N2}$ vs W_{mol} (b) Dimensionless time t^* vs $x_{I,N2}$ vs $x_{II,O2}$ 67

2.12 Master curves for the closed system with heat transfer through the piston wall (a) Dimensionless time t^* vs $x_{I,N2}$ vs W_{mol} (b) Dimensionless time t^* vs $x_{I,N2}$ vs $x_{II,O2}$ 68

2.13 Master curves for the open system (a) Dimensionless time t^* vs $x_{I,N2}$ vs W_{mol} (b) Dimensionless time t^* vs $x_{I,N2}$ vs $x_{II,O2}$ 69

3.1 O_2/N_2 separation in the Membrane Piston process, using inputs from Table 1. Continuous line: Compartment I. Dashed line: Compartment II. Dash-dotted line: steady-state results (a) Volume evolution versus time (b) Temperature evolution versus time. In both cases, curves are overlayed (c) Pressure evolution versus time (d) Molar composition (e) Composition path (f) Molar work for nitrogen production. 74

3.2 Recap of the parameters of interest in the parametric study. 77

3.3 Impact of velocity, selectivity and permeability on energy requirement of the Membrane Piston for Nitrogen Enrichment. (a) Closed mode (b) Open mode. Full symbol: Membrane piston system; Hollow symbol: Steady-state following the reference process ; black: base case; red: $50\alpha^*$, green: $5\alpha^*$; blue: $5\mathscr{P}_{\text{fast component}}$; purple: $50\mathscr{P}_{\text{fast component}}$. 79

3.4 Impact of velocity, selectivity and permeability on energy requirement of the Membrane Piston for Biogas separation. (a) Closed mode (b) Open mode. See Fig 3.3 for description. 82

3.5 Minimal molar work for slow component enrichment in closed mode, with $x_{\text{in, slow component}} = 0.8$ & $x_{\text{I, slow component}} = 0.95$, from 5 cases to a broad range of possible materials 86

3.6 Minimal molar work ratio for different initial compositions $x_{\text{in, slow component}}$, with $x_{I,\text{slow component}} = x_{\text{obj}}$. Blue •: $x_{\text{obj}} = 0.9$; yellow ■: $x_{\text{obj}} = 0.95$; green ♦: $x_{\text{obj}} = 0.98$; red ▲: $x_{\text{obj}} = 0.99$. (a) $\alpha^* = 8$ case, (b) $\alpha^* = 40$ case. . . . 88

3.7 Steady-state membrane separation (a) Using Polaris Membrane with two stages (b) Using a reverse selectivity membrane with one stage (c) Using a reverse selectivity membrane with two stages (d) Final molar work for two $\eta = 0.8$ and $\eta = 0.9$ for all three cases presented. $\Psi_{recovered}$ corresponds to the pressure ratio of the stage where the CO_2 is recovered. 91

3.8 Membrane piston performances to reach 80% purity of CO_2 including the required molar work (red) to end pressure in the process (green) 93

3.9 Membrane piston performances for five cases of selectivity and permeance (a) Molar work evolution compared to piston velocity with respective recovery. Label at $\min(W)$. (b) Molar work for targeted recovery compared to end pressure in the system. 94

4.1 Membrane piston, from concept to experiental design 100

4.2 Experimental set-up 101

4.3 Membrane system 102

4.4 Experimental apparatus 104

4.5 Leaks in compartments (a) I and (b) II at pressure from 1 to 6 bar gauge . . 105

4.6 Comparison of experimental and simulation pressure values vs time for pure gas with and without leaks. Symbols: experimental data (•, ■, and ♦); solid lines: simulations without leaks; dashed lines (–): simulations with leaks. . 109

4.7 Parity plot experimental vs simulated values pressure in the Membrane Piston system at 300 mm (before the leaks) and at $t^* = 1$ (end of compression). Green: 0.05 $mm\,s^{-1}$; red: 0.1 $mm\,s^{-1}$; blue: 0.2 $mm\,s^{-1}$; purple: 0.5 $mm\,s^{-1}$; brown: 1 $mm\,s^{-1}$; yellow: 1.5 $mm\,s^{-1}$ (a) Compartment I, no leaks simulated (b) Compartment I with leaks in the simulation (c) Compartment II with no simulated leaks in compartment I (d) Compartment II with leaks simulated in compartment I 110

4.8 Parity plot experimental vs simulated values pressure in the Membrane Piston system at 300 mm (before the leaks) and at $t^* = 1$ (end of compression). Yellow: 0.08 $mm\,s^{-1}$; blue: 0.2 $mm\,s^{-1}$; purple: 0.5 $mm\,s^{-1}$; brown: 0.8 $mm\,s^{-1}$. Empty marker: flush/open mode; filled marker: closed mode. • & ○: initial composition 30%CO_2/70%N_2; ■ & □: initial composition 50%CO_2/50%N_2. (a) Compartment I with leaks in the simulation (b) Compartment II with leaks simulated in compartment I 111

4.9 Parity plot experimental vs simulated values for molar fraction in compartment I in the Membrane Piston system at 320 mm (before the leaks) and at 375 mm (end of compression). Blue: 0.2 $mm\,s^{-1}$; red: 0.5 $mm\,s^{-1}$. (a) Composition in N_2 (b) Composition in CO_2 112

4.10 Parity plot experimental vs simulated values for molar fraction in compartment I in the Membrane Piston system at 320 mm (before the leaks) and at 375 mm (end of compression). Blue: 0.2 $mm\,s^{-1}$; red: 0.5 $mm\,s^{-1}$. Empty marker: flush/open mode; filled marker: closed mode. • & ○: initial composition 30%CO_2/70%N_2; ■ & □: initial composition 50%CO_2/50%N_2. (a) Composition in N_2 (b) Composition in CO_2 113

5.1 Schematic representation of the minimum work for a separation 118

5.2 Perfect separation. 120

5.3 Perfect separation with partial recovery rate of a pure stream of the component of interest. 121

5.4 Perfect separation with partial recovery rate of a non-pure stream of the component of interest. 123

5.5 Initial and final state for separation using the Membrane Piston process . . . 124

5.6 System boundaries for the entropy analysis. 127

5.7 Molar work and Membrane Piston efficiency for multiple velocities for a fixed output of $x_{I,N_2} = 0.95$ for air separation 130

5.8 Impact of the velocity variation on the separation performances (a) Velocity depending on position in the piston (b) Entropy per mole of nitrogen produced (c) Pressure ratio evolution (d) Composition path (e) Work per mole of nitrogen produced (f) Nitrogen recovery. Black: reference case; blue: slow down; red: speed up; green: pulse. 132

5.9 Impact of the velocity variation on the separation performances: zoom on entropy versus work. Labels indicate the maximum of x_{N_2} reached. 133

5.10 Velocity profile minimizing S_c (a) Velocity depending on position in the piston (b) Entropy per mole of nitrogen produced (c) Pressure ratio evolution (d) Composition path (e) Work per mole of nitrogen produced (f) Nitrogen recovery. Black: optimized case; red: reference case at $\dot{V} = 4.4 \cdot 10^{-9} \mathrm{m^3\,s^{-1}}$. 135

5.11 Velocity profile minimizing W (a) Velocity depending on position in the piston (b) Entropy per mole of nitrogen produced (c) Pressure ratio evolution (d) Composition path (e) Work per mole of nitrogen produced (f) Nitrogen recovery. Black: optimized case; red: reference case at $\dot{V} = 3.3 \cdot 10^{-9} \mathrm{m^3\,s^{-1}}$. 136

A.1 Permeability–selectivity relationship for O_2/N_2. 158

A.2 Permeability–selectivity relationship for CO_2/N_2. 159

A.3 Permeability–selectivity relationship for CO_2/CH_4. 160

B.1 Compressibility factor for a $20\%O_2/80\%N_2$ mixture 162

B.2 Compressibility factor for a $40\%CO_2/60\%CH_4$ mixture 162

C.1 $x_{\text{in, slow component}} = 0.95$ 163

C.2 $x_{\text{in, slow component}} = 0.80$ - Closed mode 164

C.3 $x_{\text{in, slow component}} = 0.80$ - Open mode 164

C.4 $x_{\text{in, slow component}} = 0.60$ 165

C.5 $x_{\text{in, slow component}} = 0.40$ 166

C.6 Summary of all $x_{\text{in, slow component}}$ and $x_{\text{ret, slow component}}$ 167

E.1 Parity plot experimental vs simulated values pressure in the Membrane Piston system at 300 mm (before the leaks) and at $t^* = 1$ (end of compression). Green: 0.05 $\text{mm}\,\text{s}^{-1}$; red: 0.1 $\text{mm}\,\text{s}^{-1}$; blue: 0.2 $\text{mm}\,\text{s}^{-1}$; purple: 0.5 $\text{mm}\,\text{s}^{-1}$; brown: 1 $\text{mm}\,\text{s}^{-1}$; yellow: 1.5 $\text{mm}\,\text{s}^{-1}$ (a) Compartment I, no leaks simulated (b) Compartment I with leaks in the simulation (c) Compartment II with no simulated leaks in compartment I (d) Compartment II with leaks simulated in compartment I 171

List of Tables

1.1 Representative polymeric membranes and their typical gas separation applications. 13

1.2 Summary of the steps for Feng's processes. 21

1.3 Performance data for the Pressure Swing Permeation (PSP) process. 22

1.4 Performance data for the Pressure–Vacuum Swing Permeation (PVSP) process – Oxygen-Enriched Air (OEA) case. 22

1.5 Summary of transient and cyclic membrane separation processes with operational descriptions 30

1.6 Comparison between minimum and real work of separation for various processes and process efficiency [4]. 35

2.1 Comparison of separation approaches 48

2.2 Activation energy and pre-exponential permeability factor for N_2 and O_2 from laboratory data. 61

2.3 Dimensionless numbers organized by similarity across phases. 65

3.1 Input parameters and results for a O_2/N_2 separation using the Membrane Piston system and comparison to the steady-state with permeate vacuum and retentate compression 76

3.2 Model input parameters 78

3.3 Velocity, selectivity and permeance impact on required molar work for air separation in closed mode. SS = steady-state, referring to the classical compression then membrane module unit. 79

3.4 Velocity, selectivity and permeance impact on required molar work for air separation in open mode. SS = Steady-state. 80

3.5 Velocity, selectivity and permeability impact on required molar work for biogas separation in closed mode. SS = Steady-state. 81

3.6 Velocity, selectivity and permeability impact on required molar work for biogas separation in open mode. SS = Steady-state. 83

3.7 Comparison of minimal molar work ratio $W_{\text{mol}}^{x_{\text{slow}}}$ for two membrane configurations 87

3.8 Performance metrics for different configurations in steady-state 92

3.9 Performance parameters for five membrane type cases using the Membrane Piston. Upper part of the table: parameters and performances at minimum work; lower part: performances for 80 and 90% recovery 95

4.1 Permeance comparison of the PolyActive with different measurement methods compared to the lab database 103

4.2 Selectivity comparison of the PolyActive compared to the lab database . . . 103

5.1 Fixed parameters and geometry for the piston optimization study. 129

5.2 Summary of piston configurations and corresponding thermodynamic results. 134

D.1 Performances of N_2-selective membranes 169

Abstract, Résumé & Résumé étendu

Abstract

Gas separation plays a crucial role in many industrial sectors, including energy, environment, and chemical production. Conventional technologies such as cryogenics, adsorption, or absorption are often energy-intensive and depend on phase changes or solvents. Membrane processes offer a promising alternative, combining modularity, small footprint, and potential energy savings. However, most membrane systems operate at steady state, which limits performance and efficiency due to fixed driving forces and the intrinsic trade-off between selectivity and permeability of polymeric materials. This thesis investigates an innovative unsteady-state process, the Membrane Piston, which integrates gas compression and separation within a single unit. The concept combines the high mechanical efficiency of piston compression with selective permeation through a moving membrane that separates two compartments. As the piston moves, pressure and composition vary dynamically, creating time-dependent driving forces that enhance selectivity while potentially reducing energy consumption compared to conventional feed compression or vacuum systems. A theoretical model was developed based on mass and energy balances under perfect gas assumptions for binary mixtures between 5 and 15 bar. Dimensionless parameters were introduced to characterize the system's behavior and scaling. Parametric studies revealed the influence of membrane selectivity, permeance, feed composition, and piston velocity. For air separation and biogas upgrading, the Membrane Piston achieved comparable purity and recovery to standard membrane systems while reducing specific energy consumption by 30–60%. Selectivity controls achievable purity, whereas permeance and piston velocity determine productivity and energetic efficiency. The open-mode configuration, where one compartment acts as an infinite sink, proved the most effective. The concept was also applied to CO_2 capture. Although conventional membranes favor fast CO_2 permeation, the Membrane Piston tends to recover the slower-permeating component. Simulations with emerging reverse selectivity membranes predict CO_2 purities up to 80% at 5 bar, with markedly lower energy requirements than steady-state systems. An experimental proof of concept confirmed the feasibility of the process. Despite leakage issues linked to moving parts, measured pressures

and composition agreed with simulations within about 10%. A thermodynamic analysis based on entropy generation was finally conducted to evaluate efficiency and identify optimization paths. Results show that the Membrane Piston operates more efficiently than conventional configurations. Optimizing the piston velocity profile, particularly through acceleration during compression, reduces entropy generation, minimizes molar work, and can increase product purity. Overall, this work demonstrates that coupling compression and separation in a dynamic membrane system provides a promising route toward more energy-efficient gas separations. The Membrane Piston thus represents a conceptual advance at the interface between mechanical and membrane technologies. Future research will focus on CFD simulations, prototype optimization, and multistage or divergent-nozzle configurations to further enhance performance and broaden industrial applicability.

Résumé

La séparation des gaz joue un rôle essentiel dans de nombreux secteurs industriels, notamment l'énergie, l'environnement et la production chimique. Les technologies conventionnelles, telles que la cryogénie, l'adsorption ou l'absorption, sont souvent énergivores et reposent sur des changements de phase ou l'utilisation de solvants. Les procédés membranaires constituent une alternative prometteuse, offrant modularité, faible empreinte environnementale et économies d'énergie potentielles. Toutefois, la plupart des systèmes membranaires fonctionnent en régime permanent, ce qui limite leurs performances et leur efficacité énergétique en raison de forces motrices fixes et du compromis intrinsèque entre sélectivité et perméance des matériaux polymères. Cette thèse étudie un procédé innovant fonctionnant en régime transitoire, le Piston Membranaire, qui intègre la compression et la séparation des gaz au sein d'un même dispositif. Le concept associe l'efficacité mécanique de la compression par piston à la perméation sélective d'une membrane mobile séparant deux compartiments. Le mouvement du piston entraîne des variations dynamiques de pression et de composition, générant des forces motrices variables susceptibles d'améliorer la sélectivité tout en réduisant la consommation énergétique par rapport aux systèmes classiques à compression ou à vide. Un modèle théorique a été développé à partir des bilans de masse et d'énergie pour des gaz parfaits, appliqué à des mélanges binaires entre 5 et 15 bar. Des paramètres sans dimension ont été introduits pour caractériser le comportement du système et faciliter son dimensionnement. Les études paramétriques ont mis en évidence l'influence de la sélectivité, de la perméance, de la composition d'alimentation et de la vitesse du piston. Pour la séparation de l'air et l'épuration du biogaz, le Piston Membranaire atteint des puretés et rendements comparables à ceux des systèmes conventionnels, tout en réduisant la consommation énergétique spécifique de 30 à 60%. La sélectivité détermine la pureté atteignable, tandis que la perméance et la vitesse du piston influencent la productivité et l'efficacité énergétique. La configuration en mode ouvert, où un compartiment agit comme réservoir infini, s'est révélée la plus performante. L'application du concept à la capture du CO_2 a également été explorée. Bien que les membranes actuelles favorisent la perméation rapide du CO_2,

le Piston Membranaire tend à récupérer le composé le plus lent. Des simulations menées avec des membranes à sélectivité inversée prédisent des puretés de CO_2 atteignant 80% à 5 bar, pour des besoins énergétiques nettement inférieurs à ceux des procédés stationnaires. Une validation expérimentale a permis de confirmer la faisabilité du procédé. Malgré des fuites résiduelles liées aux pièces mobiles, les pressions et débits mesurés concordent avec les simulations à environ 10% près. Enfin, une analyse thermodynamique fondée sur la création entropique a été réalisée pour évaluer et optimiser l'efficacité du procédé. Les résultats montrent que le Piston Membranaire présente une efficacité supérieure aux systèmes conventionnels. L'optimisation du profil de vitesse du piston, notamment une accélération en phase de compression, réduit la création d'entropie, diminue le travail molaire et améliore la pureté obtenue. Dans l'ensemble, ces travaux démontrent que l'intégration simultanée de la compression et de la séparation au sein d'un système dynamique ouvre la voie à des procédés membranaires plus sobres en énergie. Le Piston Membranaire représente ainsi une avancée conceptuelle majeure à l'interface entre technologies mécaniques et séparatives. Les perspectives incluent des simulations CFD, l'optimisation du prototype et l'étude de configurations multi-étagées ou à tuyère divergente pour renforcer encore les performances et élargir les applications industrielles.

Résumé étendu

Les procédés de séparation industriels, tels que la cryogénie, l'adsorption ou l'absorption, sont utilisés depuis longtemps pour la séparation des gaz [1]. Plus récemment, les procédés à membranes se sont imposés comme une alternative prometteuse pour des applications variées : production d'azote, purification d'hydrogène, valorisation du biogaz ou récupération de composés organiques volatils. Leur attrait réside dans leur modularité, leur faible encombrement, l'absence de solvants et les économies d'énergie potentielles par rapport aux méthodes classiques comme la distillation [2, 19, 3]. Cependant, l'efficacité énergétique de ces procédés reste un enjeu majeur. Bien que les membranes soient souvent présentées comme peu énergivores, les performances observées varient fortement. Deux stratégies dominent : la compression de l'alimentation, plus courante mais énergétiquement coûteuse, et le pompage sous vide, plus limité en efficacité et en mise à l'échelle. Dans les deux cas, la consommation énergétique dépend du débit traité, du rapport de pression et du rendement des équipements [4, 5].
Dans un contexte de transition énergétique et de décarbonation, il est essentiel d'optimiser ces procédés. C'est dans cette optique qu'a été développé le concept du Piston Membranaire, un système innovant qui combine séparation et compression dans une seule opération. Il tire parti à la fois de la réduction progressive de la quantité de gaz à comprimer et de la grande efficacité mécanique des compresseurs à piston, ouvrant la voie à des procédés de séparation plus compacts et économes en énergie. L'objectif de cette thèse est de développer un concept innovant visant à réduire les besoins énergétiques et à améliorer l'efficacité globale des procédés en intégrant les opérations de séparation et de compression dans un seul système, appelé Piston Membranaire. La thèse est structurée en cinq chapitres :

- **Chapitre 1** : État de l'art. Présente les principes fondamentaux de la séparation par membranes, l'évolution historique des procédés transitoires et les approches existantes d'amélioration de l'efficacité énergétique, en soulignant les limites qui justifient cette recherche.

- **Chapitre 2** : Le concept de Piston Membranaire. Décrit en détail le fonctionnement du système, ses bases physiques et les nombres sans dimension qui caractérisent son comportement.
- **Chapitre 3** : Étude numérique du comportement du Piston Membranaire. Analyse le comportement dynamique du système à travers des simulations, notamment pour la séparation de l'air, du biogaz et pour la capture du CO_2 à l'aide de membranes à sélectivité inverse.
- **Chapitre 4** : Validation expérimentale. Présente la conception et la mise en œuvre d'un prototype expérimental, ainsi que les mesures de pression et de composition réalisées sur différents mélanges gazeux.
- **Chapitre 5** : Analyse d'efficacité énergétique. Évalue l'efficacité thermodynamique du procédé, détermine le travail minimal requis et explore l'usage de l'entropie comme fonction objectif pour optimiser le profil de vitesse du piston.

La perméation gazeuse est un procédé de séparation dans lequel une membrane laisse passer certains gaz plus facilement que d'autres, créant une différence de composition entre les deux côtés. Le mélange d'alimentation (feed) est introduit sur une face de la membrane : les gaz les plus lents forment le rétentat, tandis que les plus rapides (les plus *perméables*) constituent le perméat [27]. Les performances d'une membrane sont caractérisées par sa perméabilité (capacité d'un gaz à traverser le matériau) et sa sélectivité (aptitude à séparer deux gaz). La perméance, qui tient compte de l'épaisseur de la membrane, est souvent utilisée en ingénierie. Ces paramètres dépendent du matériau, de la pression, de la température et des interactions gaz-membrane. Dans les membranes denses, le transport suit le modèle solution-diffusion [9, 19] : les molécules se dissolvent dans le matériau, diffusent à travers lui, puis ressortent de l'autre côté. La séparation résulte des différences de solubilité et de diffusivité entre les gaz. Enfin, la perméance constitue un indicateur global du transport, essentiel pour la conception, la mise à l'échelle et l'optimisation des systèmes de séparation par membrane [19].

De nombreux matériaux sont utilisés pour la perméation des gaz. Les membranes polymères dominent le marché industriel en raison de leur faible coût, de leur flexibilité et de leur facilité de fabrication. Elles sont largement employées pour la séparation de l'air, la récupération d'hydrogène ou l'élimination du CO_2. Leur performance est toutefois limitée par le compromis entre perméabilité et sélectivité, décrit par la courbe limite de Robeson [34]. Les recherches actuelles visent à dépasser cette limite grâce à de nouveaux polymères ou à des structures composites [35, 30, 36].

Les procédés transitoires en séparation membranaire représentent une approche alternative aux opérations classiques en régime permanent [16]. En introduisant une dépendance temporelle, par impulsions, cycles de pression ou phases fermées, ils visent à exploiter les différences de cinétique de diffusion entre gaz pour améliorer la sélectivité ou la récupération. Ces méthodes, inspirées d'expériences fondamentales (comme le time-lag) ou d'analogies avec d'autres technologies cycliques (PSA, distillation périodique), ont évolué depuis les années 1970 vers des concepts plus performants et applicables industriellement. Les principales variantes, présentées ci-dessous, illustrent les stratégies et avantages de cette approche dynamique.

- **Time-lag** [43] : Méthode expérimentale classique pour mesurer la diffusivité et la perméabilité d'un gaz dans une membrane dense. On observe le retard de l'arrivée du perméat après mise sous pression du côté amont ; la durée de retard permet de calculer D puis la perméabilité et la solubilité, données essentielles pour la modélisation.

- **Paul (pulsed membrane)** [10] : Ce procédé consiste à réaliser des opérations cycliques. Dans une première phase, un mélange est placé dans le compartiment du rétentat et comprimé sur une durée choisie de sorte à récupérer un perméat enrichi en composé rapide avant que le composé lent n'ait le temps de traverser la membrane. Puis le rétentat est vidé et l'opération recommence. Ce procédé permet d'augmenter fortement la sélectivité au prix d'une productivité réduite et d'une complexité opérationnelle élevée .

- **Pressure Swing Permeation (PSP)** [11] : Il s'agit d'un système continu à plusieurs modules alternés, inspiré du PSA, qui récupère le perméat à haute pression via un cycle synchronisé entre plusieurs modules. Il améliore la récupération et la composition du perméat par rapport à l'état stationnaire, mais il nécessite une coordination opératoire précise entre les modules et des cycles courts.

- **Pressure–Vacuum Swing Permeation (PVSP)** [12, 13] : C'est une variante monoprocédé du PSP qui utilise un seul module et une pompe basculante (capable de comprimer et de réaliser le vide). Cette variante simplifie l'architecture du procédé PSP tout en améliorant la récupération et les performances sur certains cas (O_2, CO_2) ; l'optimisation du rapport volumes amont/aval et des pressions conditionne l'efficacité du procédé.

- **Cyclic batch / free diffusion (Wang)** [46, 15] : Le procédé opère en mode fermé dans lequel la composition et la pression évoluent librement au sein d'un seul module ; des

cycles longs ou courts définissent deux régimes (régime instationnaire sur temps court dans lequel la diffusion domine ou régime pseudo-stationnaire sur temps long). Ce procédé peut atteindre des combinaisons de variables pureté/récupération inaccessibles en continu, mais il demande une gestion précise des volumes et des opérations de mise sous vide.

- **Pulsed retentate** [14, 48, 49] : Ce cycle est centré sur la fermeture temporaire de la vanne du rétentat puis une brève vidange du rétentat enrichi. Il est conçu pour extraire le composé lent sans perte de productivité, il est compatible avec l'utilisation de membranes ultrafines et intégrable à des PSA ; il offre des gains de séparation sans contrainte forte sur l'épaisseur des membranes .

Ces technologies transitoires montrent qu'on peut dépasser certaines limites stationnaires en jouant sur le temps et la configuration des cycles ; toutefois, l'impact énergétique reste peu traité systématiquement et mérite d'être intégré comme critère d'optimisation.
L'optimisation énergétique est un enjeu central pour tout procédé de séparation. Chaque opération consomme une certaine quantité d'énergie, qu'il s'agit de réduire au maximum pour tendre vers le rendement thermodynamique idéal (celui associé à une opération de séparation réversible). Cette idée est souvent illustrée par le paradoxe du démon de Maxwell, qui met en évidence la limite entre séparation idéale et irréversibilités réelles. En pratique, aucune séparation ne peut être parfaitement réversible : les membranes, compresseurs ou vannes introduisent des dégradations énergétiques liées aux frottements, aux mélanges ainsi qu'aux pertes thermiques. Ces phénomènes sont associés à une production d'entropie, marqueur de l'irréversibilité du processus. La comparaison entre le travail minimal théorique (W_{min}) et le travail réel (W_{real}) permet de définir l'efficacité énergétique du procédé ($\eta = W_{min}/W_{real}$). Les procédés membranaires, bien qu'avantageux par leur simplicité et leur modularité, ne sont pas toujours les plus performants énergétiquement. Leur amélioration repose donc sur la réduction des irréversibilités et l'optimisation de la répartition des forces motrices et de la production d'entropie dans le système. Les concepts d'équipartition des forces, de la production d'entropie, ou de la vitesse thermodynamique, offrent ainsi un cadre théorique pour concevoir des procédés plus efficaces, en minimisant la dissipation d'énergie tout au long du transfert de matière.

Le concept de Piston Membranaire a été proposé afin de réduire la consommation énergétique des procédés de séparation gazeuse par membrane [17]. Dans les systèmes classiques, le coût énergétique provient presque entièrement de la compression du gaz d'alimentation ou du pompage sous vide du perméat, deux opérations efficaces mais coûteuses et parfois difficiles

à mettre en œuvre, notamment concernant le pompage sous vide [9]. L'idée novatrice du procédé Piston Membranaire est de combiner la compression et la séparation dans une même étape, en utilisant un piston pour comprimer uniquement une fraction réduite de gaz tout en générant la différence de pression nécessaire à la perméation. Ce couplage dynamique permettrait ainsi de limiter le travail mécanique global et d'améliorer significativement l'efficacité énergétique du procédé. Le fonctionnement du procédé membranaire classique en régime permanent est d'abord présenté, avant de détailler le principe du concept du Piston Membranaire, opéré en régime transitoire.

Les procédés en régime permanent sont classiquement modélisés à l'aide de bilans globaux et de bilans partiels (sur les composés impliqués) dans des modules de type cross-flow, comme présenté par [47], permettant de prédire les compositions et les flux de sortie ainsi que l'effort énergétique requis pour la compression ou la mise sous vide. Le régime permanent constitue la référence pour comparer les avantages des approches transitoires en termes de pureté, récupération et efficacité énergétique.

Pour évaluer les performances du procédé de séparation présenté, il est essentiel de combiner les critères de séparation (compositions finales) et d'énergie, tout en tenant compte de l'état thermodynamique des mélanges finaux. En effet, un mélange à haute pression possède possède un capital énergétique (c'est-à-dire une valeur exergétique) supérieur à un mélange identique sous basse pression. La prise en compte de l'état thermodynamique des mélanges produits par le procédé doit donc être prise en compte dans l'évaluation énergétique globale dudit procédé. Afin de comparer équitablement le procédé proposé dans cette étude (Piston Membranaire) et les procédés usuels, les conditions finales de pression ont été choisies identiques : si nécessaire, afin d'assurer une comparaison la plus équitable possible, le rétentat du procédé usuel en régime permanent le plus économe en énergie est comprimé afin que ce rétentat soit obtenu au même niveau exergétique que celui produit par le Piston Membranaire.

La modélisation du Piston Membranaire s'effectue à partir de bilans de matière et d'énergie sur le procédé et ses sous-systèmes, en tenant compte d'hypothèses simplificatrices - telles que l'hypothèse des gaz parfaits (très efficace pour des systèmes dont la pression n'excède pas 10 à 15 bar) et l'absence de limitation au transfert en dehors de la membrane - et en prenant en compte les phénomènes de transfert thermique entre le corps du piston et le milieu extérieur. Ces choix sont discutés indépendamment, tout comme la dépendance de la sélectivité du matériau membranaire à la température.

Le modèle proposé est résumé par l'équation (2.29).

$$
\begin{cases}
\dfrac{dn_{I,i}}{dt} = -\Phi_i, \quad \text{for } i \in \{1,\dots,p\} \\
\dfrac{dn_{II,i}}{dt} = \Phi_i, \quad \text{for } i \in \{1,\dots,p\} \\
\dfrac{dV_I}{dt} = -\dot{V} \\
\dfrac{dV_{II}}{dt} = +\dot{V} \\
\underbrace{n_I}_{\sum_i n_{I,i}} \cdot c_{v,I} \dfrac{dT_I}{dt} = -\dfrac{\lambda A}{\varepsilon - mem}(T_I - T_{II}) - \dfrac{\lambda_{\text{wall}} S_{\text{I, ext}}}{\varepsilon_{\text{piston}}}(T_I - T_{atm}) + P_I \dot{V} - RT_I \sum_i \Phi_i \\
\underbrace{n_{II}}_{\sum_i n_{II,i}} \cdot c_{v,II} \dfrac{dT_{II}}{dt} = +\dfrac{\lambda A}{\varepsilon_{mem}}(T_I - T_{II}) - \dfrac{\lambda_{\text{wall}} S_{\text{II, ext}}}{\varepsilon_{\text{piston}}}(T_{II} - T_{atm}) - P_{II} \dot{V} + RT_{II} \sum_i \Phi_i \\
\dot{W}_{\text{compression}} = -(P_{II} - P_I) \cdot \dot{V} - \sum_i \dfrac{dn_i}{dt} \left[h^{\bullet}_{i\ \text{pure}}(T_{II}) - h^{\bullet}_{i\ \text{pure}}(T_I) \right] \\
P_I = \dfrac{n_I R T_I}{V_I} \\
P_{II} = \dfrac{n_{II} R T_{II}}{V_{II}}
\end{cases}
\tag{2.29}
$$

Un modèle adimensionnel est également proposé, afin de pouvoir comparer plus facilement le fonctionnement du Piston Membranaire à celui d'une séparation membranaire en régime permanent.

Plusieurs études de cas ont été conduites sur les applications potentielles de ce système transitoire. Pour illustrer le concept de Piston Membranaire, une étude de cas sur la séparation de l'air [17], a été menée. Le système utilise une membrane commerciale typique pour l'air enrichi en azote (NEA) avec une sélectivité $\alpha^* = 7$, choisie sur la courbe de compromis (trade-off) entre perméance et sélectivité [34]. Le transfert thermique à travers la membrane et le corps du piston en aluminium tend à maintenir un processus quasi-isotherme. Sur la période de relaxation, la séparation continue légèrement, améliorant la pureté finale. La composition maximale en azote dans le compartiment I atteint 97,1%, suffisante pour de nombreuses applications d'inertage ou comme étape de pré-concentration a une pression de 12,4 bar. Comparé à un processus classique en régime permanent avec compression du rétentat et tirage sous vide du perméat, le processus Piston Membranaire réduit de 45% le travail molaire nécessaire pour produire de l'azote à 95% de pureté et de 24% pour atteindre la pureté maximale. Ces résultats démontrent le potentiel du processus transitoire piston-

membrane pour améliorer significativement l'efficacité énergétique tout en conservant des performances de séparation proches des processus en régime permanent.
Pour explorer les performances potentielles du système Piston Membranaire, une série d'études paramétriques a été menée en faisant varier la vitesse du piston, la perméance et la sélectivité des membranes. L'objectif a été d'évaluer l'efficacité énergétique réalisable par ce procédé transitoire par rapport aux modules à membrane classiques en régime permanent. Ces investigations s'appuient sur des études précédentes sur la séparation de l'air pour l'obtention d'air enrichi en azote [17] et étendent les résultats en considérant différentes conditions de vitesse du piston et de propriétés membranaires [18].
Dans le cas de l'air, le Piston Membranaire montre un impact significatif de la vitesse du piston et de la sélectivité sur le travail molaire nécessaire pour atteindre une pureté industrielle en azote. Il existe une vitesse optimale du piston permettant de minimiser le travail de séparation, souvent inférieure à celui requis par un processus classique en régime permanent, ce qui suggère un potentiel de réduction d'énergie substantiel. La sélectivité influence fortement l'énergie minimale, tandis que la perméance agit principalement sur la vitesse du piston nécessaire pour atteindre la pureté cible. De plus, le mode ouvert, où le compartiment de perméat est relié à l'atmosphère, permet de réduire encore davantage le travail énergétique par rapport au mode fermé.
Pour le biogaz, le Piston Membranaire permet également d'atteindre des enrichissements élevés en méthane avec une consommation énergétique plus faible que le procédé classique, suivant des tendances similaires à celles observées pour l'air. Les performances dépendent de la vitesse du piston et des caractéristiques de la membrane, en particulier pour des perméances élevées, certaines configurations ne permettant pas d'atteindre la pureté souhaitée. Comme pour l'air, le mode ouvert offre un avantage énergétique supplémentaire, réduisant notablement le travail minimal requis pour la séparation. Ces résultats confirment que le procédé est prometteur pour différents types de mélanges gazeux et que l'optimisation de la vitesse et des propriétés membranaires est essentielle pour maximiser l'efficacité énergétique.
Les tendances observées dans les études de cas sont confirmées lorsque les plages de sélectivité et de perméance sont élargies. À sélectivité constante, la variation de la perméance conduit à des courbes d'iso-sélectivité quasi linéaires, indiquant que le travail molaire minimal requis pour une séparation donnée ne dépend pas de la perméance, bien que l'augmentation de celle-ci entraîne une hausse de la vitesse du piston, influençant la productivité du procédé. Inversement, lorsque la perméance est maintenue constante et que la sélectivité augmente, le travail minimal diminue mais tend à se stabiliser pour des valeurs élevées, traduisant une saturation de l'effet bénéfique de la sélectivité lorsque le rapport de pression devient limitant. Enfin, cette étude propose un outil graphique sous forme de grille permettant

d'estimer l'énergie requise pour une composition d'alimentation donnée en fonction des caractéristiques membranaires, généralisable à tout gaz léger sous hypothèse de gaz parfait, et donc applicable à un large spectre d'applications industrielles.
Deux cas représentatifs ont été étudiés afin de comparer plus finement les performances du système Piston Membranaire à celles du régime permanent : un à faible sélectivité et un à sélectivité élevée. Les résultats montrent que, selon la composition d'alimentation et la pureté visée, le système transitoire permet une réduction significative du travail molaire par rapport au procédé à l'état stationnaire. Cette amélioration est particulièrement marquée en mode ouvert, où le ratio minimal du travail requis peut descendre jusqu'à environ 0,2. Toutefois, lorsque la fraction initiale du composé lent est faible, la séparation devient plus difficile et nécessiterait une optimisation du dimensionnement ou une configuration multi-étagée. Globalement, le procédé Piston Membranaire confirme ainsi son fort potentiel pour réduire la consommation énergétique des séparations membranaires.
Une dernière étude explore l'application du concept Membrane–Piston au catpage du dioxyde de carbone, un domaine encore peu étudié pour ce type de procédé. L'objectif a été d'évaluer si la combinaison d'un fonctionnement transitoire et de nouvelles membranes à sélectivité inversée (N_2-sélectives) peut permettre une réduction drastique de l'énergie requise pour la séparation. Après avoir comparé plusieurs configurations en régime permanent, les résultats montrent que le système Piston Membranaire, en mode ouvert, atteint des performances nettement supérieures : pour une récupération de 80 à 90 % du CO_2, la consommation énergétique chute à environ 60–70 kWh/tCO_2, soit près de deux à trois fois moins que les meilleures technologies membranaires actuelles. De plus, le CO_2 est récupéré directement sous pression, évitant un surcoût de recompression. Enfin, une étude prospective indique qu'avec l'amélioration des matériaux N_2-sélectifs, le potentiel du procédé pourrait encore s'accroître, positionnant le Membrane–Piston comme une voie prometteuse pour une capture du carbone plus efficiente.

La mise en œuvre expérimentale du système Membrane–Piston, réalisée dans le cadre de cette thèse, s'est avérée particulièrement complexe en raison de la présence de pièces mobiles et de fuites multiples, difficiles à quantifier. Afin de valider expérimentalement le concept du Piston Membranaire et confronter les résultats expérimentaux obtenus à ceux issus du modèle développé, le modèle a été légèrement modifié afin de tenir compte de la présence de fuites. Un terme de fuite utilisant pour paramètre un coefficient de fuite ajusté a été introduit. Ce coefficient a été déterminé à partir de différents gaz et mélanges.
Les mesures de pression réalisées au sein du dispositif montrent un bon accord avec les simulations dans le compartiment I, tandis que des écarts supérieurs à 10 % sont observés dans le

compartiment II, probablement liés à des fuites difficilement quantifiables. Des tendances similaires sont relevées pour l'évolution de la fraction molaire dans le compartiment I. Pour améliorer l'accord entre expérience et modèle, les prochaines étapes envisagées incluent un réalignement du piston afin de réduire les pertes et l'utilisation de membranes à plus forte sélectivité pour accentuer les différences mesurables de composition.
Malgré ces limitations, cette première démonstration expérimentale constitue une preuve de concept encourageante : elle valide partiellement le modèle en reproduisant de manière raisonnable les évolutions de pression et de composition observées, tout en soulignant les points à perfectionner pour de futures investigations.

L'efficacité énergétique du Piston Membranaire est directement liée à ses performances, car elle reflète le niveau d'irréversibilités générées au cours de l'opération. Le calcul du travail minimal W_{min}, calculé pour un cas non-isobare (c'est-à-dire en tenant compte du fait que les deux mélanges produits par le dispositif de séparation de gaz sont à des pressions différentes, supérieures à celle du mélange initial), montre que le procédé est nettement plus efficace que les séparations conventionnelles, avec une efficacité croissante lorsque la vitesse du piston augmente.
L'analyse de différents profils de vitesse du piston met en évidence l'influence marquée des phases d'accélération et de décélération sur la génération d'entropie et le travail molaire, impactant directement les performances de séparation. Si l'accélération tend à réduire l'entropie créée et le travail requis à partir d'une vitesse optimisée, elle améliore également l'efficacité globale de récupération du diazote. Une première optimisation a été réalisée en découpant le mouvement du piston en plusieurs phases sur lesquelles les vitesses sont différentes. Cela a permis de mettre en évidence l'intérêt d'accélérer ou de décélérer le mouvement du piston. En particulier, les configurations comportant une accélération en seconde partie de course offrent un bon compromis entre réduction des irréversibilités, diminution du travail à fournir et amélioration de la pureté en dioxygène pour la valorisation du compartiment II. Des travaux d'optimisation complémentaires sont néanmoins nécessaires pour affiner ces profils et atteindre un équilibre optimal entre efficacité, travail fourni et pureté du produit.

Les séparations membranaires constituent une technologie essentielle pour accompagner la transition énergétique. Cependant, leur fonctionnement en régime permanent limite leurs performances, notamment en raison des contraintes liées aux matériaux disponibles. Le concept de Piston Membranaire propose une approche innovante en combinant, dans un même dispositif, la compression et la séparation, permettant ainsi une évolution temporelle de la force motrice, à la différence des systèmes conventionnels. Les résultats obtenus dé-

montrent que ce procédé peut atteindre des performances industrielles pertinentes, tout en réduisant considérablement la consommation énergétique, que ce soit pour la séparation de l'air, la valorisation du biogaz ou encore le captage du dioxyde de carbone. Les simulations menées montrent notamment que le travail molaire minimal dépend fortement de la vitesse du piston, de la sélectivité et de la perméance de la membrane, et que des réductions d'énergie de 30 à 60 % peuvent être atteintes par rapport aux procédés stationnaires. Les premiers essais expérimentaux, bien que limités par des fuites difficiles à maîtriser, confirment la validité partielle du modèle et confortent la faisabilité du concept. Enfin, l'analyse entropique réalisée montre une nette amélioration du rendement thermodynamique, renforcée par l'optimisation du profil de vitesse du piston, dont l'accélération apparaît comme un levier efficace pour améliorer à la fois l'efficacité et la pureté des gaz produits.

Les perspectives de ce travail s'articulent autour de deux axes principaux. D'une part, le développement théorique se poursuivra avec la modélisation approfondie de systèmes à pistons multiples, associée à des simulations CFD, afin d'affiner la compréhension des phénomènes d'écoulement et de valider les tendances thermodynamiques observées. D'autre part, un axe expérimental visera l'amélioration du prototype, notamment par la réduction des fuites et l'intégration de membranes à plus forte sélectivité. Ces avancées s'appuieront sur des collaborations industrielles pour envisager une mise à l'échelle du concept. Enfin, de nouvelles configurations de procédés, comme l'intégration de tuyères divergentes ou de cycles de compression alternés, pourront être explorées pour optimiser encore les performances énergétiques et élargir le champ d'applications de ce système prometteur.

Remerciements

Quelques mots ne suffiront pas à résumer tout ce qui s'est passé ces trois dernières années, mais je tiens quand même à essayer de l'exprimer : je voudrais adresser mes plus sincères remerciements à toutes les personnes qui m'ont entourée pendant cette aventure : elle n'a été possible que grâce à votre soutien inconditionnel.

Tout d'abord, je remercie les membres de mon jury, Christophe Coquelet, Xuan-Mi Meyer, Pierrette Guichardon, Torsten Brinkmann et Yann Le Moullec, d'avoir accepté de faire partie de cette discussion. Merci d'avoir fait le déplacement, d'avoir pris le temps de vous intéresser à ce concept. Merci pour vos remarques pertinentes et vos questions, qui nous ont permis d'avoir une discussion enrichissante. Je pense que nous attendons tous impatiemment de voir ce qui adviendra du piston membranaire, mais merci d'avoir fait partie de cette première étape de développement.

À ceux qui ont mis les mains à la pâte, Hervé, le SERM et le SIEL, merci pour votre bienveillance, pour avoir toujours pris le temps de m'aider, d'écouter les problèmes et de créer des solutions toujours innovantes. Une petite pensée également pour Rebeca et Maxime, qui ont grandement contribué à tous les résultats expérimentaux : sans vous, ce chapitre serait bien vide. Vous avez fait un travail extraordinaire en peu de temps ; votre aide a été très précieuse.

À tous les collègues qui ont croisé ma route, je vous remercie pour les discussions au détour d'un couloir ou d'une manipulation, pour votre entrain à partager votre savoir.

Je ne peux évidemment pas oublier de mentionner le BJC : ce fut un plaisir d'organiser les événements du laboratoire à vos côtés et d'apprendre à vous connaître en dehors. Vous avez rendu les semaines bien plus agréables et je suis très heureuse de vous avoir rencontrés. Christophe, Romain, Éric, un énorme merci pour tout ce que vous avez fait ces trois dernières années. J'ai tellement appris à vos côtés. Vos encouragements incessants sont vraiment la raison pour laquelle je suis fière d'avoir pu finir cette thèse et de la présenter. Votre bonne humeur, les réunions-repas et les discussions au bar, les pauses tisanes… J'ai beaucoup de

bons souvenirs associés à tout ce que nous avons accompli et je suis fière d'avoir pu travailler à vos côtés.

La team membrane originelle, Margarita, Omar, Andres, merci pour votre accueil chaleureux et vos conseils, les sorties impromptues et les fous rires. Merci d'avoir été des amis autant que des collègues. Zahia, Omar, merci pour votre soutien et pour toutes ces discussions, parfois sérieuses, parfois plus légères, mais toujours précieuses.

La vie (et une thèse) serait bien monotone sans les amis pour l'égayer un peu : ceux qui sont là depuis le début (coucou Corentin et Hugo) ou depuis quelques années déjà, remontrés lors des études (les Sporwer et Arthur), merci d'être venue me soutenir dans ce jour de présentation, votre soutien m'a fait chaud au cœur. Teva, merci pour tout le soutien dans cette dernière ligne droite, pour les distractions et les discussions.

Eglé, Alexis, Louis, Lubin et tous les autres, merci de m'avoir supporté quand je radotais sur mon sujet, pour m'avoir toujours accompagnée et soutenue (avec une bonne bière au bar), grâce a vous le temps et passe si vite et on ne s'est jamais ennuyé.

Je n'en serai pas arrivée la sans ma famille : mes parents, ma grand-mère, mes frères. Même sans comprendre ce que je fais ou pourquoi, vous m'avez toujours encouragé à continuer encore et encore.

Elise, Chloé, Adrien, ma team Ouin-Ouin. Je ne sais pas ce qu'aurait été ces années sans vous, mais elles auraient été bien plus tristes c'est sûr. Les pauses thés, les jeux du midi, les sorties et les vacances en passant par les crises de quart de siècle, vous avez tellement contribue à rendre cette aventure plus belle. C'était un plaisir de partager cette étape de ma vie avec vous, je suis fière de tout ce que vous avez accompli.

Enzo, tout le temps passe ensemble m'est très précieux. Tu as toujours cru en moi et c'est grâce à toi que j'ai commencé cette thèse, et c'est aussi en partie grâce à toi que j'ai pu la finir. Je chérirai tous les bons moments que nous avons partagé. Un gros bisous a Zoya, mon chat, ma princesse, pour le soutien émotionnel (sous forme de miaulement dans les oreilles et de câlins quand on s'y attend le moins.)

Et enfin, les filles, le Consejo, mon soutien émotionnel et mes repères depuis déjà 15 ans, j'espère que vous savez a quel point vous avez été essentielle dans cette aventure. Jamais vous n'avez doute de moi et de mes capacités, vous m'avez toujours soutenue et poussée vers le haut, à viser toujours plus haut et à ne pas me laisser abattre. Alors Mathilde et Doriane, merci.